Dynamical properties of vortices and quasiparticles in superconductors

Vadim Plastovets

THÈSE PRÉSENTÉE

pour obtenir le grade de

Docteur de l'Université de Bordeaux

ÉCOLE DOCTORALE DES SCIENCES PHYSIQUES ET DE L'INGÉNIEUR

SPÉCIALITÉ LASERS, MATIÈRE, NANOSCIENCES

Par **Vadim PLASTOVETS**

Propriétés dynamiques des vortex et des quasiparticules dans les supraconducteurs

(Dynamical properties of vortices and quasiparticles in superconductors)

Sous la direction de : **Alexandre Bouzdine**

Soutenue le 18 octobre 2023

Membres du jury :

M. Manuel HOUZET	Directeur de Recherche	CEA Grenoble	Rapporteur
M. Pascal SIMON	Professeur	Université Paris-Saclay	Rapporteur
M. Vladimir KRASNOV	Professeur	Université de Stockholm	Examinateur
M. Javier VILLEGAS	Directeur de Recherche	CNRS/Thales	Examinateur
M. Philippe TAMARAT	Professeur	Université de Bordeaux	Président
M. Alexandre BOUZDINE	Professeur	Université de Bordeaux	Directeur de thése

Laboratoire Ondes et Matière d'Aquitaine UMR 5798, 33405 Talence, France.

Abstract

The growing interest in superconductivity and its applications in modern ultrafast microelectronics stimulates the active study of various problems in this vast field of condensed matter physics. This dissertation, based on several publications, presents theoretical studies on some new aspects of the physics of vortices and quasiparticle excitations in a superconducting condensate.

The first chapter is devoted to the most prominent manifestation of the superconductivity - quantum vortices, which nowadays are actively considered as possible elements of quantum computer and other microelectronic devices. An important means of physical control of such systems is the manipulation of individual vortices. Dynamic properties and associated dissipative processes caused by the vortex motion are determined both by the structure of vortex magnetic field and electronic arrangement of quasiparticles inside the vortex normal core. The vortex structure can be strongly modified in superconductors with defects of quite various sizes, especially in real crystals, where the appearance of imperfections is unavoidable. As an example we studied the electronic (or subgap) and electromagnetic configuration of the vortex in the vicinity of the planar defects. Our predictions can be useful in interpreting the current experimental results related to vortex imaging and may become a guide for the development of electronic vortex-based devices.

In the second chapter the dynamics of the superconducting condensate exposed to the circularly polarized light radiation is discussed in the context of recently developed theory of inverse Faraday effect (IFE) for superconductors. More precisely we consider strongly nonlinear regime of IFE with respect to the order parameter and discuss the possibility of the trapping of the Abrikosov vortices by superconducting currents. The latter can be utilized as a useful tool for optical vortex generation giving rise to on-demand creation of the vortices without applying magnetic field. We have also studied IFE in the fluctuational regime above the critical temperature for the case of small superconducting rings, which, in turn, can be regarded as a promising application for superconducting fluxonics.

The third chapter deals with nonequilibrium dynamics of the superconducting condensate in the presence of spin-splitting field mediated by spin-orbit interaction. In particular we examined the excitation of the amplitude modes of the order parameter (so-called Higgs modes) whose resonant behaviour is strongly determined by the applied Zeeman field. Such modes strongly modify the electromagnetic response of a superconductor and can be directly coupled to the external spin-splitting field. In addition, we considered how the intersection of different branches in the quasiparticle spectrum, caused by the Zeeman field, provokes a nonadiabatic tunneling of quasiparticle states. This leads to significant dynamic change of order parameter as well as the distribution function of quasiparticles, which can affect the transport and/or optical response of the superconductor.

Keywords: Superconductivity, Abrikosov vortex, Inverse Faraday effect, Nonequilibrium dynamics

Résumé

L'intérêt croissant pour la supraconductivité et ses applications dans la microélectronique ultrarapide moderne stimule l'étude active de divers problèmes dans ce vaste domaine de la matière condensée. Cette thèse, basée sur plusieurs publications, présente des études théoriques des quelques nouveaux aspects de la physique des vortex et des excitations de quasiparticules dans un condensat supraconducteur.

Le premier chapitre est consacré à la manifestation la plus importante de la supraconductivité - les vortex quantiques, qui sont aujourd'hui activement considérés comme des éléments possibles de l'ordinateur quantique et d'autres dispositifs microélectroniques. Un moyen important de contrôle physique de tels systèmes est la manipulation de vortex individuels. Les propriétés dynamiques et les processus dissipatifs associés provoqués par le mouvement du vortex sont déterminés à la fois par la structure du champ magnétique du vortex et l'arrangement électronique des quasiparticules à l'intérieur du noyau normal du vortex. La structure de vortex peut être fortement déformée dans les supraconducteurs présentant des défauts de tailles assez diverses, notamment dans les cristaux réels, où l'apparition d'imperfections est inévitable. A titre d'exemple nous avons étudié la configuration électronique (ou sous-gap) et électromagnétique du vortex au voisinage des défauts planaires. Nos prédictions peuvent être utiles pour interpréter les résultats expérimentaux récents liés à l'imagerie de vortex et peuvent devenir un guide utile pour le développement de dispositifs électroniques à base de vortex.

Dans le deuxième chapitre, la dynamique du condensat supraconducteur exposé au rayonnement lumineux polarisé circulairement est étudié dans le contexte de la théorie récemment développée de l'effet Faraday inverse (EFI) pour les supraconducteurs. Plus précisément, nous considérons un régime fortement non linéaire du régime EFI par rapport au paramètre d'ordre et discutons la possibilité du piégeage des vortex d'Abrikosov par des courants supraconducteurs. Ce dernier peut être utilisé comme un outil utile pour la génération optiques des vortex donnant lieu à la création à la demande des vortex sans application de champ magnétique. Nous avons également étudié l'EFI dans le régime de fluctuationnel au-dessus de la température critique pour le cas de petits anneaux supraconducteurs, ce qui, à son tour, peut être considéré comme une application prometteuse pour la fluxonique supraconductrice.

Le troisième chapitre traite la dynamique hors d'équilibre du condensat supraconducteur en présence d'un champ Zeeman médié par l'interaction spin-orbite. En particulier nous avons examiné l'excitation des modes d'amplitude du paramètre d'ordre (appelés modes de Higgs) dont le comportement résonant est fortement déterminé par le champ de Zeeman appliqué. De tels modes modifient fortement la réponse électromagnétique d'un supraconducteur et peuvent être directement couplés au champ Zeeman externe. De plus, nous avons examiné comment l'intersection de différentes branches dans le spectre des quasiparticules, causée par le champ de Zeeman, provoque un effet tunnel non adiabatique des états des quasiparticules. Cela conduit à un changement dynamique important du paramètre d'ordre ainsi que de la fonction de distribution des quasiparticules, ce qui peut affecter le transport et/ou la réponse optique du supraconducteur.

Mots-clés : Supraconductivité, Vortex d'Abrikosov, Effet Faraday inverse, Dynamique hors équilibre

Acknowledgements

I especially thank the members of the committee for the time and effort devoted to my defence.

This dissertation is the result of my work in Condensed Matter Theory Group of Laboratoire Ondes et Matière d'Aquitaine. I would like to express my deepest gratitude to my supervisor, Alexander Buzdin, for his engagement, encouragement and patience, which helped me to develop as a young researcher. I extend my sincere thanks to to Alexander Mel'nikov for the invaluable support in my PhD work and for inspiring scientific discussions.

Thanks to LOMA team for hospitality and enjoable time. To Bishal and Jérémy for helping with the adaptation after my arrival and for kind atmosphere during the long COVID months. Thanks to Alpesh, Jonathan, Elena, Aditya and Benjamin for the lab routine and all kinds of distractions both in and out of the lab. To Jerôme Cayssol for a little teaching experience. Thanks also to Pierre, Nicolas, Thomas and Guillaume for the music sessions and some great live performances.

Part of my PhD journey was spent in Laboratoire Photonique Numérique et Nanosciences. I would like to thank Brahim Lounis for his help and extreme curiosity about my work, always evolving into useful discussions. Thank to the local team: Malo, Matthias, Elise, Quentin and Sid for their kindness, various scientific and non-scientific conversations and time spent together.

I thank my mom and sister for their constant support and faith, which have brought me to this point.

Thank you Polina for the loving patience, empathy and motivation which I have felt throughout all these years.

List of publications

[1] A. V. Samokhvalov, **V. Plastovets** and A. S. Mel'nikov, "TOPOLOGICAL TRANSITIONS IN ELECTRONIC SPECTRA: CROSSOVER BETWEEN ABRIKOSOV AND JOSEPHSON VORTICES", Phys. Rev. **B** 102, 174501 (2020). DOI:10.1103/PhysRevB.102.174501

Author's contribution: analytical solution of the Bogoliubov-de Gennes equation, calculation of the density of states and participation in writing the manuscript.

[2] **V. Plastovets** and A. S. Mel'nikov, "ELECTRONIC STRUCTURE OF A JOSEPHSON VORTEX IN A SIS JUNCTION", Phys. Rev. **B** 105, 094516 (2022). DOI:10.1103/PhysRevB.105.094516

Author's contribution: derivation of main results and writing the manuscript.

[3] **V. Plastovets** and A. I. Buzdin, "DELOCALIZATION OF THE VORTEX MAGNETIC FIELD NEAR A PLANAR DEFECT", Phys. Rev. **B** 108, L180502 (2023). DOI:10.1103/PhysRevB.108.L180502

Author's contribution: derivation of a part of the results and participation in writing the manuscript

[4] A. Gutfreund, H. Matsuki, **V. Plastovets**, A. Noah, L. Gorzawski, N. Fridman, G. Yang, A. Buzdin, O. Millo, J.W.A. Robinson, Y. Anahory, "DIRECT OBSERVATION OF A SUPERCONDUCTING VORTEX DIODE", Nat Commun 14, 1630 (2023). DOI:10.1038/s41467-023-37294-2

Author's contribution: discussion of the theoretical model and writing the theoretical part of the manuscript.

[5] **V. Plastovets**, I. D. Tokman, B. Lounis, A. S. Mel'nikov, and A. I. Buzdin, "ALL-OPTICAL GENERATION OF ABRIKOSOV VORTICES BY THE INVERSE FARADAY EFFECT", Phys. Rev. **B** 106, 174504 (2022). DOI:10.1103/PhysRevB.106.1745042

Author's contribution: writing of numerical codes, analysis of the main results and writing the manuscript.

[6] **V. Plastovets**, A. I. Buzdin, "FLUCTUATION-MEDIATED INVERSE FARADAY EFFECT IN A SUPERCONDUCTING RING", Physics Letters A 481, 129001 (2023). DOI:10.1016/j.physleta.2023.129001

Author's contribution: derivation of main results and writing the manuscript.

[7] **V. Plastovets**, A. S. Mel'nikov, A. I. Buzdin, "COLLISIONLESS DYNAMICS OF THE SUPERCONDUCTING GAP EXCITED BY A SPIN-SPLITTING FIELD", Phys. Rev. **B** 108, 104507 (2023). DOI:10.1103/PhysRevB.108.104507

Author's contribution: derivation of main results and writing the manuscript.

Contents

Introduction

Since the discovery of superconductivity for more than 110 years, many of its manifestations have been studied in various aspects of condensed matter physics. One of the most prominent effects is the interaction of the superconducting condensate with an external magnetic field. A startling example is a type II superconductor which shows perfect diamagnetism (Meißner effect) below the critical field H_{c1} and reveals "Abrikosov's vortex"/"mixed"/"Shubnikov" state up to the normal state for $H_{c1}(T) < H < H_{c2}(T)$. After breakthrough experimental discovery of high-T_c superconductivity in cuprates by Bednorz and Miiller [1], and subsequent various compounds (such as BSCCO [2], MgB_2 [3], Fe-pnictides [4] or Fe-chalcogenides [5] and nickelates [6]), most of which belong to type II, the study of the vortex state has become crucial to understanding the physics of superconductors. Indeed, the presence of the vortex lines in the material strongly modifies the fundamental thermodynamical, heat, transport, optical, etc. properties of the superconductor and provides plenty of novel effects that are of interest in applied physics. A rich and complex picture of the interaction of vortices with each other, with external drive, with disorder, crystal defects and various geometric shapes of superconductors, led to the emergence of the term "vortex matter", which can be studied separately against the background of a self-consistent theory of superconductivity.

The observation of a rich variety of vortex phases in superconductors and superfluids is known to be one of the convincing manifestations of the quantum coherence in these systems, which can be described phenomenologically within the complex-valued order parameter $\Psi(\mathbf{r},t) = |\Psi|e^{i\theta}$. According to a textbook picture quantum vortex has a normal core with the size of the order of coherence length $\xi(T)$ with 2π circulation of the order parameter phase $\theta(\mathbf{r},t)$. The vortex core is surrounded by the circular supercurrent on the scale of the London penetration depth $\lambda(T)$, which carries the magnetic flux quantum $\Phi_0 = \pi\hbar c/e \approx 2\times10^{-7}$ G cm^2 in the bulk systems. The supercurrents flowing around the vortex are responsible for the hydrodynamic interaction of the vortex with the external transport current $\mathbf{j}$, which leads to the appearance of an effective Lorentz force $\mathbf{F}_L = \mathbf{j}\times\mathbf{\Phi}_0/c$ which moves the vortex in a direction perpendicular to $\mathbf{j}$ [7]. The core of the vortex consists of normal electrons and therefore provides a dissipation processes both inside and outside the core due to the interaction with transport electric field. This results in the appearance of the friction force $-\eta\mathbf{v}_L$ which balances the Lorentz's force $\mathbf{F}_L$ and thereby provides a steady-state velocity of the vortex $\mathbf{v}_L = \mathbf{j}\times\mathbf{\Phi}_0/c\eta$. The motion of the vortices under applying of the transport current is called the "flux-flow" regime. Due to the Faraday's law the moving magnetic flux produces spatially averaged electric field $\langle\mathbf{E}\rangle = \mathbf{B}\times\mathbf{v}_L/c$ [8] which is parallel to $\mathbf{j}$ and therefore results in the losses and finite longitudinal conductivity $\sigma_{xx} = \sigma_n H_{c2}/B$. Here we use the expression for the viscosity $\eta = \sigma_n\Phi_0 H_{c2}/c^2$ derived in the Bardeen-Stephen model with the normal conductivity σ_n [9]. Thus, the flux-flow regime leads to the dissipation even in the clean homogeneous superconductor, and a finite voltage on $I(V)$ curves is observed in all typical transport measurements in the vortex state. Such an interaction of the vortex and the transport current in the hybrid superconductor/ferromagnet structure will be considered in the Chapter 1, where the experimental observation of the diode effect in the flux-flow regime is discussed.

In addition to the Lorentz force, there are many other contributions that play a significant role in the dynamics of vortices under the action of external perturbations. For instance, there is a well known pinning force [10] existing in inhomogeneous superconductors with defects, or

more intricate force $\mathbf{F}_{\text{env}}$, which originates from the back action of the quasiparticle environment (subsystem) induced by the vortex displacement [11]. The exact form of $\mathbf{F}_{\text{env}}$ can be found from the Boltzmann kinetic equation for the quasiparticle distribution function, taking into account the electronic structure of the vortex normal core. This approach allows one to describe both clean/dirty limits and the steady motion of the vortex is simply defined as $\mathbf{F}_L + \mathbf{F}_{\text{env}} = 0$. Besides the mentioned friction (Bardeen-Stephen result), the force $\mathbf{F}_{\text{env}}$ may contain more complicated contributions generally provoking the motion of the vortex line *along* the transport current [11]. One of them is purely hydrodynamic Magnus force, which naturally enhances the dissipationless dynamics in the clean regime and is inherent in neutral superfluids. Another important contribution to $\mathbf{F}_{\text{env}}$ is so-called quasiparticle *spectral flow force* [1] , which is especially of interest in the context of Chapter 1. It is known that quantum vortices in superconductors affect the local gap function and, thus, perturb the quasiparticle spectrum provoking the formation of the subgap quasiparticle states. These states are capable of participating in the transfer of linear momentum to quasiparticles from the motion of a vortex, and such an interaction (effectively leading to the breaking of Cooper pairs) is dissipative [11]. The specific details of the quasiparticle dynamics in the vortex system depend on the vortex electronic structure, especially its subgap part.

Generally, experimental detection and study of the vortex subgap spectrum can provide an information about the nature of the superconducting state, i.e. about the symmetry and structure of the superconducting gap function [13–24]. This approach to the probing of the gap structure can be applied for different types of vortex systems including a standard Abrikosov vortex in isotropic superconductors and strongly disturbed vortex solutions in anisotropic or layered superconductors with Josephson interaction between the layers[10, 25, 26]. The electronic structure of a singly quantized Abrikosov vortex has been studied for decades both experimentally and theoretically [10, 27–29]. Circulation of the phase of the order parameter is responsible for the formation of the subgap bound quasiparticle states, which form a so-called anomalous spectral branch, originally discovered in the work of Caroli-de Gennes-Matricon (CdGM)[30]. In the quasiclassical limit $k_F\xi \gg 1$, where k_F is the Fermi momentum, the quasiparticles propagate along the straight classical trajectories, which can be parametrized by the impact parameter $b = -\mu/k_\perp$, where μ is the angular momentum (half an odd integer) defined with respect to the vortex axis and $k_\perp$ is the momentum component perpendicular to the vortex axis. The anomalous spectral branch crosses the Fermi level and varies from $-\Delta_0$ to Δ_0 as μ changes. The low-energy CdGM spectrum is a linear function of the angular momentum μ: $E_{CdGM} \approx -\mu\Delta_0/k_F\xi$. We neglect the quantization of the CdGM spectrum in the quasiclassical regime ($k_F\xi \gg 1$) due to small interlevel spacing $\propto \Delta/E_F$, while in the quantum regime ($k_F\xi \sim 1$) the discreteness of μ becomes important. The discrete CdGM levels have been recently observed in the Fe-chalcogenides with $\Delta \lesssim E_F$ [31, 32]).

In real superconducting crystals, the spectral features described above can be strongly affected by defects of different nature, such as columnar defects, point impurities, and twinning planes. In particular, these inhomogeneities can modify the shape of the vortex core and, consequently, the subgap spectrum. Another aspect of the influence of the defects on the vortex electronic structure originates from the elastic scattering of quasiparticles at the defect potential profile. The consequences of this scattering effect have been investigated for point impurities [33–36], for columnar [37, 38] and planar [39–41] defects and for a vortices near the surface of various shape [42–44]. It has been shown [40], in particular, that for a vortex pinned at a high-transparent

[1] This effect is quite general for bosonic (^{4}He) and uncharged (^{3}He)/charged (superconductors) fermionic superfluids [12].

insulating plane the electron scattering can cause the essential changes in the structure of the low-energy part of the CdGM spectrum even without perturbation of the vortex core shape. This leads to a significant increase in the spectral minigap at the Fermi level and deviation of the low-energy spectrum structure from the above equidistant behavior. For the low-transparent insulating plane the vortex core no longer exists and the minigap in the spectrum tends to the bulk gap value Δ_0 [45].

In addition to transport, rearrangement of subgap quasiparticle states has a significant effect on the high frequency properties of the vortex [38, 46]. Moreover, the changes in the quasiparticle spectrum of the vortex pinned at a linear defect are of particular interest in the context of the problem of manipulating of the topologically protected Majorana states [47–52]. The controllable motion of the vortex along the linear defect in an exemplary hybrid structure consisting of a primary superconductor with conventional pairing and a two-dimensional (2D) layer with a nontrivial topology provides a unique possibility to manipulate the Majorana state located in the 2D layer. The value of the minigap in the vortex spectrum in the primary superconductor is of the crucial importance for the topological protection of these operations [53, 54].

Practical implementation of microelectronic devices based on superconducting vortices poses two key questions: how to create vortices and how to control them efficiently. Addressing these challenges, the utilization of light emerges as a promising solution. Notably, the ongoing achievements in terahertz technologies play an important role for the study of non-stationary and non-equilibrium processes in superconducting materials. This naturally led to the rapid growth of the field of optoelectronics, focused in particular on the optical manipulation of Abrikosov vortices. A simple mechanism of the light - vortex interaction originates from the local heating of superconductor by a tightly focused laser beam [55–58]. The induced thermal gradient ∇T [59, 60] offers a possibility of fast and precise manipulation of individual Abrikosov vortices, demonstrated recently in Ref. [61]. Interestingly, a strong laser pulse by itself is able to generate vortices in superconductors by the Kibble-Zurek mechanism. First introduced in cosmology [62, 63] and later generalized to the systems with broken U(1) symmetry [64–66], this mechanism can describe the formation of topological defects during rapid thermal quench after heating the sample with a thermal pulse. Such a scenario has been observed in a superfluid helium ^{3}He [67–69], superconducting systems [70–74] and cold atoms condensate [75, 76]. In nonequilibrium superconductors, Kibble-Zurek mechanism always results in the creation of vortex-antivortex pairs which should annihilate during the post-quench dynamics. The presence of pinning centers in the superconductor prevents the annihilation process making it possible to experimentally visualize the generated vortex-antivortex pairs [72, 73]. In order to generate the vortex with a desired polarity at a desired position, one can use a focused laser pulse, which initiates the local rapid quench of the superconductor in the presence of a weak magnetic field (see Ref. [77]). The combined effect of the thermal force $\mathbf{f}_T \propto -\nabla T$ and the Lorentz force arising from Meissner currents $\mathbf{f}_L = \mathbf{j}_M \times \Phi_0/c$ is able to separate vortex-antivortex pairs formed after quench with further transfer of desired polarity at the position of the laser spot and expelling the opposite fluxes to the edges of the superconductor. The current which can be used for a separation of vortex-antivortex pairs in a superconductor can be induced by optical mechanism. The basic idea is to replace an external magnetic field with a light radiation carrying a nonzero angular momentum. For instance, transfer of the *orbital* angular momentum from Laguerre-Gaussian mode to the trapped Bose-Einstein condensate can excite persistent currents, which have been observed experimentally [78, 79]. On the other hand, it is expected that the electromagnetic wave with a *spin* angular momentum or just characterized by the circular polarization of a given

helicity $\sigma_\pm$ can excite the circulating dc currents in a superconductor.

This problem is very similar to the so-called inverse Faraday effect (IFE), which is one of the types of interaction between light and matter. General theory of IFE has been developed several decades ago [80] and describes the generation of the magnetic moment in the media by a circularly polarized electric field. This general mechanism was considered more detailed in various systems: magnetics [81, 82], normal metals [83–85], ballistic nanorings [86–90] and recently in superconductors [91]. In a normal metal IFE appears due to the circular motion of an electric charge along the boundaries of the metal, which makes their presence critical for this effect. In the case of a superconducting system, the light-induced dynamics of the order parameter $\Psi(\mathbf{r},t)$ comprises a nondissipative oscillatory contribution from the coupled modes of the phase and the modulus of $\Psi(\mathbf{r},t)$ and creates the dc currents maintaining a nonzero magnetic moment. The IFE for supeconductors was theoretically considered within the framework of the Ginzburg-Landau theory for a disc [91, 92] and thin rings [93, 94]. According to Ref. [91], the nontrivial dynamics of the order parameter responsible for IFE can present in superconductors with broken particle-hole symmetry in the quasiparticle spectrum. On the microscopic level this asymmetry can appear as a consequence of a finite slope of the density of states at the Fermi level $\nu(E) \approx \nu(E_F) + \gamma(E - E_F)$, where $\gamma \propto \nu'(E_F)$. In the phenomenological Ginzburg-Landau theory, this effect manifests itself as the appearance of the imaginary part of the relaxation constant Γ of the time-dependent order parameter, and $\mathrm{Im}\Gamma \propto \gamma$ [95–98]. Despite the fact that the contribution of $\mathrm{Im}\Gamma$ to the superconductor's dynamics is usually negligible, since $\gamma \propto T_c/E_F$ and for typical low-temperature superconductors $T_c/E_F \ll 1$, there are some effects which crucially depend on this parameter.

For example, the electron-hole asymmetry appears in the Hall effect observed in the vortex state of superconductors. If the imaginary part of Γ is taken into account when describing the vortex dynamics in the framework of the TDGL theory, then the equation of vortex motion will be modified by an additional term: $\mathbf{j}_{tr} \times \mathbf{\Phi}_0 = \alpha_1 \mathbf{v}_L + \alpha_2(\gamma)\mathbf{v}_L \times \mathbf{\Phi}_0$, where $\mathbf{v}_L$ is the local vortex velocity and $\alpha_1 \mathbf{v}_L$ is the viscous drag force [99]. The parameter α_2 corresponds to the nondissipative *Magnus-like* force (given by small $\sim T_c/E_F$ curvature of the quasiparticle spectrum) , which pushes the vortex along the transport current j_{tr} and leads to the generation of the longitudinal voltage and nondiagonal components of the conductivity σ_{xy}. Note that $\alpha_2(\gamma = 0) = 0$ [11, 99, 100]. The measurements of the Hall effect in the high-T_c compounds, such as layered cuprates, indicate relatively large value of γ [101–105]. Among other possible candidates with quite a large relation $T_c/E_F \sim 0.3$ one can mention the class of actively studied FeSe-based materials [106, 107].

Another well known manifestation of the particle-hole asymmetry is the Hall effect observed in superconductors in fluctuation regime above T_c, where there are no vortices and the supercurrents are carried by the fluctuating Cooper pairs [108]. This effect can be noticeable, since usually the response of the fluctuating system induced by some external perturbation has a strong (divergence) dependence on the temperature detuning $\epsilon = (T - T_c)/T_c$ in the vicinity of the phase transition. The theoretical calculation of so-called paraconductivity (or Aslamazov-Larkin [109]) contribution to the nondiagonal component of the conductivity tensor (Hall effect) in the layered superconductor exposed to perpendicular magnetic field shows that $\sigma_{xy} \propto \gamma$ [108]. The particle-hole asymmetry also plays an important role in the recently studied photon drag of superconducting fluctuations in two-dimensional electron gas [110]. The direct transfer of the momentum of the electromagnetic wave to the fluctuations produces the supercurrent $j_s \propto \gamma$, which can compete with the response from the normal electrons in the region $\epsilon \ll 1$. The general nature of these effects can be a promising prerequisite for observing the inverse Faraday effect

maintained by fluctuating Cooper pairs [111], which may complement the theory of fluctuation spectroscopy [112] in superconductors.

To describe effects such as vortex dynamics, the Hall effect or IFE, it may be sufficient to use the GL phenomenological approach, which has proven to be very successful. However, this approach has strict limits, especially for the time-dependent problems. For example, regarding the IFE for superconductors the theory predicts that the effective generation of the dc magnetic moment requires THz frequency range of the external electromagnetic radiation for high T_c ($\Delta(0) \sim 90$ K $= 1.8$ Thz) and far infrared for low T_c ($\Delta(0) \sim 10$ K $= 0.2$ Thz) compounds. If the applied frequency lies above at the edge of the quasiparticle continuum, then the total electromagnetic response of the superconductor (in the general case) will be supplemented by the contribution from various nonequilibrium processes associated, for instance, with the direct excitation of quasiparticles by photons [113]. Note that the study of many nonequilibrium processes has become experimentally available in the last decade due to the growing field of THz spectroscopy [114]. The TDGL theory is not capable of describing strongly nonequilibrium processes and has a natural constraint $\omega \ll \Delta(0) \sim T_c$, e.g. the characteristic frequency of the external disturbance must be less then the gap in the quasiparticle spectrum. To study out-of-equilibrium physics one can apply different methods. The TDGL can be applicable if the energy relaxation of the quasiparticles τ_ε is much less than the characteristic time of the order parameter $\tau_\Delta \propto (T_c - T)^{-1}$. Such situation can be realized either in the vicinity of the critical temperature [115, 116], or in the gapless superconductor with strong inelastic electron-phonon interaction [117]). In the opposite limit $\tau_\varepsilon \gg \tau_\Delta$ the temporal evolution of QP is governed by the Boltzmann kinetic equation together with the self-consistency equation for the order parameter (which is assumed to have small variations in space and time), which is applicable for clean superconductors [11, 118, 119]. Finally, the most general approach for the nonequilibrium regime is a comprehensive Gorkov-Keldysh theory for Green functions.

The quench and subsequent relaxation of the quasiparticles above the gap can trigger *collective excitations* (or modes - long-lived coherent motion of a large fraction of the particles in a system), which are the brilliant example of complex phenomena in condensed matter physics [120]. Collective modes are diverse and the most well-known are, for example, phonos, magnons and plasmons. Some of the collective modes have fundamental nature according to Goldstone theorem and are connected to the spontaneous breaking of a global continuous symmetry in the system [121]. Thus, phonon modes appear due to the broken translational symmetry and they naturally participate in the energy relaxation of nonequilibrium electrons through the electron-phonon interaction [122]. Superconductors have intrinsic collective excitations originated from the broken U(1) symmetry (rotational symmetry with respect to the phase of a macroscopic wave function), which gives rise to the modes of the modulus and the phase of the complex-valued order parameter, or the gap function $\Delta(t) = |\Delta|e^{i\theta}$ around its equilibrium value $\Delta_0(T)$. For conventional superconductors the phase (or Nambu-Goldstone) modes are not of particular interest, since due to the gauge invariance they are coupled to the electromagnetic field and, therefore, their dynamics occurs at typical electron plasma frequencies (Anderson-Higgs mechanism [123]). On the contrary, the mode of the order parameter modulus, which is called Higgs mode by analogy with electro-weak particle theory [124, 125] or Schmid mode [126], is a low-energy excitation with the energy $2\Delta_0$, coinciding with the bottom of the quasiparticle spectrum. Note that in the presence of a particle-hole asymmetry both types of modes are coupled to each other [125]. Aforementioned quench of electrons above the energy gap can provoke the effective excitation of the Higgs mode [127–129]. Despite the fact that the contribution of

collective modes to the response of a superconductor is fairly well studied [130], the question of modifying such a contribution in the presence of broken time reversal symmetry remains unexplored.

Extensive studies of nonequilibrium states of superconductors [11, 131] pay considerable attention to the so-called collisionless dynamics of a superconducting condensate, described by the pairing potential $\Delta(t)$. At timescales shorter than the typical inelastic relaxation time $t \ll \tau_\varepsilon$ the dynamics of Cooper pairs is in coherent regime, which can be described, for instance, by the Keldysh technique for Green's functions or its quasiclassical approximation [132, 133]. The collisionless regime manifests itself most clearly in the existence of oscillations of the amplitude of the order parameter $\Delta(t) = \Delta_0 + \delta\Delta(t)$ near the equilibrium gap value Δ_0. This mode comes from excited interference interaction between the wave functions of the quasiparticles (QP) from broken Cooper pairs. Due to the QP dispersion the summation over all interference contributions results in an inhomogeneous broadening of the total gap mode, which is equivalent to a weak damping with a typical time evolution $\delta\Delta(t) \propto \cos(2\Delta_0 t)/\sqrt{\Delta_0 t}$ [132]. Since the Higgs mode is a scalar excitation, it can not be coupled to the electromagnetic field $\mathbf{A}(t)$ linearly and several indirect mechanisms have been studied, such as linear excitation by the THz radiation in the presence of dc supercurrent [134, 135]. Also it possible to realize a nonlinear and coherent (or incoherent [136]) Higgs mode excitation using high-intensity THz light with frequency just above the equilibrium superconducting gap Δ_0, which can be detected by ultrafast pump-probe spectroscopy and third harmonic generation measurements [130, 137–140].

It is known that, in addition to electromagnetic fields, superconductors also respond to nonstationary spin-splitting fields $\mathbf{h}(t)$. Typically, this field is produced by an external magnetic field $\mathbf{h} = \mu_B \mathbf{H}$ or by the exchange field of an adjacent ferromagnetic layer $\mathbf{h} \sim J_{\text{ex}} \mathbf{M}_F$, which is induced by proximity to the superconductor. Spin-split systems serve as a good platform for spintronic applications and extensive study of various non-equilibrium processes has been done over the last few decades [141–143]. In particular, by inducing magnetic moment dynamics in S/F junctions an effective spin-triplet component of the superconducting gap is generated resulting in long-range proximity effects [144–148]. On the other hand experimental observations indicate that the superconducting subsystem has a direct impact on the ferromagnetic resonance in hybrid S/F structures [149–151].

In recent years there has been a growing interest in studying of the Higgs modes in the proximitized superconducting systems [152, 153] as well as the interaction of collective modes in S/F systems [154]. For instance, it was recently shown that in a superconductor in the helical phase, which can be achieved in the presence of a strong spin-orbit coupling (SOC) and an exchange field, the Higgs mode can be linearly coupled to the electromagnetic field through the nonzero superconducting phase gradient in the ground state [155]. Also, it was revealed that the coupling of the Higgs mode $\delta\Delta(t)$ in a superconductor to external light $\mathbf{A}(t)$ and magnetic dynamics $\mathbf{m}(t)$ in the F layer allows the generation of time-dependent spin currents [156]. These currents can themselves excite the Higgs mode in the superconductor through the resonance of the ferromagnet due to the reciprocal effect [156]. Another example is an interplay between the superconducting Higgs mode and a magnon mode in the adjacent F layer in the presence of a SOC and static proximity effect [157]. Interestingly, the Higgs mode here is coupled to the Zeeman field $\mathbf{h}(t)$ linearly due to the presence of both the spin-orbit interaction and some preferred direction given by wave-vector of the magnetic mode.

According to the aforementioned works, the SOC is critical for interaction of different spin subbands of the QP spectrum, which directly leads to the gap dynamics $\Delta(t)$. Some preconditions for this can be taken from the elementary analysis of the equilibrium state. The equilibrium

superconducting gap does not depend on the Zeeman field below the so-called paramagnetic limit $h_{\rm cr} = \Delta_0/\sqrt{2}$, so that $\Delta(h < h_{\rm cr}, T = 0) = \Delta_0$; and above this limit the superconductivity is completely suppressed with $\Delta(h > h_{\rm cr}, T = 0) = 0$ [158, 159]. The SOC drastically changes the dependence $\Delta(h)$ and promotes a generation of triplet component superconducting correlations, leading to the survival of the gap at $h > h_{\rm cr}$ [160]. This effect is associated with mixing of the different spin states of QP, and the appearance of such mixing is naturally expected in the dynamic regime. Consideration of the temporal evolution of the quasiparticles and the self-consistent field $\Delta(t)$ and in the presence of a Zeeman field and mediated by SOC can be performed using time-dependent Bogoliubov-de Gennes theory [142, 161]. This allows one to study the collisionless regime of a superconducting condensate at low temperatures in a purely quantum-mechanical or coherent regime, and calculate its response within a theory for QP wave functions [162–164].

This manuscript attempts to cover several specific and diverse problems of the modern theory of superconductivity. This includes a microscopic description of the stationary states and dynamic properties of quasiparticles, as well as the macroscopic behavior of the mean field order parameter in a superconducting condensate. In fact, each chapter represents an independent study on the specific topic, which, nevertheless, are interconnected as was discussed in the Introduction. In particular, we will address the following questions

• The influence of the planar insulating defect of various transperency on the *electronic* [Ch.1/Sec.1-2] and *magnetic* [Ch.1/Sec.3] structure of the superconducting vortices

• The origin of the flux-flow diode effect in the vortex state of the inhomogeneous superconductor - ferromagnet structure [Ch.1/Sec.4]

• Generation of the inverse Faraday effect in the superconduting media and its application to the optical vortex generation [Ch.2/Sec.1-2]

• Properties of the inverse Faraday effect in superconductors in the fluctuation regime above the critical temperature [Ch.2/Sec.3]

• General features of the dynamics of a superconducting condensate driving out of equilibrium by a spin-spitting field in the presence of a spin-orbit interaction [Ch.3]

Both analytical (mostly) and numerical methods has been widely used in this work. Despite the purely theoretical nature of the study, we comment on its relationship with existing experimental observations and also discuss possible experiments that can be based on our findings. The research summarized in this dissertation can find an application in various aspects of applied superconducting nano-/optoelectronics and spintronics.

Chapter 1

Vortices in inhomogeneous systems

This Chapter is devoted to a theoretical study of the electronic and magnetic structure of a vortex line trapped by a planar defect of various electronic transparency. For this, we consider two limiting cases of Abrikosov and Josephson regimes. In addition, we discuss the mechanism of vortex generation in the S/F bilayer and associated diode flux-flow effect observed in a recent experiment.

The most general definition of different vortex type solutions for the order parameter in superconducting and superfluid systems is based on the calculation of the so-called circulation of the gradient of the order parameter phase around the line of singularity. Provided this circulation equals to 2π we get a singly quantized vortex. The particular structure of the order parameter and magnetic field distributions strongly depends then on the specific system. In a homogeneous isotropic superconductor the vortex solution possessing a cylindrical symmetry is well known as an Abrikosov vortex [165] while the presence of any anisotropy or inhomogeneity can strongly deform this vortex line in the plane (x, y) perpendicular to its axis (see Fig.1). An extreme example of such anisotropic solution which does not even possess the normal core can be realized for a vortex pinned at the Josephson junction [166]. Such quasi-one dimensional vortices are also called Josephson vortices (see Fig. 1.1c) and are known to play an important role in magnetic and transport properties of layered and nano-structured systems. Provided the junction critical current density j_c is much smaller than depairing current density

$$j_d = c\Phi_0/12\sqrt{3}\pi^2\lambda^2\xi\,, \tag{1.1}$$

the Josephson penetration depth

$$\lambda_J = \sqrt{c\Phi_0/16\pi^2 j_c\lambda}\,, \tag{1.2}$$

appears to be much larger than the London penetration depth λ. Here $\Phi_0 = \pi\hbar c/e$ is the magnetic flux quantum, and ξ is the superconducting coherence length. Clearly, changing the electron transparency of the junction one can get a variety of intermediate vortex states corresponding to a crossover from the Josephson to the Abrikosov vortex [167–169]. This situation with the intermediate transparencies naturally appears in many superconducting systems studied in experiments, e.g. in superconductors with twinning planes [170], low-angle grain boundaries [171, 172] or other types of defects [173–175]. An appropriate theoretical treatment needed, for instance, for the interpretation of the experimental data on the magnetic field distribution can be

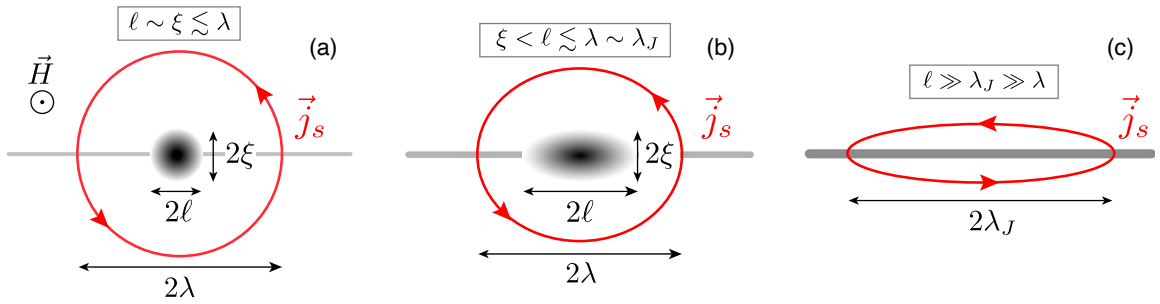

Figure 1.1: Vortex pinned by a planar defect positioned in the $y = 0$ plane for several values of the barrier transparency $\mathcal{T}$: (a) $\mathcal{T} \sim \mathcal{T}_\xi$ – Abrikosov vortex; (b) $\mathcal{T} \sim \mathcal{T}_\xi/\kappa$ – Abrikosov-like vortex for strong coupling; (c) $\mathcal{T} \ll \mathcal{T}_\xi/\kappa$ – Josephson vortex for weak coupling . The region of the vortex core is shown by grey color. Current streamline around the vortex in the plane $(x,\, y)$ perpendicular to its axis is shown by a solid red line.

well developed on the basis of the Ginzburg–Landau theory. Indeed, using a general expression [176] for the critical current I_c across the junction with a cross-section area S

$$I_c = j_c S = \pi\Delta_0/2eR_N\,, \tag{1.3}$$

and relation between the contact resistance and the angle-averaged transmission probability of the barrier $\mathcal{T}$

$$R_N^{-1} = k_F^2 S\,(2e^2/\hbar)\,\mathcal{T}\,, \tag{1.4}$$

we derive the following simple relation

$$\lambda_J^2 = \lambda\,\xi/12\pi^2\mathcal{T}\,. \tag{1.5}$$

It is natural that the Josephson length λ_J grows if the transmission probability of the barrier $\mathcal{T}$ decreases. Keeping in mind type-II superconductors we should take $\xi \lesssim \lambda$ what is equivalent to relatively large Ginzburg-Landau parameter $\kappa = \lambda/\xi$. Using the introduced notations one can qualitatively describe the structure of the vortex assuming electron transmission probability $\mathcal{T}$ to be an arbitrary parameter:

• [Fig. 1.1a] In the case of the extremely strong Josephson coupling $\mathcal{T} \gtrsim \mathcal{T}_\xi = 1/12\pi^2$ the anisotropy of the vortex core is negligible, and at this initial stage of the crossover the order parameter profile in the Abrikosov vortex core is almost insensitive to the defect.

• [Fig. 1.1b] As $\mathcal{T}$ decreases, the vortex supercurrent starts to shrink and when its density $j(r)$ in the vortex core ($r \lesssim \xi$) becomes of order of the depairing one j_d, the length ℓ of the core along the defect can be estimated from the continuity of currents flowing parallel and perpendicular to the defect within the core [167]: $\ell\, j_c \sim j_d\xi$, whence $\ell \sim j_d\xi/j_c \sim \lambda_J^2/\lambda$. The case $\mathcal{T}_\xi > \mathcal{T} \gtrsim \mathcal{T}_\xi/\kappa \ll 1$ (equivalent to $\xi < \ell \lesssim \lambda \sim \lambda_J$) corresponds to the limit of strong Josephson coupling with $j_c \gtrsim j_d/\kappa$ and we get the crossover to the Abrikosov-like vortex having strongly deformed anisotropic core ($\ell \times \xi$), where the superconducting order parameter is suppressed. The distributions of the magnetic field and circular screening currents outside the core ($r \gg \ell,\, \xi$) approach now with the ones for the Abrikosov vortex in a uniform superconductor.

• [Fig. 1.1c] For the weak Josephson coupling $\mathcal{T} \ll \mathcal{T}_\xi/\kappa$ ($\lambda_J \gg \lambda$) the low supercurrent density through the barrier is only enough to form the coreless Josephson vortex with strongly delocalized magnetic field.

Despite general correctness of the above qualitative picture there exist several important physical issues which definitely cannot be described within the phenomenological model and demand a more careful microscopic consideration. This statement surely relates to the scanning

tunneling microscopy (STM) and spectroscopy (STS) data which provide detailed spatially resolved excitation spectra [177–181] and also to the problem of the vortex dynamics and dissipation [11, 33, 182–185]. In the latter case the crossover from the Abrikosov to the Josephson vortex is particularly important since it is accompanied by the disappearance of the normal vortex core which provides the dominating contribution to the dissipation and resulting vortex viscosity [171]. It is the goal of the present work to develop a theoretical description of the changes in the electronic structure of the pinned vortex core which occur during the crossover between the Abrikosov and Josephson vortices and unveil a nontrivial topological nature of this vortex core transformation.

1.1 Electronic structure of an Abrikosov vortex in a SIS junction

Considering the microscopic theory one should take into account the behavior of the subgap fermionic states bound to the Abrikosov vortex core which are known to determine both the structure and dynamics of vortex lines in the low temperature limit (see Ref. [11] for details). These subgap states are known to form the so–called anomalous spectral branch crossing the Fermi level. For well separated vortices the behavior of the anomalous branches can be described by the Caroli–de Gennes–Matricon (CdGM) theory [30]: for each individual vortex the energy $\varepsilon_{CdGM}(\mu)$ of subgap states varies from $-\Delta_0$ to $+\Delta_0$ as one changes the angular momentum μ defined with respect to the vortex axis. Here Δ_0 is the superconducting gap value far from the vortex axis. At small energies $|\varepsilon| \ll \Delta_0$ the spectrum is a linear function of μ: $\varepsilon_{CdGM}(\mu) \simeq -\mu\hbar\omega_0$, where $\hbar\omega_0 \approx \Delta_0/(k_F\xi) = \Delta_0^2/2E_F \ll \Delta_0$ is the interlevel spacing, $\xi = \hbar V_F/\Delta_0$, and $p_F = \hbar k_F$, V_F, E_F are Fermi momentum, velocity and energy, respectively. We shall use here the quasiclassical approach, which is valid if the characteristic size ξ of the vortex core is much larger than the Fermi wavelength of quasiparticles $\lambda_F = 2\pi/k_F$. As a result, the quasiparticles propagate along almost straight classical trajectories which are characterized by the direction of the quasiparticle momentum $\mathbf{p}_F = \hbar k_\perp (\cos\theta_p\, \mathbf{e}_x + \sin\theta_p\, \mathbf{e}_y) + \hbar k_z\, \mathbf{e}_z$ and the impact parameter $b = -\mu/k_\perp$. The subgap bound states of quasiparticles form at these straight trajectories due to the Andreev reflection [186] from the gap profile inside the vortex core. Neglecting the quantization of the angular momentum μ one can get the anomalous spectral branch crossing the Fermi level at $\mu = 0$ for all orientations of the momentum $\mathbf{p}_F$. Thus, in the space $(\mu - \mathbf{p}_F)$ we obtain a Fermi surface (FS) for excitations localized within the vortex core (see Ref. [187] for review). For fixed values of the energy ε and the momentum projection at the vortex axis $\hbar k_z$ we can define a quasiclassical orbit in the plane $(\mu - \theta_p)$: $\mu(\theta_p) = -\varepsilon/\hbar\omega_0$. Each point at this orbit corresponds to a straight trajectory passing through the vortex core, which is determined by the impact parameter b and the angle θ_p (Fig. 1.2). For an isotropic vortex core a θ_p-dependence of the energy ε is lacking, and isoenergetic lines form open orbits shown by dotted lines in Fig. 1.3a. The 2D quantum mechanical nature of the quasiclassical solution can be restored if one takes account of the precession of the quasiparticle trajectories which is triggered by the small deviations from the exact backscattering in the Andreev reflection processes and described by the Hamilton equation: $\hbar\partial\theta_p/\partial t = \partial\varepsilon/\partial\mu$. For a free Abrikosov vortex the straight trajectories precess (or just rotate) around the vortex center by the angle 2π (see Ref. [11]).

Any additional normal scattering process should modify the behavior of the anomalous spectral branch. Such modification can be noticeable even for impurity atoms introduced in a vortex core [33] and becomes much more pronounced provided we consider a vortex pinned by a normal-metal [188, 189] or an insulating [37, 38, 190, 191] columnar defect of the size

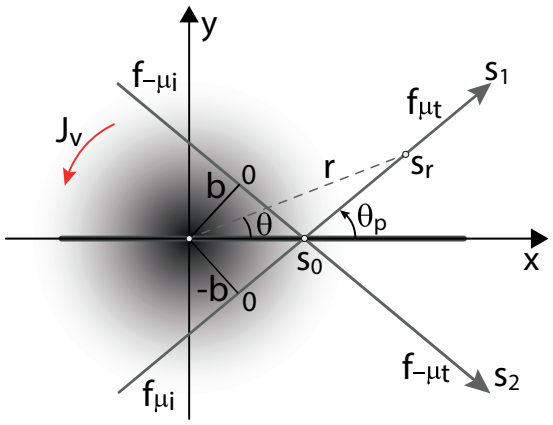

Figure 1.2: Specular reflection of quasiclassical trajectories s_1 and s_2 with opposite values of the angular momentum $\mu = \pm k_\perp |b|$ at the defect in the plane $y = 0$. The region of the vortex core is marked by the gray color. The red arrow shows the direction of the supercurrent in the vortex.

$R \ll \xi$ well exceeding the Fermi wavelength. In the last case the scattering at the defect is responsible for the opening of the minigap $\varepsilon_0 \sim \Delta_0 R/\xi$ in the spectrum of localized states and resulting suppression of the dissipation at low temperatures $T \ll \varepsilon_0$ [11, 192]. For a vortex approaching a flat or curved sample boundary an appropriate spectrum transformation was studied in Refs. [43, 193–195]. Change in the anomalous spectral branch is accompanied by the changes in the topology of quasiclassical orbits in the $(\mu - \theta_p)$ plane. Such topological transitions in quasiparticle spectra of vortex systems are similar to the well–known Lifshits transitions which occur in the band spectra of metals [196, 197]. The generic examples of such transitions in vortex matter including the opening of the closed segments of the orbits in the $(\mu - \theta_p)$ plane or merging and reconnection of the different segments via the Landau-Zener tunneling have been previously studied in Refs. [43, 198, 199]. The basic properties of vortex matter such as pinning and transport characteristics, heat transport in the vortex state and peculiarities of the local density of states should be strongly affected by these changes in the topology of the subgap spectral branches.

To elucidate our main findings we start from the simplified qualitative picture illustrating the effect of the barrier on the quasiparticle subgap states. Our idea is that the scattering at the plane defect with some finite transparency $\mathcal{T}$ can strongly affect the quasiparticle trajectory precession preventing the trajectory to rotate by the full angle 2π. This destruction of the trajectory rotation around the vortex center should be accompanied by the changes in the topology of the quasiclassical orbits and qualitative modification of the quasiparticle spectrum. We restrict ourselves to situations when the barrier is rather weak assuming $\mathcal{T}_\xi \lesssim \mathcal{T} < 1$, and focus on the modification of the anomalous energy branches which occurs in a vortex pinned by a planar defect due to the quasiparticle normal reflection at the defect boundary. First, considering the specular reflection of the quasiclassical trajectories at the plane defect in Fig. (1.2) one can clearly see that the scattering couples the wave functions with the opposite angular momenta $\pm\mu$. Overlapping of these wave functions transforms the quasiclassical spectrum resulting modification of the topology of isoenergetic lines in the $(\mu - \theta_p)$ plane. Phenomenologically one can describe this coupling by a standard two-level problem, which yields the secular equation

$$(\varepsilon - \varepsilon_\mu)(\varepsilon - \varepsilon_{-\mu}) \approx (V_{gap}(\theta_p))^2 \ , \tag{1.6}$$

where ε_μ denotes the anomalous spectral branch for a linear trajectory passing through the core

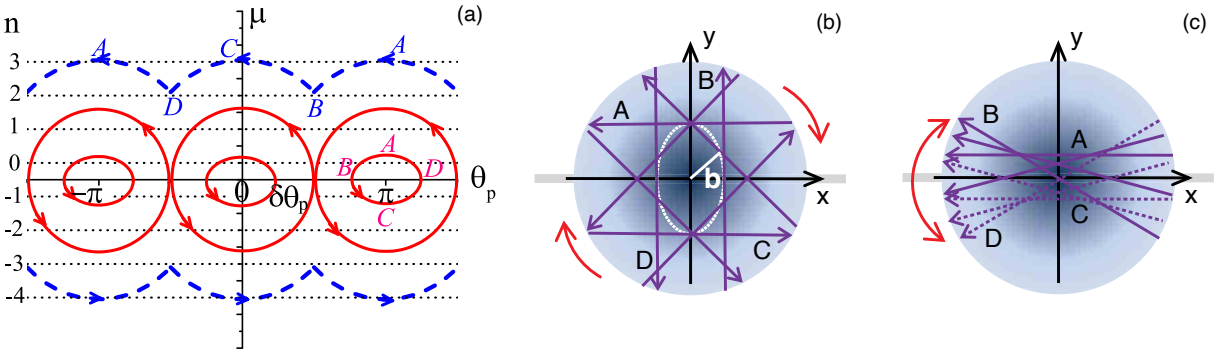

Figure 1.3: Quasiparticle orbits (1.8) in the $(\mu - \theta_p)$ plane corresponding to different energy levels n are shown schematically by red solid lines. For reference dashed lines show the orbits for a single Abrikosov vortex in absence of a barrier. Arrows show the direction of the quasiparticle trajectory precession along the orbit.

of a free vortex. The scattering obviously cannot couple the trajectories with $\theta_p = 0\,, \pm\pi$, which are parallel to the defect plane. Considering now the limit of small angles θ_p one can expect that even for the barriers with rather good transparency $\mathcal{T}$ the tunneling probability should vanish in this angular interval. The splitting of the energy levels around $\varepsilon = 0$ should originate from the superconducting phase difference ϕ at the ends of the incident $f_{-\mu i}$ ($f_{\mu i}$) and reflected $f_{\mu t}$ ($f_{-\mu t}$) trajectories (see Fig. 1.2). This phase difference ϕ equals to $\pm(\pi - 2\theta_p)$. Using now a standard expression for the subgap Andreev state energy in a one-dimensional Josephson junction [200] we find:

$$\varepsilon = \pm\Delta_0\sqrt{1 - \mathcal{T}\sin^2(\phi/2)} \simeq \pm\Delta_0\sqrt{1 - \mathcal{T} + \mathcal{T}\,\theta_p^2}\,. \tag{1.7}$$

This energy splitting gives us the estimate for the coupling coefficient in the above two-level problem (1.6): $V_{gap}(\theta_p) \sim \Delta_0\theta_p$ for planar defect with a high transparency $\mathcal{T} \to 1$.

As a result, one obtains a set of quasiclassical orbits in $(\mu - \theta_p)$ space

$$\mu(\theta_p) = \pm\frac{1}{\hbar\omega_0}\sqrt{\varepsilon^2 - \Delta_0^2\theta_p^2}\,. \tag{1.8}$$

These orbits (1.8) corresponding to the precession of the quasiparticle trajectory are schematically shown in Fig. 1.3. For low energy levels one can clearly observe the formation of closed orbits near the points $\theta_p = 0, \pm\pi$, which are separated by the prohibited angular domains centered at $\theta_p = \pm\pi/2$. The closed orbits are nothing more but skipping (or gliding) quasiparticle states formed due to the scattering at the defect plane. The discrete subgap energy levels of quasiparticles can be obtained from the semiclassical Bohr-Sommerfeld quantization rule for canonically conjugate variables μ and θ_p [201, 202]:

$$\Sigma(\varepsilon) = \int_0^{2\pi} \mu(\varepsilon, \theta_p)d\theta_p = 2\pi(n + \beta)\,, \tag{1.9}$$

where n is integer, 2π is the period of $\mu(\theta_p)$, and β is of the order unity. Applying the Bohr-Sommerfeld rule (1.9) to the closed paths in $(\mu - \theta_p)$ space, we obtain the spectrum in the form

$$\varepsilon_n^2 = \frac{\Delta_0^3}{E_F}(n + \beta)\,, \tag{1.10}$$

which is dramatically different from the CdGM spectrum $\varepsilon_n = \hbar\omega_0(n + 1/2)$ and reminds the square-root quantization of the quasiparticle spectra in different types of nodal problems (like graphene [203, 204] or d-wave superconductors in magnetic fields [205]). Note, that this draft

estimate of the energy of low subgap spectrum levels appears to be in good agreement with the explicit expression for the energy levels (1.34) on the basis of the full quantitative description in Sec. 1.1.1. The novel minigap $\varepsilon_0 \simeq \Delta_0\sqrt{\Delta_0/E_F}$ determined by Eq. 1.10 well exceeds the CdGM interlevel spacing $\hbar\omega_0$. This minigap increase obviously manifests the partial suppression of the spectral flow which should give the origin to all the dissipation phenomena inside the vortex core during its motion. In this sense this spectrum change can be viewed as a precursor to the crossover to the Josephson vortex where all the subgap quasiparticle levels are repelled from the Fermi energy to the gap value Δ_0. On the other hand, the limit of the moderate barrier strength studied here provides a possibility to observe a novel type of the vortex core with the peculiar quantization rule arising from the splitting of the orbit segments in the $\mu - \theta_p$ plane. This splitting destroys the trajectory precession in the whole angular interval $0 < \theta_p < 2\pi$ changing, thus, the topology of the quasiclassical orbits. The precession region $|\theta_p| \leq \delta\theta_p$ expands with an increase of the energy level n. As a result, for rather high levels the prohibited angular domains shrink, the precession over the full region $0 \leq \theta_p \leq 2\pi$ restores, and we get the crossover to a CdGM type of spectrum $\varepsilon_n \sim n$.

1.1.1 Quasiclassical approximation of BdG equations

Hereafter we consider a planar defect in the plane $y = 0$ as a $\delta-$function repulsive potential for quasiparticles, i.e. $V(y) = H\delta(y)$. The magnetic field $\mathbf{B} = B\mathbf{z}_0$ is assumed to create a single quantum vortex line parallel to the $z-$axis trapped inside the attractive potential well within the defect [206]. The vortex center defined as a point of the order parameter phase singularity is positioned at the point $x = y = 0$.

We assume the system to be homogeneous along the $z-$axis, thus, the $\hbar k_z-$projection of the momentum is conserved. The quantum mechanics of quasiparticle excitations in a superconductor is governed by the two dimensional BdG equations for particlelike (u) and holelike (v) parts of the two-component quasiparticle wave functions $\hat{\Psi}(x,\, y)\exp(ik_z z) = (u(\mathbf{r}),\, v(\mathbf{r}))^T\, \exp(ik_z z)$:

$$-\frac{\hbar^2}{2m}\left(\nabla^2 + k_\perp^2\right) u + \Delta(\mathbf{r})v = \epsilon u \tag{1.11a}$$

$$\frac{\hbar^2}{2m}\left(\nabla^2 + k_\perp^2\right)\, v + \Delta^*(\mathbf{r})\, u = \epsilon\, v\,. \tag{1.11b}$$

Here $\nabla = \partial_x\mathbf{x}_0 + \partial_y\mathbf{y}_0$, $\mathbf{r} = (x,\, y)$ is a radius vector in the plane perpendicular to the magnetic-field direction, $\Delta(\mathbf{r})$ is the gap function and $k_\perp^2 = k_F^2 - k_z^2$.

The potential barrier is assumed to be partially transparent for electrons, and the appropriate boundary conditions for wave function $\hat{\Psi}(x,\, y) = (u(\mathbf{r}),\, v(\mathbf{r}))^T$ at $y = 0$ read [207]:

$$\hat{\Psi}(x, 0+) = \hat{\Psi}(x, 0-) = \hat{\Psi}_0\,, \tag{1.12a}$$

$$\partial_y\hat{\Psi}(x, 0+) - \partial_y\hat{\Psi}(x, 0-) = 2k_\perp Z\hat{\Psi}_0\,, \tag{1.12b}$$

where the dimensionless barrier strength $Z = H/\hbar V_\perp$ ($mV_\perp = \hbar k_\perp$) defines the transmission $\mathcal{T} = 1/(1+Z^2)$ and reflection $Z^2/(1+Z^2)$ coefficients in the normal state. For extremely weak barrier ($\mathcal{T} \gtrsim \mathcal{T}_\xi$) we can neglect the anisotropy of the order parameter $\Delta(\mathbf{r})$ within the vortex core and assume that

$$\Delta(\mathbf{r}) = \Delta_0\,\delta_v(r)\,\mathrm{e}^{i\theta}\,, \quad r = \sqrt{x^2+y^2}\,, \tag{1.13}$$

where $(r,\, \theta)$ is a polar coordinate system. Here $\delta_v(r)$ is a normalized order parameter magnitude for a vortex centered at $r = 0$, such that $\delta_v(r) = 1$ for $r \to \infty$.

Following the procedure described in [43, 194, 199] (see Appendix 1.1.4 for details) we introduce the momentum representation:

$$\hat{\Psi}(\mathbf{r}) = \frac{1}{(2\pi\hbar)^2}\int_{-\infty}^{+\infty} d^2\mathbf{p}\, \mathrm{e}^{i\mathbf{p}\mathbf{r}/\hbar}\,\hat{\psi}(\mathbf{p}) \tag{1.14}$$

where $\mathbf{p} = |\mathbf{p}|\,(\cos\theta_p\,, \sin\theta_p) = p\,\mathbf{p}_0$. The unit vector $\mathbf{p}_0$ parametrized by the angle θ_p defines the trajectory direction in the $(x,\, y)$ plane. We assume that our solutions correspond to the momentum absolute values p close to the value $\hbar k_\perp$: $p = \hbar k_\perp + q$ ($|q| \ll \hbar k_\perp$). Within the quasiclassical approach the wave function in the momentum representation assumes the form

$$\hat{\psi}(\mathbf{p}) = \frac{1}{k_\perp}\int_{-\infty}^{+\infty} ds\, \mathrm{e}^{i(k_\perp - |\mathbf{p}|/\hbar)\,s}\hat{\psi}(s,\theta_p)\,, \tag{1.15}$$

where s is a coordinate along a quasiclassical trajectory, which is a straight line along the direction of the quasiparticle momentum. Finally, the wave function $\hat{\Psi}(\mathbf{r})$ in the real space $\mathbf{r} = r(\cos\theta, \sin\theta)$ is expressed in the following way via the slowly varying functions $\hat{\psi}(s,\theta_p)$ defined at the trajectory:

$$\hat{\Psi}(r,\,\theta) = \int_0^{2\pi} \mathrm{e}^{ik_\perp r cos(\theta_p-\theta)}\hat{\psi}(r\cos(\theta_p-\theta),\theta_p)\frac{d\theta_p}{2\pi}\,. \tag{1.16}$$

The solution (1.16) cannot be characterized by a definite angular momentum μ because the partial transparency of the barrier makes it possible to couple four quasiclassical rays at the plane defect. As a result, the angular harmonics $f_{\pm\mu i}$ and $f_{\pm\mu t}$ (see Fig. 1.2) with opposite momentum μ and $-\mu$ become interacting, contrary to the case considered in [37]. To account for this four–wave coupling, we follow Ref. [208] introduce the angular momentum expansion for the solution (1.16)

$$\hat{\psi}(s,\,\theta_p) = \sum_\mu \mathrm{e}^{i\mu\theta_p + i\,\hat{\sigma}_z\theta_p/\,2}\hat{f}_\mu(s)\,, \tag{1.17}$$

where the discreteness of the angular momentum $\mu = n + 1/2$ (n is an integer) arises from the obvious condition that the wave function (1.17) is single-valued. The function $\hat{f}_\mu(s)$ satisfies the Andreev equation along the quasiclassical trajectory with the impact parameter $b = -\mu/k_\perp$

$$-i\hbar V_\perp\hat{\sigma}_z\,\partial_s\hat{f}_\mu + \hat{\Delta}_b(s)\hat{f}_\mu = \varepsilon\hat{f}_\mu\,, \tag{1.18}$$

where

$$\hat{\Delta}_b(s) = \hat{\sigma}_x\,\mathrm{Re}D_b(s) - \hat{\sigma}_y\,\mathrm{Im}D_b(s) \tag{1.19}$$

is the gap operator, $\hat{\sigma}_i$ are the Pauli matrices and the expression for the order parameter $\Delta = D_b(s)\,\mathrm{e}^{i\theta_p}$ around the vortex in $(s,\,\theta_p)$ variables

$$D_b(s) = \Delta_0\,\frac{\delta_v(\sqrt{s^2+b^2})}{\sqrt{s^2+b^2}}(s+ib)\,. \tag{1.20}$$

can be obtained from (1.13) taking into account the evident relations:

$$x = s\cos\theta_p - b\sin\theta_p\,,\quad y = s\sin\theta_p + b\cos\theta_p\,,$$
$$x \pm iy = (s \pm ib)\,\mathrm{e}^{\pm i\theta_p}\,.$$

Note, that the impact parameter b and the trajectory orientation angle θ_p are two independent

quantities which parametrize the linear quasiclassical trajectory in the $(x,\, y)$ plane.

General solution

To find the solution of Eqs. (1.18)–(1.20) we can use the results of Ref. [194]. For low energies ($\mu \ll k_\perp \xi$) we take the function $\hat{f}_\mu$ as a sum

$$\hat{f}_\mu = \begin{pmatrix} u_\mu \\ v_\mu \end{pmatrix} = c_{\mu 1}\hat{G}_{\mu 1} + c_{\mu 2}\hat{G}_{\mu 2} \tag{1.21}$$

of the two linearly independent solutions

$$\hat{G}_{\mu 1} = \mathrm{e}^{i\,\hat{\sigma}_z \pi/\,4}\left(\mathrm{e}^{-|K_\mu(s)|} - i\,\mathrm{sgn}(s)\frac{\gamma_\mu}{2}\hat{\sigma}_z \mathrm{e}^{|K_\mu(s)|}\right)\hat{\lambda}\,, \tag{1.22a}$$

$$\hat{G}_{\mu 2} = \mathrm{e}^{i\,\hat{\sigma}_z \pi/\,4}\mathrm{e}^{-|K_\mu(s)|}\,\hat{\sigma}_z\,\hat{\lambda}\,, \tag{1.22b}$$

where $\hat{\lambda} = (1,1)^T$,

$$K_\mu(s) = \frac{k_F}{k_\perp \xi}\int_0^s dt\,\frac{t\,\delta_v\left(\sqrt{t^2+b^2}\right)}{\sqrt{t^2+b^2}}\,, \tag{1.23}$$

$$\Lambda_\mu = \frac{2\,k_F}{k_\perp \xi}\int_0^\infty ds\,\mathrm{e}^{-2K_\mu(s)}\,, \tag{1.24}$$

$$\gamma_\mu = \frac{\Lambda_\mu}{\Delta_0}\,(\,\varepsilon_\mu - \varepsilon\,) \tag{1.25}$$

and

$$\varepsilon_\mu = -\frac{2\Delta_0\,k_F\mu}{k_\perp^2\,\xi\,\Lambda_\mu}\int_0^\infty ds\,\frac{\delta_v\left(\sqrt{s^2+b^2}\right)}{\sqrt{s^2+b^2}}\,\mathrm{e}^{-2K_\mu(s)} \tag{1.26}$$

is the CdGM excitation spectrum. Here $\xi = \hbar V_F/\Delta_0$ is the coherence length (V_F is the Fermi velocity).

Boundary condition

As a next step we rewrite the boundary condition (1.12) for wave functions $\hat{f}_{\pm\mu}(s)$ defined at the trajectories s_1 and s_2 (see Fig. 1.2). Due to normal reflection of quasiparticles at the defect the trajectories s_1 and s_2 with opposite momentum ($+\mu$ and $-\mu$) directions are coupled. Substituting the expressions (1.16,1.17) into the boundary condition (1.12), we obtain the following relation between the amplitudes of incident $\hat{f}_{\pm\mu i}(s)$ and transmitted $\hat{f}_{\pm\mu t}(s)$ two-component quasiparticle wave functions at the point $s_0 = -b/\tan\theta_p$ where the trajectories cross the barrier:

$$(\eta + i)\,\hat{f}_{\pm\mu t} = \eta\,\hat{f}_{\pm\mu i} - i\mathrm{e}^{\mp i\,\hat{\sigma}_z\theta_p}\hat{f}_{\mp\mu i}\,, \tag{1.27}$$

where $\eta = \sin\theta_p/Z$. Our further analysis of quasiparticle excitations is based on the solutions (1.21,1.22) which must be supplemented by the boundary conditions (1.27).

1.1.2 Quasiparticle spectrum of the vortex

We now proceed with the analysis of the subgap spectrum for a singly quantized vortex trapped by the planar defect. Hereafter in this section we assume the angular momentum to be positive,

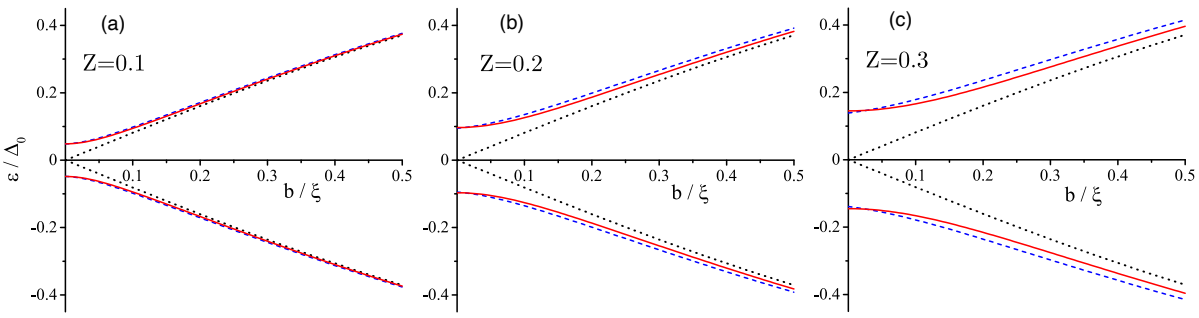

Figure 1.4: Quasiparticle spectra $\varepsilon(b,\,\theta_p)$ calculated using Eq. (1.31) for different values of the dimensionless barrier strength Z and the trajectory direction θ_p in the $(x,\,y)$ plane ($k_z = 0$): (a) $Z = 0.1$; (b) $Z = 0.2$; (c) $Z = 0.3$. Dotted lines for $\theta_p = 0$ correspond to the CdGM branch of the spectrum. The dash blue lines show the dependence for $\theta_p = \pi/4$; solid red lines show the dependence for $\theta_p = \pi/2$.

i.e. $\mu > 0$. The form of the two-component quasiparticle wave functions $\hat{f}_{\pm\mu}(s)$ depends on a position of the point s_0 at the trajectory. If the coordinate $s_0 \geq 0$ than the general solution (1.21,1.22) takes the following form

$$\hat{f}_{\pm\mu}(s) = \begin{cases} c_{\pm\mu i}\, \mathrm{e}^{i(\hat{\sigma_z}\mp 1)\pi/4} \mathrm{e}^{-|K_\mu(s)|}\, \hat{\lambda}\,, & s \leq 0\,, \\ c_{\pm\mu i}\, \mathrm{e}^{i(\hat{\sigma_z}\mp 1)\pi/4} \left(\mathrm{e}^{-|K_\mu(s)|} - i\gamma_{\pm\mu}\hat{\sigma_z}\mathrm{e}^{|K_\mu(s)|}\right) \hat{\lambda}\,, & 0 \leq s \leq s_0\,, \\ c_{\pm\mu t}\, \mathrm{e}^{i(\hat{\sigma_z}\mp 1)\pi/4} \mathrm{e}^{-|K_\mu(s)|}\, \hat{\lambda}\,, & s \geq s_0\,, \end{cases} \quad , \tag{1.28}$$

where

$$\gamma_{+\mu} = -\frac{\Lambda_\mu}{\Delta_0}\left(|\varepsilon_\mu| + \varepsilon\right)\,, \quad \gamma_{-\mu} = \frac{\Lambda_\mu}{\Delta_0}\left(|\varepsilon_\mu| - \varepsilon\right)\,.$$

Otherwise, if $s_0 \leq 0$

$$\hat{f}_{\pm\mu}(s) = \begin{cases} c_{\pm\mu i}\, \mathrm{e}^{i(\hat{\sigma_z}\mp 1)\pi/4} \mathrm{e}^{-|K_\mu(s)|}\, \hat{\lambda}\,, & s \leq s_0\,, \\ c_{\pm\mu t}\, \mathrm{e}^{i(\hat{\sigma_z}\mp 1)\pi/4} \left(\mathrm{e}^{-|K_\mu(s)|} + i\gamma_{\pm\mu}\hat{\sigma_z}\mathrm{e}^{|K_\mu(s)|}\right) \hat{\lambda}\,, & s_0 \leq s \leq 0\,, \\ c_{\pm\mu t}\, \mathrm{e}^{i(\hat{\sigma_z}\mp 1)\pi/4} \mathrm{e}^{-|K_\mu(s)|}\, \hat{\lambda}\,, & s \geq 0\,. \end{cases} \tag{1.29}$$

The unknown coefficients $c_{\pm\mu i}$, $c_{\pm\mu t}$ in (1.28) and (1.29) are determined by the boundary conditions (1.27). The eigenfunctions $\hat{f}_{\pm\mu}(s)$ have to be normalized such that

$$\int_{-\infty}^{\infty} ds \left(|\hat{f}_{+\mu}(s)|^2 + |\hat{f}_{-\mu}(s)|^2\right) = k_\perp\,.$$

Substituting the above expressions (1.28) or (1.29) into the boundary conditions (1.27), we obtain the following system of algebraic equations with respect to the amplitude $c_{\pm\mu i}$ of the incident waves

$$\eta\,\gamma_{+\mu}\,c_{+\mu i} + \left(\gamma_{\mp\mu}\,\cos\theta_p + \mathrm{e}^{-2K_0}\,\sin\theta_p\right)\,c_{-\mu i} = 0\,, \tag{1.30a}$$

$$\eta\,\gamma_{-\mu}\,c_{-\mu i} - \left(\gamma_{\pm\mu}\,\cos\theta_p - \mathrm{e}^{-2K_0}\,\sin\theta_p\right)\,c_{+\mu i} = 0\,. \tag{1.30b}$$

The case $s_0 \geq 0$ ($s_0 < 0$) corresponds to the choice of upper (lower) sign in Eqs. (1.30), $K_0 = K_\mu(s_0)$ and the angle θ_p defines the direction of the ray with the angular momentum $+\mu$. To find the subgap quasiparticle excitation spectrum we should find the determinant of the

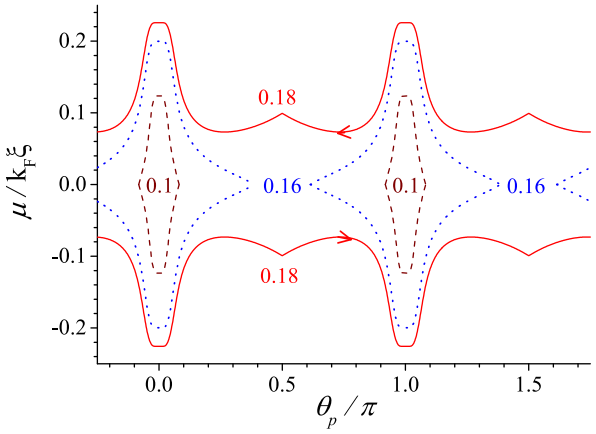

Figure 1.5: Quasiparticle orbits in the $\mu - \theta_p$ plane corresponding to different energy levels for the dimensionless barrier strength $Z = 0.3$. The numbers near the curves denote the corresponding values of ε/Δ_0. The direction of trajectory precession along the orbits is shown by arrow. We put here $k_z = 0$.

algebraic system, and its zero give us the equation for the energy spectrum ε:

$$\varepsilon^2(b\,,\theta_p) = \varepsilon_\mu^2 + \left(\frac{\Delta_0}{\Lambda_\mu}\right)^2 \frac{\mathrm{e}^{-2K_0}}{\eta^2 + \cos^2\theta_p}\left[\Lambda_\mu \frac{|\varepsilon_\mu|}{\Delta_0}|\sin(2\theta_p)| + \mathrm{e}^{-2K_0}\,\sin^2\theta_p\right].$$

Figure 1.4 shows the anomalous spectral branches as functions of the impact parameter $b = -\mu/k_F$ for different values of the dimensionless barrier strength Z and the trajectory directions in the (x, y) plane determined by the angle θ_p. The qualitative behavior of the spectrum is weakly sensitive to the concrete profile of the gap amplitude inside the core and we choose a simple model dependence

$$\delta_v(r) = r/\sqrt{r^2 + \xi^2} \tag{1.31}$$

neglecting, thus, the influence of the defect on the behavior of the gap profile. Contrary to the CdGM case the spectrum branch (1.31) does not cross the Fermi level in presence of the defect. For rather small Z the minigap in the quasiparticle spectrum

$$\Delta_m(\theta_p) = \varepsilon(0, \theta_p) = \frac{\Delta_0}{\Lambda_0}\frac{Z}{\sqrt{1 + Z^2/\tan^2\theta_p}}$$

appears to be almost independent of θ_p in a wide range of angles except the small angular intervals close to $\theta_p = 0$ and $\theta_p = \pi$. It is natural to expect that in the patterns of the local density of states (LDOS) this angular independent quantity should reveal itself as a soft gap $\Delta_{Soft} \sim Z\Delta_0$ growing with the increasing barrier strength Z (see the Section 1.1.3). We emphasize here the fact that this gap is soft since the spectrum (1.31) for small $|\tan\theta_p| \lesssim Z$ is gapless and, thus, these angular intervals can contribute to the LDOS at the Fermi level. This nonzero contribution exists, of course, only in the quasiclassical limit when we completely neglect the quantum mechanical nature of the trajectory precession which should be responsible for the opening of the hard minigap for the energies below Δ_{Soft}.

To derive the corresponding quantization rules in the limit $Z \ll 1$ we consider isoenergetic lines $\mu(\theta_p) = -k_\perp b(\theta_p)$ in $(\mu - \theta_b)$ plane. The resulting classical orbits are shown in Fig. 1.5. Generally, one can distinguish two types of the isoenergetic lines behavior. If the quasiparticle

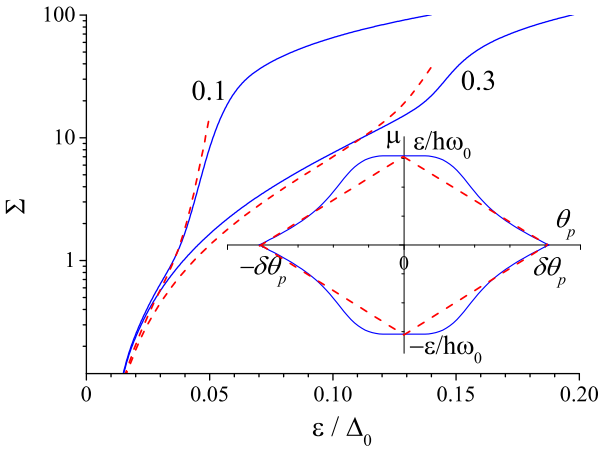

Figure 1.6: Dependence $\Sigma(\varepsilon)$ (1.9) for two values of the dimensionless barrier strength Z. Results of numerical calculations are shown by the blue solid lines. Dashed red curves show approximate values of $\Sigma(\varepsilon)$ obtained from Eq. (1.33). The insert shows quasiparticle orbit in the $(\mu - \theta_b)$ plane (blue solid line) and its approximation (red dashed line) described by the equation (1.33). We put here $k_z = 0$ and $E_F/\Delta_0 = 50$.

energy is of the order of the minigap ($\varepsilon \lesssim \Delta_{Soft}$) there appear prohibited angular domains centered at the points $\theta_p = \pm\pi/2$ due to the normal reflection of quasiparticles at the defect. In this case classical orbits form close paths in $(\mu - \theta_b)$ space corresponding to the precession of the trajectory in the region with the width $2\,\delta\theta_p(\varepsilon)$ near the points $\theta_p = 0, \pm\pi$. The width $2\,\delta\theta_p$ of the precession region grows with an increase in energy level. For small $|\mu| \ll k_\perp \xi$ the value $\delta\theta_p$ can be estimated as follows:

$$\delta\theta_p \simeq \frac{\varepsilon\,\Lambda_0/\Delta_0}{\sqrt{1-(\varepsilon\,\Lambda_0/Z\Delta_0)^2}}. \tag{1.32}$$

Shrinking of the prohibited angular domains and the crossover from the closed orbits to the open ones occur at the energy ε^* satisfying the condition $\delta\theta_p(\varepsilon^*) = \pi/2$.

The low lying energy levels of quasiparticles can be obtained by applying the Bohr-Sommerfeld quantization rule (1.9) for closed paths in the plane of canonically conjugate variables μ and θ_p. Figure 1.6 shows the typical dependence $\Sigma(\varepsilon)$ calculated using the spectrum (1.31). Taking $\varepsilon_\mu \simeq -\hbar\omega_0\mu$ for small μ values and replacing the real classical orbits in $(\mu - \theta_b)$ plane by the model one (see the insert Fig. 1.6), one can obtain a reasonable fit (dashed curve) to the numerical results (solid curve):

$$\Sigma(\varepsilon) \approx 2\frac{\varepsilon}{\hbar\omega_0}\delta\theta_p = \frac{2\varepsilon^2\Lambda_0/\Delta_0}{\hbar\omega_0\sqrt{1-(\varepsilon\,\Lambda_0/Z\Delta_0)^2}}. \tag{1.33}$$

The above relation together with the Bohr-Sommerfeld rule (1.9) results in the following explicit expression for discrete subgap energy levels

$$\varepsilon_n \simeq \frac{\Delta_0 Z}{\Lambda_0}\left[p_n\sqrt{1+p_n^2/4} - p_n^2/2\right]^{1/2}, \quad p_n = \frac{\pi\Lambda_0\Delta_0}{2E_F Z^2}\,(n+\beta)\,, \tag{1.34}$$

which appears to be justified for $\varepsilon_n/\Delta_0 \lesssim Z^2 \ll 1$. The expression (1.34) can be strongly simplified provided $p_n \ll 1$ for low lying energy levels:

$$\varepsilon_n^2 \simeq \frac{\pi}{2\Lambda_0}\frac{\Delta_0^3}{E_F}\,(n+\beta)\left[1 - \frac{\pi\Lambda_0\Delta_0}{4E_F Z^2}\,(n+\beta)\right].$$

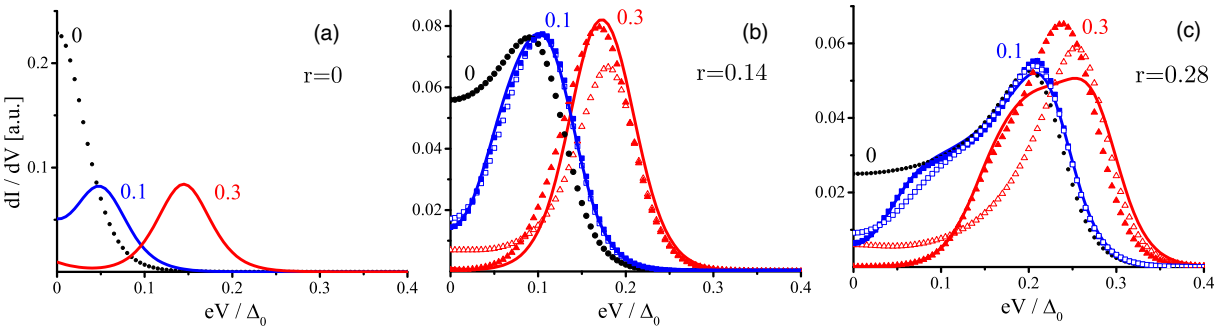

Figure 1.7: Local differential conductance dI/dV versus bias voltage (eV) in different points (r, θ) at the plane (x, y): (a) $r = 0$; (b) $r = 0.14\,\xi$; (c) $r = 0.28\,\xi$. The numbers near the curves denote the corresponding values of the dimensionless barrier strength Z. The lines correspond to the case $\theta = \pi/4$; empty symbols – $\theta = 0$; filled symbols – $\theta = \pi/2$. We put here $T/\Delta_0 = 0.02$. For reference black filled circles (•) show the local dI/dV curves for the free Abrikosov vortex ($Z = 0$).

The main term of the last relation appears to be in good agreement with the estimate (1.10) and describes qualitatively the new behavior of spectrum of subgap quasiparticle states ($\varepsilon_n \sim n^{1/2}$) due to the normal scattering at the planar defect. Both the hard minigap $\varepsilon_0 \lesssim \Delta_0\sqrt{\Delta_0/E_F} \ll \Delta_{Soft}$ in the discrete spectrum (1.34) and the interlevel spacing $\hbar\omega = \varepsilon_n - \varepsilon_{n-1}$ grow with the increase in the barrier strength Z.

Besides its fundamental interest, the problem of pinned vortex spectrum important for understanding the nature of dissipation in the presence of planar defects. In particular, according to the spectral flow theory [11], it is the behavior of the anomalous branch which determines the high-frequency conductivity and Kerr effect [38, 191]. One can expect that the opening of the hard minigap ε_0 in discrete quasiparticle spectrum (1.34) and change in the slope $\varepsilon(\mu)$ dependence (1.31) can cause the suppression of the dissipation accompanying the vortex motion and the resulting changes in the relation between the Ohmic and Hall conductivities. As a result, the quasiparticle subgap spectrum can be tested by the measurements of the conductivity tensor at finite frequencies.

1.1.3 Local density of states of the vortex

We now proceed with the calculations of the local density of states for a singly quantized vortex pinned at the planar defect. This quantity is known to be directly probed in the scanning tunneling microscopy/spectroscopy experiments [181]. For the sake of simplicity we assume here the Fermi surface to be a cylinder and neglect the dependence of the quasiparticle energy on the momentum component k_z along the cylinder axis z considering a motion of quasiparticles only in (x, y) plane. The peculiarities of the LDOS are usually determined from the analysis of the local differential conductance (LDC):

$$\frac{dI/dV}{(dI/dV)_N} = \int_{-\infty}^{\infty} d\varepsilon\, \frac{N(\mathbf{r},\,\varepsilon)}{N_0}\, \frac{\partial f(\varepsilon - eV)}{\partial V}\,, \tag{1.35}$$

where V is the applied voltage, $(dI/dV)_N$ is a conductance of the normal metal junction, and $f(\varepsilon) = 1/\left(1 + \exp(\varepsilon/T)\right)$ is a Fermi function. Within the quasiclassical approach the LDOS

$$N(\mathbf{r},\,\varepsilon) = k_F \int db\, |u_b(\mathbf{r})|^2\, \delta(\varepsilon - \varepsilon(b)) \tag{1.36}$$

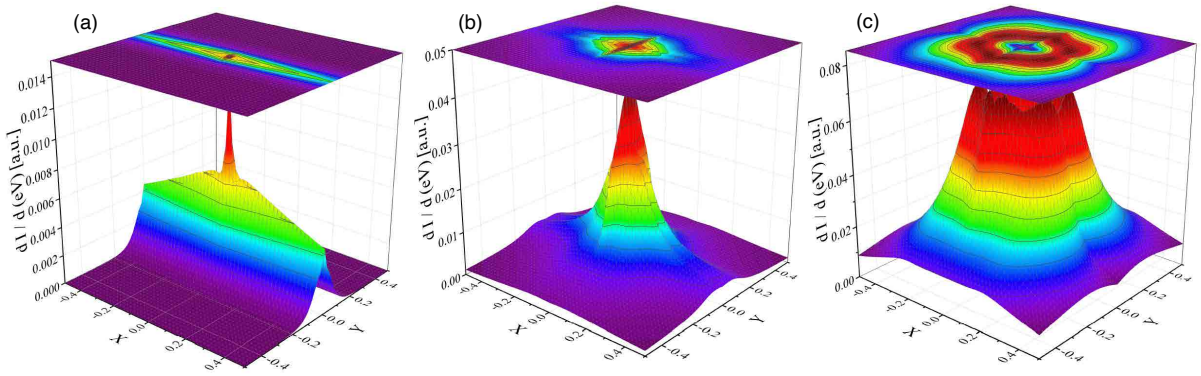

Figure 1.8: Evolution of the local differential conductance $dI/dV(eV,\, x,\, y)$ corresponding to different bias voltages $eV/\Delta_0 = 0$(a); 0.1(b); 0.2(c), for the dimensionless barrier strength $Z = 0.3$. We put here $T/\Delta_0 = 0.02$.

can be expressed through the electron component $u(r,\, \theta)$ of quasiparticle eigenfunctions (1.14) corresponding to the energy $\varepsilon(b,\, \theta_p)$ determined by Eqs. (1.31),(1.23),(1.24),(1.25),(1.26). The wave function $\hat{\psi}(r, \theta)$ parametrized by the impact parameter $b = -\mu/k_F$

$$\hat{\psi}(r,\theta) = \begin{pmatrix} u(r,\theta) \\ v(r,\theta) \end{pmatrix} = \mathrm{e}^{i(2\mu+\hat{\sigma}_z)\theta/2} \int_0^{2\pi} \frac{d\alpha}{2\pi}\, \mathrm{e}^{ik_F r\cos\alpha + i(2\mu+\hat{\sigma}_z)\alpha/2}\, \hat{f}_\mu(r\cos\alpha)$$

in the limit $k_F\, r \gg 1$ can be evaluated using the stationary phase method. For an impact parameter $|b| \le r$ the stationary phase points are given by the condition: $\sin\alpha_{1,2} = -b/r$. Summing over two contributions in the vicinity of the stationary angles $\alpha_1 = \theta_{p1} - \theta = \alpha_r$ and $\alpha_2 = \theta_{p2} - \theta = \pi - \alpha_r$, we can write the electron component $u(r, \theta)$ of quasiparticle eigenfunctions as follows:

$$u(r,\, \theta) = \left(\frac{1}{2\pi k_F s_r}\right)^{1/2} \mathrm{e}^{i(2\mu+1)\theta/2} \left[f_\mu^u(s_r)\, \mathrm{e}^{i\varphi_r} + f_\mu^u(-s_r)\, \mathrm{e}^{-i\varphi_r + i(2\mu+1)\pi/2} \right],$$

where $s_r = r|\cos\alpha_r| = \sqrt{r^2 - b^2}$. The phase

$$\varphi_r = k_F r\cos\alpha_r + |\mu|\alpha_r + \mathrm{sgn}(\mu)\, \alpha_r/2 - \pi/4$$

is determined by the trajectory orientation angle $\alpha_r = -\arcsin(b/r)$. Neglecting the oscillations at the atomic length scale we obtain the following slowly varying envelope function:

$$|u(r,\, \theta)|^2 \simeq \frac{1}{2\pi k_F s_r} \left[|f_\mu^u(s_r)|^2 + |f_\mu^u(-s_r)|^2 \right], \tag{1.37}$$

where the function $f_\mu^u(\pm s_r)$ is determined by the relations (1.28) or (1.29).

We have calculated the differential conductance using Eqs. (1.35),(1.36),(1.37) for low temperature $T/\Delta_0 = 0.02$ for different values of the dimensionless barrier strength Z. The typical examples of dependence of the local differential conductance dI/dV vs the bias voltage eV at various distances r from the vortex axis are shown in Fig. 1.7. In order to compare our results with the standard CdGM ones, we present the dependence of the local dI/dV vs voltage at different distances r from the Abrikosov vortex axis in the absence of the barrier ($Z = 0$). One can clearly observe the disappearance of the zero bias peak in the core ($r = 0$) and opening of the soft spectral minigap Δ_{Soft} caused by the normal scattering at the defect (Fig. 1.7(a)). The barrier results in the anisotropy of the LDC structure in the plane $(x,\, y)$ (Fig. 1.7(b, c)).

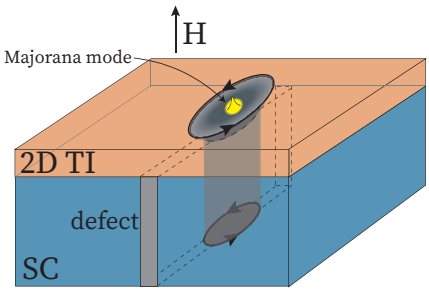

Figure 1.9: Possible setup of the Majorana-type system based on the vortex pinned by a planar defect. A robust Majorana fermion can be localized inside the vortex core created on the surface of the topological insulator (TI) by the proximity effect to the primary s-wave superconductor (SC).

The anisotropy of the LDC grows when barrier strength Z increases. Figure 1.8 illustrates the evolution of the local differential conductance $dI/dV(eV, x, y)$ distribution in the plane (x, y) for several values of the bias voltage V and dimensionless barrier strength Z. In Fig. 1.8(a, b) we can see the spread of the zero bias peak along the defect which appears to be another hallmark of the crossover from the Abrikosov to the Josephson vortex type. Due to the normal reflection of electrons and holes at the defect plane we get the azimuthal modulation of the LDC developing with the growth of the barrier strength Z.

Let us qualitatively discuss the transformation of the *shape of the vortex core* which is, of course, related to the changes in the low energy spectrum since the latter cause both the change in the supercurrent density and gap profile. At large barrier transparency $\mathcal{T} \gtrsim \mathcal{T}_\xi$ we see that the appearance of the nutating states strongly suppresses the DOS below the soft minigap $\Delta_{Soft} \sim Z\Delta_0$ which should result in the partial increase in the gap value inside the core. Without the self-consistent calculations we can only assume that further decrease in the barrier transparency fully suppresses the quasiparticle states nutating around the direction parallel to the barrier and only the high energy states close to the gap can survive (See Section 1.2). Such suppression of the low energy DOS obviously gives the disappearance of the normal vortex core which will be discussed in the next Section.

Finally, we note that recently the vortices pinned by the defects are studied as the hosts for the Majorana states in the systems consisting of a primary superconductor with conventional pairing and a low dimensional layer with a nontrivial topology[47–50]. The isolating inclusions in the vortex core in the primary superconductor allow to shift the low energy core spectrum from the Fermi level improving the topological protection of the Majorana states in the 2D topological superconductor. The vortex at the planar defect considered in our work can provide a perspective platform for such states since the hard minigap in the core can exhibit a strong increase even in the limit of the defect with high transparency when the shape of the gap inside the vortex core is only weakly perturbed by the scattering. Another advantage of this geometry [Fig. 1.9] is related to the possibility to move the vortices along the defects changing, thus, the positions of the Majorana states in the attached 2D layer without changing the minigap responsible for the desired topological protection.

1.1.4 Appendix: Andreev equations

The BdG equations for particle-(u) and holelike v parts of the two-component quasiparticle wave functions $(U,\, V)^T = (u(\mathbf{r}),\, v(\mathbf{r}))^T \exp(ik_z z)$ have the following form:

$$-\frac{\hbar^2}{2m}\left(\nabla^2 + k_\perp^2\right)\, u + \Delta(\mathbf{r})\, v = \epsilon\, u \tag{1.38a}$$

$$\frac{\hbar^2}{2m}\left(\nabla^2 + k_\perp^2\right)\, v + \Delta^*(\mathbf{r})\, u = \epsilon\, v\,. \tag{1.38b}$$

Here $\nabla = \partial_x \mathbf{x}_0 + \partial_y \mathbf{y}_0$, $\mathbf{r} = (x,\, y)$ is a radius vector in the plane perpendicular to the magnetic-field direction, $\Delta(\mathbf{r})$ is the gap function and $k_\perp^2 = k_F^2 - k_z^2$. We assume the system to be homogeneous along the z axis, thus, the $\hbar k_z$ projection of the momentum is conserved, and restrict our analysis with the case of the weak external magnetic field and the extreme type-II superconductors where the vector potential $\mathbf{A}$ can be neglected.

The two–component wave function $\hat{\Psi} = (u(\mathbf{r}),\, v(\mathbf{r}))^T$ in the momentum representation can be written as follows:

$$\hat{\Psi}(\mathbf{r}) = \frac{1}{(2\pi\hbar)^2}\int_{-\infty}^{+\infty} d^2\mathbf{p}\; \mathrm{e}^{i\mathbf{p}\mathbf{r}/\hbar}\,\hat{\psi}(\mathbf{p})\,, \tag{1.39}$$

where $\mathbf{p} = p\,(\cos\theta_p\,, \sin\theta_p) = p\,\mathbf{p}_0$ defines the polar coordinate system in momentum space. The unit vector $\mathbf{p}_0 = (\cos\theta_p\,, \sin\theta_p)$ is parametrized by the angle θ_p which determines the trajectory direction in the $(x,\, y)$ plane. The coordinate operator in the polar coordinate system $(p,\, \theta_p)$ can be written as follows:

$$\hat{\mathbf{r}} = i\hbar\frac{\partial}{\partial\mathbf{p}} = i\hbar\left(\mathbf{p}_0\frac{\partial}{\partial p} + \frac{i}{p}\,[\mathbf{z}_0,\, \mathbf{p}_0]\;\hat{\mu}\right)\,, \tag{1.40}$$

where operator of z projection of angular momentum $\hat{\mu}$ is given by the expression:

$$\hat{\mu} = \frac{1}{\hbar}\,[\mathbf{r},\, \mathbf{p}]\;\mathbf{z}_0 = -i\frac{\partial}{\partial\theta_p}\,. \tag{1.41}$$

Within the quasiclassical approach the characteristic length scale of envelopes of quasiparticle waves is determined by the superconducting coherence length ξ, and the quasiparticle wave function can be viewed as a wave packet with momenta absolute values close to $\hbar k_\perp$ since $k_F\xi \gg 1$ is assumed. Therefore, we look for solutions with absolute values $\mathbf{p}$ close to the value $\hbar k_\perp$: $p = \hbar k_\perp + q$ ($q \ll \hbar k_\perp$). In this case one can obtain the following expression for the coordinate operator:

$$\hat{\mathbf{r}} = i\hbar\mathbf{p}_0\frac{\partial}{\partial q} + \frac{i}{2k_\perp}\left\{[\mathbf{z}_0,\, \mathbf{p}_0]\,,\, \frac{\partial}{\partial\theta_p}\right\}\,, \tag{1.42}$$

where $\{\ldots\}$ is an anticommutator. Let us now introduce a Fourier transformation:

$$\hat{\psi}(\mathbf{p}) = \frac{1}{k_\perp}\int_{-\infty}^{+\infty} ds\,\mathrm{e}^{-i\,q\,s\,/\hbar}\hat{\psi}(s,\theta_p)\,, \tag{1.43}$$

where $s = r\,\cos(\theta_p - \theta)$ is a coordinate along a quasiclassical trajectory, which is a straight line along the direction of the quasiparticle momentum $\mathbf{p}$. The trajectory orientation angle is given by the θ_p value. The wave function $\hat{\Psi}(\mathbf{r})$ in polar coordinate system $(r,\, \theta)$ can be found from Eqs. (1.39) and (1.43):

$$\hat{\Psi}(r,\, \theta) = \int_0^{2\pi} \mathrm{e}^{ik_\perp r cos(\theta_p - \theta)}\hat{\psi}(r\cos(\theta_p - \theta), \theta_p)\frac{d\theta_p}{2\pi}\,, \tag{1.44}$$

where functions $\hat{\psi}(s,\theta_p)$ vary slowly at the trajectory θ_p. The expression for coordinate operator (1.42) in (s, θ_p) representation reads:

$$\hat{\mathbf{r}} = s\,\mathbf{p}_0 + \frac{i}{2k_\perp}\left\{[\mathbf{z}_0,\,\mathbf{p}_0]\,,\,\frac{\partial}{\partial\theta_p}\right\}\,. \tag{1.45}$$

Then, BdG Eqs.(1.38) in (s, θ_p) representation takes the form

$$\begin{aligned}\hat{H}\,\hat{\psi}(s,\theta_p) &= \epsilon\,\hat{\psi}(s,\theta_p)\,, \\ \hat{H} &= -i\hat{\sigma}_z\frac{\hbar^2 k_\perp}{m}\frac{\partial}{\partial s} + \begin{bmatrix} 0 & \Delta(\hat{\mathbf{r}}) \\ \Delta^*(\hat{\mathbf{r}}) & 0 \end{bmatrix}\,,\end{aligned} \tag{1.46}$$

where $\hat{\sigma}_x$, $\hat{\sigma}_y$ and $\hat{\sigma}_z$ are the Pauli matrices. Considering eikonal approximation for the angular dependence of wave function

$$\hat{\psi}(s,\theta_p) = \mathrm{e}^{iS_e(\theta_p)}\,\hat{f}(s,\theta_p)\,,$$

where

$$-\frac{1}{k_\perp}\frac{\partial S_e}{\partial\theta_p} = b(\theta_p)$$

is an impact parameter of a quasiclassical trajectory, and assuming a rather slow angular dependence of $\hat{f}(s,\theta_p)$ ($\hat{f}(s,\theta_p) \simeq \hat{f}_\mu(s)$), one can neglect a differential operator $\partial/\partial\theta_p$ in the Hamiltonian (1.46). The function $\hat{f}_\mu(s)$ satisfies the Andreev equations along the quasiclassical trajectory with a certain orientational angle θ_p an impact parameter $b = -\mu/k_\perp$

$$-i\hat{\sigma}_z\frac{\hbar^2 k_\perp}{m}\frac{\partial\hat{f}_\mu}{\partial s} + \hat{\sigma}_x\,\mathrm{Re}\Delta(x,y)\,\hat{f}_\mu - \hat{\sigma}_y\,\mathrm{Im}\Delta(x,y)\,\hat{f}_\mu = \epsilon\,\hat{f}_\mu\,,$$

where

$$x = s\cos\theta_p - b\sin\theta_p\,,\quad y = s\sin\theta_p + b\cos\theta_p\,.$$

Changing the sign of the coordinate s one can observe a useful symmetry property of the solution of Eq.(1.47):

$$\hat{f}_\mu(-s) = \pm\,\hat{\sigma}_y\hat{f}_\mu(s)\,.$$

1.2 Electronic structure of a Josephson vortex in a SIS junction

First, we give a small comment of the previous problem of the pinned vortex. The solution and discussion presented in Section 1.1 is not self-consistent in the sense that it does not take into account the deformation of the vortex core and the redistribution of the order parameter phase along the defect. The self-consistent numerical analysis of the quasiparticle spectrum and DOS for a vortex pinned by the plane defect has been carried out in Ref. [39] on the basis of the BdG theory for a two-dimensional tight-binding model on a square lattice. The effect of perturbation correction to the gap profile has been discussed in Ref. [41]. Such approximation is valid as long as the electronic transparency of the barrier $\mathcal{T}$ is close to unity. This limit allows one to observe the changes in the LDOS distribution in the vortex area corresponding to the transition from the pinned Abrikosov vortex to the intermediate Abrikosov-Josephson vortex regime [167, 209, 210]. However, a generic problem of the electronic structure of the disturbed vortex pinned by a defect with arbitrary transparency remained unsolved.

In the present Section we suggest a theoretical description of the electronic structure of a vortex pinned by a *low-transparent* defect [45]. The spatial distribution of the order parameter phase in this limit becomes strongly anisotropic, and the corresponding circulating supercurrent along the defect is characterized by the length ℓ_J strongly exceeding ξ and λ. This extreme anisotropy allows one to consider the quasiparticle motion along the junction in the adiabatic approximation.

1.2.1 WKB approximation of BdG equations

We restrict our consideration to the case of a SIS system (Fig. 1.10) in a rather thick superconducting film neglecting all the effects related to the peculiarities of thin film electrodynamics. The isolating barrier is positioned at $y = 0$ and modeled by the delta function potential $V(y) = \hbar^2 k_F m^{-1} Z_0 \delta(y)$, where Z_0 is the dimensionless barrier strength. The quantum mechanics of quasiparticles in such junction is described by the following BdG equations:

$$\begin{pmatrix} \hat{H}_0 - \mu & \Delta \\ \Delta^* & \mu - \hat{H}_0 \end{pmatrix} \hat{\Psi}(x,y) = E\hat{\Psi}(x,y), \tag{1.47}$$

where

$$\hat{H}_0 = -\frac{\hbar^2}{2m}\left(\frac{\partial^2}{\partial x^2} + \frac{\partial^2}{\partial y^2}\right) + V(y)$$

is the single-particle Hamiltonian, μ is the chemical potential which is equal to the Fermi energy, $\Delta(x,y)$ is the complex-valued gap function, $\hat{\Psi}(x,y) = (u(x,y), v(x,y))$ is the wave function with electron- u and hole- v like components. For simplicity we consider here the motion of quasiparticles only in the x-y plane assuming that the Fermi surface is a cylinder and therefore neglecting the dependence of the quasiparticle energy on the momentum component k_z along the cylinder axis z. The potential $V(y)$ can be taken into account by introducing specific boundary conditions:

$$\begin{gathered} \hat{\Psi}(x,+0) = \hat{\Psi}(x,-0) \\ \frac{\partial\hat{\Psi}}{\partial y}(x,+0) - \frac{\partial\hat{\Psi}}{\partial y}(x,-0) = 2k_F Z_0 \hat{\Psi}(x,+0) \end{gathered} \tag{1.48}$$

For rather low electron transmission through the barrier the system can be described taking a standard approximation for a Josephson junction, i.e., neglecting the spatial dependence of the absolute value of the order parameter Δ_0 and assuming a jumpwise behavior of the superconducting phase:

$$\Delta(x,y) = \Delta_0 \begin{cases} e^{i\theta_2(x)}, & y > 0 \\ e^{i\theta_1(x)}, & y < 0 \end{cases}$$

The phase difference $\varphi(x) = \theta_1(x) - \theta_2(x)$ is a continuous smooth function changing at a certain length scale ℓ_J. The length ℓ_J increases with the decrease of the barrier transparency from the values of the order of several superconducting coherence lengths to value of the so-called Josephson penetration depth $\lambda_J = \sqrt{c\Phi_0/16\pi^2 j_c \lambda}$, where j_c is the critical current density through the junction. The spatial distribution of the function $\varphi(x)$ in the Josephson junction can be obtained from the solution of a standard electrodynamic problem (see e.g. [167]) which is based on some particular form of the Josephson current-phase relation. The latter, in principle, should be found from the above consideration of the quasiparticle spectrum and wave functions. In our further consideration we do not consider the solution of this full self-consistent problem and just analyze the quasiparticle spectral properties for some typical profiles of the superconducting phase. Moreover, in our BdG equations we completely neglect the vector potential assuming, thus, that the supercurrents flowing in superconducting leads are too weak to affect the subgap energy spectrum under consideration.

The model introduced in the previous section contains several important length scales: (i) the Fermi wavelength k_F^{-1}; (ii) the typical length scale of the wave function decay for the subgap quasiparticles which is roughly the coherence length ξ; (iii) the characteristic length of the superconducting phase profile ℓ_J. The Fermi wavelength is certainly the smallest length scale among these values which allows us to use a standard quasiclassical approach, i.e., the so-called Andreev approximation. Moreover, for the junctions with not too large transparency we can introduce an additional simplification valid for the small value of the coherence length compared to the phase distribution length scale ℓ_J.

The appearance of the small parameter ξ/ℓ_J allows one to construct the solution of Eq. (1.47) using the semiclassical Wentzel-Kramers-Brillouin (WKB) approximation. Indeed, the slow change of the phase difference φ along the junction allows to define the semiclassical energy $E(x,k_x)$ assuming the momentum component k_x and coordinate x to be classical commuting variables. As a next step, we can restore the quantum mechanical commutation rule for these variables using a standard Bohr-Sommerfeld relation. This kind of semiclassical procedure allows to find the true quantum mechanical bound states.

We consider the structure of the wave function in the form $\hat{\Psi}(x,y) = f(x)\hat{g}(y,x)$. Similarly to the WKB approach, the function $f(x)$ can be written as the following asymptotic expansion:

$$f(x) = e^{i\kappa^{-1}S(x)}\big[f_0(x) + \kappa f_1(x) + O(\kappa^2)\big]. \tag{1.49}$$

Here $S(x)$ is the eikonal, the functions S, f_0 and f_1 are real and $\kappa = (k_F\ell_J)^{-1}$. After substituting this solution into the equation (1.47) and separating different orders in κ we get:

$$\kappa^0 : \left[-\hat{\tau}_3 \frac{\hbar^2}{2m}\Big(\frac{\partial^2}{\partial y^2} + k_F^2 - (S')^2\Big) + \begin{pmatrix} -E & \Delta(x) \\ \Delta^*(x) & -E \end{pmatrix} \right] \hat{g} f_0 = 0 \tag{1.50}$$

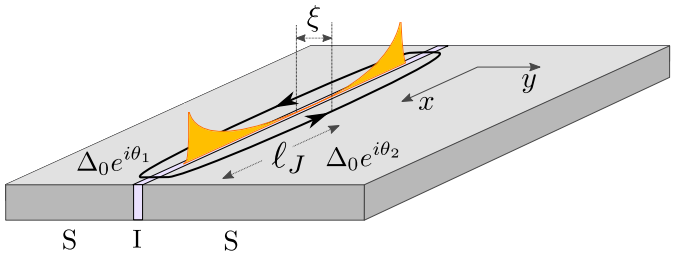

Figure 1.10: Sketch of a SIS structure with a Josephson vortex, created by a circulation of the order parameter phase (black solid line). Spatially separated peaks of the local density of subgap states are schematically shown in orange color.

$$\kappa^1: \quad -\frac{\hbar^2}{2m}\Big(iS''f_0+2iS'f_0'\Big)\hat{\tau}_3\hat{g}=\left[-\hat{\tau}_3\frac{\hbar^2}{2m}\Big(\frac{\partial^2}{\partial y^2}+k_F^2-(S')^2\Big)+\begin{pmatrix}-E & \Delta(x)\\ \Delta^*(x) & -E\end{pmatrix}\right]\hat{g}f_1, \tag{1.51}$$

where the prime means the derivative $\partial/\partial x$ and $\hat{\tau}_3$ is the Pauli matrix in the electron-hole Nambu space. The equation (1.50) contains a one-dimensional equation which together with the boundary conditions (1.48) can be viewed as the short SIS junction problem [211, 212] in which, due to the semiclassical approximation, the momentum k_x is replaced by S', and the coordinate x is a parameter. Introducing an auxiliary equation

$$-\hat{\tau}_3\frac{\hbar^2}{2m}\Big(\frac{\partial^2}{\partial y^2}+k_F^2-(S')^2\Big)\hat{g}+\begin{pmatrix}0 & \Delta(x)\\ \Delta^*(x) & 0\end{pmatrix}\hat{g}=\omega(x)\hat{g} \tag{1.52}$$

and using (1.48) we obtain a quasiparticle spectrum ω in the presence of a "frozen" phase distribution $\varphi(x)$. Eigenfunctions $\hat{g}(y,x)=(g_u,g_v)^T$ can be written as:

$$\hat{g}(y,x)=e^{i\text{sign}(y)\frac{\varphi(x)}{4}\hat{\tau}_3}\begin{cases}\Big(c_1e^{-iq_+y}+d_1e^{iq_-y}\hat{\tau}_1\Big)\hat{g}_0 & y<0\\ \Big(c_2e^{iq_+y}+d_2e^{-iq_-y}\hat{\tau}_1\Big)\hat{g}_0 & y>0\end{cases} \tag{1.53}$$

Here the vector $\hat{g}_0=(\tilde{u},\tilde{v})^T$ has the electron-like and hole-like parts:

$$\tilde{u}=\frac{1}{\sqrt{2}}\sqrt{1+i\frac{\sqrt{\Delta_0^2-\omega^2}}{\omega}},\quad \tilde{v}=\frac{1}{\sqrt{2}}\sqrt{1-i\frac{\sqrt{\Delta_0^2-\omega^2}}{\omega}}$$

and the wave vector is

$$q_\pm=\sqrt{k_F^2-(S')^2}\pm i\frac{m}{\hbar^2}\frac{\sqrt{\Delta_0^2-\omega^2}}{\sqrt{k_F^2-(S')^2}}.$$

Note, that in the latter expression we use the expansion in the parameter $(k_F\xi)^{-1}$, which is valid due to the quasiclassical condition $\Delta_0/E_F\sim(k_F\xi)^{-1}\ll 1$. The coefficients $c_{1,2}$ and $d_{1,2}$ are determined by the boundary conditions (1.48) and normalization condition:

$$\int\hat{g}^\dagger(y,x)\hat{g}(y,x)dy=k_F^{-1}.$$

1.2.2 Quasiparticle spectrum of the vortex

With the help of equations (1.53) and (1.48) we obtain the resulting spectrum of such a system, which is essentially the spectrum of the short SIS system [212]

$$\omega(x) = \pm\Delta_0\sqrt{1 - \mathcal{T}\sin^2\Big(\frac{\varphi(x)}{2}\Big)}, \tag{1.54}$$

where

$$\mathcal{T} = \left(1 + \frac{k_F^2 Z_0^2}{k_F^2 - (S'(x))^2}\right)^{-1}.$$

Substituting (1.52) into (1.50) and using the condition of existence of a nontrivial solution we easily get

$$E = \omega(x). \tag{1.55}$$

To obtain f_0 from the matrix equation (1.51) one has to use the Fredholm theorem [213] which gives us the solvability condition for the Eq. (1.51):

$$f_0\hat{g}^\dagger\Big(-\frac{\hbar^2}{2m}i\big[S''\hat{f}_0 + 2S'\hat{f}_0'\big]\hat{\tau}_3\hat{g}\Big) = 0,$$

which can be rewritten as

$$\big(\hat{g}^\dagger\hat{\tau}_3\hat{g}\big)\frac{\partial}{\partial x}\big(f_0^2 S'\big) = 0, \tag{1.56}$$

The term $\big(\hat{g}^\dagger\hat{\tau}_3\hat{g}\big)$ can be expressed as

$$\big(\hat{g}^\dagger\hat{\tau}_3\hat{g}\big) \sim \frac{1}{S'}\frac{\partial\omega}{\partial S'}$$

using equation (1.52) and it tends to zero only at the specific points $\varphi(x) = 2\pi k$ with an integer k. Therefore, we come to the equation $\big(f_0^2 S'\big)' = 0$ from which the function f_0 can be found. In the first-order WKB approximation, the function (1.49) has a standard form:

$$f(x) = \frac{C}{\sqrt{S'}}e^{\pm i\int S'(\xi)d\xi}, \tag{1.57}$$

where C is an arbitrary constant. The quantity S' is the gradient of the eikonal, therefore it can be interpreted as the x-component of the classical local quasiparticle momentum and here it is convenient to use the notation $S' \equiv k_x$. The expression for this momentum follows from (1.55):

$$\frac{k_x(x)}{k_F} = \sqrt{1 + Z_0^2\frac{\Delta_0^2 - E^2}{\Delta_0^2\cos^2(\varphi(x)/2) - E^2}}. \tag{1.58}$$

The above dependence of the momentum k_x on the coordinate x at a fixed energy E allows one to view the motion of quasiparticles in the presence of the superconducting phase profile as the motion in a smooth adiabatic potential. This potential has a set of turning points where $k_x(x) = 0$, therefore one can define closed semiclassical orbits in the plane (k_x, x). A set of exemplary semiclassical orbits for the particular case of a linearly growing phase difference

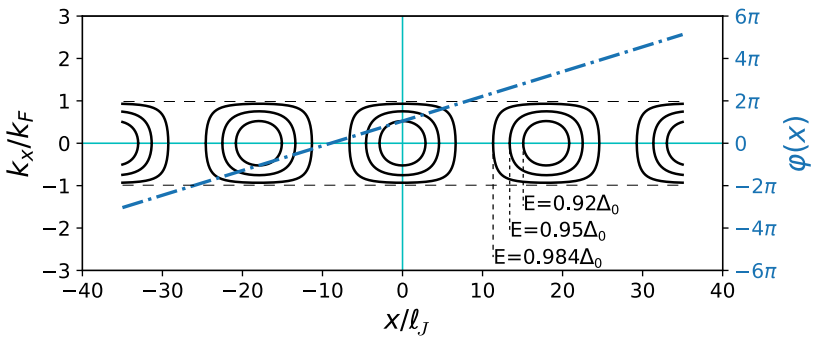

Figure 1.11: Semiclassical orbits (black lines) in the plane (k_x, x) described by the Eq. (1.58) for the linearly growing phase difference $\varphi(x)$ (blue dash-dotted line) for a fixed value of the parameter $Z_0 = 2$ and different energies E. Each set of concentric orbits corresponds to a single vortex in a vortex chain.

$\varphi(x) = 0.35(x/\ell_J) + \pi$ is shown in Fig. 1.11. Obviously, to restore the true quantum mechanics one can apply the Bohr-Sommerfeld quantization rule

$$\oint k_x(x)dx = 2\pi(n+\beta), \tag{1.59}$$

where n is an integer, and obtain the discrete spectrum levels. Certainly, the interlevel distance should be small due to the small parameter κ. Similarly to a standard quasiclassical version of the quantum mechanics the parameter β is of the order of the unity and its effect on the behavior of the discrete energy spectrum at large quantum numbers n is rather weak. In order to determine the appropriate value of β one needs to solve the quantum mechanical problem near the turning points beyond the quasiclassical approximation. This calculation is beyond the scope of our work.

Note, that the value of k_x does not exceed k_F in the classically allowed region, but the denominator of Eq. (1.58) tends to zero at some singular points. This is a direct consequence of using of the "frozen" phase approximation; however, since these points are in the forbidden region, the semiclassical approximation is not violated.

It should be noticed that the lower bound of the spectrum is determined by the general expression $E_b = \Delta_0 Z_0/\sqrt{1+Z_0^2}$ for a minimal energy value of localized states $\omega(x)$. For rather large values Z_0 this condition means that all the features related to the bound states in the Josephson junction can be observed only at energies rather close to Δ_0. The expression for the low-lying energy levels close to E_b can be obtained explicitly from the Eq. (1.59). Using a linearized expression for the phase difference $\varphi \approx ax + \pi$ with a slope a in the vicinity of the orbit center and assuming the condition $Z_0 \gtrsim 1$ in the Eq. (1.58) we find the discrete spectrum

$$E_n \approx E_b\sqrt{1+\frac{(n+\beta)a\pi\kappa}{Z_0\sqrt{1+Z_0^2}}}. \tag{1.60}$$

It is interesting to note that the square root dependence of the spectrum on the level number n has already been observed in the case of an Abrikosov vortex pinned at a high-transparent defect with $Z_0 \ll 1$ [40]. In such a system the deformation of the bound CdGM states in a vortex core results in the appearance of a "hard" minigap, which determines the value of the lowest energy level in the spectrum, besides this the electron scattering at the defect plane also provides a "soft" minigap which is $\Delta_{soft} \sim \Delta_0 Z_0$. Although direct comparison of (1.60) and the result for the high-transparency limit is not possible, it can be seen that quantitatively this "soft" minigap Δ_{soft} coincides with the lowest energy level $E_{n=0} \approx \Delta_0 Z_0$ (for $Z_0 \lesssim 1$) from (1.60), which is actually

a "hard" minigap in the present system where the vortex core is absent. The energy value $\Delta_0 Z_0$ always appears in the systems with a barrier of the finite transparency; therefore, one can expect this quantity to play an essential role throughout the entire crossover from the pinned Abrikosov to the Josephson vortex with an increase of the barrier strength Z_0.

Finally, we get the adiabatic solution of the BdG problem $\hat{\Psi}(x,y)$, which consists of two parts: $\hat{g}$ from (1.53) and f from (1.57). Following the standard procedure of constructing semiclassical solution in the potential well [214] we find the function $f(x)$ which has an oscillating behavior in the classically allowed region and decays exponentially in the classically forbidden region.

1.2.3 Local density of states of the vortex

As we discussed in the previous section, the distance between the true quantum mechanical levels appears to be extremely small due to the small value of the inverse quasiclassical parameter κ. For example, a low-lying part of the discrete spectrum (1.60) provides $E_{n+1} - E_n \approx a\pi\kappa\Delta_0/2(1+Z_0^2)$. Considering possible experimentally measurable hallmarks of the subgap quasiparticle states it may be much more important to analyze the local density of states in the semiclassical limit neglecting the level quantization. An appropriate expression for the local DOS reads:

$$\nu(x,y,E) = k_F \int_{-k_F}^{k_F} \frac{dk_x}{2\pi} |g_u(x,y)|^2 \delta\big(E - \omega(k_x)\big), \tag{1.61}$$

where the function $g_u(x,y)$ is defined in (1.53). Evaluating the integral we find:

$$\frac{\nu(x,y,E)}{\nu_{2D}} = \frac{|g_u|^2}{\tilde{k}_x} \frac{2E/\Delta_0\big(1-\tilde{k}_x^2\big)\big(1-\tilde{k}_x^2+Z_0^2\big)}{Z_0^2(1-E^2/\Delta_0^2)}, \tag{1.62}$$

where $\nu_{2D} = m/\pi\hbar^2$ is a local density of states of a two-dimensional electron gas and dimensionless momentum $\tilde{k}_x(x) = k_x/k_F$ is taken from (1.58). A singularity $\nu(k_x \to 0) \sim k_x^{-1}$ in the vicinity of each turning point $k_x = 0$ should be both regularized by a more accurate solution of a WKB problem and smeared by various broadening effects. Since the position of these peculiarities is defined by the turning points, their existence is restricted by the energy interval $E_b < E < \Delta_0$, as it was discussed above.

- **single Josephson vortex**

Now we proceed with consideration of several specific models for the phase distribution $\varphi(x)$. First, consider the limit $j_c \ll j_d\xi/\lambda$, which is realized for a low transparent insulating barrier with $Z_0 \gg \sqrt{12\pi^2\lambda/\xi}$ [40, 167]. In this case the electrodynamics of the Josephson system is local therefore the phase distribution obeys the sine-Gordon equation with the well-known soliton solution [215]:

$$\tilde{\varphi}(x) = 4\arctan e^{x/\ell_J}, \tag{1.63}$$

which corresponds to a single isolated Josephson vortex with the size of $\ell_J \sim \lambda_J \gg \lambda \gg \xi \gg k_F^{-1}$. Two last inequalities assume the limit of a strong type-II superconductor and the validity of the quasiclassical approximation described above. With the help of the relation $\sin^2(\tilde{\varphi}(z)/2) =$

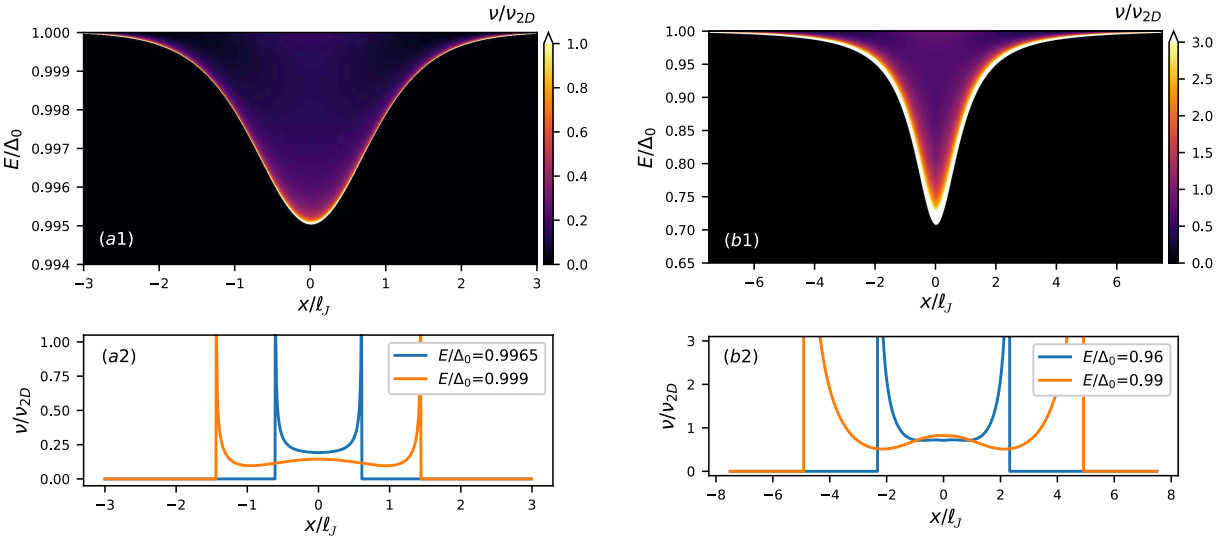

Figure 1.12: Distribution of the LDOS of the quasiparticles in the Josephson vortex $\nu(x, y = 0, E)$ as a function of the energy E and coordinate along the barrier x for local $(a1)$ (1.63) and nonlocal $(b1)$ (1.65) regimes. Subplots $(a2)$ and $(b2)$ show the cross section of the LDOS at a certain energy value for $Z_0 = 10$ (a) and $Z_0 = 1$ (b). The maximum values are truncated at $\nu/\nu_{2D} = (1, 3)$ for (a,b) for illustrative purposes.

$\cosh^{-2}(z)$ we obtain an explicit expression for the turning points:

$$\frac{x_{a,b}}{\ell_J} = \pm \ln \left(\frac{\Delta_0 - \sqrt{\Delta_0^2 - (\Delta_0^2 - E^2)(1 + Z_0^2)}}{\sqrt{(\Delta_0^2 - E^2)(1 + Z_0^2)}} \right). \tag{1.64}$$

Using the expression (1.58) for $k_x(x)$ and the wave function $\hat{g}$ we can plot the dependence of the LDOS (1.62) on the coordinate along the junction x directly at the junction line $y = 0$. A typical example of the spatial distribution of LDOS for different energy values is shown in Fig. 1.12(a). The local DOS along the junction clearly reveals two peaks (schematically shown in Fig. 1.10). The formation of these peaks, which are essentially signatures of the Josephson vortex, is a direct consequence of the semiclassical motion of trapped quasiparticles described above. At the same time, the exact form of the function $\varphi(x)$ does not qualitatively affect the formation of closed orbits in the plane (k_x, x). Therefore, the observation of the above spectral features is possible for various kinds of 2π-soliton, proposed for different parameters of the Josephson SIS junction [167].

For example, one can consider a so-called nonlocal regime of a Josephson junction, which is realized for the opposite limit $j_d \gg j_c \gg j_d\xi/\lambda$. In our model, this limit can be realized when the transparency of the barrier is sufficiently low, i.e. $1 \lesssim Z_0 \lesssim \sqrt{12\pi^2\lambda/\xi}$. In such a case the nonlocal equation for the phase has a soliton-like solution

$$\tilde{\varphi}(x) = \pi + 2\arctan(x/\ell_J), \tag{1.65}$$

which corresponds to a single Josephson-Abrikosov vortex with the size of ℓ_J, where $\lambda \gg \lambda_J \gg \ell_J \gg \xi$. As in the local case, this solution assumes the condition $\kappa = (k_F\ell_J)^{-1} \ll 1$ to be fulfilled, therefore, it is possible to use the WKB approximation for (1.65). With the help of relation $\sin^2(\tilde{\varphi}(z)/2) = (1 + z^2)^{-1}$ we obtain an explicit expression for the turning points:

$$\frac{x_{a,b}}{\ell_J} = \pm \sqrt{\frac{\Delta_0^2}{(\Delta_0^2 - E^2)(1 + Z_0^2)} - 1}. \tag{1.66}$$

Spatial dependence of quasiparticle LDOS for a nonlocal vortex is shown in Fig. 1.12(b). Considering both limits we find that described peculiarities in the LDOS can be observed in the wide range of transparencies.

Let us note that some basic features of the LDOS and quasiparticle spectrum discussed above are qualitatively close to the ones predicted in Ref. [39] on the basis of the numerical BdG calculations. This qualitative similarity reveals itself, in particular, in the behavior of the lowest energy level of the subgap spectrum: the energy of this level grows with the decreasing barrier transparency (i.e., the hopping strength at the defect line) resulting in the suppression of the LDOS at low energies and the splitting of the subgap energy peak (see Figs. 2 and 3 of the Ref. [39]). The quantitative comparison is however difficult since our calculations are based on the quasiclassical approach assuming rather large ratio E_F/Δ_0, while in the Ref. [39] this ratio is not so large.

We also note that a two-peak LDOS pattern is also characteristic of the Abrikosov vortex pinned by a plane defect (see the spatial profile of LDOS along the defect in Fig. 1.8(c)). What makes the case of the Josephson vortex distinctive is that the distance between the peaks $\sim \ell_J/\sqrt{1-E^2/\Delta_0^2}$ can well exceed the corresponding distance for Abrikosov vortex $\sim \xi/\sqrt{1-E^2/\Delta_0^2}$. In the high-resolution scanning tunneling microscopy (STM) and scanning tunneling spectroscopy (STS) measurements this feature can be obviously viewed as the spectral signature of precisely the *Josephson vortex*.

- **array of Josephson vortices**

The idea of formation of an adiabatic potential for quasiparticles in the Josephson vortex holds for a quite general form of the function $\varphi(x)$. Consider as an example a general solution of the Ferrell-Prange equation describing the local limit of the Josephson junction

$$\frac{\lambda_J}{\sqrt{2}}\int_{\varphi_0}^{\varphi}\frac{d\varphi}{\sqrt{C-\cos\varphi}}=x,$$

where C is a constant, φ_0 is a phase difference value at $x=0$ and the scale of the spatial distribution of the phase along the junction is $\ell_J\sim\lambda_J$. The case $C=1$ corresponds to the phase soliton described in the previous subsection, while at $C>1$ the phase grows continuously and each increase of the phase by 2π corresponds to a Josephson vortex. For such a solution, an array of semiclassical potential wells is formed and, consequently, we get an array of LDOS peaks corresponding to these wells.

For illustration we take the limit of high magnetic fields and dense vortex lattices which corresponds to the values $C\gg 1$. The solution can be chosen in the following form: $\tilde{\varphi}(x)=ax/\lambda_J+\pi$, where the constant a is proportional to the external magnetic field in the contact. Then, using (1.58) we find a set of the turning points

$$\frac{x_{a,b}}{\lambda_J}=\mp\frac{2}{a}\arccos\sqrt{(Z_0^2+1)(1-E^2/\Delta_0^2)}\pm\frac{2\pi}{a}n, \tag{1.67}$$

where n is an integer corresponding to different vortices in the vortex array. The result is a double-period peak structure shown in Fig. (1.13). As the quasiparticle energy approaches the gap value, the distance between the peaks in each vortex increases and the peaks from different vortices approach each other. This leads to the coupling of states in the neighboring classically allowed regions, which is not taken into account in the present work.

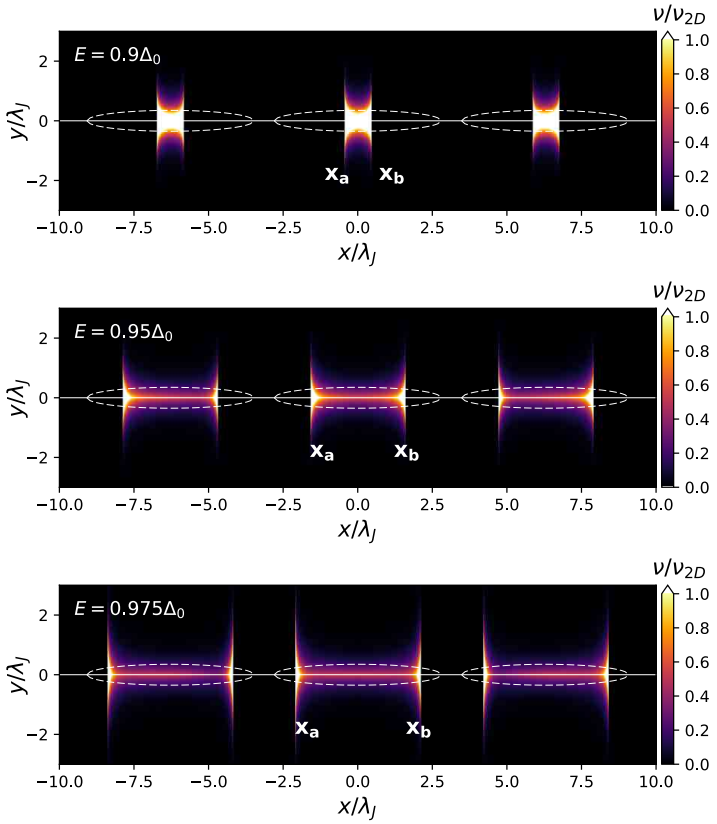

Figure 1.13: Spatial distribution of the quasiparticle LDOS $\nu(x, y, E)$ for a set of three Josephson vortices, schematically shown by the dashed lines for the different values of the energy. White solid line shows the barrier position. The positions of the peaks of LDOS $x_{a,b}$ correspond to the turning points (1.67) for each vortex. The parameters are: $a = 1$, $Z_0 = 2$, $k_F\xi = 30$, $k_F\lambda_J = 100$.

1.3 Magnetic structure of vortices in the vicinity of a plane defect

We have elucidated how the electronic structure of the vortex pinned at the plane defect changes throughout the crossover between Abrikosov and Josephson regimes. Since the defect potential affects the electronic transparency it will inevitably modify the electromagnetic (or current) part of the vortex as well. In this Section we investigate the physical mechanisms for delocalization of the magnetic field of Abrikosov vortex in superconductors in the presence of planar defects of various electronic transparency. Although the electrodynamic properties of the vortices are well-studied and intuitive, the particular cases (such as plane defects) require detailed analysis, especially when it comes to interpreting experimental results.

Very recently in Ref. [216] the observation of the superconducting vortices carrying a flux smaller than the flux quantum $\Phi_0 = \pi\hbar c/e$ in the $Ba_{1-x}K_xFe_2As_2$ superconductor was reported. These fractional vortices were observed in the hole overdoped $Ba_{1-x}K_xFe_2As_2$ ($x = 0.77$) compound with a critical temperature $T_c \sim 11$K which is substantially smaller the critical temperature of 38K for the optimally doped $x = 0.4$ compound [217]. The fractional vortices coexist with the standard single quantum vortices but disappear below 9K. In Refs. [216, 218] it was suggested that the appearance of the fractional vortices is related with the multiband superconductivity in $Ba_{1-x}K_xFe_2As_2$ when the vortex exists only in one band.

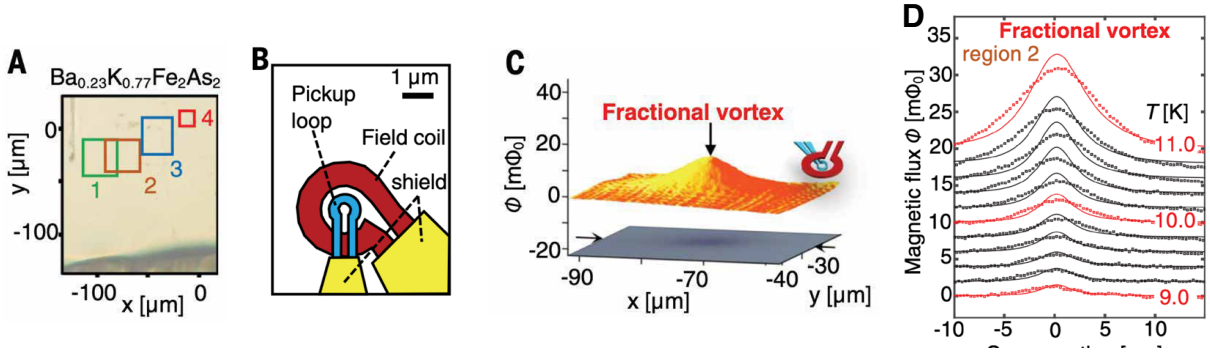

Figure 1.14: Scanning SQUID imaging fractional vortices in $Ba_{1-x}K_xFe_2As_2$.(A) Optical image of the sample with scan regions 1 to 4. (B) Pickup loop and field coil of the SQUID susceptometer. (C) SQUID measurements of isolated fractional vortex carrying ~0.3 of the flux quantum. (D) Measured cross sections of the fractional vortex along the x axis, where the y position is indicated by horizontal arrows in (C). From Ref. [216].

This interpretation arises some doubts because of the inevitable interband interaction in 3D $Ba_{1-x}K_xFe_2As_2$ superconductor which near T_c effectively results in a single order parameter superconductivity with usual vortices. In present article we analyze how the vortex magnetic field distribution can be modified by the presence of the nearby planar defects of different type and demonstrate that vortex itself can carry a flux substantially smaller than Φ_0, while the remaining flux may be strongly delocalized at distances of the order of the defect's size. Similar situation may be realized if the Abrikosov vortex is situated near the Josephson junction [219, 220] - it also can carry only a part the flux quantum while the remaining flux will be absorbed by the part of the Josephson vortex. As the result a hybrid Arikosov-Josephson vortex satisfies the condition of flux quantization but the flux of Abrikosov vortex (located at the distance of the order of London penetration depth λ) is smaller than Φ_0 and the remaining flux is accumulated at the distances of the order of Josephson length $\lambda_J \gg \lambda$. We believe that on experiment this situation may be seen as a fractional "bright" Abrikosov vortex supplemented by remaining weak field existing at

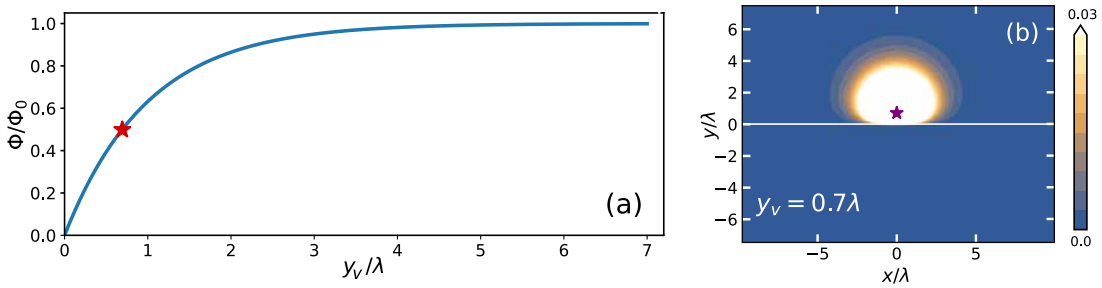

Figure 1.15: (a) Dependence of the magnetic flux on the vortex distance y_v from the infinite isolating plane. (b) Spatial distribution of the magnetic field $h_z/\frac{\Phi_0}{2\pi\lambda^2}$ of the vortex located at $y_v = 0.7\lambda$ (marked by the star) from the plane (shown by the white line).

distances much larger than λ and hardly detected above the noise level. Note that different types of defects can greatly alter the superconducting current distribution, which can even mimic a generation of vortex-antivortex pairs [221, 222].

We consider a planar defect of the thickness $d \ll \lambda$ lying in the plane $y = 0$ whose transparency is characterized by angle-averaged probability of electron transmission $\mathcal{T}$ (see the introduction in the Chapter 1) which determines the amplitude of the critical current density j_c and is temperature independent [223].

- **Vortex near a long planar defect with $\mathcal{T} = 0$.**

Strongly insulating plane is nontransparent for the supercurrent, hence the Abrikosov vortex placed nearby has the same magnetic field distribution as a vortex near the edge of the sample [224]. The latter is defined by a solution of the London equation with corresponding boundary conditions of vanishing supercurrent through the defect's plane

$$(\nabla^2 - \lambda^{-2})h_z = \frac{\Phi_0}{2\pi\lambda^2}\delta(\mathbf{r}_v); \quad \left(\nabla \times \mathbf{h} \cdot \mathbf{y}_0\right)|_{x\in(-\infty,\infty)} = 0, \tag{1.68}$$

where $\delta(\mathbf{r})$ is delta function. Using the image method [224] the magnetic field can be written as a superposition of the fields of a free vortex placed at the point $(x_v,\ y_v > 0)$

$$\mathbf{h}_v(\mathbf{r}) = \frac{\Phi_0}{2\pi\lambda^2} K_0\Big[\frac{|\mathbf{r} - \mathbf{r}_v|}{\lambda}\Big]\mathbf{z}_0$$

and mirrored antivortex, such that

$$h_z(\mathbf{r}) = \begin{cases} h_v(\mathbf{r}) - h_v(\mathbf{r})|_{y_v\to -y_v},\ y \geqslant 0 \\ 0,\ y < 0 \end{cases}. \tag{1.69}$$

The total magnetic flux of the vortex may be easily calculated and is given by the expression [220]

$$\Phi\left(y_v\right) = \Phi_0\left[1 - \frac{y_v}{\pi\lambda}\int_{-\infty}^{\infty}\frac{K_1\left(\frac{y_v\sqrt{1+t^2}}{\lambda}\right)}{\sqrt{1+t^2}}dt\right], \tag{1.70}$$

where y_v is the distance between vortex and the boundary and K_i is modified Bessel function. At $y_v \gg \lambda$ the flux is equal to its standard value Φ_0, but it vanishes when $y_v \to 0$. The evolution of the vortex flux $\Phi\left(\frac{y_v}{\lambda}\right)$ is presented in Fig. 1.15(a). Naturally, a similar situation occurs in a

superconductor with planar defects provoking a local weakening of superconductivity.

• **Vortex near a short planar defect with $\mathcal{T} = 0$.**

Here we consider an Abrikosov vortex near finite-sized insulating xz-plane of the size 2ℓ in the x-direction. The distribution of the vortex magnetic field can be easily obtained from Eq. (1.68) with the same boundary conditions, which at short distances $|\mathbf{r}| \ll \lambda$ can be approximated as a Poisson equation [225]

$$\nabla^2 h_z = \frac{\Phi_0}{2\pi\lambda^2}\delta(\mathbf{r}_v); \quad \big(\nabla \times \mathbf{h}\cdot\mathbf{y}_0\big)|_{x\in(-\ell,\ell)} = 0. \tag{1.71}$$

This problem is similar to the electrostatic one and can be solved by conformal transformation method [226]. The solution reads

$$h_z(\mathbf{r}) = \frac{\Phi_0}{2\pi\lambda^2}\left[\ln\frac{\lambda}{2\ell} + \ln\left|\frac{2}{e^{\gamma+i\varphi} - e^{\gamma_v+i\varphi_v}}\right| + \ln\left|1 - e^{-(\gamma+\gamma_v)-i(\varphi-\varphi_v)}\right|\right], \tag{1.72}$$

where

$$\gamma(\mathbf{r}) = \frac{1}{2}\cosh^{-1}\left[\frac{r^2}{\ell^2} + \sqrt{\left(\frac{r^2}{\ell^2} - 1\right)^2 + 4\frac{y^2}{\ell^2}}\right],$$

the phase is defined as $e^{i\varphi(x,y)} = x\ \mathrm{sech}(\gamma)/\ell + iy\ \mathrm{csch}(\gamma)/\ell$; and index v means vortex coordinates. Note that at $\ell \ll \lambda$ the magnetic field of the vortex changes slightly, while at $\ell \gg \lambda$ the strong deformation is described by the limiting case (1.69). The most nontrivial redistribution of the field occurs in the case $\ell \approx \lambda$, and the corresponding illustrative examples are presented in Fig. 1.16. We clearly see that substantial part of vortex flux comes from the remote region with a weak magnetic field, especially when the vortex is placed close to the plane. When the vortex is pinned by the plane its magnetic field is smeared over the entire defect and the flux is strongly delocalized [Fig. 1.16(e)].

Interaction with a defect is described by the potential energy which can be calculated using the field (1.72) and reads up to a constant [227]

$$U_p = \left(\frac{\Phi_0}{4\pi\lambda}\right)^2\left[\ln\left(1 - e^{-2\gamma_v}\right) + \ln\left|1 - e^{-2(\gamma_v+i\varphi_v)}\right|\right]. \tag{1.73}$$

The interaction of the plane segment and the vortex line is purely attractive and has anisotropy as shown in Fig. 1.16(f). The pinning force $\mathbf{F}_p$ in the vicinity of the defect (for $\ell \approx \lambda$) can be estimated in the limit $\delta x_v, \delta y_v \ll \ell$ as follows

$$F_{px}(\ell + \delta x_v, 0) \approx \Big[-\frac{1}{\delta x_v} + \sqrt{\frac{2}{\ell}}\frac{1}{\sqrt{\delta x_v}}\Big]\Big(\frac{\Phi_0}{4\pi\lambda}\Big)^2, \qquad F_{py}(0, \delta y_v) \approx -\frac{1}{\delta y_v}\Big(\frac{\Phi_0}{4\pi\lambda}\Big)^2$$

and we see that the vortex attraction is much stronger near the central part of the defect comparing with its edges. Conversely, away from the defect (for the case $\ell \ll \lambda$) the force scales as

$$F_{px}(x_v \gg \ell, 0) \approx -\frac{\ell^2}{x_v^3}\Big(\frac{\Phi_0}{4\pi\lambda}\Big)^2, \qquad F_{py}(0, y_v \gg \ell) \approx -\frac{\ell^4}{4y_v^5}\Big(\frac{\Phi_0}{4\pi\lambda}\Big)^2$$

and attraction from the edges becomes dominant.

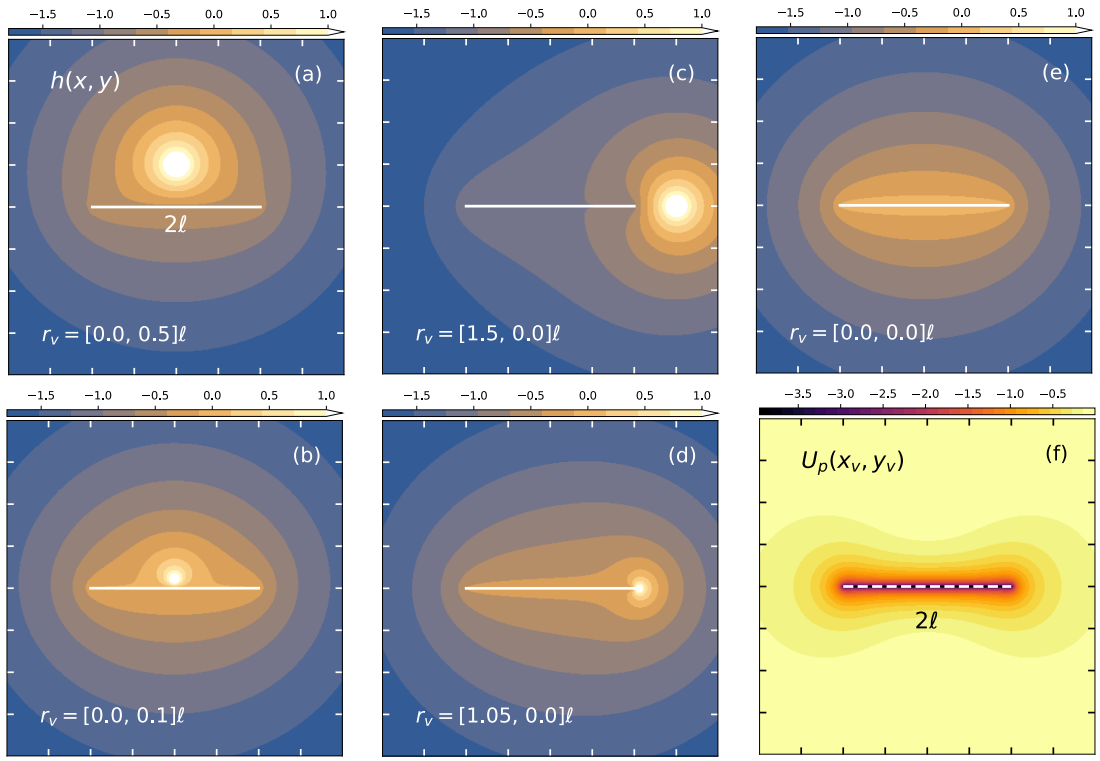

Figure 1.16: (a-e) Distribution of the magnetic field $h_z(x,y)/\frac{\Phi_0}{2\pi\lambda^2}$ of the Abrikosov vortex in the vicinity of the isolating plane (shown by the white line) of the length 2ℓ for different vortex position $r_v = [x_v, y_v]\ell$. (f) Pinning energy profile $U_p/(\frac{\Phi_0}{2\pi\lambda^2})^2$ as a function of the vortex position $\mathbf{r}_v/\ell$.

• **Vortex near the plane with $\mathcal{T} \ll 1$.**

Now we consider the case of the Abrikosov vortex situated near a long Josephson junction with $\ell \gtrsim \lambda_J$ which can model a situation when the vortex is near a segment-like defect with low transparency (or small critical current). The Abrikosov vortex creates a local phase difference at the Josephson junction at the nearby region $\sim \lambda$, which at the scale of the Josephson length $\lambda_J \gg \lambda$ can be considered as a local phase jump. This phase jump κ is generated by vortex current at the junction and is directly related with the vortex flux Φ from Eq. (1.70).

$$\kappa = 2\pi \frac{\Phi_0 - \Phi(y_v)}{\Phi_0}. \tag{1.74}$$

This situation is somewhat similar to the Josephson junction with a pair of tiny current injectors generating a local phase jump [228]. In our case a vortex plays a role of these injectors. The evolution of the phase difference φ on the Josephson junction is described by the Ferrell-Prange equation [229]

$$\frac{d^2\varphi}{dx^2} = \frac{1}{\lambda_J^2}\sin\varphi \tag{1.75}$$

and for the Abrikosov vortex situated at $x_v = 0$ and at the distance y_v from the junction the Abrikosov vortex generates only the flux $\Phi(y_v)$ and the remaining flux $\Phi_0 - \Phi(y_v)$ is generated by the Josephson vortex in the region $\sim 2\lambda_J$. Naturally the total flux of such a hybrid vortex is equal to one quantum Φ_0.

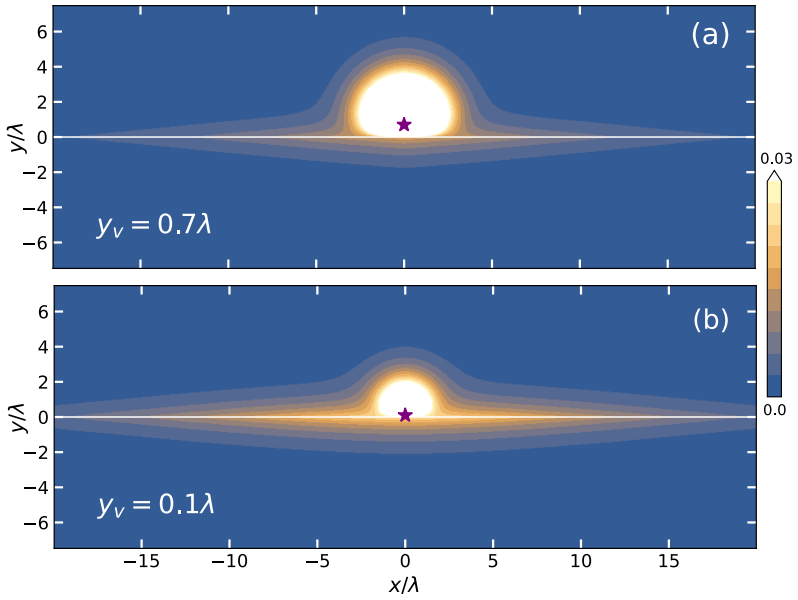

Figure 1.17: Spatial distribution of the magnetic field $h_z/\frac{\Phi_0}{2\pi\lambda^2}$ of the Abrikosov vortex located at y_v (marked by the star) in the vicinity of the infinite Josephson junction (shown by the white line) for $\lambda_J/\lambda = 10$.

Magnetic field at the center of Josephson junction (we suppose that the thickness d of the weak coupling region is much smaller than λ) is $h_z(x, y = 0) = -\frac{\Phi_0}{4\pi\lambda}\nabla_x\varphi$ [229]. Taking into account that it decays along the y-axis exponentially at distance λ from the junction we get

$$h_z(x,y) = \frac{\Phi_0}{4\pi\lambda\lambda_J}\frac{e^{-|x|/\lambda_J}\tan\left(\frac{\kappa(y_v)}{8}\right)}{1+e^{-2|x|/\lambda_J}\tan^2\left(\frac{\kappa(y_v)}{8}\right)}e^{-|y|/\lambda}. \tag{1.76}$$

The characteristic magnetic field of such a partial Josephson junction $\sim \frac{\Phi_0}{\lambda\lambda_J}$ is much smaller than the field of Abrikosov vortex and can be hardly detected on experiment. In Fig. 1.17 we present the field distribution for such a composite Abrikosov[Eq. (1.69)] + Josephson[Eq. (1.76)] vortex for: (i) $y_v = 0.7\lambda$ ($\kappa = \pi$), where half of the flux is carried by Abrikosov vortex and Josephson vortex; and (ii) $y_v = 0.1\lambda$ ($\kappa = 1.8\pi$), where almost all of the flux has been transferred to the Josephson vortex. Note that this effect may be important in the context of the generation of the Josephson phase shift controlled by the Abrikosov vortex [220, 230, 231].

• **Vortex near the plane with $\mathcal{T} \approx 1$.**

As a last case we address the opposite limit of long ($\ell \gtrsim \lambda$) planar defect of high transparency, which can be treated with the help of spatially modulated diffusion coefficient $D(\mathbf{r}) \propto \lambda^{-2}(\mathbf{r})$ or London penetration depth. The local increase of the latter in the vicinity of the defect plane can be simply modeled as $\lambda^2(y) = \lambda^2 + \alpha\lambda^2\delta(y)$, where we introduced the dimensionless coefficient $0 \leqslant \alpha \propto (1-\mathcal{T}) \ll 1$. Note that the energy of the vortex $U_p \propto \lambda^{-2}(y)$ decreases in the vicinity of the plane, therefore the local suppression of transparency ($\alpha > 0$) leads to an attractive interaction. Local change of the supercurrent situated close to the defect plane $\mathbf{j} = (c/4\pi\lambda^2(y))(\frac{\Phi_0}{2\pi}\nabla\theta - \mathbf{A})$ obeys the London equation which reads

$$(\nabla^2 - \lambda^{-2})h_z - \frac{\Phi_0}{2\pi\lambda^2}\delta(\mathbf{r}_v) = \alpha\lambda\delta(y)\nabla^2 h_z + \alpha\lambda\nabla_y\delta(y)\nabla_y h_z. \tag{1.77}$$

Following approach of Ref. [232] we treat the RHS of the Eq. (1.77) as a perturbation and obtain

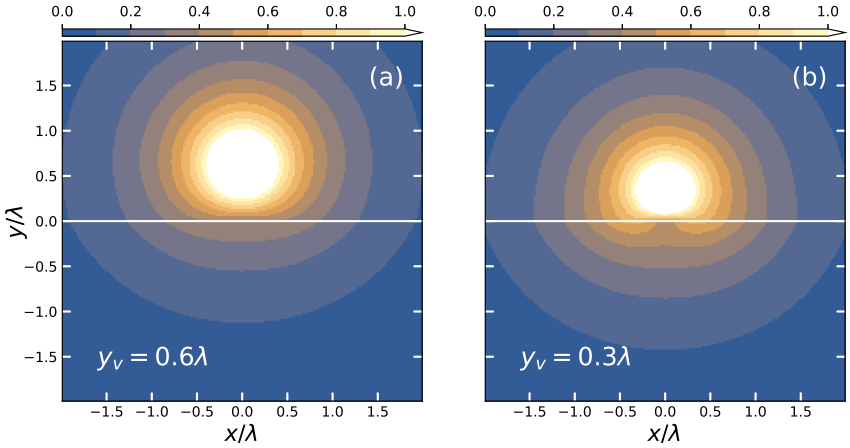

Figure 1.18: Distribution of the magnetic field $h_z/\frac{\Phi_0}{2\pi\lambda^2}$ of the Abrikosov vortex in the vicinity of the planar defect of the strength $\alpha = 0.3$ (shown by the white line) for different vortex positions y_v.

the distribution of the field $h_z(\mathbf{r}) = h_v(\mathbf{r}) + \alpha h_{z1}(\mathbf{r}) + \mathcal{O}(\alpha^2)$ using Fourier transform

$$h_z(\mathbf{r}) = \frac{\Phi_0}{2\pi\lambda^2} K_0\Big[\frac{|\mathbf{r}-\mathbf{r}_v|}{\lambda}\Big] - \alpha\frac{\Phi_0}{2\pi\lambda^2}\frac{|y|+|y_v|}{\sqrt{(|y|+|y_v|)^2+x^2}} K_1\Big[\frac{\sqrt{(|y|+|y_v|)^2+x^2}}{\lambda}\Big]. \qquad (1.78)$$

Naturally, the field distribution is weakly extended along the defect with local anisotropy of the order of α. It confirms the general tendency for the vortex magnetic field to spread with the decrease of $\mathcal{T}$, and this effect may be noticeable even in the intermediate regime $\mathcal{T} \lesssim 1$.

We believe that the fractional vortices observed in Ref. [216] close to T_c may be the Abrikosov vortices near the planar defects (which can appear in $Ba_{1-x}K_xFe_2As_2$ due to the local doping variation). The remote field of such vortices may be too small for local magnetometry resolution above the noise level. Our results show that Abrikosov vortices are attracted to the planar defect and the attractive force (1.73) increases with the decrease of the temperature through $\lambda(T)$, which may explain why the fractional vortices [216] disappeared below 9K - they were absorbed by the defect or if the defect presents a local critical temperature increase, the short range repulsion will maintain vortex near the defect. The situation is somewhat similar to the vortex near the twinning plane with a local increase of superconducting pairing [233].

1.4 Flux-flow vortex diode effect in S/F bilayer

In the last Section of this Chapter we will discuss the mechanism of a spontaneous vortex nucleation in the superconductor-ferromagnet bilayer structure and elucidate the origin of the vortex diode effect observed in Nb/EuS sample in the recent experiment [234]. We build a theoretical model based on the setup from Ref. [234], which is sketched out in Fig. 1.19.

stripe width	$L = 15\mu$m
Nb film	
thickness	$d_s = 8$ nm
coherence length	$\xi \sim 50$ nm
London penetration depth	$\lambda_{\text{bulk}} \sim 50$ nm $\lambda_{\text{film}}(0) \sim 220$ nm
effective Pearl length	$\lambda_{\text{eff}} = \lambda^2/d_s \sim 1\mu$m
EuS film	
thickness	$d_f = 30$ nm
magnetization	$4\pi M \approx 1,5$ T

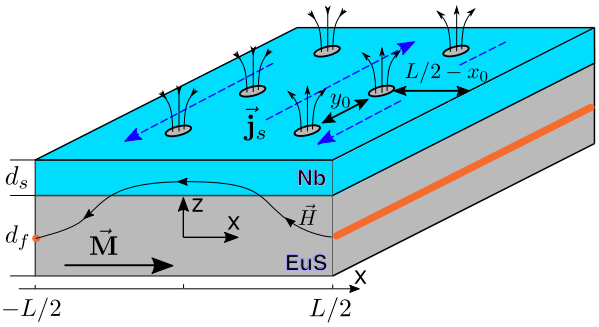

Figure 1.19: Sketch of the proposed S(blue)/F(grey) system. Orange lines represent auxiliary (imaginary) wires with magnetic charge $\beta = Md_f$, to which a field $\mathbf{H}$ corresponds. This field produces supercurrents $\mathbf{j}_s$ (blue dashed lines), that provoke the entry of Abrikosov vortices.

Consider the infinite strip consisting of S and F layers. The F layer has a magnetization $4\pi\mathbf{M}$ [1] along the x-axis, which produces a stray magnetic field $\mathbf{H}$ inside and outside the F layer. We omit the discussion about the demagnetization effect caused by stray field and focus on the supercurrents induced in the S layer. The calculation of the vector potential $\mathbf{A} = A(x,z)\mathbf{y}_0$ produced by the magnetization is straightforward using the following model [235]. In the limit $L \gg d_f$ the field from F strip can be modeled by the field induced by two infinite wires with opposite magnetic charge densities $\pm Md_f$ positioned at $x = \pm L/2$ and $z = 0$. Note here that the plane $z = 0$ is chosen to pass through the middle of the F layer.. In the Pearl regime when $d_s \ll \lambda$ we can consider S strip as a delta layer placed in the $z = -d_f/2$ plane. Therefore the vector potential produced by the magnetization M in the superconducting layer takes the form

$$A_{\text{M}}(x, d_f/2) = -2Md_f\left[\text{arctg}\left(\frac{2x+L}{d_f}\right) - \text{arctg}\left(\frac{2x-L}{d_f}\right)\right]. \tag{1.79}$$

- **Simplified model for the case $L \lesssim \lambda_{\text{eff}}$**

For a qualitative analysis consider first the case $L \lesssim \lambda_{\text{eff}}$, where it is natural to neglect the contribution to the vector potential from the screening current. Thus, the supercurrent is defined through the local vector potential generated by the ferromagnet:

$$\mathbf{j}_s(x) = j_s(x)\mathbf{y}_0 = -\frac{c}{4\pi\lambda^2}\Big[\mathbf{A}_{\text{M}}(x) + \mathbf{A}_0\Big], \tag{1.80}$$

where $\mathbf{A}_0$ is a gauge term which can be found from the condition $\int_{-L/2}^{L/2} j_s(x)dx = 0$. This gives

[1] Magnetization of the F layer can be estimated knowing the density $\rho(\text{EuS}) = 5,7 \times 10^3 \text{kg/m}^{-3}$, number density $\rho_N(\text{EuS}) = 2 \times 10^{28}\text{m}^{-3}$ and magnetization per formula unit $M_{\text{EuS}} = 7\mu_B$, which gives us a value $4\pi M \approx 1,5$T.

us simple analytical expression for spatial distribution of the screening current density

$$j_s(x)/j_0 = M_0\Big[\text{arctg}\big((2x+L)/d_f\big)-\text{arctg}\big((2x-L)/d_f\big)-2\text{arctg}\big(2L/d_f\big)+(d_f/L)\ln\big(1+4L^2/d_f^2\big)\Big]. \tag{1.81}$$

Here we introduced a dimensionless magnetization $M_0 = 4\pi M d_f/\Phi_0$, where the value $4\pi M \approx 2$T corresponds to $M_0 \approx 1$. Current density is expressed in terms of $j_0 = \Phi_0 c/8\pi^2 d_f \lambda^2$, where in SI units for $d_f = 30$nm and $\lambda \approx 220$nm we have $j_0 \approx 17\times 10^6$ A/cm^2. The distribution of $j_s(x)$ is shown in Fig. (1.19). The sharp increase in the screening current density in the vicinity of the sample edge is due to the large ratio L/d_f. It is important to note that the model under consideration [235] is not valid in the range $|x \pm L/2| < d_f$, where the cutoff should be introduced. Note that the current value j_s does noe exceed the depairing current for this system $j_d \sim 200\times 10^6$A/cm^2 (see Ref. [236]). Large value of the current at the edge induces the entrance of the vortices (antivortices) in the superconductor film. At moderate magnetization M one expects an equilibrium chain of vortices along the y axis located close to the edge. As a result the supercurrent from the vortex will reduce the total current at the edge.

Note that similar S/F systems have been considered both theoretically and experimentally in the context of diode effect in Ref. [237] (see also Ref. [238]), where the authors studied the distribution of the screening current in Nb bridge induced by the narrow Co strip and its impact of the critical current $I_c(M)$. In our case we focus on the vortex nucleation problem inside the strip with commensurate S/F layers and on interaction of the vortices with ac transport current.

Consider first the single vortex problem. Hereafter we will discuss only vortices at the $x \approx L/2$ edge and neglect the interaction of these vortices with the antivortices at $x \approx -L/2$, which is weak for the intervortex distances larder than $\sim L/\pi$ [239]. From the work [240] we can extract the energy of the Pearl vortex in the finite-sized film per unit length for the case of $L \ll \lambda_{\text{eff}}$:

$$\epsilon_{\text{v}}(x_0) = \left(\frac{\Phi_0}{4\pi\lambda}\right)^2 \ln\left(\frac{\lambda}{\xi}\right) + \left(\frac{\Phi_0}{4\pi\lambda}\right)^2 \ln\left[\frac{L}{\pi\lambda}\cos\left(\frac{\pi x_0}{L}\right)\right] = \left(\frac{\Phi_0}{4\pi\lambda}\right)^2 \ln\left[\frac{L}{\pi\xi}\cos\left(\frac{\pi x_0}{L}\right)\right], \tag{1.82}$$

where $x \in [-L/2, L/2]$ and the cutoff $|x-x_0| = \xi$ is introduced. The balance of the effective force acting on the vortex from the boundaries (confinement effect) and from the induces supercurrent j_s (Lorentz force) at the equilibrium position x_0 reads

$$-\nabla_x \epsilon_{\text{v}}\big|_{x_0} - \frac{\Phi_0}{c} j_s(x_0) = 0 \tag{1.83}$$

or

$$\text{arctg}\Big(\frac{2x_0+L}{d_f}\Big) - \text{arctg}\Big(\frac{2x_0-L}{d_f}\Big) - 2\text{arctg}\Big(2\frac{L}{d_f}\Big) + \frac{d_f}{2L}\ln\Big(1+4\frac{L^2}{d_f^2}\Big) + \frac{\pi d_f}{2M_0 L}\text{tg}\Big(\frac{\pi x_0}{L}\Big) = 0. \tag{1.84}$$

It makes sense to consider the position of the vortex x_0 near the edge $L/2$ (see Fig. 1.19). For $d_f \ll L/2 - x_0 \ll L$ the approximate solution of Eq. (1.84) is

$$x_0 \approx \frac{L}{2}\left(1 - \frac{1-\frac{1}{M_0}}{\ln(2L/d_f)}\right) \tag{1.85}$$

The vortex entry condition can be formulated as $M_0 > 1$, what in dimensional units is equivalent to $4\pi M \gtrsim 2$T. This value is comparable to our estimation for the EuS layer $4\pi M \approx 1,5$ T.

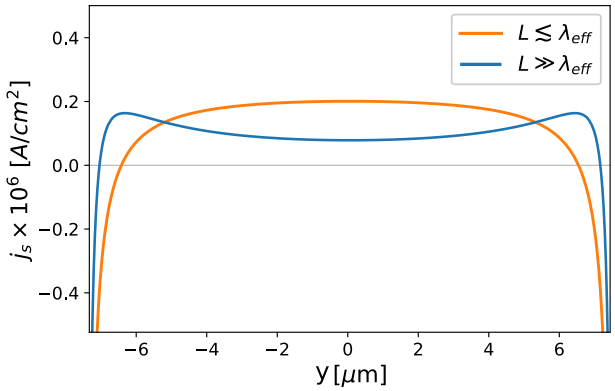

Figure 1.20: Spatial distribution of the supercurrent $j_s(x)$ induced by the ferromagnet layer with $4\pi M = 2$ T, $L/d_f = 500$ and $L/\lambda_{\text{eff}} = 15$ (for the blue line).

This result is valid for a rather sparse vortex array, while for a dense chain of vortices it is necessary to take into account the short-range vortex interaction in the Pearl regime [239]. For example consider an infinite linear chain of vortices along the y axis (see Fig. 1.19). The equilibrium state of such a system can be obtained by balancing all the forces acting on an elementary cell (a pair of vortices):

$$-\nabla_i \epsilon_{\text{v}}\big|_{x_0} - \nabla_i \epsilon_{\text{v}}^{(\text{int})}\big|_{x_0,y_0} - \frac{\pi y_0}{L}\frac{\Phi_0}{c} j_s(x_0) = 0, \tag{1.86}$$

where $i = x, y$ and we have taken into account the interaction of the nearest vortices [239]

$$\epsilon_{\text{v}}^{(\text{int})}(x_0, y_0) = \frac{\Phi_0^2}{16\pi^2\lambda^2} \ln\left[1 + \frac{2\cos^2(\frac{\pi x_0}{L})}{\cosh(\frac{\pi y_0}{L}) - 1}\right]. \tag{1.87}$$

The solution of Eq. (1.86) can be easily estimated as follows

$$y_0 \approx \frac{L}{\pi M_0}, \quad x_0 \approx \frac{L}{2}\left(1 - \frac{1 - \frac{L}{y_0 \pi M_0}}{\ln(2L_d)}\right).$$

For $M_0 \sim 1$ the intervortex interaction is negligible and we formally repeat Eq. (1.85). Note that with an increase in M_0 (and the density of induced supercurrent j_s) the vortex chain may be unstable to rearrangement into a zigzag pattern.

- **Model for the case $L \gg \lambda_{\text{eff}}$**

In the case of a wide stripe, which may be more appropriate for the experiment described in [234], the expression for both the current j_s and the vortex energy ϵ_{v} should be corrected and found in a self-consistent manner. Using London equation we can write the screening supercurrent in terms of total vector potential as follows:

$$\mathbf{j}_s(x) = -\frac{c}{4\pi\lambda^2}\Big[\mathbf{A}_{\text{s}}(x) + \mathbf{A}_{\text{M}}(x) + \mathbf{A}_0\Big], \tag{1.88}$$

where the gauge term is $\mathbf{A}_0 = -\int_{-L/2}^{L/2}\big(\mathbf{A}_s + \mathbf{A}_{\text{M}}\big)dx/L$. The vector potential induced in the superconductor can be defined with the help of Biot-Savart's law:

$$\mathbf{A}_s(\mathbf{r}) = \frac{1}{c}\int \frac{d\mathbf{j}_s}{R} = \frac{1}{c}\int \frac{\mathbf{j}_s(\mathbf{r}')d^3r'}{|\mathbf{r} - \mathbf{r}'|}. \tag{1.89}$$

In the case of the thin superconducting film one has

$$\mathbf{A}_s(x,y) = \frac{d_s}{c}\int_{-L/2}^{L/2} dx' \int_{-l}^{l} dy' \frac{\vec{j}_s(x',y')}{\sqrt{(x-x')^2+(y-y')^2)}}. \tag{1.90}$$

Consider a strip that is infinite in x direction with the length $l \to \infty$ in the presence of the supercurrent $\mathbf{j}_s = j_s(x)\mathbf{y}_0$. After integration the vector potential gains a simple form:

$$A_s(x) = -\frac{2d_s}{c}\int_{-L/2}^{-L/2} \ln|x-x'| j_s(x')dx'. \tag{1.91}$$

The last expression can be rewritten as an implicit equation for A_s:

$$A_s(x) = \frac{d_s}{2\pi\lambda^2}\int_{-\frac{L}{2}}^{-\frac{L}{2}} \ln|x-x'|\Big(A_s(x') + A_{\mathrm{M}}(x')\Big)dx' \tag{1.92}$$
$$-\frac{d_s}{2\pi\lambda^2}\frac{1}{L}\int_{-\frac{L}{2}}^{-\frac{L}{2}}\Big(A_s(x'') + A_{\mathrm{M}}(x'')\Big)dx''\int_{-\frac{L}{2}}^{-\frac{L}{2}}\ln|x-x'|dx'.$$

This equation can be solved iteratively, starting with the ansatz $A_s(x) = 0$. The numerically integrated current distribution is shown in Fig. 1.20. It is clearly seen that a simple analytical approach for $L \ll \lambda_{\mathrm{eff}}$ qualitatively gives reasonable profile of the supercurrent.

We briefly discuss the single vortex problem. The energy of Pearl vortex near the boundary of the strip (which is effectively semi-infinite for $L \gg \lambda_{\mathrm{eff}}$) can be found from the interaction of the vortex with its image. The corresponding vortex-antivortex interaction energy can be taken from [239]:

$$\epsilon_{\mathrm{v}} = -\frac{\Phi_0^2}{8\pi\lambda^2}\Big[\mathbf{H}_0\Big(\frac{L/2-x_0}{\lambda_{\mathrm{eff}}}\Big) - Y_0\Big(\frac{L/2-x_0}{\lambda_{\mathrm{eff}}}\Big)\Big], \tag{1.93}$$

where $\mathbf{H}_0$ and Y_0 are the Struve and Bessel functions. The equilibrium position of the vortex x_0 can be extracted from the condition of the balance of forces acting on the vortex. The corresponding equation is:

$$-\frac{\partial\epsilon_{\mathrm{v}}}{\partial x}\Big|_{x_0} - \frac{\Phi_0}{c}j_s(x_0) = 0 \tag{1.94}$$

This equation (can be solved numerically) gives qualitatively the same dependence $x_0(M_0)$ like in the case $L \lesssim \lambda_{\mathrm{eff}}$ (see Eq. (1.85)).

- **Diode effect with AC transport current**

The vortices induced by the magnetization of the F layer inevitably affect the transport measurements in the flux-flow regime, what was indeed observed in the experiment in [234]. In this work the ac transport supercurrent $\mathbf{j}_{\mathrm{tr}} = j_{\mathrm{tr}}(t,x)\mathbf{y}_0$ was applied in addition to the current $\mathbf{j}_s(x)$ generated by the magnetic layer. The spatial distribution of the transport current is almost homogeneous over the strip and is described by the Bean critical state model [241, 242]. The amplitude of ac current is strong enough to reduce the screening current $j_s(x)$ and even change its sign of in the middle of the strip at some phase of ac oscillation [Fig. 1.21]. As soon as the total supercurrent $j_s + j_{\mathrm{tr}}$ becomes the same sign in the entire strip, this provokes a flow of vortices driven by the Lorentz force (flux-flow) (see Fig. 1.22(c,e)). After half a period the transport current increases the screening current $j_s(x)$ in the middle and slightly affect it at the

edges, so that there is almost no vortex motion and flux-flow is significantly suppressed [Fig. 1.21].

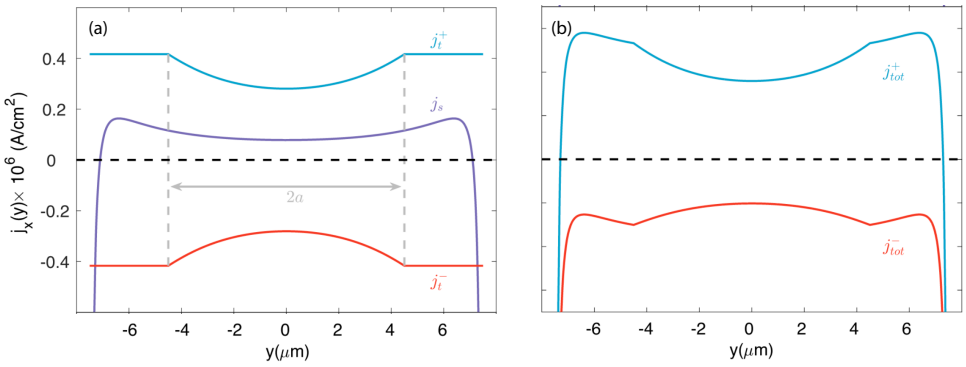

Figure 1.21: *(Fig. 4 from Ref. [234])*. (a) Spatial distribution of the screening current j_s from Eq. (1.88) induced by the F layer and applied transport current $j_{\rm tr}$ (from Bean model, see [234] for details). (b) Total supercurrent $j_s + j_{\rm tr}$ at opposite phases of ac cycle. Note that our notation differs from [234] by replacing $x \leftrightarrow y$.

Averaging this process over a sufficiently fast period of the AC signal ($f \approx 1$ kHz) gives an effective DC diode effect, which manifests itself in the dependence $I_{\rm dc}(V_{\rm dc})$ [Fig. 1.22(a)]. Reversing the direction of magnetization in the F-layer reverses the direction of vortex motion [Fig. 1.22(c-e)], as our theoretical model suggests. When the magnetization is directed along the strip (Fig. 1.22(f-h)], vortex formation is absent and the diode effect is not observed. Thus, the experimental results from Ref. [234] are in good agreement with our simple theoretical model.

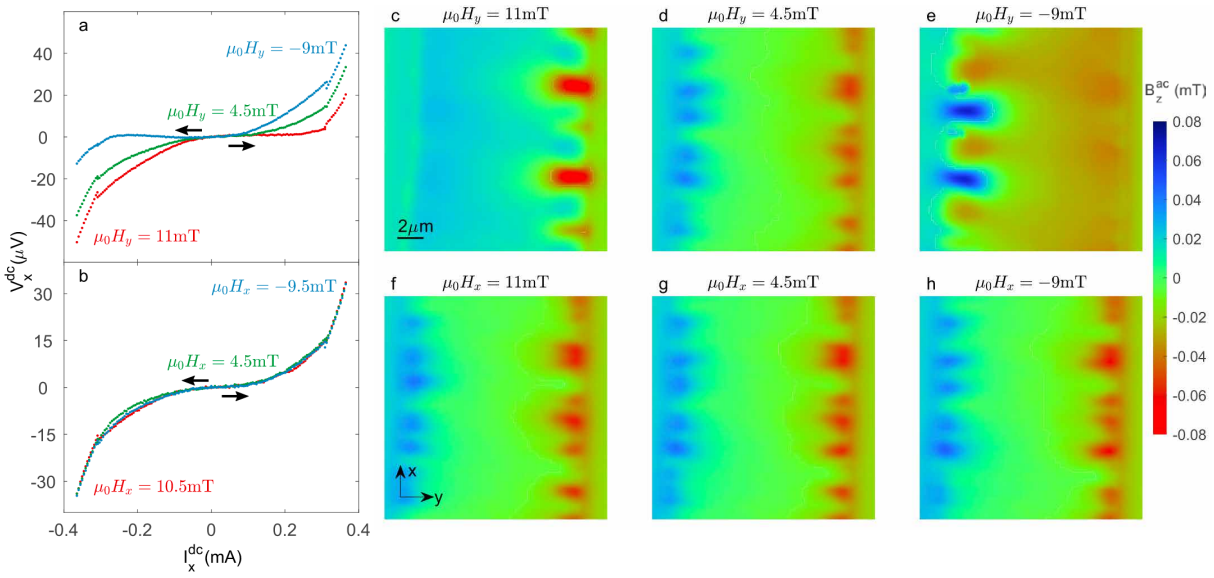

Figure 1.22: *(Fig. 2 from Ref. [234])*. $I(V)$ characteristics for different transverse (a) and longitudinal (b) magnetic fields. (c-h) SQUID-on-tip image of the ac out-of-plane component of the magnetic field $B_z^{ac}(x, y)$, modulated with respect to an oscillating transport current with an RMS value $I_x^{ac}(x)$. The polarity of the signal depends on whether the magnetic feature appears in phase (blue) or at a π-phase (red) with respect to the oscillating current. For (c-e) the magnetization of the F layer is oriented along y-axis, and for (f-h) along x-axis. Note that our notation differs from [234] by replacing $x \leftrightarrow y$.

1.5 Summary and outlook

We have investigated the transformation of the subgap spectrum of quasiparticle excitations in the Abrikosov vortex pinned by the planar defect with a high transparency. We find that the normal scattering at the defect surface results in the opening of a soft minigap Δ_{Soft} in the elementary excitation spectrum near the Fermi level. The minigap size grows with the decrease in the transparency of the barrier. The increase in the resulting soft gap affects the splitting of the zero bias anomaly in the tunneling spectral characteristics and perturb the circular symmetry of the LDOS peaks. The normal reflection of electrons and holes at the defect plane changes the topology of the isoenergetic orbits in $(\mu - \theta_p)$ space. This topological transition revealing in the specific behavior of the quantized quasiparticle levels and density of states, can be considered as a hallmark of the crossover from the Abrikosov to the Josephson vortex. As a result, there appears a new type of subgap quasiparticle states gliding along the defect, which reveal the qualitatively new behavior of discrete spectrum $\varepsilon_n \sim n^{1/2}$. The hard minigap $\varepsilon_0 \ll \Delta_{Soft}$ in the spectrum of energy levels exceeds noticeably the value of the CdGM minigap $\hbar\omega_0 \ll \varepsilon_0$. The decrease in the barrier transparency is accompanied by the increase in the hard minigap ε_0 in the spectrum which can be observed in the measurements of the Ohmic and Hall conductivities at finite frequencies. The basic properties of the vortex such as pinning and mobility along the defect plane are strongly affected by these changes in the orbit topology. We have also analyzed the distinctive features of the quasiparticle density of states for an Abrikosov vortex pinned by a planar defect with a perfect boundary. One can expect, however, that barrier imperfections and roughness should result in a partial smearing of both the hard and soft gap features similarly to the effect of the point impurity scattering.

We analyzed the subgap spectrum of localized quasiparticle states in a SIS junction with a low transparency in the presence of an inhomogeneous phase difference along the junction, which corresponds to an array of Josephson vortices. Since the spatial scale of the Josephson vortex is usually much larger than the characteristic quasiparticle wavelength, the phase difference profile can be treated as an effective adiabatic potential. This potential affects the quasiparticle motion along the barrier and leads to the appearance of the closed semiclassical orbits in the plane of (k_x, x). We restored the quantum spectrum corresponding to this orbits by using the Bohr-Sommerfeld quantization rule. The obtained discrete spectrum E_n reveals a minigap $E_0 \approx \Delta_0 Z_0/\sqrt{1+Z_0^2}$ which increases with an increase in the barrier strength Z_0. We found, that the semiclassical orbits are responsible for the formation of a set of turning points at which momentum along the barrier plane k_x goes to zero. Corresponding local increase in the quasiparticle wave function near each turning point leads to the formation of the corresponding peak of the LDOS. We claim that these peaks can be observed in the STS/STM experiments in both local and nonlocal Josephson junction regimes in a fairly large energy range below the gap.

We have shown that in addition to the electronic structure inside the vortex core, planar defects of various electronic transparency can strongly modify the structure of supercurrents surrounding the vortex oriented parallel to the defect plane. Thus, for highly transparent defect plane the magnetic field of the vortex is only slightly perturbed, while the low transparency leads to the significant elongation of the field along the plane. Moreover, if the size of the defect exceeds the London penetration depth λ a substantial part of the magnetic flux of the vortex should be delocalized from its center. Since a low-transparent defect is essentially a Josephson junction, one can expect effective transfer of the flux from the Abrikosov vortex situated near the

defect to the Josephson vortex whose magnetic field is smeared at a distance of $\lambda_J \gg \lambda$. As a result such deformations may affect the local ($\lesssim \lambda$) flux measurements in superconductors with high concentration of crystal defects.

We developed a theoretical model for the vortex nucleation in a bilayer superconductor/ferromagnet strip. The magnetization of the F layer (oriented perpendicular to the strip) produces the stray magnetic field which induces the screening supercurrent in the S layer. The inhomogeneous spatial distribution of this current provokes the entrance of the vortices inside the bilayer. Applying an alternating transport current will cause the motion of the induced vortices and generation of corresponding flux-flow resistance. The flux-flow effect is naturally different for the opposite phase of the ac cycle, since the magnetization of the F layer breaks the spatial symmetry in the system. Eventually, time-averaged measurements of the $I_{\rm dc}(V_{\rm dc})$ curves clearly reveal the diode effect, which have been recently discovered experimentally in the Nb/EuS structure Ref. [234].

Chapter 2

Inverse Faraday effect in superconductors

The present Chapter is devoted to a theoretical study of inverse Faraday effect in superconducting media. We start with a brief introduction to the Ginzburg-Landau theory with broken particle-hole symmetry. We then provide the details of the IFE generation for a superconducting film at $T < T_c$ and a ring geometry at $T > T_c$.

2.1 Time-dependent Ginzburg-Landau theory

The dynamics of the superconducting condensate in the vicinity of the critical temperature can be described within the complex-valued order parameter $\Psi(\mathbf{r}, t)$ connected to the microscopical pairing parameter (or the gap function) $\Delta(\mathbf{r}, t)$. According to the Ginzburg-Landau (GL) theory the free energy of the superconductors in the presence of the magnetic field reads

$$\mathcal{F} = \int d^3r \Big[a|\Psi|^2 + \frac{b}{2}|\Psi|^4 + \frac{1}{4m}\Big|\Big(\frac{\hbar}{i}\nabla - \frac{2e}{c}\mathbf{A}\Big)\Psi\Big|^2 + \frac{|\nabla \times \mathbf{A}|^2}{8\pi}\Big]. \tag{2.1}$$

Here $\mathbf{A}$ is the vector potential, m is the electron mass, e is the electron charge, $a \propto T - T_c$ and b are phenomenological parameters. The equilibrium state must satisfy the GL equations for the order parameter $\delta\mathcal{F}/\delta\Psi^* = 0$ and for the supercurrent $\delta\mathcal{F}/\delta\mathbf{A} = -\mathbf{j}_s/c$. A deviation from the equilibrium state should be governed by some time-dependent extension of the GL equations. On the first sight, the equation $\delta\mathcal{F}/\delta\Psi^* = 0$ resembles the nonlinear Schrodinger equation, and the natural idea is to add a time derivative such that $i\partial_t\Psi = \delta\mathcal{F}/\delta\Psi^*$. It was shown that this type extension leads to contradictions [122] and the question of the order parameter dynamics requires comprehensive microscopic analysis. The derivation of the time-dependent Ginzburg-Landau (TDGL) equations from the microscopic theory (using, for instance, the quasiclassical version of Gorkov equations) implies an expansion of the Greens function which is impossible in the presence of the gap in the quasiparticle spectrum. First derivation of TDGL [115, 116] was made within the assumptions of small gap $\Delta \to 0$, which takes place extremely close to the critical temperature. The resulting dynamical dynamical equation is appears to be of a diffusion type $-\Gamma\partial_t\Psi = \delta\mathcal{F}/\delta\Psi^*$, where $\Gamma > 0$ is a relaxation coefficient. The TDGL equation in this form is rather simple both for analytical and numerical calculations and is heavily utilized for the description of nonequilibrium superconductors. Later it was shown that the described TDGL model is *exact* for the gapless superconductors and can be derived in the case of

paramagnetic impurities, which suppress the energy gap due to a spin-dependent scattering that breaks spin-singlet Cooper pairs [243]. Another possible case providing gapless state is the strong electron-phonon interaction, which results in the modified Kramer–Watts-Tobin equation [117, 244–246]. For large electron-phonon relaxation rate $\tau_{ph}^{-1} \gg \Delta/\hbar$ this equation can be reduced to the standard TDGL form, however, such a gapless regime is hardly achievable in real systems [247]. In the opposite limit this equation corresponds to the gapful superconductor [248]. In the case of unconventional superconductivity, possessing, for example, d-wave symmetry, the gapless regime can be easily achieved in the dirty limit. In the presence of nonmagnetic impurities, which effectively suppress the $\mathbf{k}$-dependent gap close to the critical temperature $\sqrt{1-T/T_c} \ll (\tau_{\text{imp}} T_c)^{-1}$ (this is equivalent to a small mean free path $\ell \ll \xi(T)$) one can obtain gapless TDGL equations, which are modified by the additional relaxation term [249]. Note that in the present chapter we will discuss only the gapless s-wave superconductors. From this discussion, we conclude that the relaxation dynamics of the order parameter seems to be the most expected for a superconducting system, since the origin of dissipations is naturally related to the strong pair breaking mechanism underlying the simplified phenomenological theory.

Dynamics of the order parameter relaxation should satisfy the gauge invariance, which leads to the appearance of the scalar potential φ

$$-\Gamma\Big(\frac{\partial}{\partial t} - \frac{2ie\varphi}{\hbar}\Big)\Psi = \frac{\delta \mathcal{F}}{\delta \Psi^*} = -|a|\Psi + b\Psi^2 + \frac{1}{4m}\Big(\frac{\hbar}{i}\nabla - \frac{2e}{c}\mathbf{A}\Big)^2\Psi. \tag{2.2}$$

The preserving of the gauge-invariance brings a contribution to the current from the normal electrons and we obtain the expression for the total current

$$\mathbf{j} = \mathbf{j}_n + \mathbf{j}_s = \sigma_n\Big(-\nabla\varphi - \frac{1}{c}\frac{\partial \mathbf{A}}{\partial t}\Big) + \frac{e}{m}\Big[\Psi^*\Big(-i\hbar\nabla - \frac{2e}{c}\mathbf{A}\Big)\Psi + \Psi\Big(i\hbar\nabla - \frac{2e}{c}\mathbf{A}\Big)\Psi^*\Big]. \tag{2.3}$$

The vector potential $\mathbf{A}(\mathbf{r}, t)$ can be included to the TDGL equations through the Maxwell equation $\nabla \times \nabla \times \mathbf{A} = -\frac{4\pi}{c}\mathbf{j}$. Some assumptions have been made in order to obtain rather simple form of Eq. (2.2). For instance, we neglect the requirement of the Galilean invariance for the macroscopic "wave function" $\Psi(\mathbf{r}, t)$, which should modify the chemical potential and therefore the term with time derivative [250, 251]. This effect is rather weak and we will not consider it in the present work. The more significant is the neglecting of particle-hole asymmetry in the quasiparticle spectrum, which can strongly modify the dynamics of the order parameter and give rise to the nondissipative contribution.

2.1.1 Particle-hole asymmetry

What is particle-hole symmetry and how it enters the TDGL equations? The order parameter represents the energy gap which drastically changes the quasiparticle spectrum of the metal in the superconducting state. Physical processes related to small perturbation of the ground state typically involve scattering of the electron states in the vicinity of the Fermi energy $E_F = \mu(0)$, therefore it is convenient to introduce the concept of quasiparticle excitations with $E_p \ll E_F$. For ideal degenerate electron gas one can define the QP energy as follows

$$\begin{aligned} \xi_p &= \frac{\mathbf{p}^2}{2m} - E_F \approx \mathbf{v}_F(\mathbf{p} - \mathbf{p}_F) + \frac{(\mathbf{p} - \mathbf{p}_F)^2}{2m} \quad \text{for particle-like excitation,} \\ \xi_p &= E_F - \frac{\mathbf{p}^2}{2m} \approx -\mathbf{v}_F(\mathbf{p} - \mathbf{p}_F) - \frac{(\mathbf{p} - \mathbf{p}_F)^2}{2m} \quad \text{for hole-like excitation.} \end{aligned} \tag{2.4}$$

where $v_F = p_F/m$. Note that according to the theory of the Fermi liquid the spectrum of the quasiparticle excitation in the strongly interacting isotropic system is identical to one of the ideal (free) electron gas, with expansion $\xi_p \approx \pm\frac{\partial E_p}{\partial \mathbf{p}}(\mathbf{p}-\mathbf{p}_F)$. The spectrum of (2.4) is symmetrical with respect to $\mathbf{p} \leftrightarrow \mathbf{p}_F$ only for $\mathbf{p}-\mathbf{p}_F \ll p_F$, however the deviation from this symmetry becomes noticeable far from Fermi level [1].

In s-wave superconductors the QP spectrum is gapped $E_p = \pm\sqrt{\xi_p^2 + |\Delta|^2}$, which leads to the mixing of the hole-like and particle-like states at $\mathbf{p} \approx \mathbf{p}_F$. For large energies $\xi_p \gg |\Delta|$ the asymmetry between particle and hole QP branches can be significant (see Fig. 2.1). Linearization of QP spectrum is connected to the simplification of the DOS of the electron gas at $\xi_p \approx 0$:

$$\nu(\xi_p) = \frac{(2m)^{3/2}}{4\pi^2\hbar^3}\sqrt{\xi_p + E_F} \approx \nu(0) + \nu(0)\frac{\xi_p}{E_F} + O\Big(\frac{\xi_p^2}{E_F^2}\Big).$$

In the theory of conventional phonon-mediated superconductivity one usually considers the pairing region $\xi_p \in (-\omega_D, \omega_D)$, where the DOS is approximated by the first term $\nu(\xi_p) = \nu(0)$, since $E_F \gg \omega_D, |\Delta|$. The second term is naturally represents the particle-hole asymmetry and has the order of $\Delta/E_F \sim T_c/E_F$. Let us elucidate how this effect modify the TDGL theory.

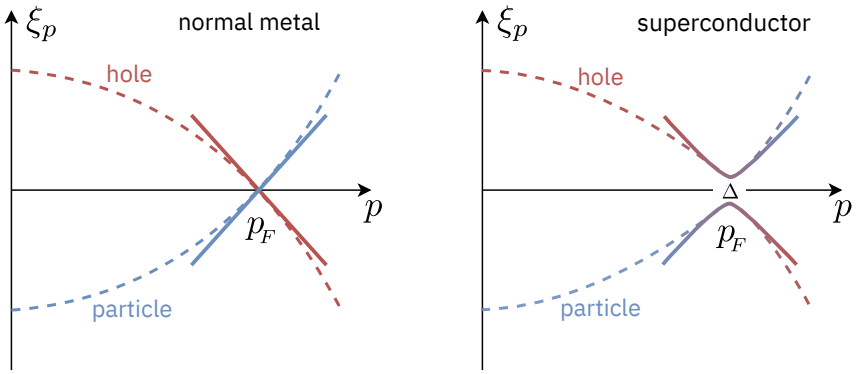

Figure 2.1: Particle/hole spectrum (dashed lines) and quasiparticle spectrum (solid lines) in the vicinity of p_F for normal and superconducting metals.

The order parameter used in the TDGL equations is related to anomalous Green function $F(\mathbf{r}_1,\tau_1;\mathbf{r}_2,\tau_2) = \langle \hat{T}_\tau \hat{\psi}_\uparrow(\mathbf{r}_1,\tau_1)\hat{\psi}_\downarrow(\mathbf{r}_2,\tau_2)\rangle_{st}$ which is defined is the system of Gor'kov equations [252] . Here $\hat{\psi}_\sigma$ is the Heisenberg fermion field operator, $\langle \dots \rangle_{st}$ means statistical averaging and $\hat{T}_\tau$ orders imaginary (Matsubara) time τ. We will show an elegant derivation of the TDGL equation while preserving the particle-hole asymmetry. This derivation can be easily implemented in the spirit of [243] (assuming a large number of paramagnetic impurities with short scattering time $\tau_s\Delta \ll 1$) or [95, 253] (for fluctuation regime at $T > T_c$) in the Matsubara formalism. The dynamics of the superconducting pairing potential can be traced from the self-consistency equation for the gap function

$$\frac{\Delta^*(\omega_k)}{g} = T\sum_n \frac{d^3p}{(2\pi\hbar)^3} F^\dagger(\mathbf{p},\omega_n,\omega_n+\omega_k), \tag{2.5}$$

which is assumed to be homogeneous for the sake of simplicity. Here $\omega_n = \pi T(2n+1)$ - fermionic

[1] Effect of the broken particle-hole symmetry is well known in the Hall effect. From the Drude theory we have nondiagonal component of the conductivity tensor $\sigma_{xy} \propto \omega_c\tau \propto 1/m^* \propto \partial^2 E_p/\partial p^2 \neq 0$ only for the asymmetrical QP spectrum. See also Section 2.3.

and $\omega_k = 2\pi T k$ - bosonic Matsubara frequencies, $\mathbf{p}$ is a momentum, g is a BCS coupling constant and T is a temperature. The anomalous Green function can be expanded in Δ in the gapless regime $\Delta \to 0$ using Gor'kov equations and we get a linearized expression

$$L^{-1}(\mathbf{p}, \omega_k)\Delta^*(\omega_k) = 0, \tag{2.6}$$

where we have defined propagator $L^{-1} = g^{-1} - \Pi(\omega_k)$ and polarization operator

$$\Pi(\omega_k) = -T\sum_n \int \frac{d^3p}{(2\pi\hbar)^3} G_0(-\mathbf{p}, -\omega_n) G_0(\mathbf{p}, \omega_n + \omega_k). \tag{2.7}$$

with the bare Green function $G_0 = (i\omega_n - \xi_p)^{-1}$. Calculating the sum in $\Pi(\omega_k)$ with the help of analytical continuation method [254] and setting $i\omega_k \to \omega$ we obtain

$$\Pi(\omega) = \int \frac{d^3p}{(2\pi\hbar)^3} \frac{\tanh\left(\frac{\xi_p}{2T}\right)}{\xi_p - \omega/2} \approx \int \frac{d^3p}{(2\pi\hbar)^3} \frac{\tanh\left(\frac{\xi_p}{2T}\right)}{\xi_p} \left(1 + \frac{\omega}{2\xi_p}\right). \tag{2.8}$$

Further we use $\int \frac{d^3p}{(2\pi\hbar)^3} = \int \nu(\xi_p) d\xi_p$ and take into account the dependence of DOS on the energy at the Fermi level $\nu(\xi_p) \approx \nu(0) + \xi_p \frac{\partial \nu}{\partial \xi_p}|_{\xi_p=0}$. Thus, the polarization operator can be written as follows

$$\Pi(\omega) \approx \nu(0) \int_0^{\frac{\omega_D}{2T}} \frac{\tanh(x)}{x} dx + \omega \frac{\nu(0)}{4T} \int_0^{\infty} \frac{\tanh(x)}{x^2} dx + \frac{\omega}{2} \frac{\partial \nu}{\partial \xi_p}\Big|_{\xi_p=0} \int_0^{\frac{\omega_D}{2T}} \frac{\tanh(x)}{x} dx. \tag{2.9}$$

Here $\frac{\partial \nu}{\partial \xi_p}|_{\xi_p=0}$ reflects the particle-hole asymmetry and we use the Debye frequency ω_D for truncation. The first two terms constitute the standard TDGL propagator

$$\Pi_0(\omega) = \frac{1}{g} + \nu(0) \ln \frac{T_c}{T} + \frac{\nu(0)\pi\hbar}{8T_c} i\omega, \tag{2.10}$$

where we use $\Delta_0 = \pi T_c/\gamma_E$ with $\gamma_E \approx 1.78...$ and $g^{-1} = \nu(0)\ln(2\omega_D/\Delta_0)$ and we have restored $\hbar$. The term with $i\omega$ correspond to time derivative $-i\omega \to \frac{\partial}{\partial t}$, which proves the dissipative nature of TDGL equation. Integrating and transforming the last term in Eq.(2.9) we get

$$\Pi(\omega) = \Pi_0(\omega) + \frac{\omega}{2} \frac{\hbar}{g\nu(0)} \frac{\partial \nu}{\partial \xi_p}\Big|_{\xi_p=0} \approx \Pi_0(\omega) + \omega \frac{\nu(0)\hbar}{2} \frac{\partial \ln T_c}{\partial E_F}. \tag{2.11}$$

Here the frequency ω brings nondissipative contribution to the time derivative of the gap function. Finally the linearized TDGL equation can be written as follows

$$-\frac{\pi\hbar}{8T_c}\left(1 - i\frac{4}{\pi}\frac{\partial T_c}{\partial E_F}\right)\frac{\partial \Delta(t)}{\partial t} + \frac{T_c - T}{T}\Delta(t) = 0. \tag{2.12}$$

This result repeats that from [95, 253] if we assume $T > T_c$. Note that the more detailed microscopic derivation of the TDGL equation for the fluctuation regime was first done in the seminal work [95].

The nonlinear and gradient terms of the GL equation (see Eq. 2.2) are not affected by particle-hole asymmetry, therefore resulting gauge-invariant equation for the dimensionless order

parameter reads

$$\tau_\psi\big(1+i\gamma\big)\Big(\frac{\partial}{\partial t}+\frac{2e}{\hbar}i\varphi\Big)\psi=\Big[1-|\psi|^2-\xi^2\Big(-i\nabla-\frac{2\pi}{\Phi_0}\mathbf{A}\Big)^2\Big]\psi, \tag{2.13}$$

where

$$\gamma=-\frac{4}{\pi}\frac{\partial T_c}{\partial E_F}\sim\frac{T_c}{E_F};$$

$\tau_\psi(T)=(\pi\hbar/8T_c)/(1-T/T_c)$ is relaxation time; Φ_0 is magnetic flux quanta; and $\xi(T)=\xi_0/\sqrt{1-T/T_c}$ is coherence length. The derivation of Eq. (2.13) can also be done by using the action formalism [255], where it was shown that the particle-hole asymmetry effectively couples the electronic density and superconducting energy gap. Note, that it is possible to introduce parameter γ in (2.13) starting directly from Eq. (2.2) and examining of the impact of the electric potential on the chemical potential of superconductor (see chapter 12.9 in [11]). The first experimental studies of the high-T_c compounds reported small imaginary part of the relaxation constant (actually $\gamma\sim10^{-3}$), however, as will be discussed in Section 1.2, some recent experiments indicate the possibility of relatively high values of γ. Another potential source of the broken particle-hole symmetry giving nonzero γ is the nontrivial topological structure of the Fermi surface [256].

From the mathematical point of view there is a clear analogy between the modified TDGL equation (2.13) and time-dependent Gross-Pitaevskii (TDGP) equation used for the helium superfluid [257]. Interestingly, that original TDGP equations constitute the steady (Schrödinger-like) dynamics of the superfluid condensate and Pitaevskii introduced the real part of the relaxation constant in order to describe relaxation towards the equilibrium state (or conversion of the superfluid into the normal one) [258]. Despite the fact that the TDGP model describes essentially different physical system and has a plethora of constraints (for instance, it works only for $T=0$), some general similarities has been considered in Ref. [259]. To uncover the features of the dynamics of the condensate in the modified TDGL model (and compare it with TDGP model) we examine its linear regime.

2.1.2 Linear analysis

Let us consider the order parameter dynamics in the presence of imaginary part of the relaxation time γ. We assume a superconductor of the size $\xi\ll L\ll\ell_E$ and therefore neglect scalar potential keeping $\mathbf{A}=0$. In the vicinity of the critical temperature $T_c-T\ll T_c$ one can linearize Eq. (2.13) with $\psi(t)\to\psi_0+\delta\psi(t)$ and put the equilibrium solution $\psi_0=1$

$$\tau_\psi(1+i\gamma)\frac{\partial\delta\psi}{\partial t}=-\delta\psi-\delta\psi^*+\xi^2\nabla^2\delta\psi, \tag{2.14}$$

Consider small harmonic perturbation to the ground state of the form

$$\delta\psi(\mathbf{r},t)=\big[ue^{i\omega t+i\mathbf{kr}}+v^*e^{-i\omega t-i\mathbf{kr}}\big]$$

using which we obtain the dispersion relation for the complex frequency $\omega=\omega'+i\omega''$

$$\omega(k)=i\tau_\psi^{-1}\frac{1+\xi^2\mathbf{k}^2}{1+\gamma^2}\left[1\pm|\gamma|\frac{\sqrt{2\xi^{-2}+\mathbf{k}_c^2+\mathbf{k}^2}}{\xi^{-2}+\mathbf{k}^2}\sqrt{\mathbf{k}_c^2-\mathbf{k}^2}\right], \tag{2.15}$$

where the critical value of the wave vector is $\xi^2\mathbf{k}_c^2(\gamma) = \sqrt{1+\gamma^{-2}} - 1$. The dispersion shows that the nondissipative contribution to the order parameter dynamics ω' exists only for $|\mathbf{k}| > |\mathbf{k}_c|$.

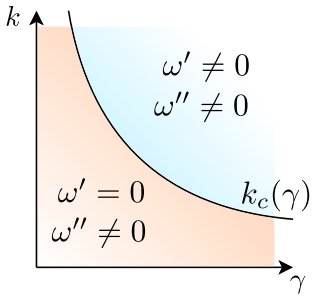

Figure 2.2: Dependence of the critical momentum $k_c(\gamma)$ separating two region with damped (blue) and purely dissipative (orange) dynamics.

For $\gamma \ll 1$ only shortwave excitations of the order parameter carry nondissipative oscillations, which are inevitably damped. The hydrodynamic or GP regime can be restored formally by putting $\gamma \gg 1$ (what is physically unreachable for superconductors). Therefore the spectrum becomes linear for small $k \to 0$

$$\omega(k) \approx \pm\frac{\sqrt{2}\xi}{\gamma\tau_\psi}k \tag{2.16}$$

and therefore provides soft (sound) modes, as TDGP model predicts.

In contrary, the strongly damped oscillations of the superconducting modes for $\gamma \ll 1$ can be hardly defined as the sound. As an example we discuss the propagation of the damped modes of the superconducting condensate caused by the effective variation of the critical temperature T_c. For the sake of simplicity we consider delta pulse which locally reduce the critical temperature and induce response-like dynamics of $\psi(\mathbf{r}, t)$. The corresponding equation reads

$$\tau_\psi(1+i\gamma)\frac{\partial\delta\psi}{\partial t} = -a_\delta\delta(t/\tau_\psi)\delta(\mathbf{r}/\xi) - \delta\psi - \delta\psi^* + \xi^2\nabla^2\delta\psi. \tag{2.17}$$

The resulting radially symmetrical profile of the order parameter $|\psi|(r,t) = 1 + \delta|\psi|(r,t)$ has the following form

$$|\psi| = 1 - \frac{a_\delta}{(1+\gamma^2)}\int_0^\infty \left[\frac{i\omega_1(s)(1-\gamma^2)+s^2}{i\omega_1(s)-i\omega_2(s)}e^{i\omega_1(s)t} - \frac{i\omega_2(s)(1-\gamma^2)+s^2}{i\omega_1(s)-i\omega_2(s)}e^{i\omega_2(s)t}\right]J_0(sr)s\frac{ds}{2\pi}, \tag{2.18}$$

where $\omega_{1,2}(k)$ is a dimensionless frequency taken from dispersion relation (2.15) and the upper limit of the integration (which restricts the spatial resolution of the GL theory as $k < \xi_0^{-1}$ [215]) was approximated as $(1 - T/T_c)^{-1/2} \to \infty$. The spatial-time distribution of $\psi(r,t)$ is shown in Fig. (2.3). Since the delta pulse excites all frequencies/wavevectors, we are guaranteed to get a undamped contribution to the total order parameter response, which naturally vanishes at $\gamma = 0$. Considering the superconducting condensate as an oscillatory system (albeit a strongly damped one) may reveal some curious effects. For instance, one can expect that the attachment of such a superconductor to a ferromagnet will couple the dynamics of the superconducting order parameter, described by TDGL model, and the precessing magnetic moment obeying the Landau-Lifshitz equation. In this case, the standard problem of the ferromagnetic resonance will be inevitably modified by the coupling to the superconductor, whose oscillatory contribution can

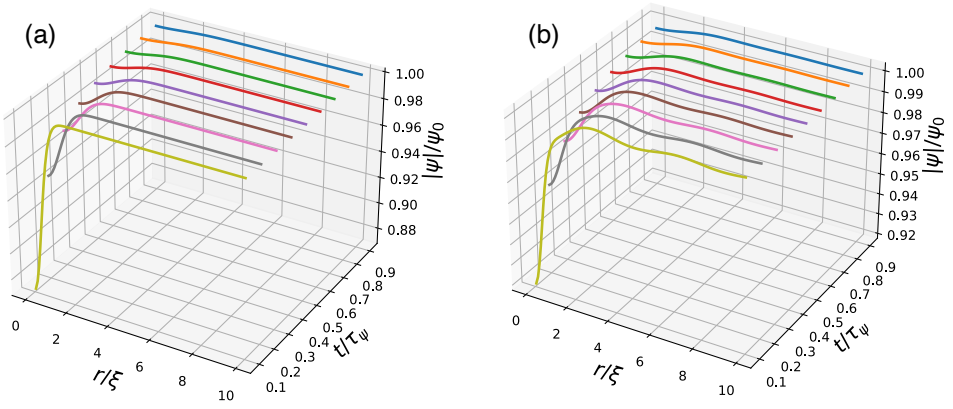

Figure 2.3: Sequential spatial profile of the $\psi(r,t)$ for $t \in [0.1,...,0.9]\tau_\psi$ for zero $\gamma = 0$ (a) and nonzero $\gamma = 0.3$ (b) particle-hole asymmetry. The amplitude of the initial perturbation is $a_\delta = 0.2$.

shift the resonance frequency.

Another example of the effects caused by the particle-hole asymmetry is the modification of the collective modes existing in the superconductor. First of all, it is known that the imaginary part of the GL relaxation constant γ directly couples the fluctuations of the phase and the modulus of the order parameter ψ on the microscopic level, thereby hybridizing the gapped Higgs and gapless Goldstone modes [125, 255]. Secondly, close to the critical temperature T_c the normal current became strong enough to screen the supercurrent fluctuations and prevent the shift of the Goldstone mode to the plasma frequency. Such a low energy mode of counterflow currents is called the Carlson-Goldman modes [260–262] and in the presence of $\gamma \neq 0$ it is natural to expect the resonance-like behavior of the current oscillations coming from the nondissipative dynamics of the order parameter. However, in general case, the dynamical structure and the interaction of different collective modes is complicated [255, 263] and its detailed analysis requires further investigation.

Less extravagant manifestation of the broken electron-hole symmetry is the interaction of the superconductor with the external electromagnetic radiation. Specifically, it was shown in Ref. [91] that the nondissipative modes of the order parameter localized close to the sample boundaries can carry the nondissipative steady supercurrents, which result in so-called inverse Faraday effect. Discussion of this phenomenon is the contents of the rest part of the present Chapter.

2.1.3 IFE in the linearized TDGL model

Direct Faraday effect is a well-known example of an optomagnetic phenomenon, which describes the rotation of the polarization plane of the light passing through the active media in the presence of a magnetic field. In turn the *inverse* Faraday effect (IFE) consists of the generation of the DC magnetic moment by the circularly polarized light. Firstly discussed in the context of transparent dispersive media by Pitaevskii [80] and discovered experimentally few years later in the nonabsorbing Eu^{2+}:CaF_2 crystal [264] this effect has been studied in many physical systems ranging from the harmonic atom [265] to magnetics [82] and graphene [266].

For superconducting metals two contributions are naturally expected in the vicinity of the critical temperature T_c from the normal and superfluid electrons. The first one is rather simple and can be described in classical regime and an excellent microscopic explanation was given in Ref. [83]. It states that the instant electric field of the EM wave incident normally to the metal's

surface induces the excess of the electron density δn at the samples' boundary, which is dragged by the circular rotation of the field with velocity $\delta\mathbf{v}$ along the boundary. This spatial motion results in the nonzero dc current $\langle\mathbf{j}_n\rangle = e\langle\delta n\delta\mathbf{v}\rangle$ averaged over the rotation period. The second one is more tricky and has been discussed only recently in [91], where an origin of that IFE was proposed for superconductors with broken particle-hole symmetry. As we discussed in the previous subsection, the inhomogeneities (such as the disk boundary considered in Ref. [91]) provoke the local excitation of the partially nondissipative order-parameter modes. The interaction of these modes with external circularly polarized electromagnetic field occurs through the gauge-invariant vector potential $\mathbf{A}(\mathbf{r},t)$, which induces the current response of the condensate. It was shown that in the second order $j_s(\mathbf{r},t) \propto \mathbf{A}^2$ the supercurrent from (2.3) has nonzero dc component $\langle j_s\rangle \propto \gamma$, which explicitly arises from the broken particle-hole symmetry.

This result from Ref. [91] has been obtained analytically within the linearized TDGL model. In order to study *nonlinear* (with respect to the order parameter) properties of IFE and its possible application to the optical generation of quantum vortices we made a numerical analysis of the TDGL Eqs. (2.3, 2.13), which is presented below.

2.2 IFE in the nonlinear TDGL model

In this section we address specific model of the 2D mesoscopic superconductor attached to the isolating substrate of the temperature T_0 (which can effectively remove the heat from the sample) and exposed to the circularly polarized THz radiation. The temporal evolution of the complex-valued order parameter $\psi(\mathbf{r},t)$ and the electric scalar potential $\varphi(\mathbf{r},t)$ in a superconductor square film is described by the modified TDGL equations in the compact form

$$\tau_\psi\big(1+i\gamma\big)\tilde{\partial}_t\psi = \big\{a(t)-|\psi|^2-\xi^2\mathbf{D}^2\big\}\psi + f(\mathbf{r},t), \tag{2.19}$$

$$\nabla^2\varphi + \frac{\hbar}{2e\tau_{\text{GL}}}\text{div}\mathbf{j}_s = 0, \tag{2.20}$$

which are supplemented by the boundary conditions

$$\mathbf{D}\cdot\mathbf{n}\Big|_S\psi = 0, \quad \nabla\varphi\cdot\mathbf{n}\Big|_S = 0. \tag{2.21}$$

Here covariant operators $\mathbf{D} = (-i\boldsymbol{\nabla} - \frac{2\pi}{\Phi_0}\mathbf{A})$ and $\tilde{\partial}_t = (\frac{\partial}{\partial t} + \frac{2e}{\hbar}i\varphi)$ are introduced; ψ is expressed in terms of the equilibrium value of the order parameter in the absence of fields ψ_0; $\mathbf{A}$ is a vector potential; $\mathbf{j}_s = \text{Im}[\psi(\boldsymbol{\nabla} + i\frac{2\pi}{\Phi_0}\mathbf{A})\psi^*]$ is a supercurrent density;

$$a(t) = \frac{T_c - T(t)}{T_c - T_0}$$

is a temperature profile created by the homogeneous laser heating (which can also model a quench of a superconductor). The parameter $\tau_\psi = (\pi\hbar/8k_BT_c)/(1-T_0/T_c)$ is an order parameter relaxation time at the temperature T_0. As a length unit we use here the coherence length $\xi = \xi_0/\sqrt{1-T_0/T_c}$ and the time unit is $\tau_{\text{GL}} = \tau_\psi/u$, where u is the dimensionless characteristic time scale of the TDGL theory [11, 247]. Thermal fluctuations in a superconductor can be simulated using a delta-correlated stochastic force $f(\mathbf{r},t)$ [108, 267, 268], which is normalized as

$$\langle f(r,t)f(r',t')\rangle \approx (4\pi 16\xi^2\lambda_L^2\tau_\psi T_c/\Phi_0^2)\delta(r-r')\delta(t-t'),$$

where $\langle\ldots\rangle$ means averaging over fluctuations, λ_L is the London penetration depth and Φ_0 is a magnetic flux quantum. The origin of the coordinate system is chosen in the center of the sample, so that $\{x,y\}\in[-L/2,L/2]$.

For a rather small sample of the size L much less than the wavelength of the electromagnetic radiation one can assume the electric field $\mathbf{E}_{\text{ext}}(\mathbf{r},t)$ of the electromagnetic wave to be uniform over the superconductor (see Fig. 2.6(a)), and the corresponding time-dependent dimensionless vector potential can be written as follows

$$\mathbf{A}_{\text{ext}}(t) = \text{Re}\Big[-ic\frac{E_{\text{ext}}}{\omega}(\mathbf{x}_0+\sigma_\pm i\mathbf{y}_0)e^{-i\omega t}\Big].$$

Here c is the speed of light and the circular polarization is defined as $\sigma_\pm = \pm 1$ for different helicity of the electromagnetic wave. Dimensional unit for an electric field amplitude is $E_0 = \hbar/2e\tau_{\text{GL}}\xi$, for a supercurrent and magnetic moment per unit area is $j_0 = M_0c = \sigma_nE_0$, where σ_n is a conductivity of a superconductor in a normal state and c is the speed of light. We consider the case of small lateral sizes $L \ll \lambda_L^2/d$, where d is the sample thickness, therefore we can neglect the contribution to the magnetic field induced by the supercurrents. This condition allows us to treat the function $\mathbf{A}_{\text{ext}}(t)$ as an external source in the Eqs. (2.19, 2.20) by using a direct

substitution $\mathbf{A} \equiv \mathbf{A}_{\text{ext}}$.

Numerical calculation [92] is implemented as follows: for each moment of time, the Poisson's equation (2.20) for the potential φ is solved using the Fourier method; then using the value of $\varphi(x, y, t)$ we find the order parameter from Eq. (2.19) in the next time step $\psi(x, y, t + \Delta t)$ using the semi-implicit Crank-Nicolson scheme (needed to treat the nonlinear term).

2.2.1 Stationary regime of IFE

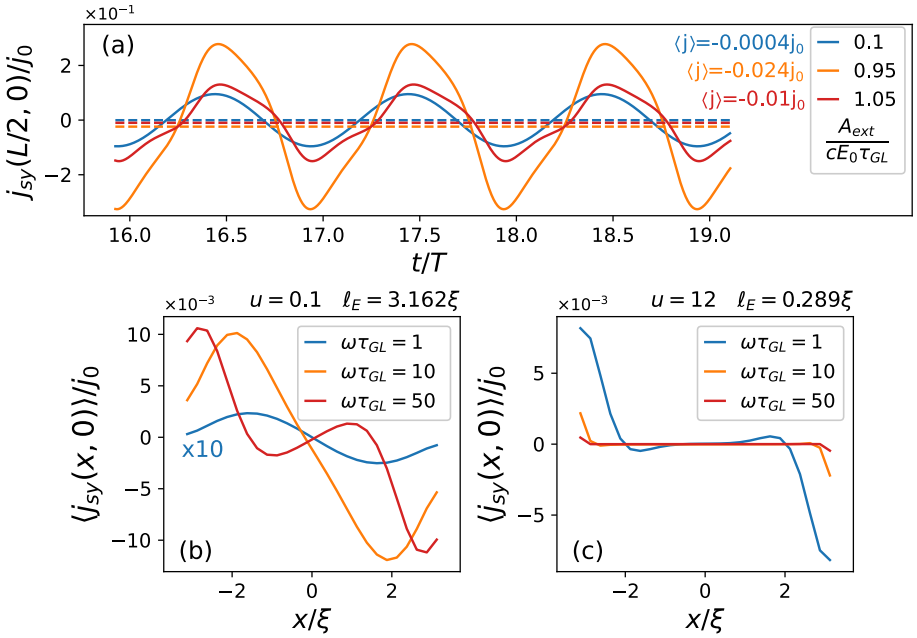

Figure 2.4: (a) Steady-state oscillations of the supercurrent $j_{sy}(x = L/2, y = 0, t)$ in the square superconductor with a side $L = 7\xi$ with a nonzero average $\langle j_{sy}\rangle_T$ (dashed lines) under the radiation of an external field with a frequency $\omega\tau_{\text{GL}} = 2$ (period $T = \pi\tau_{\text{GL}}$) for parameters $u = 1$, $\gamma = 0.3$. (b, c) Spatial distribution of the averaged supercurrent $\langle j_{sy}(x, y = 0)\rangle_T$ along a central section of the superconductor for different values of the electric field penetration length ℓ_E and frequency ω for $\gamma = 0.3$; the amplitude of the external field is different for the different frequencies with the fixed relation $E_{\text{ext}}/\omega = A_{\text{ext}}/c = 0.75(E_0\tau_{\text{GL}})$.

First, we address the stationary case - without heating and quench dynamics. An alternating harmonic electric field of a circularly polarized THz radiation of frequency ω induces a supercurrent with the density $\mathbf{j}_s(\mathbf{r}, t) = \text{Re}\sum_n \mathbf{j}_{s,n}(\mathbf{r})e^{in\omega t}$ including all harmonics $n\omega$ with an integer n. Note here that the even-n harmonics in the superconducting condensate response appear only for a nonzero imaginary part of the order parameter relaxation time: $\gamma \neq 0$. An example of the multi-harmonic oscillations of the supercurrent $\mathbf{j}_s$ is shown in Fig. 2.4(a). According to the IFE theory for the superconducting condensate [91], the same parameter γ is responsible for a nonzero averaged supercurrent induced by the electromagnetic wave

$$\langle \mathbf{j}_s(\mathbf{r})\rangle_T = \frac{1}{T}\int_0^T \mathbf{j}_s(\mathbf{r}, t)dt, \tag{2.22}$$

where $T = 2\pi/\omega$ is a period of the electric field. The direction of the current flow is determined by the helicity of the circular polarized wave $\sigma_\pm$. The spatial distribution of the dc current is controlled by two characteristic length scales: (i) the electric field penetration length [11, 269] $\ell_E = \xi/\sqrt{u}$; (ii) the phenomenological frequency-dependent length $\ell_\omega \sim \xi/\sqrt{\omega}$. While the first length ℓ_E is the length of conversion of normal currents to the superconducting ones, the ℓ_ω

value can be qualitatively considered as a localization scale of the order parameter amplitude and phase [91]. It is worth noting that the applicability of the TDGL model for externally driven processes is provided by a condition $\omega\tau_{\text{GL}} < T_c/(T_c - T_0)$, where T_c is a critical temperature of a superconductor and T_0 is a substrate temperature. From the general constraint on the time variation of the order parameter $\omega_{GL} \equiv \tau_{\text{GL}}^{-1} \ll \tau_\varepsilon^{-1}$, where τ_ε is the inelastic relaxation time of quasiparticles [11, 269], we obtain an additional condition $\omega \ll T_c/(T_c - T_0)\tau_\varepsilon^{-1}$, which is always satisfied in the vicinity of T_c.

The distribution of y-component of the dc current $\langle \mathbf{j}_s \rangle_T$ induced by the radiation with σ_+ polarization for different values of ω and u is presented in Fig. 2.4. It is straightforward from the fourfold symmetry of the problem that the distribution $\langle j_{sx}(x = 0, y)\rangle_T$ can be obtained by $\pi/2$ rotation. For convenience, the amplitude of the time-dependent vector potential $A_{\text{ext}} = cE_{\text{ext}}/\omega$ is fixed for all plots: $A_{\text{ext}} = 0.75(cE_0\tau_{\text{GL}})$. We observe that the transition from the adiabatic $\omega\tau_{\text{GL}} \lesssim 1$ to the nonadiabatic $\omega\tau_{\text{GL}} \gg 1$ regime is accompanied by the strong decrease of the localization length of the supercurrent $\langle \mathbf{j}_s(\mathbf{r})\rangle_T$ for $u \ll 1$ and rather weak decrease for $u \gg 1$. The localization length of the supercurrent is determined by the frequency ω when the largest length scale in the superconductor is $\ell_E \sim L$ and mainly by the parameter u when this length scale is $\ell_\omega \lesssim L$ (see Fig. 2.4). Therefore the supercurrent is always localized at the smallest length scale $\sim \min\{\ell_E, \ell_\omega\}$.

2.2.2 DC magnetic moment

The averaged current $\langle \mathbf{j}_s \rangle_T$ produces a dc magnetic moment per unit area

$$\mathbf{M}_T = L^{-2} \int [\mathbf{r} \times \langle \mathbf{j}_s(\mathbf{r})\rangle_T] d\mathbf{r},$$

with a direction determined by the light polarization. The dependencies of the modulus of the magnetic moment $|\mathbf{M}_T| \equiv M_T$ on different parameters are shown in Fig. 2.5. Figure 2.5a demonstrate that with a small amplitude of the vector potential, the moment grows quadratically as $M_T \sim A_{\text{ext}}^2$ and after passing the maximum value at $A_{\text{ext}} \approx 0.75(cE_0\tau_{\text{GL}})$ the moment begins to decrease due to the suppression of the order parameter ψ, shown in Fig. 2.5(b). The term $|\mathbf{A}|^2$ in the TDGL equation for the order parameter can be treated as a negative contribution to the critical temperature T_c, therefore superconductivity is destroyed and the moment decreases to zero at $A_{\text{ext}} \approx 1.0(cE_0\tau_{\text{GL}})$, which corresponds to $E_{\text{ext}} \approx \omega\sqrt{0.5H_{c2}(T_0)\Phi_0}/c^2$ in dimensional units. At low frequencies and large amplitudes of the external field, the distribution of the order parameter and, correspondingly, the supercurrent $\mathbf{j}_s$ become strongly inhomogeneous, which leads to a shift of the maximum of $M_T(E_{\text{ext}})$ at $\omega\tau_{\text{GL}} = 1$ relative to the curves plotted for larger frequencies. The moment M_T as a function the frequency ω has a peak shown in Fig. 2.5(d). For the fixed amplitude of the external filed E_{ext} the moment grows linearly $M_T \sim \omega$ at $\omega\tau_{\text{GL}} \ll 1$ and decreases as $M_T \sim \omega^{-3}$ at $\omega\tau_{\text{GL}} \gtrsim 1$. This behavior is in a good agreement with the perturbative analytical solution provided in [91]. Using the optimal parameters one can achieve the most efficient interaction of the dc current produced by IFE with Abrikosov vortices generated by the thermal quench, which is discussed below.

2.2.3 All-optical Abrikosov vortex generation

Numerical simulation shows that the dc component of the supercurrent $\langle \mathbf{j}_s(\mathbf{r})\rangle_T$ is too weak to create the Abrikosov vortex on its own (e.g. strongly suppress the critical field H_{c1}), but

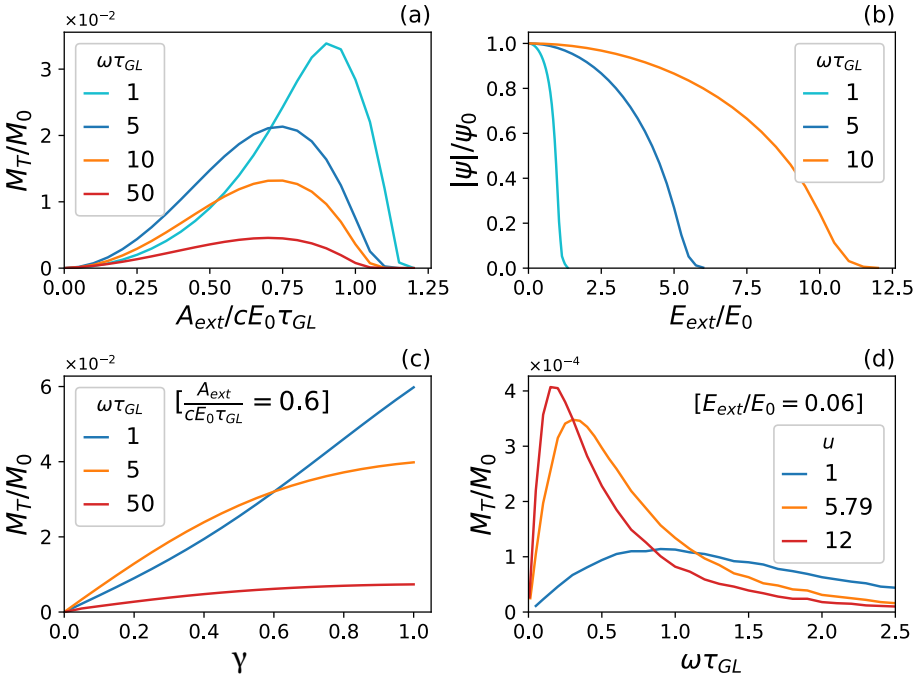

Figure 2.5: Dependence of the dc magnetic moment M_T in the square superconductor with a side $L = 7\xi$ on different parameters (a, c, d). Subplot (b) shows the dependence of the amplitude of the order parameter $|\psi|(x = 0, y = 0)$ on the E_{ext} and corresponds to (a). Sets of parameters are chosen as follows: (a, b) $u = 1$, $\gamma = 0.3$; (c) $u = 1$, $A_{\text{ext}} = 0.6(cE_0\tau_{\text{GL}})$; (d) $\gamma = 0.3$, $E_{\text{ext}} = 0.06E_0$;

nevertheless it opens the possibility to implement purely optical generation using a thermal quench of the superconductor.

Note that the question of the vortex generation due to the direct transfer of the angular momentum to the superconducting condensate has already been addressed in Ref. [270]. However, the analysis in Ref. [270] was based on the linearized TDGL equation which can not properly describe an essentially nonlinear problem of the vortex generation. The linearized model simply does not allow selecting the stable solutions. Moreover, in Ref. [270] the purely real relaxation constant is considered, but in this case, the IFE is merely absent. In contrast, the present study proposes different mechanism of the vortex generation, where the IFE plays the key role and the nonlinear TDGL model was used for the correct description of all stages of nucleation and evolution of vortices.

In order to implement the optical generation of the Abrikosov vortices with a desired polarity, we consider a process consisting of two subsequent illumination stages (see Fig.2.6(a)):

• before the time instant $t = 0$ the superconductivity in the film is completely destroyed due to the sample heating by a strong laser pulse with the beam radius well exceeding the size L;

• a rapid thermal quench occurs at the second stage for $t > 0$ in the presence of a weak circularly polarized electromagnetic wave.

We assume that the temperature distribution over the film is uniform and its time evolution can be described by the phenomenological expression [74]: $T(t) = T_0 + (T_i - T_0)e^{-t/\tau_q}$, where T_i is an initial temperature of the superconductor and τ_q is a characteristic heat drain time. Following this model and taking $T_i > T_c$ we assume the homogeneous initial conditions $\psi(\mathbf{r}, t = 0) = 0$. After the start of the quench at $t = 0$, superconductivity begins to recover in the presence of the thermal fluctuations $f(\mathbf{r}, t)$ and, according to the Kibble-Zurek mechanism, the vortex-antivortex pairs appear throughout the sample. Further dynamics of these vortex pairs at times $t \gg \tau_q$ is affected by the circularly polarized radiation with the frequency ω. Since the induced current has

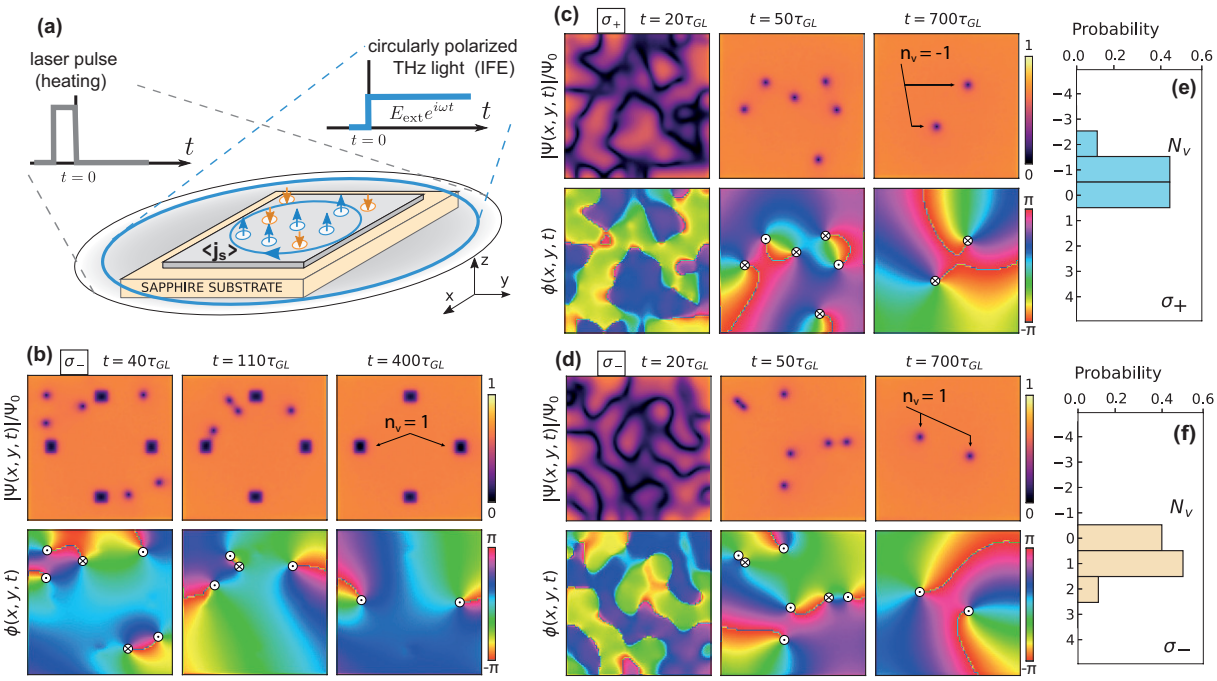

Figure 2.6: (a) Sketch of the proposed experimental setup: superconductor placed on a sapphire substrate is heated by an external laser pulse and then quenched in the presence of a circularly polarized light. (Orange)blue arrows show (anti-)vortices created after the rapid thermal quench. (c, d) Numerical simulations of a vortex nucleation and dynamics in the presence of a circularly polarized light with σ_+ and σ_- polarization. (b) Pinning of the vortex by a small square defect after vortex nucleation. Panels (b-d) show the modulus $|\psi|$ and the phase ϕ of the order parameter for different time instants. White circles with a dot(cross) denote vortices with a polarity $n_\mathrm{v} = 1(-1)$. (e, f) Probability of the creation of the vortices with a certain vorticity the for different polarizations σ_+ and σ_-. The number of the implementations (unique simulations) is $N_\mathrm{imp} = 20$ for each subplot. The set of parameters used for the calculation (b-f): $L = 80\xi$, $u = 1$, $\omega\tau_\mathrm{GL} = 10$, $\gamma = 0.3$, $E_\mathrm{ext} = 7.5E_0$, $\tau_q = 1.0\tau_\mathrm{GL}$.

both dc and ac components, the equation of the motion for the vortex has a quite complicated form. The alternating electric field produces local oscillations of the vortex position which are observable at $\omega \lesssim \tau_\mathrm{GL}^{-1}$ and are averaged at larger frequencies. The averaged part of the current produces a Lorentz force $f_L \sim \langle j \rangle_T$ acting on a single vortex. The direction of the force is defined both by the sign of the polarization $\sigma_\pm$ and the vortex winding number, or polarity:

$$n_\mathrm{v} = \frac{1}{2\pi} \oint_l \nabla \arg(\psi) dl,$$

where l is the anticlockwise oriented contour around a single vortex. In the following we use the term 'vortex' for $n_\mathrm{v} = 1$ and 'antivortex' for $n_\mathrm{v} = -1$. In the presence of the imaginary part of the relaxation time $\gamma \neq 0$ there is a Hall component of the vortex motion (see, e.g., [11]). Phenomenologically one can describe this effect as

$$\sigma n_\mathrm{v} \langle \mathbf{j}_s \rangle_T \times \mathbf{z}_0 = \alpha_1 \mathbf{v}_L + n_\mathrm{v} \alpha_2(\gamma) \mathbf{v}_L \times \mathbf{z}_0,$$

where $\mathbf{v}_L$ is the local vortex velocity, $\alpha_1 \mathbf{v}_L$ is the viscous drag force and α_2 corresponds to the Hall effect. It is useful to note that $\alpha_2(\gamma = 0) = 0$ [11, 99, 100].

The dynamics of the superconducting condensate during the quench process are presented in Fig. 2.6(c,d). At the initial stage $t \approx 20\tau_\mathrm{GL}$ we observe the nucleation of the vortex-antivortex pairs which are distributed randomly over the superconductor area since the quench is homogeneous. After that at $t \approx 50\tau_\mathrm{GL}$ the part of the pairs annihilates and the remaining (anti)vortices begin

to move in the presence of the induced supercurrent. Since the (anti)vortex-current interaction depends on the direction of the dc supercurrent, the current acts selectively expelling the vortices with a certain polarity from the sample. It is shown in Fig. 2.6(c,d) that for the $\sigma_\pm$ polarization only antivortices/vortices with $n_\mathrm{v} = \mp 1$ survive in the sample at the times $t \sim 700\tau_\mathrm{GL}$. In the absence of the pinning surviving (anti)vortices stay in the superconductor for quite a long time: they escape from the superconductor only for $t \gg 700\tau_\mathrm{GL}$. The formation of vortex-antivortex pairs is controlled by a stochastic force and in order to establish the correlation between a given polarization and the polarity of vortices surviving at large times one needs to consider a statistical dependence $N_\mathrm{v}(\sigma)$, where $N_\mathrm{v} = \sum n_\mathrm{v}$ is the sum over all vortices. This dependence is shown in Fig. 2.6(e,f) and it is clearly seen that $N_v(\sigma_+) \leq 0$ and $N_v(\sigma_-) \geq 0$ for $N_\mathrm{imp} = 20$ implementations for each polarization. Obviously, the distributions for σ_+ and σ_- should be symmetric in the limit $N_\mathrm{imp} \to \infty$. Note that among the results of calculations we also observe the implementations with $N_v = 0$ when all the vortices and antivortices are either annihilated or leaving the sample for the times $t \sim 700\tau_\mathrm{GL}$. In the case of linear polarization, which is the sum of two waves with opposite helicities, we observe only $N_v = 0$ for the times $t \gtrsim 700\tau_\mathrm{GL}$, since the IFE is absent.

Obviously, the escape of vortices from the superconductor can be additionally prevented by introduction of pinning centers. In order to strengthen the influence of pinning we should place these centers near the edges of the superconductor, where the dc supercurrent $\langle \mathbf{j}_s \rangle_T$ is maximal and plays, thus, a stronger role in separation of vortex-antivortex pairs [Fig. 2.5(b,c)]. An example of such a process is shown in Fig. 2.6(b) for the case of the square defects with locally suppressed superconducting critical temperature T_c. Numerical simulation shows that the polarity of the pinned vortices is consistent with the helicity of the light polarization, according to the statistical dependence $N_\mathrm{v}(\sigma)$. One can also consider a wide-ring geometry with the width $W \gg \xi$. In such a system the pinning of the locked vortices is replaced by the flux trapping. Numerical simulations (not presented here) again shows the correlation between the direction of the trapped flux and the light polarization. These observations prove the possibility of creation of vortices with a certain polarity in the absence of the applied magnetic field only by the circularly polarized electromagnetic wave. Generated vortices contribute to the dc magnetic moment providing, thus, a possibility to observe the enhanced IFE.

2.2.4 Proposals for experiments

Reduction in the parameter γ, used in the simulation of the vortex dynamics above, leads to a decrease in the amplitude of the averaged current (see Fig. 2.5(c)), which makes locking of a vortex with a desired polarity less likely. Therefore, an experimental observation of the light-induced vortex generation is possible in materials with relatively large imaginary part of the superconducting relaxation time $\gamma \sim T_c/E_F \lesssim 1$. Since the parameter γ is also responsible for the Hall effect and the Hall-anomaly in the vortex state of type-II superconductors [11, 99, 100], promising candidates for an experiment can be high-T_c compounds, where studies indicate relatively large Hall effect [101–105]. Among other possible candidates with quite a large relation $T_c/E_F \sim 0.3$ one can mention the class of actively studied iron selenides [106, 107].

Consider a specific example of a thin YBCO sample with the size $L \sim 0.1 - 4$ μm and $d \sim 10$nm. For the substrate temperature $T_0 \approx 0.98T_c$ (with $T_c \approx 90$ K) the typical frequency of the circularly polarized radiation used in the calculation corresponds to the far infrared range $\omega \sim 10/\tau_\mathrm{GL} \sim 50$ THz. Corresponding intensity of the polarized radiation at which the effect is the most pronounced is $\mathcal{I} \approx 5 \cdot 10^{-2}$ μW/μm^2. Note, that low temperature materials Nb or FeSe

with $T_c \sim 9$ K require a terahertz frequency range $\omega \sim 1 - 10$ THz. The control of the quench time τ_q in an experiment is possible due to good heat removal from the superconductor ensured by, for example, sapphire substrate film (see Fig. 2.4) with a typical thickness ~ 1 μm [77]. It provides large thermal conductivity $\sim 10^3$ W/mK [271], which ensures the heat transfer of a surface power density of the order of ~ 10 μW/μm^2 at the temperature change of the superconductor $\Delta T \sim 10^{-2}$ K.

Vortex polarity can be detected with the local vortex imaging provided by the SQUID measurements with sub-micron spatial resolution [272–274] the scanning magnetometry with nitrogen-vacancy centers in diamonds [275, 276], the magneto-optical imaging based on Faraday rotation of light polarization [61, 77, 277] or magnetic force microscopy technique [278, 279]. It is also possible to use an array of superconducting disks [280] simultaneously irradiated with polarized radiation, while the average magnetic moment can be measured using a standard SQUID magnetometer technique [281].

In summary, we theoretically showed that vortex-antivortex pairs created by a thermal laser pulse in a superconductor can be separated by the dc supercurrent induced by an external circularly polarized radiation due to IFE. This leads to effective locking of vortices with a certain polarity inside the superconductor, determined by the light polarization. The findings of this research can be applied in experiments on a fast vortex manipulation in mesoscopic superconductors.

2.3 Fluctuation-mediated IFE in a superconducting ring

In this subsection we want to study the problem of IFE in superconductors at temperatures above the critical T_c, where the superconductivity is maintained by fluctuating Cooper pairs [111]. It is known that superconductors in the fluctuation regime are sensitive to the particle-hole asymmetry and can exhibit Hall effect [2] , resulting in the appearance of the nondiagonal component of conductivity tensor $\sigma_{xy} \propto \gamma$ [96, 108, 282–284]. This may serve as a hint for the observation of IFE due to their similar physical nature [91].

Note that at $T > T_c$ the normal contribution to the total response of the superconductor is large and Hall effect comes from both subsystems simultaneously. It is curious that the *normal* Hall effect is also associated with the particle-hole asymmetry (see Fig. 2.1(left)). The Hall conductivity in the Drude model reads $\sigma_{xy} = \sigma_D \omega_c \tau/(1+\omega_c^2\tau^2)$, where τ is the scattering time and $\omega_c = |eH/m^*c|$ is the cyclotron frequency. The effective mass near the Fermi level is defined as $1/m^* \propto \partial^2 E_p/\partial p^2$, which is nonzero only if the small deviation of the QP spectrum from linearity is taken into account [Eq. (2.4)]. Thus, the finite curvature of the QP spectrum affects both normal and superconducting [2] Hall effects [98, 285].

We consider the simple geometry of a quasi-one-dimensional ring for which both the fluctuation state [286–290] and the IFE below T_c [93, 94] are well studied. For the ring system the IFE reveals itself as a generation of the dc component of the fluctuation supercurrent induced by an external circularly polarized radiation. This current can be manipulated by an applied magnetic flux Φ, which additionally controls the dynamics of order parameter (see Fig. 2.7). Fluctuation regime is of particular interest because of singular behavior of the response function in the vicinity of the critical temperature (due to formally infinite correlation $\xi(T)$ in the system). Although the IFE associated with particle-hole asymmetry is usually of the order of $\sim T_c/E_F \ll 1$, the fluctuation enhancement of the supercurrent for $T \to T_c$ can be noticeable against the background of the normal IFE, which in weakly sensitive to the temperature.

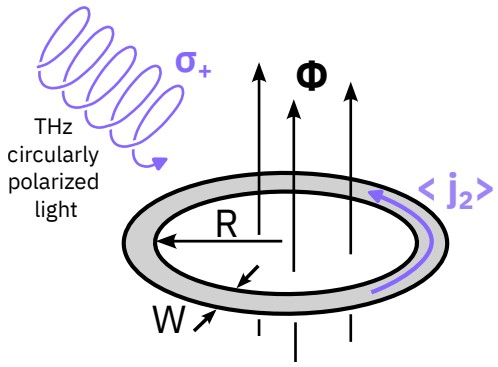

Figure 2.7: Sketch of a ring with dc supercurrent $\langle j_2 \rangle$ induced by the circularly polarized radiation with σ_+ polarization in the presence of external magnetic flux Φ.

Consider a superconducting ring with a radius R and a width $W \ll \xi_0/\sqrt{\epsilon}$, where ξ_0 is a coherence length at zero temperature and ϵ is the reduced temperature. The ring is exposed to (i) circularly polarized light radiation, which is assumed to be homogeneous and described with the electric field $\boldsymbol{E}(\theta,t) = E_0 \cos(\theta - \omega t)\boldsymbol{\theta}_0$ and (ii) constant magnetic flux Φ. The dynamics of fluctuating order parameter $\Psi(\theta,t)$ is described within a time-dependent Ginzburg-Landau

[2] Note that this fluctuating Hall effect is due to the direct interaction of the Cooper pair and the electromagnetic field, while below T_c the Hall effect is usually associated with vortex motion.

theory [108], and the corresponding linearized equation reads

$$\frac{\pi\alpha}{8}(1+i\gamma)\frac{\partial\Psi}{\partial t}+\alpha T_{c0}\Big[\epsilon+\Big\{\frac{\xi_0}{R}(\hat{n}-A_\Phi)-A_\omega(t)\Big\}^2\Big]\Psi=\zeta(\theta,t), \tag{2.23}$$

where $\alpha=(4mT_{c0}\xi_0^2)^{-1}$; $\epsilon=T/T_{c0}-1$ is the reduced temperature; and T_{c0} is a critical temperature in the absence of magnetic flux. Note, that hereafter we put $\hbar=c=1$. We introduce here the imaginary part of the relaxation constant $\gamma\propto T_{c0}/E_F$, which is responsible for IFE in superconductors [91]; the angular momentum operator $\hat{n}=-i\partial_\theta$; and dimensionless vector potential which has a part from the external magnetic flux $A_\Phi=\Phi/\Phi_0$, where $\Phi_0=\pi/e$, and from the external electric field $A_\omega(t)=A_0/2e^{i(\theta-\omega t)}+$ c.c. with the amplitude $A_0=2e\xi_0E_0/\omega$.

The stochastic (Langevin) force $\zeta(t,\theta)$ in the RHS of Eq. (2.23) originates from the thermal noise and its presence is required to maintain a nonzero thermal average of the short-lived fluctuations of the Cooper pairs above T_c. Thus, all measured quantities Q should be averaged over all possible configurations of the stochastic field $\psi(\mathbf{r},t)$ in thermal equilibrium, what in general case can be found as $\langle Q\rangle=\mathrm{Tr}(Q\exp\{-F_{GL}/T_{c0}\})/\mathrm{Tr}(\exp\{-F_{GL}/T_{c0}\})$ [108]. The correlator of Langevin force satisfies the dissipation-fluctuation theorem and reads

$$\langle\zeta^*(t,\theta)\zeta(t',\theta')\rangle=2T(\pi\alpha/8)\xi_0^{-3}\delta(\theta-\theta')\delta(t-t').$$

Using the chosen notation one can write a general expression for the averaged θ-component of the supercurrent:

$$\langle j(t)\rangle=\frac{e}{mR}\Big\langle\Psi^*\Big[\hat{n}-A_\Phi-(R/\xi_0)A_\omega\Big]\Psi+\text{c.c.}\Big\rangle. \tag{2.24}$$

2.3.1 DC response of the superconductor

Next we consider the amplitude of the vector potential A_0 as a small parameter, which allows us to use a perturbation theory with the expansion $\Psi=\sum_{i=0}\Psi_i$, where $\Psi_i\propto(A_0)^i$. In order to get a dc part of the supercurrent we consider only 0-th and 2-nd orders in the expansion of the current (2.24), which read

$$\langle j_0\rangle=\frac{2e}{mR}\mathrm{Re}\langle\Psi_0^*(\hat{n}-A_\Phi)\Psi_0\rangle, \tag{2.25}$$

$$\langle j_2\rangle=\frac{2e}{mR}\int_0^{\frac{2\pi}{\omega}}\mathrm{Re}\Big[\langle\Psi_0^*(\hat{n}-A_\Phi)\Psi_2\rangle+\langle\Psi_2^*(\hat{n}-A_\Phi)\Psi_0\rangle$$
$$+\langle\Psi_1^*(\hat{n}-A_\Phi)\Psi_1\rangle-(R/\xi_0)2A_\omega(t)\mathrm{Re}\langle\Psi_0^*\Psi_1\rangle\Big]\frac{2\pi dt}{\omega}, \tag{2.26}$$

where $\langle j_i\rangle\propto(A_0)^i$. The functions Ψ_i can be found from Eq. (2.23) using perturbation method [108, 110]. One can rewrite Eq. (2.23) in the operator form as follows

$$\Big(\hat{L}_0^{-1}-\hat{L}_1-\hat{L}_2\Big)\Psi(\theta,t)=\zeta(\theta,t), \tag{2.27}$$

where

$$\hat{L}_0^{-1} = (1+i\gamma)\frac{\partial}{\partial t} + \alpha T_c\Big[\epsilon + \frac{\xi_0^2}{R^2}(\hat{n}-A_\Phi)^2\Big], \tag{2.28}$$
$$\hat{L}_1 = \alpha T_c \frac{\xi_0}{R}\Big[(\hat{n}-A_\Phi)A_\omega + A_\omega(\hat{n}-A_\Phi)\Big],$$
$$\hat{L}_2 = -\alpha T_c A_\omega^2.$$

Note that the use of perturbation theory implies restrictions on the frequency range that must satisfy

$$\omega \gg \frac{\xi_0}{R}\frac{2e\xi_0 E_0}{\epsilon}, \quad \frac{R}{\xi_0}2e\xi_0 E_0 \tag{2.29}$$

This means that the limit of low frequencies can be treated only if the condition $E_0/\omega \to 0$ is satisfied.

The expansion terms of the order parameter $\Psi(\theta,t)$ can be found straightforwardly as

$$\Psi_i = \hat{L}_0\hat{L}_1\Psi_{i-1} + \hat{L}_0\hat{L}_2\Psi_{i-2}$$

with $\Psi_0 = \hat{L}_0\zeta$. The $\hat{L}_0$ operator is diagonal in the angular momentum eigenmode representation

$$\Psi(\theta,t) = \sum_{n=-N}^{N}\int\frac{d\Omega}{2\pi}\Psi(n,\Omega)e^{i(n\theta-\Omega t)} \tag{2.30}$$

and its eigenvalue is

$$L_0(n,\Omega) = \frac{1}{\alpha T_c\varepsilon_n - i(1+i\gamma)\Omega} \quad \text{with} \quad \varepsilon_n = \epsilon + \frac{\xi_0^2}{R^2}(n-\Phi/\Phi_0)^2.$$

Note that only rings with $R \gg \xi_0$ can be considered in the framework of the Ginzburg-Landau theory, which gives us a constraint on the maximum number of modes inside the ring $N = 2\pi R/\xi_0$.

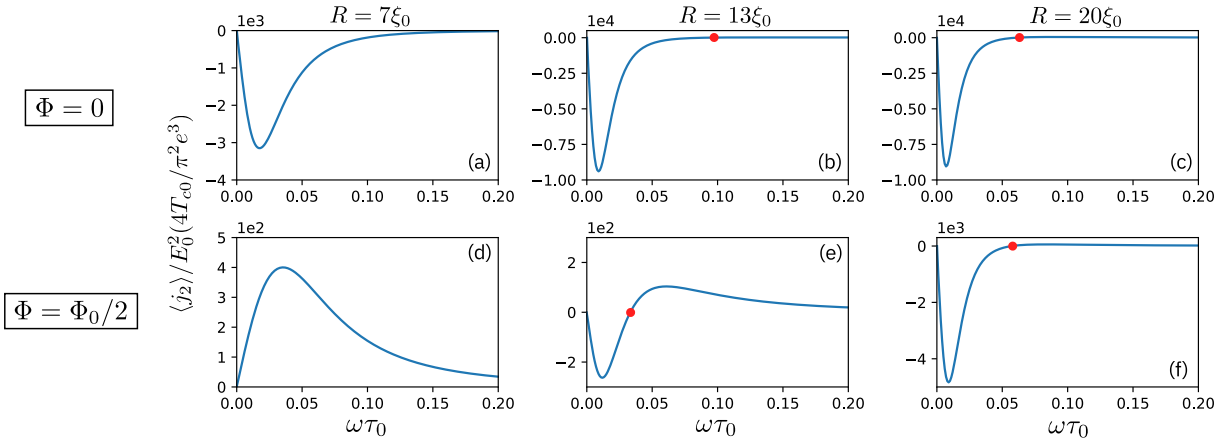

Figure 2.8: The frequency dependence of the dc supercurrent $\langle j_2\rangle/E_0^2$ from Eq. (2.33) for $\Phi = 0$ (a-c) and $\Phi = \Phi_0/2$ (d-f) for different ring radii $R/\xi_0 = 7, 13, 20$. The parameters are $\epsilon = 0.005$ and $\gamma = 0.01$. Red dots mark the zero crossing.

By substituting the wave function (2.30) into Eq. (2.25) we get the zeroth order current

produced by the magnetic flux

$$\langle j_0\rangle = \frac{8eT_{c0}}{\xi_0^2}\frac{\xi_0}{R}\sum_n \frac{n-\Phi/\Phi_0}{\epsilon+\frac{\xi^2}{R^2}(n-\Phi/\Phi_0)^2}. \tag{2.31}$$

This is a periodic function of Φ with a period of a flux quantum, hence it is sufficient to consider an interval $|\Phi| \leqslant \Phi_0/2$, within which the critical temperature depends on the flux Φ as

$$T_c = T_{c0}\Big(1-\frac{\xi_0^2}{R^2}\frac{\Phi^2}{\Phi_0^2}\Big). \tag{2.32}$$

This is nothing but Little-Parks effect [291]. Generally, the current (2.31) will dominate over small response $\langle j_2\rangle$, however, it can be shown [292] that this current vanishes exactly at $\Phi = \pm\Phi_0/2$ (and obviously at $\Phi = 0$). Namely these two cases will be considered below. The current of the second order in A_ω from Eq. (2.26) reads

$$\begin{aligned}\langle j_2\rangle = \frac{\pi^2e^3}{4T_{c0}}\frac{\xi_0}{R}\frac{E_0^2}{\omega^2\tau_0^2}\sum_n &-\frac{1}{\varepsilon_n}\frac{(2(n-A_\Phi)+1)(\varepsilon_+ +\varepsilon_n+\gamma\omega\tau_0)}{(\varepsilon_+ +\varepsilon_n)^2+2\omega\tau_0\gamma(\varepsilon_+ -\varepsilon_n)+\omega^2\tau_0^2}\\ &+\frac{1}{\varepsilon_n}\frac{(2(n-A_\Phi)-1)(\varepsilon_- +\varepsilon_n-\gamma\omega\tau_0)}{(\varepsilon_- +\varepsilon_n)^2-2\omega\tau_0\gamma(\varepsilon_- -\varepsilon_n)+\omega^2\tau_0^2}-\frac{n-A_\Phi}{\varepsilon_n^2}\\ +\frac{\xi_0^2}{R^2}\frac{n-A_\Phi}{2\varepsilon_n^2}&\left[\frac{(2n-2A_\Phi+1)^2(\varepsilon_+ +\varepsilon_n+2\gamma\omega\tau_0)}{(\varepsilon_+ +\varepsilon_n)^2+2\omega\tau_0\gamma(\varepsilon_+ -\varepsilon_n)+\omega^2\tau_0^2}+\frac{(2n-2A_\Phi-1)^2(\varepsilon_- +\varepsilon_n-2\gamma\omega\tau_0)}{(\varepsilon_- +\varepsilon_n)^2-2\omega\tau_0\gamma(\varepsilon_- -\varepsilon_n)+\omega^2\tau_0^2}\right]\\ &+\frac{\xi_0^2}{2R^2}\left[\frac{1}{\varepsilon_n\varepsilon_+}\frac{(2n-2A_\Phi+1)^2(n-A_\Phi+1)(\varepsilon_+ +\varepsilon_n)}{(\varepsilon_+ +\varepsilon_n)^2+2\omega\tau_0\gamma(\varepsilon_+ -\varepsilon_n)+\omega^2\tau_0^2}\right.\\ &\left.+\frac{1}{\varepsilon_n\varepsilon_-}\frac{(2n-2A_\Phi-1)^2(n-A_\Phi-1)(\varepsilon_- +\varepsilon_n)}{(\varepsilon_- +\varepsilon_n)^2-2\omega\tau_0\gamma(\varepsilon_- -\varepsilon_n)+\omega^2\tau_0^2}\right].\end{aligned} \tag{2.33}$$

Here we introduced the time units $\tau_0 = \pi/8T_{c0}$ and shifted functions $\varepsilon_\pm \equiv \varepsilon_{n\pm1}$.

We consider two flux values $\Phi = 0$ and $\Phi = \Phi_0/2$, so that the contribution to the total direct current is determined only by the component $\langle j_2\rangle$ induced by external light radiation. The frequency dependence of the fluctuation current from Eq. (2.33) is shown in Fig. 2.8. For $\omega > 0$ the electric field $\boldsymbol{E}(\theta,t)$ rotates counterclockwise, which can be defined as σ_+ polarization. As can be seen in Fig. 2.8, the current $\langle j_2\rangle$ can flow either with or against the rotation of the field. For rings with large radii the interplay between different harmonics of the order parameter leads to a change in the direction of the current with increasing frequency. Note that the direction of the current $\langle j_2\rangle$ is also defined by the sign of the parameter of the particle-hole asymmetry γ, which usually depends one the band structure of a material [11, 108]. Thus, for $\Phi = 0$ and $\Phi_0/2$ we have $\langle j_2\rangle(-\gamma) = -\langle j_2\rangle(\gamma)$. As expected, the dc response of a superconductor (or IFE) crucially depends on γ, so that $\langle j_2\rangle(\gamma = 0) = 0$. Changing the polarization from σ_+ to σ_- is equivalent to changing $\omega \to -\omega$, with respect to which the current is odd $\langle j_2\rangle(-\omega) = -\langle j_2\rangle(\omega)$. This reflects the correlation between the polarization of the external radiation and the orientation of the induced dc supercurrent. Naturally we have $\langle j_2\rangle(\omega \to 0) = 0$ (if the limit $E_0/\omega \to 0$ holds).

In order to find the temperature dependence of $\langle j_2\rangle$ in the vicinity of T_c it is convenient to extract leading terms in Eq. (2.33). More precisely for $\Phi = 0$ there is one leading mode with $n = 0$ which dominates in the temperature region $\epsilon \ll \xi_0^2/R^2$ and diverges at the superconducting transition. Similarly for $\Phi = \Phi_0/2$ there are two contributing modes $n = 0, 1$ in the region

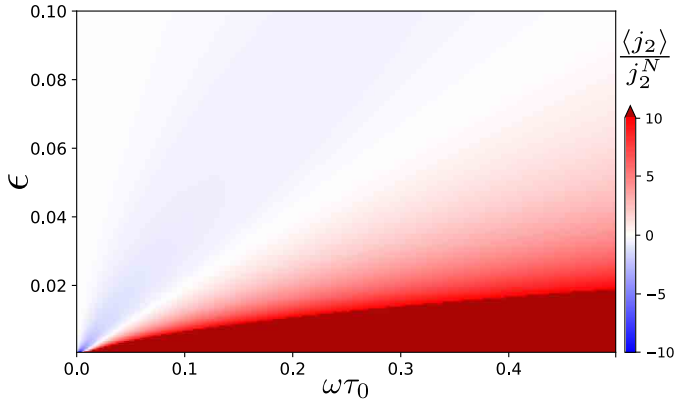

Figure 2.9: The ratio of the super- and normal dc current components generated by the circularly polarized light $\langle j_2\rangle/j_2^N$ in the ring with $R = 20\xi_0$ for different frequencies and temperature detuning $\epsilon = T/T_{c0} - 1$. The applied magnetic flux is zero $\Phi = 0$ and $\gamma = 0.01$. The amplitude of the current is truncated at the value $\langle j_2\rangle/j_2^N = 10$.

$\tilde{\epsilon} \ll \xi_0^2/R^2$, where $\tilde{\epsilon} = (T - T_c)/T_{c0}$ with $T_c = T_{c0}(1 - \xi_0^2/4R^2)$. Thus, in the vicinity of the critical temperature (2.32) the dc current (2.33) can be written as follows

$$\langle j_2\rangle \approx \gamma \frac{\pi^2 e^3}{2T_{c0}} \frac{\xi_0}{R} \frac{E_0^2}{\omega\tau_0} \begin{cases} -\frac{1}{\epsilon} \frac{\omega^2\tau_0^2 + \frac{\xi_0^2}{R^2}\epsilon}{\left[\frac{\xi_0^4}{R^4} + \omega^2\tau_0^2\right]^2 - 4\gamma^2\omega^2\tau_0^2\frac{\xi_0^4}{R^4}} & \text{for } \Phi = 0 \\ \frac{1}{\tilde{\epsilon}^2} \frac{\frac{2\xi_0^2}{R^2}\left[\omega^2\tau_0^2 - \frac{\xi_0^2}{R^2}\tilde{\epsilon}\right]}{\left[4\frac{\xi_0^4}{R^4} + \omega^2\tau_0^2\right]^2 - 16\gamma^2\omega^2\tau_0^2\frac{\xi_0^4}{R^4}} & \text{for } \Phi = \Phi_0/2. \end{cases} \tag{2.34}$$

The degeneracy of the modes $n = 0$ and $n = 1$ for $\Phi = \Phi_0/2$ strongly enhances the dependence of the dc current on the temperature detuning and change the divergence degree from $\langle j_2\rangle \propto \epsilon^{-1}$ for the case of zero magnetic flux, where only one mode strongly contributes to fluctuations, to $\langle j_2\rangle \propto \tilde{\epsilon}^{-2}$. This feature is typical for the rings with half the flux quantum and was considered in Ref. [293]. Note that the divergence peak at $T = T_c$ should be smeared by a smooth transition to the region $T < T_c$, which can be obtained by taking into account nonlinear terms in Eq. (2.23).

2.3.2 Contribution from the normal current

In general case, the dc response of the superconductor coexists with that from the normal current, and their contribution should be compared in the vicinity of T_c. For a qualitative discussion we introduce some phenomenological penetration length of the dc normal current ℓ_N. If the ring has a width $\ell_N \ll W$, then there are two oppositely directed dc currents along the inner and outer radius, which can lead to the vanishing of the total normal current averaged over the ring width. Otherwise, for a ring with $W \ll \ell_N$ there is nonzero homogeneous θ-component of the normal current $j_2^N \neq 0$, the value of which can be simply estimated using an approach developed in Ref. [83]. Consider 1D normal ring and write the continuity equation for the normal electron density ρ_e and velocity of the electron fluid:

$$\frac{\partial\rho_e}{\partial t} + \frac{1}{R}\frac{\partial}{\partial\theta}(\rho_e v) = 0. \tag{2.35}$$

The normal current is defined as $j_N = e\rho_e v = \sigma_N E$, where $\sigma_N(\omega) = i\rho_e e^2/m\omega$ is a conductivity of a metal. We assume the external electric field to be homogeneous over the size of the ring $E(\theta, t) = \frac{1}{2}(\delta E e^{-i\omega t} + \delta E^* e^{i\omega t})$, with $\delta E = E_0 e^{i\theta}$. Following Hertel's derivation in Ref. [83]

we consider a small deviation of the electron density and the velocity from their stationary (or time-averaged values) and get an expression for the dc current quadratic in the field amplitude E_0:

$$j_2^N = \frac{\rho_e e^3}{4m^2\omega^3}\Big[\delta E^*\Big(-i\frac{1}{R}\frac{\partial}{\partial\varphi}\Big)\delta E + \text{c.c}\Big] = \frac{\rho_e e^3}{2m^2\omega^3}\frac{E_0^2}{R}. \tag{2.36}$$

The two contributions from Eqs. (2.36) and (2.33) can be directly compared:

$$\langle j_2\rangle / j_2^N \approx 20\pi(\omega\tau_0)F[\omega,\epsilon]T_{c0}/E_F. \tag{2.37}$$

Here the function F corresponds to the dimensionless sum $\sum_n(\dots)$ in Eq. (2.33). For example, if we choose $T_{c0}/E_F = 0.01$ (meaning $\gamma \sim 0.01$), we get $\langle j_2\rangle/j_2^N \approx \omega\tau_0 F[\omega,T]$. The ratio of the two contributions to IFE is shown in Fig. 2.9 for different frequencies and temperatures. As expected, with a decrease in ϵ the supercurrent amplitude increases and the contribution from fluctuations dominates. The full dc response $\langle j_2\rangle + j_2^N$ is determined by the polarization of the external light, as well as by the temperature and frequency, since the supercurrent can change its direction. Note that for the $\Phi = \Phi_0/2$ case the divergency of $\langle j_2\rangle$ at the critical temperature is much stronger, which substantially increase the region of domination of superconducting IFE.

A suitable setup for *experimental observation* of the IFE in the fluctuation regime can be an array of superconducting rings made of either high-T_c cuprate compounds [99, 101], or iron-based materials such as FeSe [107], where the relatively large value of γ is expected. Such an array can be exposed to circularly polarized laser radiation in terahertz or far-infrared frequency range (with $\omega \sim T_{c0}/\hbar$). The registration of the magnetic momentum, associated with the dc current in the rings can done with standard SQUID measurements, scanning magnetometry with nitrogen-vacancy centers in diamond [275], or magneto-optical imaging [277].

2.4 Summary and outlook

We considered a general phenomenological Ginzburg-Landau approach for a superconducting condensate with broken particle-hole symmetry. We have demonstrated how this asymmetry affects the dynamics of the superconducting order parameter and modify corresponding time-dependent GL equations. As an example we study the inverse Faraday effect in the superconducting film of finite size induced by an external electromagnetic wave. In comparison with the seminal work [91] we addressed the nonlinear regime in terms of the order parameter and showed dependence of the dc magnetic moment on the amplitude of the external electromagnetic field. The obtained spatial distribution of the dc supercurrent allowed us to develop an effective scheme of all-optical vortex generation. Using numerical simulations we implemented a two-stage protocol and showed that vortex-antivortex pairs created in a superconductor by a strong *thermal laser pulse* (according to Kibble-Zurek mechanism) can be separated by the dc supercurrent induced by additional *polarized radiation* due to IFE. This leads to effective locking of vortices with a certain polarity determined by the light polarization. More precisely we established a strong statistical correlation between the polarity of the vortices generated by this protocol and the polarization (or helicity) of the external radiation. The findings of this research contribute to the rapidly developing field of optofluxonics and can be directly applied to experiments on fast vortex manipulation in mesoscopic superconductors.

We have studied the mechanism of the IFE in the fluctuation regime above the critical temperature T_c using the example of a one-dimensional superconducting ring. We demonstrated the possibility of generation of the dc supercurrent in the ring by external circularly polarized radiation. For fixed parameters the direction of the current is unambiguously determined by the light helicity. In such a geometry, the external magnetic flux Φ can significantly affect the dynamics of the order parameter. For instance, applying half of the flux quantum leads to an enhancement of the temperature dependence of the fluctuation supercurrent from $\langle j\rangle(\Phi = 0) \propto (T - T_c)$ to $\langle j\rangle(\Phi = \Phi_0/2) \propto (T - T_c)^2$. Note that the transition of the fluctuation response through the T_c point (or the region of critical fluctuations) should be smeared out due to non-Gaussian corrections to the TDGL equation [108, 215], which is beyond our linearized model [Eq. 2.23]. However, one can expect that in the vicinity of T_c the supercurrent contribution to the IFE can exceed the normal one (insensitive to T_c), which can be an observable hallmark of the fluctuation IFE in superconductors.

Chapter 3

Collisionless dynamics of a superconducting gap excited by spin-splitting field

In this Chapter we study the coherent dynamic interaction of a time-dependent spin-splitting field with the homogeneous superconducting order parameter $\Delta(t)$ mediated by spin-orbit coupling. We begin with the specific physical model and quantum mechanical theory of Bogoliubov-de Gennes. Then the linear response of the superconductor in the presence of the Zeeman field is investigated. In the last part we analyze the nonadiabatic dynamics of quasiparticle states in strong Zeeman field.

Our goal is to address the dynamical aspects of the nonequilibrium state of a superconducting condensate excited in the presence of both a spin-splitting field and SOC. For the sake of simplicity we consider specific system of an uniform superconductor at zero temperature $T = 0$ and consider short timescale $t \ll \tau_\varepsilon$ at which the collisionless regime holds, so one can treat the system with the pure quantum-mechanical approach within the time-dependent Bogoliubov-de Gennes (TDBdG) equations [161]. We assume a homogeneous SOC and a spin-splitting field with only one component $\mathbf{h}(t) = h(t)\mathbf{z}_0$.

A simple approach based on the expansion of the QP wave function in terms of the eigenstates of the BdG Hamiltonian $\psi(t) = \sum_n C_n(t)\Psi_n$ can be developed. The behavior of the QPs and related self-consistent gap function $\Delta(t)$ are determined by the coefficients $C_n(t)$, which describe how the states with a specific spin quantum number and momentum are refilled due to nonstationary transitions.

3.1 Time-dependent Bogoliubov-de Gennes theory

We consider a homogeneous s-wave superconductor in the presence of the uniform time-dependent Zeeman field $h(t)$ and Rashba spin-orbit coupling (RSOC). The coherent QP dynamics is governed by the TDBdG equations [161]

$$i\frac{\partial}{\partial t}\check{\psi}_k = \check{\mathcal{H}}(k,t)\check{\psi}_k, \tag{3.1}$$

where the Hamiltonian

$$\check{\mathcal{H}}(k,t)=\begin{pmatrix}\hat{H}(k,t) & i\hat{\sigma}_y\Delta(t)\\ -i\hat{\sigma}_y\Delta(t) & -\hat{H}^*(-k,t)\end{pmatrix} \tag{3.2}$$

is the 4×4 matrix in the Nambu×Spin space with the Pauli matrices $\hat{\sigma}_i$ acting on the four-component wave function $\check{\psi}_k(t)$. The single particle matrix Hamiltonian in the spin space $\hat{H}(k,t)=\xi_k\hat{\sigma}_0-h(t)\mathbf{z}_0\hat{\boldsymbol{\sigma}}+\alpha(\hat{\boldsymbol{\sigma}}\times\mathbf{k})\mathbf{z}_0$ depends on the modulus $k=|\mathbf{k}|$ and the relative phase $\theta_k=\arg(k_x+ik_y)$ of the momentum. Here $\xi_k=k^2/2m-E_F$ is a free particle spectrum measured from the Fermi level and α is a strength of RSOC. Hereafter we put $\hbar=1$. For simplicity we consider here the motion of QPs only in the $x-y$ plane neglecting their dispersion along the $\mathbf{z}_0$ axis, so that $\mathbf{k}=(k_x,k_y)$.

The pairing potential $\Delta(t)$ should satisfy the self-consistency equation, which at zero temperature $T=0$ can be written as follows

$$\Delta(t)=-\frac{\lambda}{2}\sum_{\text{i.c.}}\check{\psi}_k^\dagger(t)\check{\tau}_\Delta\check{\psi}_k(t), \tag{3.3}$$

where λ is the pairing constant, $\check{\tau}_\Delta=(\hat{\tau}_x+i\hat{\tau}_y)\otimes i\hat{\sigma}_y/2$ and the independence of Δ on θ_k is taken into account. The summation here is performed over all solutions of Eq. (3.1) for different initial conditions (i.c.) at $t=0$. The information about the dynamics as well as the distribution function of the QP excitations is contained in the functions $\check{\psi}_k(t)$, which self-consistently define the temporal evolution of the gap. In the homogeneous problem, the initial conditions are numbered by the momentum k, which, in the case of a spin-split superconductor, must be supplemented by the spin quantum number. All possible initial configurations of the QP states are defined by an equilibrium distribution function. The pairing potential $\Delta(t)$ can be chosen as a real function of time, and this choice will be justified below.

Generally speaking, the concept of an energy spectrum for a dynamical system is not clearly defined. However, in the case of adiabatic evolution one can introduce the eikonal approximation for the QP wave functions $\check{\psi}_k(t)\propto\check{\Psi}_k(t)e^{iS_k(t)}$, from which the adiabatic spectrum $E_k(t)=-\partial_t S_k$ can be extracted. The functions $\check{\Psi}_k(t)$ are the instantaneous eigenstates of the Hamiltonian $\check{\mathcal{H}}(t)$ from Eq. (3.2). The resulting spectrum is

$$E_{kn}(t)=\pm\sqrt{E_0^2+\alpha^2k^2+h^2(t)\mp\operatorname{sgn}(\sigma)2\sqrt{\xi_k^2\alpha^2k^2+h^2(t)E_0^2}} \tag{3.4}$$

where $E_0=\sqrt{\xi_k^2+\Delta^2}$. We use the index $n\equiv\sigma\pm=\{\uparrow+,\downarrow+,\uparrow-,\downarrow-\}$ which refers to different spin subbands and positive/negative energy (these notations will be used in the text below). There are four corresponding instantaneous eigenstates which can be written as $\check{\Psi}_{kn}(t)=(u_{k\uparrow n},u_{k\downarrow n},v_{k\uparrow n},v_{k\downarrow n})^T$. The detailed structure of the vectors is given in Appendix A. The functions $\check{\Psi}_{kn}(t)$ form an orthonormal basis with the normalization condition $\check{\Psi}_{kn}^\dagger\check{\Psi}_{kn'}=\delta_{nn'}$ and the completness relation $\sum_{kn}\check{\Psi}_{kn}\check{\Psi}_{kn}^\dagger=\check{1}$. Obviously, in the limit of the stationary Zeeman field, $\check{\Psi}_{kn}$ becomes an exact solution of stationary problem (3.1).

It is important to keep in mind that in the presence of both RSOC and spin-splitting field the equilibrium gap value depends of the values of these fields $\Delta_{\text{eq}}=\Delta_{\text{eq}}(h,\alpha)$. In what follows, the RSOC strength α will be considered as a small parameter, and the static dependence $\Delta(\alpha)$ will

be neglected for simplicity. Thus, the equilibrium gap value is defined as follows

$$\Delta_{\text{eq}} = \Delta_0 = 2\hbar\omega_D e^{-\frac{1}{\lambda N(0)}},$$

where ω_D is Debye frequency and $N(0)$ is the density of states at Fermi energy.

3.2 Linear response of a superconducting condensate

In this section we want to address the temporal evolution of a small fluctuation of the gap $\Delta_0 + \delta\Delta(t)$ in the presence of the static spin-splitting field $\mathbf{h} = h_0\mathbf{z}_0$. The gap dynamics can be excited by some external pulse at $t = 0$ or can be driven, for instance, by time-dependent spin-splitting field $\delta\mathbf{h}(t) = \delta h(t)\mathbf{z}_0$. In linear order in small perturbations $\delta\Delta(t), \delta h(t) \ll h_0 < \Delta_0$, the TDBdG equations for the QP wave functions read

$$i\frac{\partial}{\partial t}\check{\psi}_k(t) = \Big[\check{\mathcal{H}}_0 + \check{\mathcal{V}}(t)\Big]\check{\psi}_k(t), \tag{3.5}$$

where the operators in the Nambu×Spin space are

$$\check{\mathcal{H}}_0 = \begin{pmatrix} \hat{H}_0(k) & i\hat{\sigma}_y\Delta_0 \\ -i\hat{\sigma}_y\Delta_0 & -\hat{H}_0^*(-k) \end{pmatrix}, \qquad \check{\mathcal{V}}(t) = \begin{pmatrix} -\delta h(t)\hat{\sigma}_z & i\hat{\sigma}_y\delta\Delta(t) \\ -i\hat{\sigma}_y\delta\Delta(t) & -\delta h(t)\hat{\sigma}_z \end{pmatrix}, \tag{3.6}$$

and single particle Hamiltonian is $\hat{H}_0(k) = \xi_k\hat{\sigma}_0 - h_0\hat{\sigma}_z + \alpha(k_y\hat{\sigma}_x - k_x\hat{\sigma}_y)$.

Time-dependent equation (3.5) can be written in the adiabatic basis using stationary eigenfunctions $\check{\Psi}_{kn}$ of the operator $\check{\mathcal{H}}_0$. Additionally, the RSOC energy $\alpha k \approx \alpha k_F$ is considered a perturbative parameter. By approximating the eigenvectors up to first order in $\alpha k_F/\Delta_0$ (see Appendix A), we can infer from equation (3.3) that the fluctuation in the gap will have an order up to $\mathcal{O}(\alpha^2 k_F^2/\Delta_0^2)$. However, in the general case, the gap Δ should not be affected by the direction of the SOC. Therefore, the first-order change in the gap $\delta\Delta \propto \mathcal{O}(\alpha k_F/\Delta_0)$ must vanish.

Instead of the general eikonal theory, we use the perturbative approach with the ansatz written in terms of the dynamical phase

$$\check{\psi}_k(t) = \sum_n \check{\Psi}_{kn} C_{kn}(t) e^{-iE_{kn}t}. \tag{3.7}$$

The index $n = \{\uparrow +, \downarrow +, \uparrow -, \downarrow -\}$ denotes the spectral branches and all negative/positive energy terms are involved into the dynamics of QPs. Substituting the function (3.7) into Eq. (3.5) we obtain the equation for the dynamics of the coefficients

$$i\frac{\partial}{\partial t}C_{km}(t) = \sum_n \check{\Psi}_m^\dagger \check{\mathcal{V}}(t)\check{\Psi}_n e^{-i(E_n - E_m)t} C_{kn}(t), \tag{3.8}$$

which completely determine the evolution of gap $\Delta(t)$ in time through the self-consistency equation

$$\Delta_0 + \delta\Delta(t) = -\frac{\lambda}{2}\sum_{\text{i.c.}}\sum_{n,n'} C_{kn}^*(t) C_{kn'}(t) e^{-i(E_{n'} - E_n)t}\check{\Psi}_{kn}^\dagger \check{\tau}_\Delta \check{\Psi}_{kn'}. \tag{3.9}$$

The dynamics of the system is considered in the interval $t \in [0, \infty)$.

Equation (3.8) describes transitions of the states between different branches n, but with the same momenta k, which makes it possible to simplify the formulation of the initial conditions. In the case of zero temperature $T = 0$ there are two possible initial configurations at $t = 0$: all QP states with energies below Fermi level in the first(second) spin subband with $\sigma =\uparrow (\downarrow)$ are fully occupied for all momenta with $\xi_k \in (-\omega_D, \omega_D)$. This imposes two corresponding initial

conditions for Eq. (3.8)

$$\begin{aligned} &\text{(i)} \quad C_{k\uparrow-}(0)=1, \;\; C_{k[\downarrow-,\uparrow+,\downarrow+]}(0)=0; \\ &\text{(ii)} \quad C_{k\downarrow-}(0)=1, \;\; C_{k[\uparrow-,\uparrow+,\downarrow+]}(0)=0. \end{aligned} \tag{3.10}$$

Therefore it is natural to linearize the equation (3.8) as follows

$$C_{kn}(t)=C_{kn}(0)+\delta C_{kn}(t). \tag{3.11}$$

The sum in Eq. (3.9) should be taken over all QP states originating from the above i.c. (3.10).

Performing Laplace transform in the complex plane $s=i\omega+\zeta$ for the linearized equations (3.8, 3.9, 3.11) (see Appendix B) we get the following dynamic self-consistency equation

$$\delta\Delta(s)=\Big[\mathcal{K}_0(s)+\mathcal{K}_+(s)+\mathcal{K}_-(s)\Big]\delta\Delta(s)+\Big[\mathcal{F}_+(s)-\mathcal{F}_-(s)\Big]\delta h(s)+\mathcal{I}(s). \tag{3.12}$$

Here $\mathcal{K}_{0,\pm}(s)$ represents kernels of the self-consistency equation and $\mathcal{F}_\pm(s)$ defines the dynamical structure of the "force" term (in analogy with a mechanical oscillator) related with $\delta h(t)$. The term $\mathcal{I}(s)$ (see Eq. (B8) in the Appendix B) represents the initial nonequilibrium perturbation in the distribution of the QP population through the coefficients $\delta C_{kn}(t=0)$. Taking into account the Eq. (3.9) this term can be treated as an effective self-consistent initial condition for the gap dynamics $\delta\Delta(t)$.

Due to the absence of particle-hole asymmetry, which couples the phase and amplitude fluctuations [125], the imaginary part of $\delta\Delta(s)$ naturally vanishes and we consider only amplitude (or Higgs) modes of the superconducting gap. Knowing the function $\mathcal{K}(s)$ one can find eigenfrequencies and free dynamics of the system, while $\mathcal{F}_\pm(s)$ induces the driven dynamics. We will conduct a thorough examination of these terms below.

3.2.1 Spin-split Higgs modes

It is known that in the absence of a spin-splitting field and RSOC the Higgs mode has a singular behavior in the vicinity of the eigenfrequency $\omega=2\Delta_0$, which defines the free evolution of the gap perturbation $\delta\Delta(t)\propto\cos(2\Delta_0 t)/\sqrt{t}$ [130]. Since the energy of the Higgs mode lies at the lower bound of the QP spectrum, the oscillatory behavior here can be represented as a coherent decay and formation of a Cooper pair into two QPs with opposite spins and energies Δ_0 at $k\approx k_F$. The contribution from the pairs of QPs with other momenta leads to the inhomogeneous broadening of the mode with the corresponding damping law. The presence of Zeeman field and RSOC makes the dynamics more complicated. To analyze the eigenmodes of the superconductor one can set $\delta h(t)=0$ and write the self-consistency equation as follows

$$\chi^{-1}_{\Delta\Delta}(s)\delta\Delta(s)=\mathcal{I}(s),$$

where we define the bare pair susceptibility

$$\chi_{\Delta\Delta}(s)=\frac{1}{1-\mathcal{K}_0(s)-\mathcal{K}_+(s)-\mathcal{K}_-(s)}. \tag{3.13}$$

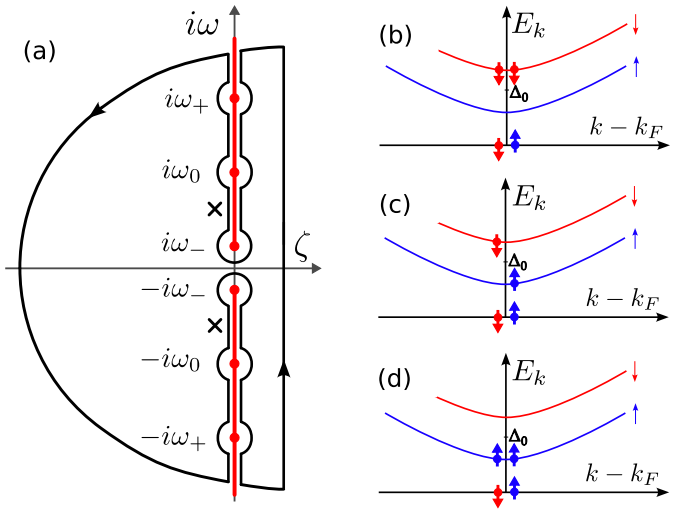

Figure 3.1: (a) Branch points $\omega_0 = 2\Delta_0, \omega_\pm = 2(\Delta_0 \pm h_0)$ (red dots) corresponding to the kernels $\mathcal{K}_0(s)$ and $\mathcal{K}_\pm(s), \mathcal{F}_\pm(s)$ [Eq. (3.12)] in the complex plane $s = i\omega + \zeta$. Red lines show the chosen branch cuts. Black crosses correspond to the poles of the external force $\delta h(s)$. (b-d) Illustration of physical mechanism behind the appearance of three eigenfrequencies ω_+ (b), ω_0 (c), ω_- (d).

The corresponding kernels read (see Appendix B)

$$\mathcal{K}_0(s) = \Big\langle \frac{2\xi^2}{E_0}\frac{1}{s^2+4E_0^2}\Big\rangle \propto \mathcal{O}\Big(\frac{\alpha^0 k_F^0}{\Delta_0^0}\Big), \tag{3.14}$$
$$\mathcal{K}_\pm(s) = \Big\langle \mathcal{A}^2(\xi)\frac{E_0 \pm h_0}{s^2+4(E_0\pm h_0)^2}\Big\rangle \propto \mathcal{O}\Big(\frac{\alpha^2 k_F^2}{\Delta_0^2}\Big),$$

where the notation $\langle \dots \rangle = \lambda N(0)\int_{-\omega_D}^{\omega_D} d\xi$ is used. The function $\mathcal{A}(\xi) \propto \check{\Psi}^{0\dagger}_{kn}\check{\tau}_\Delta\check{\Psi}^0_{kn} \propto \alpha k_F/\Delta_0$ is proportional to nonzero triplet component of the wave function, therefore the kernels $\mathcal{K}_\pm$ are of the second order in the RSOC parameter.

The frequencies of the eigenmodes of the superconducting condensate can be traced out from the condition $|\chi^{-1}_{\Delta\Delta}(\omega)| = 0$, which reflects the singular points of the kernels (3.14). Consider these points in more detail. Instead of straightforward integrating, we are going to implement the analysis in the spirit of the work [132] and analytically obtain the limit $\zeta \to 0$. The functions $\mathcal{K}_{0,\pm}(s \to \omega)$ can be represented as $\mathcal{K}(s) = \mathcal{K}'(\omega) + i\mathrm{sgn}(\omega\zeta)\mathcal{K}''(\omega)$. The real parts of the kernels

$$\frac{\mathcal{K}_0'(\omega)}{\lambda N(0)} = \int_{-\omega_D}^{\omega_D}\frac{2\xi^2}{\sqrt{\xi^2+\Delta_0^2}(4\xi^2+4\Delta_0^2-\omega^2)}d\xi, \tag{3.15}$$
$$\frac{\mathcal{K}_\pm'(\omega)}{\lambda N(0)} = \int_{-\omega_D}^{\omega_D}\frac{\mathcal{A}^2(\xi)(E_0\pm h_0)}{4(E_0-h_0)^2 \pm |\omega|^2}d\xi, \tag{3.16}$$

are regular on the imaginary axis $s = i\omega$. The imaginary parts are

$$\frac{\mathcal{K}_0''(\omega)}{\lambda N(0)} = -\frac{\pi}{2}\frac{\sqrt{\omega^2-\omega_0^2}}{|\omega|}\Theta[\omega^2-\omega_0^2], \tag{3.17}$$
$$\frac{\mathcal{K}_\pm''(\omega)}{\lambda N(0)} = -\frac{\pi}{8}\frac{|\omega|\mp 2h_0}{\xi_\pm}\mathcal{A}^2(\xi_\pm)\Theta[\omega^2-\omega_\pm^2], \tag{3.18}$$

where $\xi_\pm = \frac{1}{2}\sqrt{\big(|\omega|-\omega_\pm\big)^2 + 4\Delta_0(|\omega|-\omega_\pm)}$. The discontinuities at the real axis ζ mean the

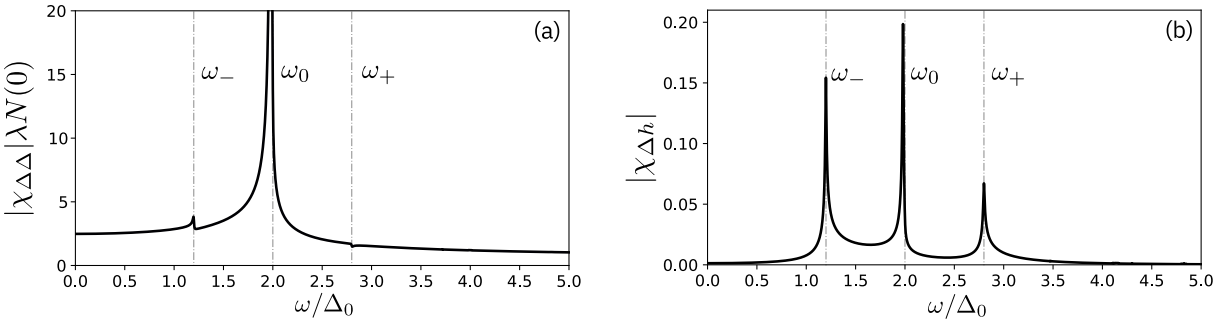

Figure 3.2: (a) The bare pair susceptibility $|\chi_{\Delta\Delta}(s)|$ from Eq. (3.13) for $s = i\omega + \zeta$. Features at the frequencies $\omega_0 = 2\Delta_0$ and $\omega_\pm = 2(\Delta_0 \pm h_0)$ correspond to Higgs modes resonances. (b) Response function $|\chi_{\Delta h}(s)|$ of the driven gap oscillations $\delta\Delta(t)$ excited by the Zeeman field $\delta h(t)$. Both plots are symmetrical with respect to $\omega \to -\omega$ and have the parameters $h_0 = 0.4\Delta_0$, $\alpha k_F = 0.09\Delta_0$. Broadening of the resonance peaks is given by $\zeta = 0.005\Delta_0$.

existence of the branch points

$$\begin{aligned} \omega_0 &= 2\Delta_0, \\ \omega_+ &= 2(\Delta_0 + h_0), \\ \omega_- &= 2(\Delta_0 - h_0), \end{aligned} \tag{3.19}$$

and corresponding cuts in the complex plane [Fig. 3.1(a)].

The analysis of the general linear response of the order parameter can be significantly simplified by expanding the susceptibility $|\chi_{\Delta\Delta}(\omega)|$ in the powers of the small parameter $\alpha k_F/\Delta_0$, since the kernels $\mathcal{K}_\pm \propto \mathcal{O}(\alpha^2 k_F^2/\Delta_0^2)$. As mentioned before, the maximum order we can take into account is $|\chi_{\Delta\Delta}| \propto \mathcal{O}(\alpha^2 k_F^2/\Delta_0^2)$. The resonance condition $|\chi^{-1}_{\Delta\Delta}(\omega)| = 0$ is satisfied at $\omega = \omega_\pm$ where the kernels $\mathcal{K}''_\pm(s)$ have a singularity (note that $\mathcal{A}$ is regular at $\xi = \xi_\pm$), and at $\omega = \omega_0$, where the function $\mathcal{K}''_0(s)$ goes to zero. Thus, the branch points (3.19) define new eigenmodes of the superconductor in the presence of spin-splitting field and weak RSOC.

One can obtain an asymptotic behavior these eigenmodes in the time domain [132]. Let us assume the specific form of the initial conditions $\mathcal{I}(s) = \mathcal{I}_0 = const$ in Eq. (3.12), which is equivalent to the instant quench of the condensate with the strength $\mathcal{I}_0$. We consider the impulse response of the gap fluctuation for $t \in [0, \infty)$ using inverse Laplace transform

$$\delta\Delta(t) = \frac{1}{2\pi i}\int_{-i\infty+\epsilon}^{i\infty+\epsilon} \chi_{\Delta\Delta}(s)\mathcal{I}_0 e^{st} ds. \tag{3.20}$$

The integral can be evaluated using closed contour shown in Fig. 3.1(a). Making sure that all integrals on infinitely large and small arcs vanish and applying residue theorem we get

$$\delta\Delta(t) = \frac{2}{\pi}\int_{\omega_-}^{\infty} \mathrm{Im}\chi_{\Delta\Delta}(s)\big|_{\zeta\to+0} \mathrm{Im}\Big[e^{i\omega t}\mathcal{I}_0\Big] d\omega. \tag{3.21}$$

One can show that the peculiarities in the vicinities of the eigenfrequencies in $\mathrm{Im}\chi_{\Delta\Delta}(s)$ lead to three partial contribution to the long-time ($h_0^{-1} \ll t$) gap dynamics

$$\delta\Delta(t) \approx \frac{4\Delta_0}{\pi^{3/2}}\frac{\mathcal{I}_0}{\lambda N(0)}\frac{\cos(\omega_0 t - \pi/4)}{\sqrt{\Delta_0 t}} - \frac{\sqrt{\pi}}{2}\frac{(\alpha k_F)^2\Delta_0}{(\Delta_0 - h_0)^2}\sum_{j=\pm}\frac{\lambda N(0)\mathcal{I}_0}{|1 - \mathcal{K}_0(\omega_j)|^2}\frac{\cos(\omega_j t - \pi/4)}{\sqrt{\Delta_0 t}}, \tag{3.22}$$

which can be identified as spin-split Higgs modes. Details of the derivation of $\delta\Delta(t)$ are provided in Appendix C.

Appearance of the frequencies (3.19) and corresponding oscillations (3.22) in the spin-split superconductor can be explained qualitatively. Coherent decay of the Cooper pairs from the Fermi level can occur into two different spin subbands of the QP spectrum. When two electrons with opposite spins from a pair dissociate into two QP at $k \approx k_F$ with the energies $\Delta_0 \pm h_0$ without spin-flipping, then the total decay energy is equal to QP threshold $\approx 2\Delta_0$. This process corresponds to the mode $2\Delta_0$ and shown in Fig. 3.1(c). A decay into two QPs with the same spins is possible in the presence of RSOC due to the effective spin-flip scattering. The energies of such two QPs are either Δ_0+h_0 or Δ_0-h_0. This process leads to the modes $2(\Delta_0\pm h_0)$ correspondingly [Fig. 3.1(b,d)]. Note that this naive interpretation of the complicated QP dynamics is valid for the sufficiently small RSOC $\alpha k_F \ll \Delta_0$.

Numerically calculated susceptibility $|\chi_{\Delta\Delta}(\omega)|$ from Eqs. (3.13-3.14) is shown in Fig. 3.2(a). The observed resonances have a different parametric order of smallness. The Higgs mode with the frequency ω_0 which exists in the absent the RCOS becomes dominating with more pronounced peak $|\chi_{\Delta\Delta}(\omega \approx \omega_0)| \propto \alpha^0 k_F^0$, whereas two other modes at shifted frequencies $\omega_\pm$ are of the order of $|\chi_{\Delta\Delta}(\omega \approx \omega_\pm)| \propto \alpha^2 k_F^2/\Delta_0^2$. These modes merge with ω_0 at $h_0 \to 0$ and disappear for $\alpha \to 0$. It is expected that the excitation of the bare response of the superconductor can be implemented with the standard THz laser pump-probe techniques. The electric field of the pump pulse produces a quench of the spin-split superconductor and subsequent probe pulse detects the multifrequency Higgs oscillations.

Note, that a similar dynamics of the order parameter was studied in the spin-orbit coupled Fermi gases [294–296]. In particular, the existence of the Higgs modes modified by the Zeeman field in the presence of strong SOC with $\alpha k_F \sim h(t) \sim E_F$ was discussed in Ref. [297]. The authors performed a numerical simulation of the one-dimensional Fermi superfluid and examined the excitation of the gap oscillations with few frequencies by abrupt change of the Zeeman field. Despite the significant differences between the models, there is a general tendency for the influence of the shift of spectral QP branches on the behavior of the order parameter modes.

We also note that in the presence of the strong Zeeman field the superconductor can be unstable to a transition to the spatially modulated FFLO state with inhomogeneous order parameter. The appearance of the broken translational symmetry gives rise to gapless Higgs and Goldstone modes, which have been investigated theoretically in Refs. [298, 299]. Hereafter we ignored the possibility of of FFLO formation, focusing on purely homogeneous case.

3.2.2 Coupling of Higgs modes and Zeeman field

We found that, in addition to an electromagnetic field, the gap dynamics in a spin-split superconductor can be excited by a nonstationary component of Zeeman field $\mathbf{h}(t) = (h_0 + \delta h(t))\mathbf{z}_0$. In this particular configuration the perturbation of the spin-splitting field $\delta h(t)$ appears in the self-consistency equation (3.12) in the first order, which is the trace of a dot product $(\mathbf{h}_0 \cdot \delta\mathbf{h})$. Note that the field $\delta h(s)$ is weighted by the functions

$$\mathcal{F}_\pm(s) = \Big\langle \mathcal{A}(\xi)\mathcal{B}(\xi)\frac{(E_0 \pm h_0)}{s^2 + 4(E_0 \pm h_0)^2}\Big\rangle \propto \mathcal{O}\Big(\frac{\alpha^2 k_F^2}{\Delta_0^2}\Big), \tag{3.23}$$

which can be written as $\mathcal{F}(s) = \mathcal{F}'(\omega) + i\mathrm{sgn}(\omega\zeta)\mathcal{F}''(\omega)$ and have the same order in αk_F and the same analytical properties as the kernels $\mathcal{K}_\pm(s)$ in (3.16,3.18), because both functions $\mathcal{A}^2(\xi)$ and $\mathcal{A}(\xi)\mathcal{B}(\xi)$ are regular for $\xi \in (-\omega_D, \omega_D)$. The presence of the singular points in the force term

makes the analysis of Eq. (3.12) more sophisticated, despite the fact that these points are shared with other kernels.

Consider the general case of forced oscillations of the order parameter driven by some field $\delta h(t)$ which is abruptly turned on at $t = 0$. It is convenient to introduce the linear response function as follows

$$\delta\Delta(s) = \chi_{\Delta h}(s)\delta h(s), \tag{3.24}$$

$$\chi_{\Delta h}(s) = \frac{\mathcal{F}_+(s) - \mathcal{F}_-(s)}{1 - \mathcal{K}_0(s) - \mathcal{K}_+(s) - \mathcal{K}_-(s)}. \tag{3.25}$$

The numerically integrated shape of $|\chi_{\Delta h}(s)|$ is shown in Fig. 3.2(b) and, as expected, it has three resonance peaks at the frequencies $\omega_{0,\pm}$. However, since the the external field $\delta\mathbf{h}(t)$ couples to the gap through the RSOC, the amplitude of the susceptibility in the vicinity of the resonances has the same order of smallness $|\chi_{\Delta h}(\omega_{0,\pm})| \propto \mathcal{O}(\alpha^2 k_F^2/\Delta_0^2)$, which differs from the bare response (3.13).

The temporal evolution of the gap fluctuation $\delta\Delta(t)$ in $[0, \infty)$ can be found using inverse Laplace transform. Similarly to Eq. (3.21) the susceptibility $\mathrm{Im}\chi_{\Delta h}$ can be expanded into series, since $\mathcal{F}_\pm, \mathcal{K}_\pm \propto \mathcal{O}(\alpha^2 k_F^2/\Delta_0^2)$, and different strongly dominant terms in the vicinity of the branch points (3.19) can be distinguished [Fig. 3.2]. Here we write the result for the superconducting gap oscillations, which at large times $h_0^{-1} \ll t$ reads (for details see Appendix C)

$$\delta\Delta(t) \approx \sum_p \chi_{\Delta h}(s_p) e^{s_p t} \operatorname*{Res}_{s=s_p}\big[\delta h(s)\big] + \frac{4\Delta_0}{\pi^{3/2}} \frac{\big[\mathcal{F}'_+(\omega_0) - \mathcal{F}'_-(\omega_0)\big]}{\lambda N(0)} \frac{\mathrm{Im}\Big[\delta h(i\omega_0) e^{i(\omega_0 t + \pi/4)}\Big]}{\sqrt{\Delta_0 t}} \tag{3.26}$$

$$+ \frac{\sqrt{\pi}}{2} \frac{(\alpha k_F)^2 \Delta_0}{(\Delta_0 - h_0)^2} \sum_{j=\pm} \frac{\lambda N(0)\big[1 - \mathcal{K}'_0(\omega_j)\big]}{|1 - \mathcal{K}_0(\omega_j)|^2} \frac{\mathrm{Im}\Big[\delta h(i\omega_j) e^{i(\omega_j t + \pi/4)}\Big]}{\sqrt{\Delta_0 t}}.$$

The first term here is related to the forced oscillations of the gap, caused by the Zeeman field $\delta h(t)$. For instance, the general harmonic perturbation $\delta h(t) = \mathrm{Re}(\delta h_0 e^{(i\omega - \beta)t})$ with $\beta \to 0$ gives two poles s_p shown in Fig. 3.1(a). The last three terms in (3.26) correspond to the free oscillations triggered by $\delta h(t)$ at $t = 0$ in the long time asymptote, with three characteristic frequencies (3.19) and square-root damping law. The latter can be interpreted as partial contribution from the Higgs modes in the spin-splitting field h_0. The eigenmodes decay at $t \to \infty$ and in the long-time asymptote the forced oscillations prevail. Consider the steady-state behavior of $\delta\Delta(t)$ (the first term in Eq. (3.26)) in the time interval restricted by the inelastic relaxation processes where the presented description of the coherent gap dynamics is valid.

In this section, we have solely focused on the longitudinal component of the field perturbation $\delta h(t)\mathbf{z}_0$ with respect to the stationary field $h_0\mathbf{z}_0$. However, it is also possible to introduce the time-dependent transversal component $\delta\mathbf{h}\perp(t)$ and examine its dynamic interaction with the superconducting system in Eq. (3.5). This component generates triplet correlations, but these do not contribute to the order parameter since only singlet pairing in (3.3) is considered. Consequently, in the second-order perturbation theory with respect to $\alpha k_F/\Delta_0$, there is no linear coupling between the field $\delta\mathbf{h}\perp(t)$ and the gap $\delta\Delta(t)$. This outcome is unsurprising since the only true scalar in this regime $(\delta\mathbf{h}_\perp \cdot \mathbf{h}_0)$ is zero.

3.3 Nonadiabatic dynamics of QPs in a strong spin-splitting field

In this section we address the case of a linearly growing spin-splitting field $h(t) = \gamma t$, which can exceed the equilibrium value of the superconducting gap $\Delta_{\text{eq}} \equiv \Delta_0$ and thus provide the crossing of the two QP spectral branches $E_{\uparrow+}(\xi_k)$ and $E_{\downarrow-}(\xi_k)$ from different spin subbands [Fig. 3.3(a, c)]. In the collisionless regime and in the absence of RSOC the intersecting spectral branches do not interact, so that the occupation of the quasiparticle states defined at $t = 0$ does not change in time. This means that the self-consistent gap function will not change even above the paramagnetic limit $h(t) > \Delta_0$ and will be defined by the initial condition $\Delta(t) = \Delta_0$. It is clear from general considerations that the spin-orbit coupling is capable of provoking the interplay between QP states with different spins, and we investigate the mechanism of such an interaction and the effect on the superconducting order parameter $\Delta(t)$. As mentioned in the Section 3.1, we will treat the RSOC energy as a small parameter $\alpha k_F/\Delta \ll 1$. Therefore, we neglect the dependence of the equilibrium gap Δ_{eq} on α and assume $\Delta_{\text{eq}} \equiv \Delta_0$.

3.3.1 Adiabatic evolution of QP states

The evolution of QP wave function of the TDBdG equations (3.1) can be regarded with the help of general adiabatic ansatz

$$\check{\psi}_k(t) = \sum_n C_{kn}(t)\check{\Psi}_{kn}(t), \tag{3.27}$$

where $\check{\Psi}_{kn}(t)$ are the instantaneous eigenstates of the Hamiltonian (3.2). Here all negative/positive energy terms with the indices $n = \{\uparrow +, \downarrow +, \uparrow -, \downarrow -\}$ are taken into account. The coefficients $C_{kn}(t)$ define the occupation of QP states and its temporal evolution (similarly to the ansatz (3.7) used in the previous Section). The initial conditions for $C(t)$ are fixed by the equilibrium distribution at $t = 0$ and have been discussed in Section 3.2 [see Eq. (3.10)]. With short notations two possible initial conditions reads $C_{kn}(t = 0) = \delta_{n,l}$, where $\delta_{n,n'}$ is Kronecker delta and $l = \{\uparrow -, \downarrow -\}$. Thus, for the given l we have $C_{kl}(t = 0) = 1$ and $C_{k(n\neq l)}(t = 0) = 0$.

We introduce the vector

$$\hat{C}_k(t) = (C_{k\uparrow+}, C_{k\downarrow+}, C_{k\uparrow-}, C_{k\downarrow-})^T, \tag{3.28}$$

which contains all the information about the dynamics of the QP states. Corresponding adiabatic temporal evolution can be described with the help of the unitary operator $\hat{C}_k(t_2) = \hat{U}_k(t_2, t_1)\hat{C}_k(t_1)$ where $\hat{U}_k = \text{diag}(U_{k\uparrow+}, U_{k\downarrow+}, U_{k\uparrow-}, U_{k\downarrow-})$ and

$$U_{kn}(t_2, t_1) = \exp\Big(-i\int_{t_1}^{t_2} E_{kn}(t)dt\Big). \tag{3.29}$$

The interaction of the branches $E_{k\uparrow+}(t)$ and $E_{k\downarrow-}(t)$ leads to *avoided crossing* of the QP levels at fixed energy ξ_k with the splitting proportional to αk_F. Thus the adiabatic approximation is justified only for the levels with $E_k(t) \gg \alpha k_F$, e.g. far enough from the crossing points. Therefore, for the Zeeman field $h(t) \lesssim \Delta_0$ all nonadiabatic transitions are suppressed and the gap function defined by the self-consistency equation (3.3) is equal to the equilibrium value $\Delta(t) = \Delta_0$.

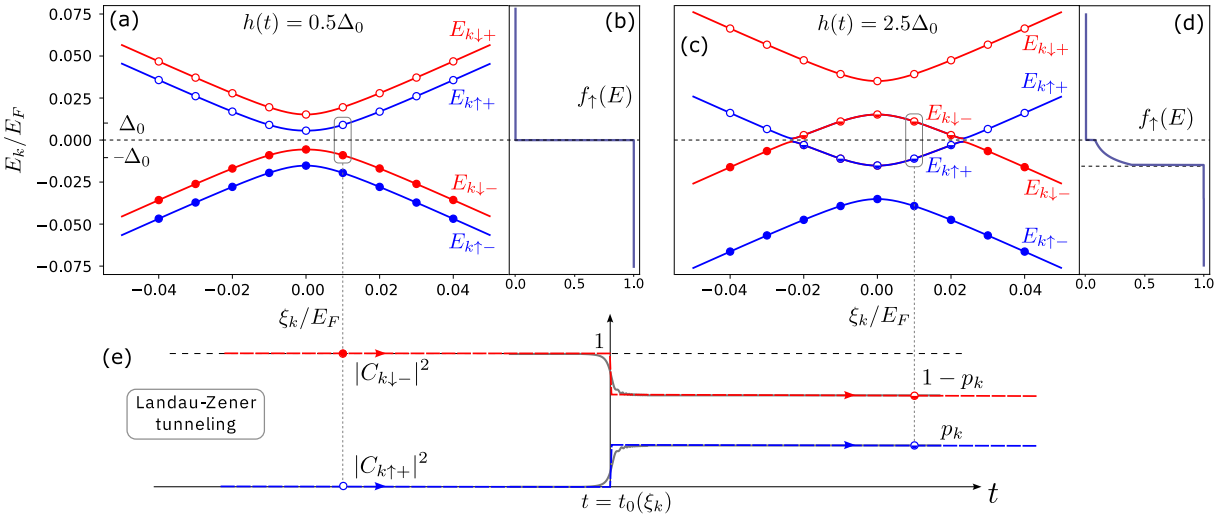

Figure 3.3: (a,b) QP spectrum E_k from Eq. (3.4) for $\Delta_0/E_F = 0.01$, $\alpha k_F/E_F = 0.0025$ and for two values of Zeeman field $h(t)$ before (a) and after (b) avoided crossing. Colored/empty circles correspond to filled/empty states. In (e) the schematic temporal evolution of the filling probabilities $|C_k|^2(t)$ for two states at fixed ξ_k is shown. The gray lines show a tunneling process similar to the real one in the vicinity of the avoided transition point $t_0(\xi_k) = \sqrt{\xi_k^2 + \Delta_0^2}/\gamma$, while red and blue lines refer to transition matrix approximation of the LZSM tunneling with the probability p_k. (b, d) The QP distribution function for one spin projection $f_\uparrow(E,t)$ from Eq. (3.44) before and after crossing of spectral branches at $\delta_{\text{LZ}} = 0.5$.

3.3.2 Transition evolution matrix

The avoided crossing between the spectral terms at $h(t) \gtrsim \Delta_0$ should be described in terms of nonadiabatic dynamics. For this we consider the branch intersection as consecutive avoided crossing of pairs of the QP states with fixed energy ξ_k at the time instant $t_0(\xi_k) = \sqrt{\xi_k^2 + \Delta^2}/\gamma$ [Fig. 3.3]. For each crossing at $\xi_k \in (-\omega_D, \omega_D)$ it is possible to formulate the time-dependent Landau-Zener-Stückelberg-Majorana (LZSM) problem [300], which describes the transitions between two QP states with different spins during their temporal evolution. Note that resulting nonadiabatic tunneling is equivalent to dynamical spin-flip process.

In general, the description of such a tunneling (or LZSM problem) requires joint solution of TDBdG equation (3.1) and self-consistency equation (3.3). However, some important results can be obtained analytically using certain approximations:

• If the time variation of the gap function $\Delta(t)$ is small on the typical tunneling time scale τ_{LZ} (see Appendix D), then the tunneling of QP states is not affected by the order parameter dynamics.

• The gap $\Delta(t)$ is defined by all states in range $\xi_k \in (-\omega_D, \omega_D)$, and a time-dependent perturbation of the states caused by the dynamical LZSM transition makes a small contribution to the sum over all ξ_k.

Thus, one can neglect the transient dynamics of the coefficients $\hat{C}_k(t)$ in the vicinity of a transition point for each ξ_k-th mode. This also means that one can investigate the tunneling problem with the help of so-called transition evolution matrix [300] connecting two adiabatic regimes before ($t < t_0-$) and after ($t > t_0+$) avoided crossing [Fig. 3.3(e)]. These conditions allow one to effectively decouple the LZSM problem from the self-consistency equation and solve them independently.

Taking into account all these assumptions, the time evolution of the vector $\hat{C}_k(t)$ from the

adiabatic ansatz (3.27) is described as follows

$$\hat{C}_k(t) = \begin{cases} \hat{U}_k(t, t_0+)\hat{S}_{\text{LZ}}\hat{U}_k(t_0-, 0)\hat{C}_k(0), & t > t_0(\xi_k) \\ \hat{U}_k(t, 0)\hat{C}_k(0), & t < t_0(\xi_k) \end{cases}. \tag{3.30}$$

Here the nonadiabatic transitions between QP states are included into transition matrix $\hat{S}_{\text{LZ}}$, which acts on the state vector $\hat{C}_k(t)$ at the time instant $t = t_0(\xi_k)$. The matrix $\hat{S}_{\text{LZ}}$ can be obtained by considering the interaction of two intersecting energy branches $E_{\uparrow+}$ and $E_{\downarrow-}$ in the TDBdG equation (3.1). Using so-called diabatic basis (basis of Hamiltonian (3.2) in the absence of RSOC) one gets a system of dynamical equations, the asymptotic solution of which forms a transition matrix describing the passage through the avoided intersection point. Then we go to the original adiabatic basis (3.27) and get the matrix $\hat{S}_{\text{LZ}}$. The complete derivation of $\hat{S}_{\text{LZ}}$ is presented in Appendix D and it reads

$$\hat{S}_{\text{LZ}} = \begin{pmatrix} \sqrt{p_k} & 0 & 0 & \sqrt{1-p_k}e^{i(\dots)} \\ 0 & 1 & 0 & 0 \\ 0 & 0 & 1 & 0 \\ -\sqrt{1-p_k}e^{-i(\dots)} & 0 & 0 & \sqrt{p_k} \end{pmatrix}, \tag{3.31}$$

where $(\dots) = \chi_k - \theta_k - \frac{\pi}{2}\text{sgn}(\alpha)$. The coefficient

$$p_k = \exp\Big[-\delta_{\text{LZ}}\frac{\Delta^2}{\xi_k^2 + \Delta^2}\Big]$$

is expressed through the dimensionless LZSM parameter $\delta_{\text{LZ}} = \pi\alpha^2 k_F^2/\gamma$ and determines the probability of tunneling between QP states with different spins. The transition is accompanied by the appearance of the Stokes phase χ_k (see Appendix D) and the phase $\theta_k = \arg\left(k_x + ik_y\right)$.

To avoid confusion, we use the same notations for the spectral branches (3.4) before ($t < t_0-$) and after ($t > t_0+$) QP transitions, as shown in Fig. 3.3. Thereby, we do not need to keep track of the indices of the eigenvectors $\check{\Psi}_{kn}(t)$ and the evolution operators $U_{kn}(t)$ from (3.29). It is sufficient that these functions take into account the permutation of the branches of the spectrum (3.4), so that all QP levels change their indices after the transition in accordance with the chosen notation.

3.3.3 Time dependence of superconducting gap

The time-dependent order parameter subjected to the field $h(t) \gtrsim \Delta_0$ depends on both the adiabatic wave function (3.27) and nonadiabatic LZSM tunneling (3.30). The calculation of $\Delta(t)$ can be accomplished using the self-consistent equation (3.3), which gets the following form

$$\Delta(t) = -\frac{\lambda}{2}\sum_l \sum_k \sum_{n,n'} C^*_{kn}(t)C_{kn'}(t)\check{\Psi}^\dagger_{kn}\check{\tau}_\Delta\check{\Psi}_{kn'}, \tag{3.32}$$

where index l means different initial configurations of the occupation of the QP spectrum at $t = 0$ (see Section 3.3.1). The first configuration with $C_{kn}(t = 0) = \delta_{n,\uparrow-}$ corresponds to occupation of all QP states belonging to the spectral branch $E_{k,\uparrow-}$ for all momenta with $\xi_k \in (-\omega_D, \omega_D)$. The evolution of the coefficients $C_{kn}(t)$ is determined by the Eq. (3.30) together with Eq. (3.28-3.29). Since the branch $E_{k,\uparrow-}$ does not cross with other branches, the coefficients $C_{kn}(t)$ have a trivial

adiabatic dynamics, which can be written as follows

$$\hat{C}_k(t) = \begin{pmatrix} 0 \\ 0 \\ U_{\uparrow -}\big(t,0\big) \\ 0 \end{pmatrix}. \tag{3.33}$$

The second initial configuration with $C_{kn}(t=0) = \delta_{n,\downarrow -}$ leads to the intersection of the filled branch $E_{k,\downarrow -}$ and empty branch $E_{k,\uparrow +}$. Using equation (3.30) we obtain a nontrivial dynamics of the states with LZSM tunneling, which reads

$$\hat{C}_k(t) = \tag{3.34}$$
$$\begin{pmatrix} \sqrt{1-p_k}e^{i(\dots)}U_{\uparrow +}\big(t,t_0+\big)U_{\downarrow -}\big(t_0-,0\big)\Theta\big[t-t_0\big] \\ 0 \\ 0 \\ \Big(\sqrt{p_k}\Theta\big[t-t_0\big] + \Theta\big[t_0-t\big]\Big)U_{\downarrow -}\big(t,0\big) \end{pmatrix}.$$

Here $(\dots) = \chi_k - \theta_k - \frac{\pi}{2}\mathrm{sgn}(\alpha)$ and $\Theta(t)$ is the Heaviside function.

Substituting coefficients (3.33) and (3.34) obtained from different initial conditions together with the QP wave functions $\hat{\Psi}_{kn}$ from (A3) into the self-consistency equation (3.32) we get

$$\Delta(t) = \lambda \sum_{|\xi_k|>\sqrt{h^2-\Delta^2}} u_0 v_0 + \lambda \sum_{|\xi_k|<\sqrt{h^2-\Delta^2}} \Bigg[\Big(\overset{=1}{|C_{k\uparrow -}|^2} + \overset{\propto p_k}{|C_{k\downarrow -}|^2} - \overset{\propto 1-p_k}{|C_{k\uparrow +}|^2} \Big) \frac{u_0 v_0}{2} \tag{3.35}$$
$$+ u_0 u_1 i e^{-i\theta_k} C^*_{k\uparrow +} C_{k\downarrow -} + v_0 v_1 (-i) e^{i\theta_k} C^*_{k\downarrow -} C_{k\uparrow +} \Bigg].$$

The last two terms are of the order of $\mathcal{O}(\alpha k_F/\Delta)$, so it is convenient to write the gap function as

$$\Delta(t) = \Delta_h[h(t)] + \delta\Delta(t). \tag{3.36}$$

We have identified two contributions that have significantly different origins: Δ_h is defined by the amplitude of the LZSM tunneling and depends on time only through the Zeeman field $h(t)$; $\delta\Delta(t) \propto \mathcal{O}(\alpha k_F/\Delta)$ is defined by cross-terms and reflects interference effects between QP wave functions caused by LZSM transitions and depends on time explicitly.

If one neglects the small perturbation $\delta\Delta(t)$ in (3.36) then it becomes possible to get a simplified self-consistency equation for $\Delta_h[h(t)]$ from Eq. (3.35). In an implicit form it reads as

$$\Delta_h = \Delta_0 \exp\left(\int_1^{h/\Delta_h} \frac{e^{-\delta_{\mathrm{LZ}}/s^2} - 1}{\sqrt{s^2-1}} ds \right), \tag{3.37}$$

where $\delta_{\mathrm{LZ}} = \pi\alpha^2 k_F^2/\gamma$ and its numerical integration is shown in Fig. 3.4. The quasistatic superconducting gap Δ_h behaves differently at $h(t) > \Delta_0$ depending on the regime by which the condensate was driven out of equilibrium.

• The value $\delta_{\mathrm{LZ}} = 0$ means zero RSOC ($\alpha = 0$), so there is no interaction of the QP states after crossing of the spectral branches and the trivial solution for the gap $\Delta_h = \Delta_0$ holds.

• The limit of $\delta_{\mathrm{LZ}} \ll 1$ with $\gamma \gtrsim \alpha^2 k_F^2$ corresponds to sudden (quench) regime. The spectral branches intersect nonadiabatically, or so rapidly that they do not feel the RSOC. The Landau-

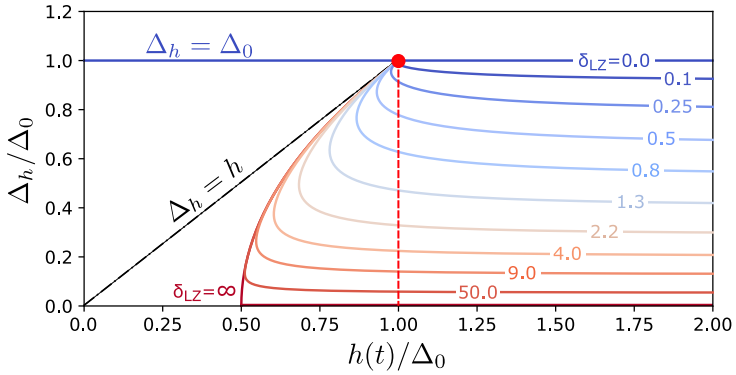

Figure 3.4: Quasistatic dependence of the superconducting gap Δ_h on the spin-splitting field $h(t)$ for different values of $\delta_{\rm LZ}$ [Eq. (3.37)]. The dashed-dotted line separates two regions where $\Delta_h \lessgtr h$. The dashed line shows the critical value of the field $h(t) = \Delta_0$ and the red circle marks the point of change in the behavior of the gap Δ_h in the region $\Delta_h > h$. After this point the equilibrium solution $\Delta_h = \Delta_0$ should jump to one of the solutions fixed by the parameter $\delta_{\rm LZ}$.

Zener tunneling is suppressed and the gap has a weak dependence on the Zeeman field at $h(t) > \Delta_0$:

$$\Delta_h \approx \Delta_0 \exp\Big(-\delta_{\rm LZ}\frac{\sqrt{h^2(t)-\Delta_h^2}}{h(t)}\Big).$$

• In the opposite limit of $\delta_{\rm LZ} \gg 1$ with $\gamma \ll \alpha^2 k_F^2$ the QPs undergo strong spin-flip tunneling during a slow (almost adiabatic) avoided crossing. This leads to the effective formation of the triplet superconducting correlations (or related triplet component of the anomalous Green function [301]) even for the small RSOC energy $\alpha k_F/\Delta \ll 1$. Such dynamically generated correlations are determined by the rate of field change γ and their effect on the gap can significantly exceed the static mixing of singlet-triplet pairs for $\alpha \neq 0$ [160]. As a result, the singlet gap function (3.3) is suppressed and the self-consistency equation reads as

$$\Delta_h \approx \begin{cases} \sqrt{\Delta_0(2h(t)-\Delta_0)} & \text{for} \quad \Delta_h > h/\delta_{\rm LZ}, \\ \Delta_0 \exp\Big(-\delta_{\rm LZ}\frac{\sqrt{h^2(t)-\Delta_h^2}}{h(t)}\Big)\frac{\exp(\sqrt{\delta_{\rm LZ}}\sqrt{\delta_{\rm LZ}-1})}{\sqrt{\delta_{\rm LZ}}+\sqrt{\delta_{\rm LZ}-1}} \\ \quad \text{for} \quad \Delta_h < h/\delta_{\rm LZ}. \end{cases}$$

However, the appearance of these triplet correlations does not result in the generation of the spin - triplet pairing order parameter, since within our model we do not introduce any nonzero coupling constant for the triplet pairing channel [302].

• The critical value $\delta_{\rm LZ} \to \infty$ corresponds to the complete Landau-Zener spin-flip tunneling, so that there are no QPs at the energies $E > 0$. In this case we have restored the thermodynamically metastable branch $\Delta_h \approx \sqrt{\Delta_0(2h(t)-\Delta_0)}$ from well-known static case [158].

The actual behavior of the gap in time must be determined by switching between different branches of $\Delta_h[h]$ as the Zeeman field $h(t)$ increases. The first solution, which is fixed by the initial condition $\Delta_h(t=0) = \Delta_0$ holds until $h(t) = \Delta_0$, where Δ_h goes to another unique possible solution $\Delta_h[h]$ for a given $\delta_{\rm LZ}$ (see the red point and black dashed line in Fig. 3.4). The question of the exact dynamics of the gap in the jump region is difficult, because due to the rapid change in the Δ_h, the decoupling of the LZSM problem and self-consistency equation may not be guaranteed [Section 3.3.2]. It is qualitatively expected that the jump at $t \approx \Delta_0/\gamma$ should be smeared both by non-zero static contribution of SOC to the gap (since the equilibrium gap

value depends on α) and by the QP tunneling dynamics. At large times $h(t) \gg \Delta_0$ there are no transitions between the QP states ($p_k \to 1$), since the splitting between the spectral branches becomes zero and therefore the gap tends to the constant asymptotics $\Delta_h(\infty)$.

3.3.4 QP interference effects

In addition to the quasistatic term Δ_h, the gap equation (3.35) also contains small rapidly oscillating term

$$\delta\Delta(t) = \lambda \sum_{|\xi_k|<\sqrt{h^2-\Delta^2}} u_0 u_1 i e^{-i\theta} C^*_{k\uparrow+} C_{k\downarrow-} + v_0 v_1 (-i) e^{i\theta} C^*_{k\downarrow-} C_{k\uparrow+}, \tag{3.38}$$

arising from the interference of the QP states which have experienced LZSM transitions. It is obvious that in its structure this function resembles the collective Higgs mode, which is excited in a natural way during the redistribution of states in the QP spectrum. Let us look at it in more details. Using the time-dependent coefficients (3.33-3.34) we obtain

$$\delta\Delta(t) = \lambda N(0) \int_{-\sqrt{h^2-\Delta^2}}^{\sqrt{h^2-\Delta^2}} \sqrt{p_k}\sqrt{1-p_k} G(\xi,t) \cos(D_k(t)) d\xi, \tag{3.39}$$

where we introduce the dynamical phase $D_k(t) = 2\int_{t_0}^{t}(E_0 - h(t))dt + \chi_k + \pi$ and the function $G(\xi,t) = \mathrm{sgn}(\alpha)(u_0u_1 + v_0v_1)$. The function $G(\xi)$ is proportional to $\alpha k_F/\Delta$, which means that $\delta\Delta(t)$ is parametrically small and can be considered against the background of the main change in the gap Δ_h from the equation (3.37).

For the integral (3.39), it is easy to estimate the asymptotic behavior at large times $\Delta_0/\gamma \ll t$. The dynamical phase is written as $D_k(t) = -(E_0^2 + \gamma^2 t^2)/\gamma + \chi_k + \pi + 2E_0 t$ for the spin-splitting field $h(t) = \gamma t$. Here $2E_0 t$ is a fast oscillating term at $t \to \infty$ and one can use a stationary phase approximation for the ξ-integration in Eq. (3.39) with the stationary phase point $\xi = 0$. Using Eq. (A6) for $G(\xi = 0, t)$, we find the asymptotic behavior of $\delta\Delta(t)$:

$$\delta\Delta(t) \approx \lambda N(0) e^{-\delta_{\mathrm{LZ}}/2}\sqrt{1-e^{-\delta_{\mathrm{LZ}}}} \frac{|\alpha|k_F}{2(\gamma t - \Delta_h)} \sqrt{\frac{\pi\Delta_h}{t}} \cos\Big[\frac{(\gamma t - \Delta_h)^2}{\gamma} + \frac{3\pi}{4} - \chi_0\Big], \tag{3.40}$$

where $\Delta_h[h(t\to\infty)]$ from Eq. (3.37) is a constant determined by δ_{LZ}. The result obtained means that the collective interference between the two QP states at each ξ_k after LZSM crossing behaves at large times as a modified Higgs mode. Due to linear dependence $h(t)$, this mode has a modulated frequency and polynomial damping law $\propto t^{-3/2}$ arising from the inhomogeneous broadening of the mode. Note that for large times only the contribution from the point $\xi = 0$ survives, so the amplitude of $\delta\Delta(t)$ does not depend on the number of redistributed states in the QP spectrum.

If the linear growth of the spin-splitting field $h(t)$ stops at a certain value $h_f > \Delta_0$ after the redistribution of some of the QP states, then the accumulated dynamic phase $D_k(t)$ and the gap fluctuation will depend only on this value h_f

$$\delta\Delta(t) \approx \lambda N(0) e^{-\delta_{\mathrm{LZ}}/2}\sqrt{1-e^{-\delta_{\mathrm{LZ}}}} \frac{|\alpha|k_F}{2(h_f - \Delta_h)} \sqrt{\frac{\pi\Delta_h}{t}} \cos\Big[2(h_f - \Delta_h)t - \frac{3\pi}{4} - \frac{\Delta_h^2 - h_f^2}{\gamma} + \chi_0\Big]. \tag{3.41}$$

The specific spectral distortion occurring between two brancher $E_{k\uparrow+}$ and $E_{k\downarrow-}$ during the Landau-

Zener dynamics at $h(t) < h_f$ acts as an initial perturbation for the gap function at $t = h_f/\gamma$. The free gap dynamics at $t > h_f/\gamma$ resembles the Higgs mode with $\delta\Delta(t) \propto \cos(2(h_f - \Delta_h)t)/\sqrt{t}$ at the frequency $\omega = 2|\Delta_h - h_f|$ (or $\omega = \omega_-$ in our previous notations) with the standard damping law. It is interesting, that the amplitude of this mode proportional to $|\alpha|k_F$ instead of $\alpha^2 k_F^2$ as it is expected in the case of small perturbations [Section 3.2]. Such amplification is a direct consequence of the intersection of two specific spectral branches and the subsequent non-adiabatic dynamics. Thus, this mode turns out to be leading in comparison with other nonadiabatic corrections arising due to the interaction of all QP spectral branches. Note, that the method for calculating the self-consistency equation developed in Section 3.2 can be combined with the Landau-Zener problem (D3) and all corrections can be computed within the perturbation theory.

3.3.5 Density of states and distribution function

Rearrangement of the spectrum as a result of the intersection of spectral branches naturally leads to a change of the structure of the density of states (DOS), that has become time dependent. Since the temporal evolution of the spectrum is adiabatic except the small region where the crossing occurs one can use the quasistatic description of the DOS. For the small RSOC the DOS for one spin projection can be written in terms of Bogoliubov-de Gennes functions

$$N_\uparrow(E,t) \approx \sum_k \sum_{n=\uparrow+,\uparrow-} |u_0|^2 \delta\Big(E - E_{kn}[h(t)]\Big) + |v_0|^2 \delta\Big(E + E_{kn}[h(t)]\Big). \tag{3.42}$$

Here we use static QP amplitudes u_0 and v_0 (see Eq. A4) to distinguish the particle/hole contributions and $E_{k\uparrow\pm}$ are defined in Eq. (3.4). The calculation of $N_\uparrow$ is cumbersome, because the RSOC shifts the spectral branches and opens a minigap $\propto \alpha k_F$ at $E = 0$ [Appendix E]. For the small RSOC parameter these changes are negligible and one can use a standard expression for the DOS

$$\frac{N_\uparrow(E,t)}{N(0)} \approx \frac{|E + h(t)|}{\sqrt{(E + h(t))^2 - \Delta_h[h(t)]^2}}. \tag{3.43}$$

Here the gap function Δ_h is taken from (3.37) and two coherence peaks are present at $E = \pm\Delta_h[h(t)] - h(t)$.

The amplitude of the QP wave function $\psi_k(t)$ from (3.27) contains the information about filling (or occupation) of the ξ_k-th state. More precisely the coefficients $|C_{k\uparrow\pm}(t)|^2$ and $|C_{k\downarrow\pm}(t)|^2$ can serve as an effective distribution functions $f_{\uparrow\downarrow}(E)$ for QPs with different spin projections. As discussed in the section 3.3.3, the temporal evolution of these coefficients is determined by the LZSM problem, and for spin-up states one has

$$\begin{aligned} |C_{k\uparrow-}(t)|^2 &= 1, \\ |C_{k\uparrow+}(t)|^2 &= (1 - p_k)\Theta\big[\sqrt{h^2(t) - \Delta_h^2} - \xi_k\big], \end{aligned}$$

which can be rewritten as a distribution function

$$f_\uparrow(E,t) \approx \begin{cases} 0, & E > 0 \\ 1 - \exp\Big[-\frac{\delta_{\text{LZ}}\Delta_h^2[h(t)]}{(E+h(t))^2}\Big], & \Delta_h - h < E < 0 \\ 1, & E < \Delta_h - h \end{cases} \tag{3.44}$$

The dependence $f_\uparrow(E)$ is shown in Fig. 3.4 for $\delta_{\rm LZ} = 0.5$. The most pronounced change of the distribution function occurs at $E \approx \Delta_h - h$, since for large QP energies the LZSM tunneling is suppressed. For the opposite spin projection the DOS $N_\downarrow(E)$ has the similar structure (3.43) with $h \to -h$, while the corresponding distribution function $f_\downarrow(E)$ is different and is given by the Eqs. (3.33-3.34). The DOS structure and effective distribution function enable the calculation of a system's optical or transport response, which can be experimentally measured.

3.3.6 Dynamical magnetization of QP gas

Nonadiabatic LZSM tunneling of QP states causes a spin imbalance in the spectrum, which results in the appearance of nonzero dynamical magnetization. Using (3.27) we can write an expression for the z-component of the magnetization per unit volume

$$m_z(t) = \mu_B \sum_{\text{i.c.}} \check{\psi}_k^\dagger(t) \check{\tau}_m \check{\psi}_k(t), \tag{3.45}$$

where $\check{\tau}_m = (\hat{\tau}_0 + \hat{\tau}_z) \otimes \hat{\sigma}_z/2$; the vector $\check{\psi}_k(t)$ is a solution of the TDBdG problem (3.27) and "i.c." means the summation over all initial conditions (see Eq. (3.3)). Due to symmetry and homogeneity of the problem for the field $\mathbf{h}(t) = h(t)\mathbf{z}_0$ the transversal components of the magnetization $m_{x,y}(t)$ are zero.

Taking the dynamical amplitudes $C_n(t)$ from (3.33-3.34) and implementing the same procedure as for the self-consistency equations (3.35-3.36) we found that the magnetization can be written as

$$m_z(t) = m_h[h(t)] + \delta m(t). \tag{3.46}$$

As in the case of the gap equation (3.36) we have two contributions: m_h which is a quasistatic function of $h(t)$ arising from the redistribution of the quaiparticle states, and $\delta m(t) \propto \alpha k_F$ which is small oscillatory term originated from the interference of the redistributed states. The first term can be easily calculated with the help of the quasiparticle density

$$n_\sigma(t) = \int N_\sigma(E,t) f_\sigma(E,t) dE, \tag{3.47}$$

where $\sigma = \{\uparrow, \downarrow\}$. Corresponding spin imbalance results in the dynamical magnetization $m_h[h(t)] = \mu_B(n_\uparrow - n_\downarrow)$, which is shown in Fig. 3.5(a).

For $h(t) < \Delta_0$ there is no crossing of the QP spectral branches and according to our model there is no tunneling between QP states, therefore $m_h = 0$. Once the intersection has occurred at $h(t) = \Delta_0$, the distribution functions $f_{\uparrow,\downarrow}(E)$ transform and nonzero spin imbalance $n_\uparrow - n_\downarrow$ is generated. Due to the jump of Δ_h function at $h(t) = \Delta_0$ [Fig. 3.4] the magnetization m_h at this point also has a jump discontinuity. At large times the tunneling of QP states is suppressed therefore the magnetization is saturated to a constant value determined by the parameter $\delta_{\rm LZ}$. Obviously, an increase in $\delta_{\rm LZ}$ makes the spin-flip tunneling more efficient and thereby increases the maximum value of m_h. The second term in (3.46) resembles the Higgs mode term (3.38) and gives negligible contribution to $m_z(t)$, therefore it can be discarded.

In addition one can compute the dynamical susceptibility of the QP gas in the Zeeman field of the general form $h(t) = \mu_{\rm B} H(t)$. It is known that an orbital and a spin parts of the magnetic susceptibility can be splitted in the case of small spin-orbital effects [301]. Since we consider a homogeneous system and neglect all orbitals effects only the spin part plays a role, which can be

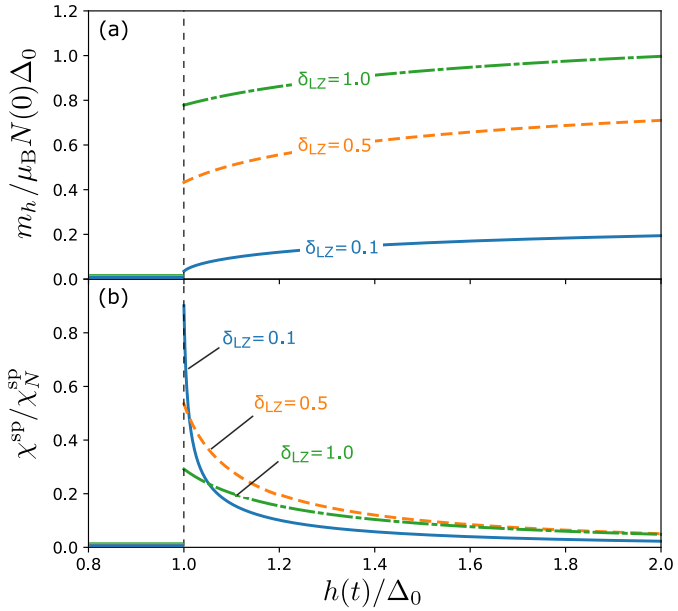

Figure 3.5: (a) Dynamical magnetization m_h per unit volume induced by the nonadiabatic tunneling of QP states and (b) corresponding spin susceptibility χ^{sp} versus time-dependent spin-splitting field $h(t)$ for different values of δ_{LZ}.

written as follows

$$\chi^{sp}[h(t)] = \mu_B \frac{\partial m_h}{\partial h}. \tag{3.48}$$

The ratio of the numerically calculated susceptibility $\chi^{sp}[h(t)]$ and the normal susceptibility $\chi^{sp}_N = 2\mu_B^2 N(0)$ [303] is shown if Fig. 3.5(b). It is seen that spin-flip tunneling in the QP spectrum provokes a paramagnetic response of the superconducting condensate. The function (3.48) should have a singularity $\chi^{sp} \propto (h(t) - \Delta_0)^{-1/2}$ in the vicinity of $h(t) \approx \Delta_0$, which is defined by the shape of the QP spectrum at $k \approx k_F$ and has the same origin as the coherence peak in the DOS (3.43). However, due to the jump of the order parameter Δ_h at this point we observe shifted peaks, which have to be smeared out near $h(t) = \Delta_0$ if more realistic model of LZSM tunneling [Section 3.3.2] is taken into account. We note again that we discuss only the dynamic contribution to the susceptibility, which, generally speaking, has to be added to the static one, which is not equal to zero at $T = 0$ in the presence of SOC [301, 303].

3.4 Experimental perspectives

We propose superconductor-ferromagnet hybrid structures as an experimental platform for detecting the described effects. The ferromagnetic layer can serve as a source of both Rashba spin-orbit coupling and an exchange field. Since it is important to remove orbital effects from the system, the most suitable geometry for superconductor is either thin film or one-dimensional nanowire [304]. For the small layer thicknesses, the exchange interaction can be averaged in the direction perpendicular to the layers giving a homogeneous effective exchange field inside the superconductor.

The excitation of spin-split Higgs modes in superconductors requires frequencies of the order of $\Delta_0/\hbar$, which vary from the far infrared to the terahertz range. The laser excitation of modes seems to be the most practical and feasible, and their detection can be implemented using the

ultrafast pump-probe spectroscopy [137–139].

We propose two possible ways to generate rapidly changing modulus of the spin-splitting field $h(t)$:

• If the S/F bilayer possesses a strongly anisotropic exchange, so that the Zeeman energy $\propto \mathbf{M}_F\hat{g}\boldsymbol{\sigma}$ in Eq. (3.6) is defined through the tensorial g-factor, then the absolute value of the exchange field is no more determined only by the absolute value of the magnetic moment $|\mathbf{M}_F(t)| = const$. Thus, we can get a pronounced component of the spin-splitting field $h_z(t)$ varying in time just for a standard precession of $\mathbf{M}_F(t)$. Such approach can be reasonable amid a progress in the ultrafast optical control of magnetization in various materials [150, 305–307].

• Another possibility is based on the obvious fact that the field $\mathbf{h}$ is determined not only by the magnetic moment but also by the penetration length of the wave functions of electrons from superconductor to the insulator. This penetration clearly depends on the potential jump at the S/F interface and, thus, can be tuned by the electric field effect. Certainly, to realize a noticeable field effect we need to take a ferromagnetic film with a rather narrow energy gap in the band spectrum, e.g., a film of ferromagnetic semiconductor. In this case the exchange field value can be modulated by simply applying a time-dependent gate potential to the semiconducting layer. As a potential reference one can mention the field control of the spin-orbit coupling in the superconducting 2D electron gas in the oxide bilayer [308, 309].

Finally, we present parameter estimates for the experimental observation of LZSM transitions in the QP spectrum. For example, consider $\Delta_0 = 0.1$ meV (for $T_c \approx 1$K) and $\alpha k_F \sim 10^{-3}$meV $\ll \Delta_0$. Then the constraint for the small tunneling rate is $\hbar\gamma \gtrsim \alpha^2 k_F^2$ in dimensional units, which is equivalent to $\gamma \gtrsim 10^{-3}$ meV/ns. Consider inelastic relaxation of QP with a typical time $\tau_{\text{ph}} \sim 100$ ns in the case of the electron-phonon scattering at low temperatures [310, 311] . The collisionless regime is maintained at $t \ll \tau_{\text{ph}}$, which corresponds to times $t \lesssim 10$ ns. Under such conditions the field $h(t) = \gamma t \sim \Delta_0$ is achievable only for $\gamma \sim 10^{-2}$ meV/ns. The measurements of the various properties of the superconducting condensate above Pauli limit at short times can be implemented with the help of ultrafast THz techniques, such as pump-probe [139] for an optical conductivity.

3.5 Summary and outlook

We have analyzed the coherent dynamics of the superconducting condensate in the presence of Zeeman field and SOC in collisionless regime. Two different nonequilibrium dynamical regimes are considered using the time-dependent Bogoliubov-de Gennes equations.

First, it was established that the Higgs mode of the superconducting gap (oscillations of the modulus of the order parameter $|\Delta|(t) = \Delta_0 + |\delta\Delta|(t)$) is sensitive to the Zeeman field h_0 and besides the standard resonant frequency $\omega_0 = 2\Delta_0$ has two additional peaks at $\omega_\pm = 2(\Delta_0 \pm h_0)$. This reflects the three possible channels of the dissociation of Cooper pairs into QP, and satellite frequencies $\omega_\pm$ correspond to decay of the pair with spin-flipping of one of the QP. Therefore, the excitation of these spin-split modes occurs in proportion to the spin-orbit interaction $\propto \alpha k_F$, which is assumed to be small in our model. The Higgs modes of the order parameter contribute to the linear response of the superconducting condensate, and can be directly triggered by either harmonic perturbation of the Zeeman field $h = h_0 + \delta h(t)$, which couples to $\delta\Delta(t)$ linearly, or by a nonadiabatic quench induced by an external laser pulse.

Second, it was shown, that the field $h(t) = \gamma t$ can provoke an avoided crossing of the QP spectral branches $E_{kn}(t)$ accompanied by adiabatic spin-flip tunneling of the QPs between the different branches. With some simplifications, this tunneling can be described by a two-level Landau-Zener-Stückelberg-Majorana problem for individual pairs of QPs. The rate of change of the field $h(t)$ makes it possible to effectively switch between two opposite adiabatic ($\gamma \ll \alpha^2 k_F^2$) and quenching ($\gamma \gtrsim \alpha^2 k_F^2$) regimes of spectrum intersection. Corresponding nonequilibrium redistribution of the QP states in the spectrum leads to (i) the appearance of the quasistatic dependence $\Delta[h(t)]$, which demonstrates the persistance of the gap above the Pauli limit in the collisionless regime; (ii) and generation of the interference effects caused by partial tunneling of states at the avoided crossing points. Emerging spin imbalance in the QP spectrum manifests itself in the effective dynamical distribution function and in a generation of a weak magnetization of the QP gas. Corresponding contribution to its spin susceptibility has a characteristic peak at $h(t) = \Delta_0$. These findings may be promising in the context of ultrafast magnetization experiments and in the study of hybrid S/F structures with complex magnetic dynamics and strong proximity effects.

3.6 Appendix

A Eigenvectors of $\check{\mathcal{H}}$

The instantaneous eigenvectors of the Hamiltonian $\check{\mathcal{H}}(k,t)$ from Eq. (3.2) can be written as follows

$$\check{\Psi}_{kn}(t) = \frac{1}{\sqrt{1+a_{1n}^2+a_{2n}^2+a_{3n}^2}} \begin{pmatrix} 1 \\ -ia_{1n}e^{i\theta_k} \\ -ia_{2n}e^{i\theta_k} \\ a_{3n} \end{pmatrix}, \tag{A1}$$

where we have defined the phase $\theta_k = \arg\left(k_x + ik_y\right)$ and real coefficients

$$\begin{aligned} a_{1n} &= \frac{(h+E_{kn})^2 - E_0^2 - \alpha^2 k^2}{2\alpha k(\xi_k + h)}, \\ a_{2n} &= \frac{\alpha k}{\Delta} - \frac{E_{kn} - \xi_k - h}{\Delta} a_{1n}, \\ a_{3n} &= \frac{E_{kn} - \xi_k + h}{\Delta} - \frac{\alpha k}{\Delta} a_{1n}. \end{aligned} \tag{A2}$$

The instantaneous eigenvalues of $\check{\mathcal{H}}(k,t)$ are

$$E_{kn}(t) \equiv E_{k\sigma\pm}(t) = \pm\sqrt{E_0^2 + \alpha^2 k^2 + h^2(t) \mp \mathrm{sgn}(\sigma) 2\sqrt{\xi_k^2 \alpha^2 k^2 + h^2(t) E_0^2}},$$

where $E_0 = \sqrt{\xi_k^2 + \Delta^2}$; the subscript $\pm$ refers to spectral branch above/below the Fermi level and $\sigma = \{\uparrow, \downarrow\}$ denotes a spin subband. Note, that the Hamiltonian (3.2) implies the symmetry relations between the energies $E_{k\uparrow+} = -E_{k\downarrow-}$ and $E_{k\downarrow+} = -E_{k\uparrow-}$, and between the corresponding eigenvectors $\check{\Psi}_{k\uparrow+} = i\hat{\tau}_y \otimes \hat{\sigma}_z \check{\Psi}^*_{k\downarrow-}$ and $\check{\Psi}_{k\downarrow+} = i\hat{\tau}_y \otimes \hat{\sigma}_z \check{\Psi}^*_{k\uparrow-}$, where $\hat{\tau}_i(\hat{\sigma}_i)$ is the Pauli matrix in the Nambu(spin) space.

For the case of weak SOC $\alpha k_F \ll \{E_F, h(t), \Delta(t)\}$ the eigenvectors (A1) can be expanded up to the first order in $\alpha k_F/\Delta$ as follows

$$\begin{aligned} \check{\Psi}_{k\uparrow+} &\approx \begin{pmatrix} u_0 \\ -iu_1 e^{i\theta_k} \\ -iv_1 e^{i\theta_k} \\ v_0 \end{pmatrix}, \quad \check{\Psi}_{k\downarrow+} \approx \begin{pmatrix} iu_1 e^{-i\theta_k} \\ -u_0 \\ v_0 \\ -iv_1 e^{-i\theta_k} \end{pmatrix}, \\ \check{\Psi}_{k\uparrow-} &\approx \begin{pmatrix} -v_0 \\ iv_1 e^{i\theta_k} \\ -iu_1 e^{i\theta_k} \\ u_0 \end{pmatrix}, \quad \check{\Psi}_{k\downarrow-} \approx \begin{pmatrix} -iv_1 e^{-i\theta_k} \\ v_0 \\ u_0 \\ -iu_1 e^{-i\theta_k} \end{pmatrix}. \end{aligned} \tag{A3}$$

Here we define equilibrium QP amplitudes

$$u_0 = \frac{1}{\sqrt{2}}\sqrt{1 + \frac{\xi_k}{E_0}}, \quad v_0 = \frac{1}{\sqrt{2}}\sqrt{1 - \frac{\xi_k}{E_0}}, \tag{A4}$$

and

$$u_1 \approx \alpha k \frac{h-\xi_k}{2h(E_0-h)} u_0, \quad v_1 \approx \alpha k \frac{(h+\xi_k)(E_0-\xi_k)}{2h\Delta(E_0-h)} u_0 \tag{A5}$$

correspond to the triplet component of the QP wave functions.

The function $G(\xi,t) = \mathrm{sgn}(\alpha)(u_0 u_1 + v_0 v_1)$ from Eq. (3.39) at the stationary phase point $\xi = 0$ can be found from (A4-A5) by putting $\Delta \approx \Delta_h$ (see Eq. (3.37)) and reads

$$G(0,t) \approx \frac{|\alpha| k_F}{2(h(t)-\Delta_h)}. \tag{A6}$$

B Derivation of linearized self-consistency equation

We start with the linearized (3.8, 3.11) dynamical equations

$$i\frac{\partial}{\partial t}\delta C_{km} = \sum_n \check{\Psi}^\dagger_m \check{\mathcal{V}}(t) \check{\Psi}_n e^{-i(E_n - E_m)t}\big(\delta_{n,l} + \delta C_{kn}\big), \tag{B1}$$

where $\delta_{n,n'}$ is Kronecker delta, the indices $n,m = \{\uparrow +, \downarrow +, \uparrow -, \downarrow -\}$ number all QP branches and $l = \{\uparrow -, \downarrow -\}$ corresponds to two possible initial configurations (see Eq. (3.10)). The compact form of the self-consistency equation for the gap (3.9) is

$$\Delta_{\mathrm{eq}} + \delta\Delta(t) = -\frac{\lambda}{2}\sum_l \sum_k \sum_{n,n'} \big(\delta_{n,l} + \delta C_{kn}(t)^*\big)\big(\delta_{n',l} + \delta C_{kn'}(t)\big) e^{-i(E_{n'} - E_n)t} \check{\Psi}^\dagger_{kn} \check{\tau}_\Delta \check{\Psi}_{kn'}. \tag{B2}$$

As was mentioned in Section 3.2, we neglect the effect of RSOC on the equilibrium value of the gap, which can be taken as $\Delta_{\mathrm{eq}} = \Delta_0$. It also makes sense to omit the negligibly small corrections from the RSOC to the energy spectrum, so one can put $E_n \equiv E_{k\sigma\pm} \approx \pm E_0 - \mathrm{sgn}(\sigma) h_0$.

The equations (B1, B2) can be simplified and written as follows

$$\begin{gathered}
\frac{\partial f_1}{\partial t} = i e^{i(2(E_0 - h_0)t)}[\mathcal{A}\delta\Delta(t) - \mathcal{B}\delta h(t)], \\
\frac{\partial f_2}{\partial t} = i e^{i(2(E_0 + h_0)t)}[\mathcal{A}\delta\Delta(t) + \mathcal{B}\delta h(t)], \\
\frac{\partial g}{\partial t} = i\frac{\xi}{E_0} e^{i(2E_0 t)}\delta\Delta(t), \\
\delta\Delta(t) = \Big\langle \frac{\mathcal{A}}{2}\mathrm{Re} f_1(t) e^{-i(2(E_0-h_0)t)} \Big\rangle + \Big\langle \frac{\mathcal{A}}{2}\mathrm{Re} f_2(t) e^{-i(2(E_0+h_0)t)} \Big\rangle + \Big\langle \frac{\xi}{E_0}\mathrm{Re} g(t) e^{-i(2E_0 t)} \Big\rangle.
\end{gathered} \tag{B3}$$

We have used the notation $\langle \dots \rangle = \lambda \sum_k \approx \lambda N(0) \int_{-\omega_D}^{\omega_D} d\xi$ and introduced new complex-valued functions

$$\begin{gathered}
f_1 \equiv -ie^{i\theta}\delta C_{\uparrow +}, \quad g_1 \equiv -\delta C_{\downarrow +}, \\
f_2 \equiv -ie^{-i\theta}\delta C_{\downarrow +}, \quad g_2 \equiv -\delta C_{\uparrow +}, \\
g = \frac{g_1 + g_2}{2},
\end{gathered} \tag{B4}$$

where the subscript corresponds to the two possible initial conditions. The functions

$$\mathcal{A}(\xi) = 2(u_0u_1 + v_0v_1) \approx \alpha k_F \frac{E_0h - \xi^2}{E_0h(E_0 - h)}, \tag{B5}$$
$$\mathcal{B}(\xi) = 2(u_0v_1 + u_1v_0) \approx \alpha k_F \frac{\Delta_0}{E_0(E_0 - h)}$$

have the lowest order in αk_F parameter [Appendix A] and are even in ξ. All terms odd in ξ in Eq. (B3) are related to the imaginary part of $\delta\Delta(t)$ and vanish due to the approximate electron-hole symmetry of BdG Hamiltonian (3.2), due to which the density of states is approximated as $N(\xi) \approx N(0)$ in the $\langle ...\rangle$-integration [312].

Applying the Laplace transform $f(s) = \int_0^\infty e^{-st} f(t)dt$ with $s = i\omega + \zeta$ (where $\zeta \to 0$) for Eq. (B3) we obtain the gap equation in the complex plane, which is found to be

$$\delta\Delta(s) = \tag{B6}$$
$$\delta\Delta(s)\Big\langle \frac{2\xi^2}{E_0}\frac{1}{s^2+4E_0^2}\Big\rangle + \delta\Delta(s)\Big\langle \mathcal{A}^2(\xi)\frac{(E_0+h_0)}{s^2+4(E_0+h_0)^2}\Big\rangle + \delta\Delta(s)\Big\langle \mathcal{A}^2(\xi)\frac{(E_0-h_0)}{s^2+4(E_0-h_0)^2}\Big\rangle$$
$$+\delta h(s)\Big\langle \mathcal{A}(\xi)\mathcal{B}(\xi)\frac{(E_0+h_0)}{s^2+4(E_0+h_0)^2}\Big\rangle - \delta h(s)\Big\langle \mathcal{A}(\xi)\mathcal{B}(\xi)\frac{(E_0-h_0)}{s^2+4(E_0-h_0)^2}\Big\rangle$$
$$+\Big\langle f_1'(0)\frac{\mathcal{A}(\xi)}{2}\frac{s}{s^2+4(E_0-h_0)^2}\Big\rangle + \Big\langle f_1''(0)\frac{\mathcal{A}(\xi)(E_0-h_0)}{s^2+4(E_0-h_0)^2}\Big\rangle$$
$$+\Big\langle f_2'(0)\frac{\mathcal{A}(\xi)}{2}\frac{s}{s^2+4(E_0+h_0)^2}\Big\rangle + \Big\langle f_2''(0)\frac{\mathcal{A}(\xi)(E_0+h_0)}{s^2+4(E_0+h_0)^2}\Big\rangle$$
$$+\Big\langle g'(0)\frac{\xi}{E_0}\frac{s}{s^2+4E_0^2}\Big\rangle + \Big\langle g''(0)\frac{2\xi}{s^2+4E_0^2}\Big\rangle.$$

Here $f = f' + if''$ and the initial conditions $f_{1,2}(0) = f_{1,2}(t=0)$, $g(0) = g(t=0)$ implicitly contain the initial value of the gap perturbation $\delta\Delta(t=0)$. Now we can single out functions of s with different singularities in the complex plane and denote them using short notations

$$\mathcal{K}_0(s) = \Big\langle \frac{2\xi^2}{E_0}\frac{1}{s^2+4E_0^2}\Big\rangle, \tag{B7}$$
$$\mathcal{K}_\pm(s) = \Big\langle \mathcal{A}^2(\xi)\frac{(E_0\pm h_0)}{s^2+4(E_0\pm h_0)^2}\Big\rangle,$$
$$\mathcal{F}_\pm(s) = \Big\langle \mathcal{A}(\xi)\mathcal{B}(\xi)\frac{(E_0\pm h_0)}{s^2+4(E_0\pm h_0)^2}\Big\rangle.$$

Other terms in Eq. (B6) can be grouped into one function

$$\mathcal{I}(s) = \Big\langle \frac{\mathcal{A}(\xi)}{2}\frac{sf_1'(0) + 2(E_0-h_0)f_1''(0)}{s^2+4(E_0-h_0)^2}\Big\rangle \tag{B8}$$
$$+\Big\langle \frac{\mathcal{A}(\xi)}{2}\frac{sf_2'(0) + 2(E_0+h_0)f_2''(0)}{s^2+4(E_0+h_0)^2}\Big\rangle$$
$$+\Big\langle \frac{\xi}{E_0}\frac{sg'(0) + 2E_0g''(0)}{s^2+4E_0^2}\Big\rangle.$$

which actually is an *effective* initial condition for the dynamics of the gap $\delta\Delta(t)$ and originated from the initial nonequilibrium perturbations of the QP population $\delta C_{kn}(t=0)$. The functions $\mathcal{A}$

and $\mathcal{B}$ are of the first order in the small parameter $\alpha k_F/\Delta$, therefore we have

$$\mathcal{K}_0(s) \propto \mathcal{O}\Big(\frac{\alpha^0 k_F^0}{\Delta_0^0}\Big), \qquad \mathcal{K}_\pm(s), \mathcal{F}_\pm(s) \propto \mathcal{O}\Big(\frac{\alpha^2 k_F^2}{\Delta_0^2}\Big).$$

It can be shown that the the difference $[\mathcal{F}_+(s) - \mathcal{F}_-(s)]$ is proportional to h_0. This allows one to write the terms with $\delta h(t)$ in (B6) as $\delta h(s)[\mathcal{F}_+(s) - \mathcal{F}_-(s)]$ or $(\mathbf{h}_0 \cdot \delta\mathbf{h}(s))[\mathcal{F}_+(s) - \mathcal{F}_-(s)]/h_0$, where both vectors are oriented along $\mathbf{z}_0$ axis. By rewriting the equation (B6) with the new introduced functions (B7) we get the self-consistency equation (3.12).

C Long-time behavior of $\delta\Delta(t)$

The susceptibility $\mathrm{Im}\chi_{\Delta\Delta}(s)|_{\zeta\to 0} = \mathrm{Im}\chi_{\Delta\Delta}(\omega)$ in Eq. (3.21) has strongly dominant terms in the vicinity of different branch points in the interval $\omega \in [\omega_-, \infty)$. In order to demonstrate this, the function $\mathrm{Im}\chi_{\Delta\Delta}(s)$ can be expanded in a series up to the second order in the parameter $\alpha k_F/\Delta$, and this expansion must be carried out accurately near the branch points and may differ in different regions of ω. Therefore, we assume that the value of the integral is determined by these dominant contributions of $\mathrm{Im}\chi_{\Delta h}(\omega)$ and can be evaluated sequentially as $\int_{\omega_-}^{\infty} = \int_{\omega_-}^{\omega_0} + \int_{\omega_0}^{\omega_+} + \int_{\omega_+}^{\infty}$. Let us consider the small regions $\Omega \ll \omega_{0,\pm}$ in the vicinity of these points separately.

- Close to the point $\omega = \omega_- + \Omega$ the term $\mathcal{K}''_-(\omega)$ dominates:

$$\mathcal{K}''_-(\Omega) \approx -\lambda N(0)\frac{\pi\Delta_0\mathcal{A}^2(0)}{4\sqrt{\Delta_0\Omega}} \propto \frac{1}{\sqrt{\Omega}}. \tag{C1}$$

Despite the kernel $1 - \mathcal{K}'_0(\omega)$ goes to zero at $\omega \to \omega_0$ there is no singularity in $\chi_{\Delta\Delta}(\omega)$ at this point due to the small terms of the order of $(\alpha k_F)^2$ in the denominator. Therefore, the region in the vicinity of ω_0 will not contribute to the integral. Thus, the behavior of the first integral for $\omega \in [\omega_-, \omega_0)$ at large time $h_0 t \gg 1$ can be estimated as follows

$$\int_{\omega_-}^{\omega_0} \approx \mathrm{Im}\left[\frac{\mathcal{I}_0 e^{i\omega_- t}}{\big[1 - \mathcal{K}'_0(\omega_-)\big]^2}\int_0^{\omega_0-\omega_-} \mathcal{K}''_-(\Omega)e^{i\Omega t}d\Omega\right] \approx -\lambda N(0)\frac{\pi^{3/2}\Delta_0\mathcal{A}^2(0)}{4\sqrt{\Delta_0 t}}\frac{\mathrm{Im}\Big[\mathcal{I}_0 e^{i(\omega_- t+\pi/4)}\Big]}{\big[1 - \mathcal{K}'_0(\omega_-)\big]^2}. \tag{C2}$$

- In the vicinity of the branch point $\omega = \omega_0 + \Omega$ the main contribution is defined by

$$\mathcal{K}''_0(\Omega) \approx -\lambda N(0)\frac{\pi}{2\Delta_0}\sqrt{\Delta_0\Omega} \propto \sqrt{\Omega}. \tag{C3}$$

Thus at large times $h_0 t \gg 1$ we get

$$\int_{\omega_0}^{\omega_+} = \int_{\omega_0}^{\omega_+} \frac{1}{\mathcal{K}''_0(\omega)}\mathrm{Im}\Big[e^{i\omega t}\mathcal{I}_0\Big]d\omega \approx -\frac{2\sqrt{\Delta_0}}{\sqrt{\pi t}}\frac{1}{\lambda N(0)}\mathrm{Im}\Big[\mathcal{I}_0 e^{i(\omega_0 t+\pi/4)}\Big]. \tag{C4}$$

- For the last branch point $\omega = \omega_+ + \Omega$ the kernel $\mathcal{K}''_+(\omega)$ dominates:

$$\mathcal{K}''_+(\Omega) \approx -\lambda N(0)\frac{\pi\Delta_0\mathcal{A}^2(0)}{4\sqrt{\Delta_0\Omega}} \propto \frac{1}{\sqrt{\Omega}}. \tag{C5}$$

At large times $h_0 t \gg 1$ we get

$$\int_{\omega_+}^{\infty} \approx \int_{\omega_+}^{\infty} \frac{\mathcal{K}_+''(\omega)\mathrm{Im}\left[e^{i\omega t}\mathcal{I}_0\right]}{\left[1-\mathcal{K}_0'(\omega_+)\right]^2+\left[\mathcal{K}_0''(\omega_+)\right]^2} d\omega \approx -\lambda N(0)\frac{\pi^{3/2}\Delta_0\mathcal{A}^2(0)}{4\sqrt{\Delta_0 t}}\frac{\mathrm{Im}\left[\mathcal{I}_0 e^{i(\omega_+ t+\pi/4)}\right]}{\left[1-\mathcal{K}_0'(\omega_+)\right]^2+\left[\mathcal{K}_0''(\omega_+)\right]^2}. \tag{C6}$$

By combining all three contribution (C2,C4,C6) we will get the equation (3.22) in the main text. Note, that discussed approximations work for $0 < h_0 < \Delta_0$.

The Eq. (3.26) can be obtained in the similar way from Eq. (3.24):

$$\delta\Delta(t) = \sum_p \chi_{\Delta h}(s_p) e^{s_p t}\underset{s=s_p}{\mathrm{Res}}\left[\delta h(s)\right] + \frac{2}{\pi}\int_{\omega_-}^{\infty}\mathrm{Im}\chi_{\Delta h}(s)\big|_{\zeta\to+0}\mathrm{Im}\left[e^{i\omega t}\delta h(i\omega)\right]d\omega. \tag{C7}$$

The kernels $\mathcal{F}_\pm(s)$ in (3.25) have the same analytical properties as $\mathcal{K}_\pm(s)$ and only differ by $\mathcal{A}^2(\xi) \to \mathcal{A}(\xi)\mathcal{B}(\xi)$. The functions $\mathcal{A}$ and $\mathcal{B}$ from (B5) at the point $\xi = 0$ are

$$\mathcal{A}(0)\mathcal{B}(0) = \mathcal{A}^2(0) = \frac{(\alpha k_F)^2}{(\Delta_0 - h_0)^2}. \tag{C8}$$

Also, the analytical expressions for the kernel $\mathcal{K}_0(\omega)$ at $\omega > 0$ reads

$$\frac{1-\mathcal{K}_0'(\omega)}{\lambda N(0)} = \begin{cases} \frac{\sqrt{4\Delta_0^2-\omega^2}}{\omega}\arctan\left(\frac{\omega}{\sqrt{4\Delta_0^2-\omega^2}}\right) & \text{for} \quad \omega < 2\Delta_0 \\ -\frac{\sqrt{\omega^2-4\Delta_0^2}}{\omega}\frac{1}{2}\ln\left(\frac{\omega-\sqrt{\omega^2-4\Delta_0^2}}{\omega+\sqrt{\omega^2-4\Delta_0^2}}\right) & \text{for} \quad \omega > 2\Delta_0 \end{cases}, \tag{C9}$$

$$\frac{\mathcal{K}_0''(\omega)}{\lambda N(0)} = -\frac{\pi}{2}\frac{\sqrt{\omega^2-4\Delta_0^2}}{\omega}\Theta[\omega-2\Delta_0]. \tag{C10}$$

Finally, the expression with the kernels $\mathcal{F}_\pm(\omega)$ from (C4) can be calculated numerically for small $\alpha k_F \ll \Delta_0$:

$$\frac{\left[\mathcal{F}_+'(\omega_0)-\mathcal{F}_-'(\omega_0)\right]}{\lambda N(0)} = h_0\int_0^{\omega_D}\mathcal{A}(\xi)\mathcal{B}(\xi)\frac{h_0^2-\xi^2-2\Delta_0^2}{(\xi^2-h_0^2)^2-4\Delta_0^2 h_0^2}d\xi. \tag{C11}$$

D Derivation and solution of LZSM problem

The dynamics of two levels with avoided crossing can be simply described with the help of so-called *diabatic* basis formed by the instantaneous eigenfunction $\check{\Phi}^0_{kn}(t)$ of the time-dependent Hamiltonian (3.1) at $\alpha = 0$. Note here that for $\alpha = 0$ the eigenstates do not depend of $h(t)$ at all and consist only of the Bogoliubov's amplitudes u_0 and v_0 (one can use (A3) and put $\alpha = 0$ there). The complete solution of the time-dependent Hamiltonian can be written as

$$\check{\Psi}_k(t) = \sum_n C^d_{kn}(t)\check{\Phi}^0_{kn}(t), \tag{D1}$$

where $n = \{\uparrow+, \downarrow+, \uparrow-, \downarrow-\}$. In order to avoid confusion with adiabatic basis in (3.27) the superscript "d" is used to denote the diabatic basis. The time-dependent coefficients obey the

following equation derived from (3.1):

$$i\frac{\partial}{\partial t}C_m^d = \sum_n C_n^d \check{\Phi}_{km}^{0\dagger}\Big[\check{\mathcal{H}}(t) - i\frac{\partial}{\partial t}\Big]\check{\Phi}_{kn}^0. \tag{D2}$$

Note that here $\check{\mathcal{H}}(t)\check{\Phi}_{kn}^0 \neq E_n(t)\check{\Phi}_{kn}^0$. By keeping in mind that $\hat{\Phi}_{kn}^0(t)$ depends on time only through $\Delta(t)$, one can rewrite (D2) as follows

$$i\frac{\partial}{\partial t}\begin{pmatrix} C_{\uparrow+}^d \\ C_{\downarrow+}^d \\ C_{\uparrow-}^d \\ C_{\downarrow-}^d \end{pmatrix} = \begin{pmatrix} E_0 - h(t) & -\frac{\xi_k}{E_0}i\alpha k e^{-i\theta_k} & i\frac{\xi_k}{2E_0^2}\frac{\partial\Delta}{\partial t} & \frac{\Delta}{E_0}i\alpha k e^{-i\theta_k} \\ \frac{\xi_k}{E_0}i\alpha k e^{i\theta_k} & E_0 + h(t) & -\frac{\Delta}{E_0}i\alpha k e^{i\theta_k} & i\frac{\xi_k}{2E_0^2}\frac{\partial\Delta}{\partial t} \\ -i\frac{\xi_k}{2E_0^2}\frac{\partial\Delta}{\partial t} & \frac{\Delta}{E_0}i\alpha k e^{-i\theta_k} & -E_0 - h(t) & \frac{\xi_k}{E_0}i\alpha k e^{-i\theta_k} \\ -\frac{\Delta}{E_0}i\alpha k e^{i\theta_k} & -i\frac{\xi_k}{2E_0^2}\frac{\partial\Delta}{\partial t} & -\frac{\xi_k}{E_0}i\alpha k e^{i\theta_k} & -E_0 + h(t) \end{pmatrix}\begin{pmatrix} C_{\uparrow+}^d \\ C_{\downarrow+}^d \\ C_{\uparrow-}^d \\ C_{\downarrow-}^d \end{pmatrix}, \tag{D3}$$

where $E_0 = \sqrt{\xi_k^2 + \Delta^2}$. One can remove the phase $\theta_k = \arg\left(k_x + ik_y\right)$ from (D3) by the unitary operator

$$\hat{U}_\theta = \begin{pmatrix} e^{i(\frac{\pi}{4} - \frac{\theta_k}{2})\hat{\sigma}_z} & 0 \\ 0 & e^{i(\frac{\pi}{4} - \frac{\theta_k}{2})\hat{\sigma}_z} \end{pmatrix}, \tag{D4}$$

so that in the new basis we have

$$i\frac{\partial}{\partial t}\begin{pmatrix} \tilde{C}_{\uparrow+}^d \\ \tilde{C}_{\downarrow+}^d \\ \tilde{C}_{\uparrow-}^d \\ \tilde{C}_{\downarrow-}^d \end{pmatrix} = \begin{pmatrix} E_0 - h(t) & -\frac{\xi}{E_0}\alpha k & i\frac{\xi}{E_0^2}\frac{\partial\Delta}{\partial t} & \frac{\Delta}{E_0}\alpha k \\ -\frac{\xi}{E_0}\alpha k & E_0 + h(t) & \frac{\Delta}{E_0}\alpha k & i\frac{\xi}{E_0^2}\frac{\partial\Delta}{\partial t} \\ -i\frac{\xi}{E_0^2}\frac{\partial\Delta}{\partial t} & \frac{\Delta}{E_0}\alpha k & -E_0 - h(t) & \frac{\xi}{E_0}\alpha k \\ \frac{\Delta}{E_0}\alpha k & -i\frac{\xi}{E_0^2}\frac{\partial\Delta}{\partial t} & \frac{\xi}{E_0}\alpha k & -E_0 + h(t) \end{pmatrix}\begin{pmatrix} \tilde{C}_{\uparrow+}^d \\ \tilde{C}_{\downarrow+}^d \\ \tilde{C}_{\uparrow-}^d \\ \tilde{C}_{\downarrow-}^d \end{pmatrix}. \tag{D5}$$

We assume that the time evolution of the gap function $\Delta(t)$ is adiabatic on the timescale of the problem (D5). Therefore one can assume Δ to be constant during the transition with the typical time $\sim \tau_{\text{LZ}}$. Since the most emphasized dynamics occurs between two crossing branches, it is convenient to consider the interaction of only the corresponding terms $C_{k\uparrow+}$ and $C_{k\downarrow-}$ [Fig. 3.3]. Hence, one can extract an effective two-level problem for the crossing levels:

$$i\frac{\partial}{\partial t}\begin{pmatrix} \tilde{C}_{k\uparrow+}^d \\ \tilde{C}_{k\downarrow-}^d \end{pmatrix} = \begin{pmatrix} E_0 - \gamma t & \frac{\Delta}{E_0}\alpha k \\ \frac{\Delta}{E_0}\alpha k & -E_0 + \gamma t \end{pmatrix}\begin{pmatrix} \tilde{C}_{k\uparrow+}^d \\ \tilde{C}_{k\downarrow-}^d \end{pmatrix}. \tag{D6}$$

This system can be viewed as the LZSM problem, which allows an exact solution [300]. However, as discussed in 3.3.2, one can neglect the transient dynamics of the $C_k(t)$ coefficients in the gap equation (3.3) and use the transition matrix approach instead. Thus, we need to obtain the relation between the long-time asymptotes of the functions $\tilde{C}_{k\uparrow\downarrow+}^d(t)$ before (t_0-) and after (t_0+) transition at the point $t_0(\xi_k) = \sqrt{\xi_k^2 + \Delta^2}/\gamma$. Here we use short notations $(t_0\mp) \approx t_0 \mp \tau_{\text{LZ}}/2$. The asymptotic solution of the problem (D6) is well-known [300] and reads

$$\begin{pmatrix} \tilde{C}_{k\uparrow+}^d(t_0+) \\ \tilde{C}_{k\downarrow-}^d(t_0+) \end{pmatrix} = \begin{pmatrix} \sqrt{p_k} & -\text{sgn}(\alpha)\sqrt{1-p_k}e^{i\chi_k} \\ \text{sgn}(\alpha)\sqrt{1-p_k}e^{-i\chi_k} & \sqrt{p_k} \end{pmatrix}\begin{pmatrix} \tilde{C}_{k\uparrow+}^d(t_0-) \\ \tilde{C}_{k\downarrow-}^d(t_0-) \end{pmatrix}, \tag{D7}$$

where the coefficient

$$p_k = \exp\Big[-\delta_{\text{LZ}}\frac{\Delta^2}{\xi_k^2 + \Delta^2}\Big]$$

with $\delta_{\rm LZ} = \pi\alpha^2 k^2/\gamma \approx \pi\alpha^2 k_F^2/\gamma$ defines the probability of tunneling. Here $\chi_k = \pi/4 + \arg\Gamma(1 + i\ln p_k/2\pi) - \ln p_k(\ln(-\ln p_k/2\pi) - 1)/2\pi$ is the Stokes phase with the Gamma function Γ.

For small energies $\xi_k \lesssim \Delta$ two different tunneling regimes are possible:

$$\begin{aligned} &\text{(weak)} \quad \gamma \gtrsim \alpha^2 k_F^2 \quad \to \quad \delta_{\rm LZ} \approx 0 \quad \to \quad p_k \approx 1, \\ &\text{(strong)} \quad \gamma \ll \alpha^2 k_F^2 \quad \to \quad \delta_{\rm LZ} \gg 1 \quad \to \quad p_k \approx 0. \end{aligned}$$

When $\xi_k \gg \Delta$, tunneling is suppressed ($p_k \to 1$) as the quasiparticle spectrum resembles that of a normal metal with no splitting between crossing spectral branches.

The typical transient time $\tau_{\rm LZ}$ for the LZSM tunneling can be estimated as follows [300]

$$\tau_{\rm LZ} \sim \sqrt{\frac{\hbar}{\gamma}} \max\left\{1, \frac{\alpha k_F}{\sqrt{2\gamma}} \frac{\Delta}{\sqrt{\xi_k^2 + \Delta^2}}\right\}.$$

If the intersection of the branches of the QP spectrum occurs at some ξ_k, then it is possible to determine the interval $\Delta\xi_k$ in which all QP states experience transient dynamics. The size of $\Delta\xi_k$ depends on transient time, however, it can be shown, that the upper limit for this interval is $\Delta\xi_k \sim \alpha k_F \ll \Delta$. The smallness of $\Delta\xi_k$ and the fact that the gap function $\Delta(t)$ is determined by all QP states in $(-\omega_D, \omega_D)$ confirm the validity of the approximations made in Section 3.3.2.

Combining all the results we write the asymptotic transition matrix $\hat{S}^d_{\rm LZ}$ in diabatic basis as

$$\begin{pmatrix} C^d_{k\uparrow+}(t_0+) \\ C^d_{k\downarrow+}(t_0+) \\ C^d_{k\uparrow-}(t_0+) \\ C^d_{k\downarrow-}(t_0+) \end{pmatrix} = \begin{pmatrix} \sqrt{p_k} & 0 & 0 & \sqrt{1-p_k}e^{i\chi_k - i\theta_k - i\frac{\pi}{2}\mathrm{sgn}(\alpha)} \\ 0 & 1 & 0 & 0 \\ 0 & 0 & 1 & 0 \\ -\sqrt{1-p_k}e^{-i\chi_k + i\theta_k + i\frac{\pi}{2}\mathrm{sgn}(\alpha)} & 0 & 0 & \sqrt{p_k} \end{pmatrix} \begin{pmatrix} C^d_{k\uparrow+}(t_0-) \\ C^d_{k\downarrow+}(t_0-) \\ C^d_{k\uparrow-}(t_0-) \\ C^d_{k\downarrow-}(t_0-) \end{pmatrix}. \tag{D8}$$

The LZSM transition matrix in the adiabatic basis (3.27) has the form $\hat{S}_{\rm LZ} = \hat{R}^{-1}(t_0+)\hat{S}^d_{\rm LZ}\hat{R}(t_0-)$, where we use the relationship between the two bases (D1) and (3.27) written in general form as a time-dependent matrix $\hat{R}(t)$. Using the perturbation theory with respect to the small parameter $\alpha k_F/\Delta$ and considering points $t_0\pm$ far from the nonadiabatic region, one can show that the matrix $\hat{R}(t_0\pm)$ can be approximated with an identity matrix. The corrections proportional to $\alpha k_F/\Delta$ in all elements of the matrix $\hat{R}(t_0\pm)$ as well as $\hat{S}_{\rm LZ}$ can be neglected, since in all equations of Section 3.3 we consider the minimum possible order of the perturbation theory with respect to the parameter $\alpha k_F/\Delta$. With these approximations the matrices $\hat{S}_{\rm LZ}$ and $\hat{S}^d_{\rm LZ}$ actually coincide and the LZSM transition matrix in the adiabatic basis can be taken taken from (D8). Thus, we get the Eq (3.31).

E Calculation of spin-split DOS

The DOS for one spin projection can be written as follows

$$N_\uparrow(E,t) \approx \sum_k \sum_{n=\uparrow+,\uparrow-} |u_0|^2 \delta\Big(E - E_{kn}[h(t)]\Big) + |v_0|^2 \delta\Big(E + E_{kn}[h(t)]\Big). \tag{E1}$$

Here we use static QP amplitudes u_0 and v_0 to distinguish the particle/hole contributions and $E_{k\uparrow\pm}$ are defined in Eq. (3.4). Note that the function $N_\uparrow(E,t)$ depends on time only through the

Zeeman field $h(t)$. The straightforward calculations for $h(t) < \Delta_0$ yield

$$\frac{N_\uparrow(E,t)}{N(0)} \approx \frac{|E|}{\xi_0}\left|1 - \mathrm{sgn}(E)\frac{\alpha^2 k_F^2 + h^2(t)}{\sqrt{\xi_0^2\alpha^2 k_F^2 + h^2(t)(\xi_0^2 + \Delta_h^2)}}\right|^{-1}, \tag{E2}$$

where

$$\xi_0(E,t) \approx \sqrt{E^2 + h^2(t) - \Delta_h^2 + \alpha^2 k_F^2 + \mathrm{sgn}(E)2\sqrt{E^2(h^2(t) + \alpha^2 k_F^2) - \Delta_h^2\alpha^2 k_F^2}} \tag{E3}$$

and we have assumed $\alpha k \approx \alpha k_F$ due to the vicinity to the Fermi energy. The time-dependent gap function $\Delta_h[h(t)]$ is defined in (3.37). Two standard coherence peaks at the energies $E = -\sqrt{(\Delta_h + h(t))^2 + \alpha^2 k_F^2}$ and $E = \sqrt{(\Delta_h - h(t))^2 + \alpha^2 k_F^2}$ appear [Fig. 6(a)].

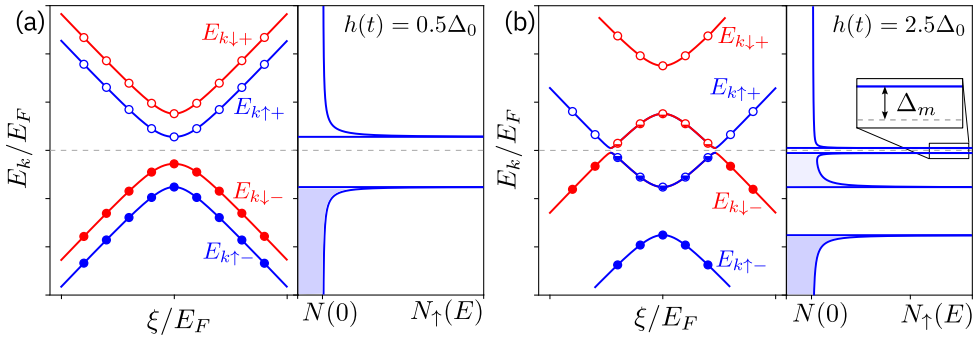

Figure 6: Spectrum (3.4) and density of states (E2- E4) for the QPs with $\uparrow$ spin for two different values of $h(t)$. The value Δ_m represents a minigap. Colored areas in DOS indicate the filling of the states in the corresponding energy intervals according to Eq. (3.44). The parameters are $\Delta_0/E_F = 0.01$, $\alpha/E_F = 0.0025$.

For the case of large Zeeman fields $h(t) > \Delta_0$ one obtains

$$\frac{N_\uparrow(E,t)}{N(0)} \approx \begin{cases} \frac{|E|}{\xi_0}\left|1 - \mathrm{sgn}(E)\frac{\alpha^2 k_F^2 + h^2(t)}{\sqrt{\xi_1^2\alpha^2 k_F^2 + h^2(t)(\xi_1^2 + \Delta_h^2)}}\right|^{-1}, & E > \Delta_m \bigcup E < -\sqrt{(\Delta_h + h(t))^2 + \alpha^2 k_F^2} \\ \frac{|E|}{\xi_0}\left|1 - \frac{\alpha^2 k_F^2 + h^2(t)}{\sqrt{\xi_2^2\alpha^2 k_F^2 + h^2(t)(\xi_2^2 + \Delta_h^2)}}\right|^{-1}, & -\sqrt{(\Delta_h - h(t))^2 + \alpha^2 k_F^2} < E < -\Delta_m \end{cases} \tag{E4}$$

where

$$\Delta_m \approx \frac{\Delta_h \alpha k_F}{\sqrt{h^2(t) + \alpha^2 k_F^2}}.$$

The splitting of the energy spectrum in the vicinity of $E = 0$ leads to the appearance of the two additional coherence peaks and corresponging minigap at the energies $E = \pm\Delta_m$, which are shown in Fig. 6(b).

Conclusion

In this dissertation we have explored the physics of quasiparticles, quantum vortices and collective modes in superconductors and superconducting hybrid structures. Diverse aspects of the static, dynamic and nonequilibrium states of the superconducting condensate were considered for a number of specific problems, each of which is closely related either to the experiments already performed or theoretically proposed in the present work.

We provided a detailed description of the electronic structure of the localized quasiparticle states inside the core of a vortex pinned by a planar insulating defect of various transparency. Our results predict that the scattering of quasiparticles by the defect potential will lead to a change in the subgap spectrum and the appearance of a soft minigap in the anomalous CdGM spectral branch at the Fermi level. This minigap grows with decreasing barrier transparency and persists even in the limit of a Josephson coreless vortex. Such a modified spectrum will affect the transport and optical properties of the pinned vortex, as well as the distribution of the local density of states, which may be its distinguishing feature observed in STM/STS measurements. In addition, the gapped low-energy spectrum can be used for developing of setups with controlled transport of Majorana fermions localized in the vortex core [313–315]. An open question here is the case of intermediate transparency, when the pinned vortex is in the Abrikosov-Josephson regime [167] and the shape of the core, as well as the electronic and magnetic structures of the vortex, are strongly anisotropic. Such a problem requires a full self-consistent BdG approach, which is, probably, analytically intractable.

We examined the effect of the plane defects on the electromagnetic structure of the vortex. We showed that the redistribution of the vortex supercurrent along the defect plane results in the delocalization of the vortex magnetic field. At low transparencies, this effect can be strong and lead to a significant decrease in the local magnetic flux compared to a free vortex. We expect that this effect can be observed in local flow measurements [272, 274, 275] in nonstoichiometric superconducting crystals [216]. We have also given an insight into the mechanism if the vortex nucleation and dynamics in the bilayer superconductor-ferromagnet structure. We theoretically showed that the nonhomogeneous stray magnetic field produced by the ferromagnet results in the vortex flux-flow diode effect, which has been observed recently in the Nb/EuS heterostructure [234].

Following the context of the previous part, we have discussed the fast optical control of vortices. We proposed a scheme for all-optical generation of vortices with desired polarity (vorticity) based on the quenching of the superconductor and induction of the inverse Faraday effect (IFE) by external circularly polarized light. To this end we numerically examine the properties of IFE in superconducting films in strong electromagnetic field and studied the possibility of the vortex nucleation and locking inside the superconductor. We have implemented a numerical simulation of the two-stage generation of Abrikosov vortices and estimate its efficiency by establishing the correlation between the light polarization and generated vorticity. Experimental realization of this idea may find an application in the optofluxonics, connected with optically driven vortex matter [61]. Beside this, we give an analytical description of the IFE in the fluctuation regime above T_c for the simplest case of a thin superconducting ring. This problem primarily contributes to the general theory of IFE, and also predicts an elegant and efficient method for generating

and controlling magnetic flux using external circularly polarized light. We expect that the last problem can become a starting point for studying the interplay of the Hall effect [108] and IFE in the fluctuation regime of superconducting films.

In the last part of the thesis we focused on the quasiparticle response of a superconductor to external perturbations. Inspired by the emerging field of spintronics [316, 317], we consider a general problem of the collisionless dynamics of the superconducting condensate driven by an exchange field in a hybrid S/F structure. In particular, we analytically predicted a modification of the Higgs mode of the time-dependent order parameter excited in the presence of an exchange field and spin-orbit coupling. The presence of Higgs modes with several resonant frequencies reflects the complex dynamics of quasiparticle states in the spin-split spectrum mediated by spin-flip transitions. Going beyond the linear response, we considered the nonadiabatic quasiparticle dynamics induced by the growing exchange field. The resulting nonequilibrium state of the superconducting condensate shows many distinctive features, such as surviving of the gap above the Pauli paramagnetic limit and the dynamically generated magnetization of the quasiparticle gas. Our findings may be promising for the experimental study of the nonequilibrium dynamics of collective exctitations in S/F heterostructures [317]. Further development of this problem involves, first of all, consideration of various mechanisms of the Higgs mode excitation associated with the imbalance of the quasiparticle spin subbands, as well as the the introduction of specific elastic and/or inelastic quasiparticle relaxations [143, 318].

Bibliography

1. Bednorz, J. G. & Müller, K. A. Possible high T_c superconductivity in the Ba- La- Cu- O system. *Zeitschrift für Physik B Condensed Matter* **64,** 189–193. doi:10.1007/BF01303701 (1986).
2. Maeda, H., Tanaka, Y., Fukutomi, M. & Asano, T. A New High-Tc Oxide Superconductor without a Rare Earth Element. *Japanese Journal of Applied Physics* **27,** L209. doi:10.1143/JJAP.27.L209 (1988).
3. Nagamatsu, J., Nakagawa, N., Muranaka, T., Zenitani, Y. & Akimitsu, J. Superconductivity at 39 K in magnesium diboride. *nature* **410,** 63–64. doi:10.1038/35065039 (2001).
4. Kamihara, Y., Watanabe, T., Hirano, M. & Hosono, H. Iron-based layered superconductor $La[O_{1-x}F_x]FeAs$ with T_c= 26 K. *Journal of the American Chemical Society* **130,** 3296–3297. doi:10.1021/ja800073m (2008).
5. Subedi, A., Zhang, L., Singh, D. J. & Du, M. H. Density functional study of FeS, FeSe, and FeTe: Electronic structure, magnetism, phonons, and superconductivity. *Phys. Rev. B* **78,** 134514. doi:10.1103/PhysRevB.78.134514 (2008).
6. Li, D. *et al.* Superconductivity in an infinite-layer nickelate. *Nature* **572,** 624–627. doi:10.1038/s41586-019-1496-5 (2019).
7. De Gennes, P. G. & Matricon, J. Collective modes of vortex lines in superconductors of the second kind. *Reviews of Modern Physics* **36,** 45. doi:10.1103/RevModPhys.36.45 (1964).
8. Josephson, B. D. Supercurrents through barriers. *Advances in Physics* **14,** 419–451. doi:10.1080/00018736500101091 (1965).
9. Bardeen, J. & Stephen, M. Theory of the motion of vortices in superconductors. *Physical Review* **140,** A1197. doi:10.1103/PhysRev.140.A1197 (1965).
10. Blatter, G., Feigel'man, M. V., Geshkenbein, V. B., Larkin, A. I. & Vinokur, V. M. Vortices in high-temperature superconductors. *Rev. Mod. Phys.* **66,** 1125–1388. doi:10.1103/RevModPhys.66.1125 (1994).
11. Kopnin, N. *Theory of Nonequilibrium Superconductivity* ISBN: 9780199566426 (OUP Oxford, 2009).
12. Kopnin, N. B., Volovik, G. E. & Parts, Ü. Spectral Flow in Vortex Dynamics of 3He-B and Superconductors. *Europhysics Letters* **32,** 651. doi:10.1209/0295-5075/32/8/006 (1995).
13. Bruér, J. *et al.* Revisiting the vortex-core tunnelling spectroscopy in YBa2Cu3O7-δ. *Nature Communications* **7,** 11139. ISSN: 2041-1723. doi:10.1038/ncomms11139 (2016).
14. Du, Z. *et al.* Anisotropic Superconducting Gap and Elongated Vortices with Caroli-De Gennes-Matricon States in the New Superconductor Ta4Pd3Te16. *Scientific Reports* **5,** 9408. ISSN: 2045-2322. doi:10.1038/srep09408 (2015).
15. Guillamón, I. *et al.* Superconducting Density of States and Vortex Cores of 2H-NbS_2. *Phys. Rev. Lett.* **101,** 166407. doi:10.1103/PhysRevLett.101.166407 (2008).
16. Nishimori, H. *et al.* First Observation of the Fourfold-symmetric and Quantum Regime Vortex Core in YNi2B2C by Scanning Tunneling Microscopy and Spectroscopy. *Journal of the Physical Society of Japan* **73,** 3247–3250. doi:10.1143/JPSJ.73.3247 (2004).

17. De Wilde, Y. *et al.* Scanning Tunneling Microscopy Observation of a Square Abrikosov Lattice in $LuNi_2B_2C$. *Phys. Rev. Lett.* **78,** 4273–4276. doi:10.1103/PhysRevLett.78.4273 (1997).
18. Suderow, H., Guillamón, I., Rodrigo, J. G. & Vieira, S. Imaging superconducting vortex cores and lattices with a scanning tunneling microscope. *Superconductor Science and Technology* **27,** 063001. doi:10.1088/0953-2048/27/6/063001 (2014).
19. Maggio-Aprile, I., Renner, C., Erb, A., Walker, E. & Fischer, Ø. Direct Vortex Lattice Imaging and Tunneling Spectroscopy of Flux Lines on $YBa_2Cu_3O_{7-\delta}$. *Phys. Rev. Lett.* **75,** 2754–2757. doi:10.1103/PhysRevLett.75.2754 (1995).
20. Berthod, C. & Giovannini, B. Density of States in High- T_c Superconductor Vortices. *Phys. Rev. Lett.* **87,** 277002. doi:10.1103/PhysRevLett.87.277002 (2001).
21. Fischer, Ø., Kugler, M., Maggio-Aprile, I., Berthod, C. & Renner, C. Scanning tunneling spectroscopy of high-temperature superconductors. *Rev. Mod. Phys.* **79,** 353–419. doi:10.1103/RevModPhys.79.353 (2007).
22. Putilov, A. V. *et al.* Vortex-core properties and vortex-lattice transformation in FeSe. *Phys. Rev. B* **99,** 144514. doi:10.1103/PhysRevB.99.144514 (2019).
23. Berthod, C., Maggio-Aprile, I., Bruér, J., Erb, A. & Renner, C. Observation of Caroli–de Gennes–Matricon Vortex States in $YBa_2Cu_3O_{7-\delta}$. *Phys. Rev. Lett.* **119,** 237001. doi:10.1103/PhysRevLett.119.237001 (2017).
24. Volovik, G. *The Universe in a Helium Droplet* ISBN: 9780199564842 (OUP Oxford, 2009).
25. Brandt, E. H. The flux-line lattice in superconductors. *Reports on Progress in Physics* **58,** 1465–1594. doi:10.1088/0034-4885/58/11/003 (1995).
26. Roditchev, D. *et al.* Direct observation of Josephson vortex cores. *Nature Physics* **11,** 332–337. ISSN: 1745-2481. doi:10.1038/nphys3240 (2015).
27. Kramer, L. & Pesch, W. Core structure and low-energy spectrum of isolated vortex lines in clean superconductors at $T \ll T_c$. *Zeitschrift für Physik* **269,** 59–64. ISSN: 0044-3328. doi:10.1007/BF01668869 (1974).
28. Klein, U. Density of bound states in a vortex core. *Phys. Rev. B* **41,** 4819–4822. doi:10.1103/PhysRevB.41.4819 (1990).
29. Hess, H. F., Robinson, R. B. & Waszczak, J. V. Vortex-core structure observed with a scanning tunneling microscope. *Phys. Rev. Lett.* **64,** 2711–2714. doi:10.1103/PhysRevLett.64.2711 (1990).
30. Caroli, C., De Gennes, P. & Matricon, J. Bound Fermion states on a vortex line in a type II superconductor. *Physics Letters* **9,** 307–309. doi:https://doi.org/10.1016/0031-9163(64)90375-0 (1964).
31. Chen, M. *et al.* Discrete energy levels of Caroli-de Gennes-Matricon states in quantum limit in $FeTe_{0.55}Se_{0.45}$. *Nature communications* **9,** 970. doi:10.1038/s41467-018-03404-8 (2018).
32. Chen, C. *et al.* Observation of Discrete Conventional Caroli–de Gennes–Matricon States in the Vortex Core of Single-Layer $FeSe/SrTiO_3$. *Phys. Rev. Lett.* **124,** 097001. doi:10.1103/PhysRevLett.124.097001 (2020).
33. Larkin, A. I. & Ovchinnikov, Y. N. Resistance of layered superclean superconductors at low temperatures. *Phys. Rev. B* **57,** 5457–5465. doi:10.1103/PhysRevB.57.5457 (1998).
34. Skvortsov, M. A., Feigel'man, M. V. & Kravtsov, V. E. Level statistics inside the core of a superconductive vortex. *Journal of Experimental and Theoretical Physics Letters* **68,** 84–90. ISSN: 1090-6487. doi:10.1134/1.567825 (1998).
35. Koulakov, A. A. & Larkin, A. I. Vortex density of states and absorption in clean layered superconductors. *Phys. Rev. B* **60,** 14597–14600. doi:10.1103/PhysRevB.60.14597 (1999).
36. Bespalov, A. A. & Plastovets, V. D. Large spectral gap and impurity-induced states in a two-dimensional Abrikosov vortex. *Phys. Rev. B* **103,** 024510. doi:10.1103/PhysRevB.103.024510 (2021).

37. Mel'nikov, A. S., Samokhvalov, A. V. & Zubarev, M. N. Electronic structure of vortices pinned by columnar defects. *Phys. Rev. B* **79,** 134529. doi:10.1103/PhysRevB.79.134529 (2009).

38. Rosenstein, B., Shapiro, I., Deutch, E. & Shapiro, B. Y. Microwave absorption in the cores of Abrikosov vortices pinned by artificial insulator inclusion. *Phys. Rev. B* **84,** 134521. doi:10.1103/PhysRevB.84.134521 (2011).

39. Kawakami, T. *et al.* Excitation spectrum of Josephson vortices on surface superconductor. *Journal of Physics: Conference Series* **568,** 022022. doi:10.1088/1742-6596/568/2/022022 (2014).

40. Samokhvalov, A. V., Plastovets, V. D. & Mel'nikov, A. S. Topological transitions in electronic spectra: Crossover between Abrikosov and Josephson vortices. *Phys. Rev. B* **102,** 174501. doi:10.1103/PhysRevB.102.174501 (2020).

41. Khodaeva, U. E. & Skvortsov, M. A. Vortex core near planar defects in a clean layered superconductor. *Phys. Rev. B* **105,** 134504. doi:10.1103/PhysRevB.105.134504 (13 Apr. 2022).

42. Graser, S., Iniotakis, C., Dahm, T. & Schopohl, N. Shadow on the Wall Cast by an Abrikosov Vortex. *Phys. Rev. Lett.* **93,** 247001. doi:10.1103/PhysRevLett.93.247001 (2004).

43. Mel'nikov, A. S., Ryzhov, D. A. & Silaev, M. A. Electronic structure and heat transport of multivortex configurations in mesoscopic superconductors. *Phys. Rev. B* **78,** 064513. doi:10.1103/PhysRevB.78.064513 (2008).

44. Iniotakis, C., Graser, S., Dahm, T. & Schopohl, N. Local density of states at polygonal boundaries of d-wave superconductors. *Phys. Rev. B* **71,** 214508. doi:10.1103/PhysRevB.71.214508 (2005).

45. Plastovets, V. & Mel'nikov, A. S. Electronic structure of a Josephson vortex in a SIS junction. *Phys. Rev. B* **105,** 094516. doi:10.1103/PhysRevB.105.094516 (2022).

46. Janko´, B. & Shore, J. D. Electromagnetic response of a static vortex line in a type-II superconductor: A microscopic study. *Phys. Rev. B* **46,** 9270–9273. doi:10.1103/PhysRevB.46.9270 (1992).

47. Rakhmanov, A. L., Rozhkov, A. V. & Nori, F. Majorana fermions in pinned vortices. *Phys. Rev. B* **84,** 075141. doi:10.1103/PhysRevB.84.075141 (2011).

48. Ioselevich, P. A. & Feigel'man, M. V. Anomalous Josephson Current via Majorana Bound States in Topological Insulators. *Phys. Rev. Lett.* **106,** 077003. doi:10.1103/PhysRevLett.106.077003 (2011).

49. Ioselevich, P. A., Ostrovsky, P. M. & Feigel'man, M. V. Majorana state on the surface of a disordered three-dimensional topological insulator. *Phys. Rev. B* **86,** 035441. doi:10.1103/PhysRevB.86.035441 (2012).

50. Akzyanov, R. S., Rozhkov, A. V., Rakhmanov, A. L. & Nori, F. Tunneling spectrum of a pinned vortex with a robust Majorana state. *Phys. Rev. B* **89,** 085409. doi:10.1103/PhysRevB.89.085409 (2014).

51. Fu, L. & Kane, C. L. Superconducting Proximity Effect and Majorana Fermions at the Surface of a Topological Insulator. *Phys. Rev. Lett.* **100,** 096407. doi:10.1103/PhysRevLett.100.096407 (2008).

52. Sau, J. D., Lutchyn, R. M., Tewari, S. & Das Sarma, S. Robustness of Majorana fermions in proximity-induced superconductors. *Phys. Rev. B* **82,** 094522. doi:10.1103/PhysRevB.82.094522 (2010).

53. Schuray, A., Frombach, D., Park, S. & Recher, P. Transport signatures of Majorana bound states in superconducting hybrid structures: A minireview. *The European Physical Journal Special Topics* **229,** 593–620. doi:10.1140/epjst/e2019-900150-7 (2020).

54. Sarma, S. D., Freedman, M. & Nayak, C. Majorana zero modes and topological quantum computation. *npj Quantum Information* **1,** 1–13. doi:10.1038/npjqi.2015.1 (2015).

55. Semenov, A. D., Gol'tsman, G. N. & Korneev, A. A. Quantum detection by current carrying superconducting film. *Physica C: Superconductivity* **351,** 349–356. doi:https://doi.org/10.1016/S0921-4534(00)01637-3 (2001).

56. Maingault, L. *et al.* Spectral dependency of superconducting single photon detectors. *Journal of Applied Physics* **107,** 116103. doi:10.1063/1.3374636 (2010).

57. Zotova, A. N. & Vodolazov, D. Y. Photon detection by current-carrying superconducting film: A time-dependent Ginzburg-Landau approach. *Phys. Rev. B* **85,** 024509. doi:10.1103/PhysRevB.85.024509 (2012).

58. Vadimov, V., Vodolazov, D., Mironov, S. & Mel'nikov, A. Photoinduced Local Nonequilibrium States in Superconductors: Hot Spot Model. *JETP Letters* **108,** 270–278. doi:10.1134/S0021364018160105 (2018).

59. Sergeev, A., Reizer, M. & Mitin, V. Thermomagnetic vortex transport: Transport entropy revisited. *EPL (Europhysics Letters)* **92,** 27003. doi:10.1209/0295-5075/92/27003 (2010).

60. Sergeev, A. & Reizer, M. *arXiv:2203.12433 [physics.gen-ph]* 2022. doi:10.48550/ARXIV.2203.12433.

61. Veshchunov, I. S. *et al.* Optical manipulation of single flux quanta. *Nature Communications* **7,** 12801. ISSN: 2041-1723. doi:10.1038/ncomms12801 (2016).

62. Zeldovich, Y. B., Kobzarev, I. Y. & Okun, L. B. Cosmological consequences of a spontaneous breakdown of a discrete symmetry. *Zhurnal Eksperimentalnoi i Teoreticheskoi Fiziki* **67,** 3–11 (1975).

63. Kibble, T. W. B. Topology of cosmic domains and strings. *Journal of Physics A: Mathematical and General* **9,** 1387–1398. doi:10.1088/0305-4470/9/8/029 (1976).

64. Zurek, W. H. Cosmological experiments in superfluid helium? *Nature* **317,** 505–508. ISSN: 1476-4687. doi:10.1038/317505a0 (1985).

65. Kopnin, N. B. & Thuneberg, E. V. Time-Dependent Ginzburg–Landau Analysis of Inhomogeneous Normal-Superfluid Transitions. *Phys. Rev. Lett.* **83,** 116–119. doi:10.1103/PhysRevLett.83.116 (1999).

66. Aranson, I., Vinokur, V. & Kopnin, N. Nucleation of vortices in superfluid 3He–B by thermal quench. *Physica C: Superconductivity* **332,** 129–130. doi:https://doi.org/10.1016/S0921-4534(99)00654-1 (2000).

67. Bäuerle, C., Bunkov, Y. M., Fisher, S. N., Godfrin, H. & Pickett, G. R. Laboratory simulation of cosmic string formation in the early Universe using superfluid 3He. *Nature* **382,** 332–334. ISSN: 1476-4687. doi:10.1038/382332a0 (1996).

68. Ruutu, V. M. H. *et al.* Vortex formation in neutron-irradiated superfluid 3He as an analogue of cosmological defect formation. *Nature* **382,** 334–336. ISSN: 1476-4687. doi:10.1038/382334a0 (1996).

69. Volovik, G. E. Defect formation in inhomogeneous second-order phase transition: theory and experiment. *Physica B: Condensed Matter* **280,** 122–127. doi:https://doi.org/10.1016/S0921-4526(99)01512-4 (2000).

70. Monaco, R., Mygind, J., Rivers, R. J. & Koshelets, V. P. Spontaneous fluxoid formation in superconducting loops. *Phys. Rev. B* **80,** 180501. doi:10.1103/PhysRevB.80.180501 (2009).

71. Maniv, A., Polturak, E. & Koren, G. Observation of Magnetic Flux Generated Spontaneously During a Rapid Quench of Superconducting Films. *Phys. Rev. Lett.* **91,** 197001. doi:10.1103/PhysRevLett.91.197001 (2003).

72. Golubchik, D., Polturak, E. & Koren, G. Evidence for Long-Range Correlations within Arrays of Spontaneously Created Magnetic Vortices in a Nb Thin-Film Superconductor. *Phys. Rev. Lett.* **104,** 247002. doi:10.1103/PhysRevLett.104.247002 (2010).

73. Golubchik, D., Polturak, E., Koren, G., Shapiro, B. Y. & Shapiro, I. Experimental Determination of Correlations Between Spontaneously Formed Vortices in a Superconductor. *Journal of Low Temperature Physics* **164,** 74–80. ISSN: 1573-7357. doi:10.1007/s10909-011-0364-y (2011).

74. Shapiro, I., Pechenik, E. & Shapiro, B. Y. Recovery of superconductivity in a quenched mesoscopic domain. *Phys. Rev. B* **63,** 184520. doi:10.1103/PhysRevB.63.184520 (2001).

75. Weiler, C. N. *et al.* Spontaneous vortices in the formation of Bose–Einstein condensates. *Nature* **455,** 948–951. ISSN: 1476-4687. doi:10.1038/nature07334 (2008).

76. Cai, Y., Allman, D. G., Sabharwal, P. & Wright, K. C. Persistent Currents in Rings of Ultracold Fermionic Atoms. *Phys. Rev. Lett.* **128,** 150401. doi:10.1103/PhysRevLett.128.150401 (2022).

77. Rochet, A. *et al.* On-Demand Optical Generation of Single Flux Quanta. *Nano Letters* **20,** 6488–6493. doi:10.1021/acs.nanolett.0c02166 (2020).

78. Beattie, S., Moulder, S., Fletcher, R. J. & Hadzibabic, Z. Persistent Currents in Spinor Condensates. *Phys. Rev. Lett.* **110,** 025301. doi:10.1103/PhysRevLett.110.025301 (2013).

79. Ryu, C. *et al.* Observation of Persistent Flow of a Bose-Einstein Condensate in a Toroidal Trap. *Phys. Rev. Lett.* **99,** 260401. doi:10.1103/PhysRevLett.99.260401 (2007).

80. Pitaevskii, L. Electric forces in a transparent dispersive medium. *Sov. Phys. JETP* **12,** 1008–1013 (1961).

81. Kirilyuk, A., Kimel, A. V. & Rasing, T. Ultrafast optical manipulation of magnetic order. *Rev. Mod. Phys.* **82,** 2731–2784. doi:10.1103/RevModPhys.82.2731 (2010).

82. Kirilyuk, A., Kimel, A. V. & Rasing, T. Laser-induced magnetization dynamics and reversal in ferrimagnetic alloys. *Reports on Progress in Physics* **76,** 026501. doi:10.1088/0034-4885/76/2/026501 (2013).

83. Hertel, R. Theory of the inverse Faraday effect in metals. *Journal of Magnetism and Magnetic Materials* **303,** L1–L4. doi:https://doi.org/10.1016/j.jmmm.2005.10.225 (2006).

84. Hertel, R. & Fähnle, M. Macroscopic drift current in the inverse Faraday effect. *Phys. Rev. B* **91,** 020411. doi:10.1103/PhysRevB.91.020411 (2015).

85. Battiato, M., Barbalinardo, G. & Oppeneer, P. M. Quantum theory of the inverse Faraday effect. *Phys. Rev. B* **89,** 014413. doi:10.1103/PhysRevB.89.014413 (2014).

86. Kibis, O. V. Dissipationless Electron Transport in Photon-Dressed Nanostructures. *Phys. Rev. Lett.* **107,** 106802. doi:10.1103/PhysRevLett.107.106802 (2011).

87. Kibis, O. V. Persistent current induced by quantum light. *Phys. Rev. B* **86,** 155108. doi:10.1103/PhysRevB.86.155108 (2012).

88. Kibis, O. V., Kyriienko, O. & Shelykh, I. A. Persistent current induced by vacuum fluctuations in a quantum ring. *Phys. Rev. B* **87,** 245437. doi:10.1103/PhysRevB.87.245437 (2013).

89. Sigurdsson, H., Kibis, O. V. & Shelykh, I. A. Optically induced Aharonov-Bohm effect in mesoscopic rings. *Phys. Rev. B* **90,** 235413. doi:10.1103/PhysRevB.90.235413 (2014).

90. Koshelev, K. L., Kachorovskii, V. Y. & Titov, M. Resonant inverse Faraday effect in nanorings. *Phys. Rev. B* **92,** 235426. doi:10.1103/PhysRevB.92.235426 (2015).

91. Mironov, S. V. *et al.* Inverse Faraday Effect for Superconducting Condensates. *Phys. Rev. Lett.* **126,** 137002. doi:10.1103/PhysRevLett.126.137002 (2021).

92. Plastovets, V. D., Tokman, I. D., Lounis, B., Mel'nikov, A. S. & Buzdin, A. I. All-optical generation of Abrikosov vortices by the inverse Faraday effect. *Phys. Rev. B* **106,** 174504. doi:10.1103/PhysRevB.106.174504 (2022).

93. Croitoru, M. D., Lounis, B. & Buzdin, A. I. Influence of a nonuniform thermal quench and circular polarized radiation on spontaneous current generation in superconducting rings. *Phys. Rev. B* **105,** L020504. doi:10.1103/PhysRevB.105.L020504 (2022).

94. Croitoru, M. D., Mironov, S. V., Lounis, B. & Buzdin, A. I. Toward the Light-Operated Superconducting Devices: Circularly Polarized Radiation Manipulates the Current-Carrying States in Superconducting Rings. *Advanced Quantum Technologies* **n/a,** 2200054. doi:https://doi.org/10.1002/qute.202200054.

95. Ebisawa, H. & Fukuyama, H. Wave Character of the Time Dependent Ginzburg Landau Equation and the Fluctuating Pair Propagator in Superconductors*). *Progress of Theoretical Physics* **46,** 1042–1053. ISSN: 0033-068X. doi:10.1143/PTP.46.1042 (Oct. 1971).

96. Fukuyama, H., Ebisawa, H. & Tsuzuki, T. Fluctuation of the order parameter and hall effect. *Progress of Theoretical Physics* **46,** 1028–1041 (1971).

97. Aronov, A., Hikami, S. & Larkin, A. Gauge invariance and transport properties in superconductors above T_c. *Phys. Rev. B* **51,** 3880. doi:10.1103/PhysRevB.51.3880 (1995).

98. Michaeli, K., Tikhonov, K. S. & Finkel'stein, A. M. Hall effect in superconducting films. *Phys. Rev. B* **86,** 014515. doi:10.1103/PhysRevB.86.014515 (2012).

99. Dorsey, A. T. Vortex motion and the Hall effect in type-II superconductors: A time-dependent Ginzburg-Landau theory approach. *Phys. Rev. B* **46,** 8376–8392. doi:10.1103/PhysRevB.46.8376 (1992).

100. Kopnin, N., Ivlev, B. & Kalatsky, V. Sign reversal of the flux-flow Hall effect in type-II superconductors. *JETP letters* **55,** 750–755 (1992).

101. Zhao, S. Y. F. *et al.* Sign-Reversing Hall Effect in Atomically Thin High-Temperature $Bi_{2.1}Sr_{1.9}CaCu_{2.0}O_{8+\delta}$ Superconductors. *Phys. Rev. Lett.* **122,** 247001. doi:10.1103/PhysRevLett.122.247001 (2019).

102. Hagen, S. J., Lobb, C. J., Greene, R. L. & Eddy, M. Flux-flow Hall effect in superconducting $Tl_2Ba_2CaCu_2O_8$ films. *Phys. Rev. B* **43,** 6246–6248. doi:10.1103/PhysRevB.43.6246 (1991).

103. Ogawa, R., Nabeshima, F., Nishizaki, T. & Maeda, A. Large Hall angle of vortex motion in high-T_c cuprate superconductors revealed by microwave flux-flow Hall effect. *Phys. Rev. B* **104,** L020503. doi:10.1103/PhysRevB.104.L020503 (2021).

104. Lang, W., Heine, G., Schwab, P., Wang, X. Z. & Bäuerle, D. Paraconductivity and excess Hall effect in epitaxial $YBa_2Cu_3O_7$ films induced by superconducting fluctuations. *Phys. Rev. B* **49,** 4209–4217. doi:10.1103/PhysRevB.49.4209 (1994).

105. Tinh, B. D., Hoc, N. Q. & Thu, L. M. The fluctuation Hall conductivity and the Hall angle in type-II superconductor under magnetic field. *Physica C: Superconductivity and its Applications* **521-522,** 29–32. doi:https://doi.org/10.1016/j.physc.2016.01.001 (2016).

106. Kreisel, A., Hirschfeld, P. J. & Andersen, B. M. On the Remarkable Superconductivity of FeSe and Its Close Cousins. *Symmetry* **12.** doi:10.3390/sym12091402 (2020).

107. Shibauchi, T., Hanaguri, T. & Matsuda, Y. Exotic Superconducting States in FeSe-based Materials. *Journal of the Physical Society of Japan* **89,** 102002. doi:10.7566/JPSJ.89.102002 (2020).

108. Larkin, A. I. & Varlamov, A. A. in *Superconductivity: Conventional and Unconventional Superconductors* (eds Bennemann, K. H. & Ketterson, J. B.) 369–458 (Springer Berlin Heidelberg, Berlin, Heidelberg, 2008). ISBN: 978-3-540-73253-2. doi:10.1007/978-3-540-73253-2_10.

109. Aslamasov, L. & Larkin, A. The influence of fluctuation pairing of electrons on the conductivity of normal metal. *Physics Letters A* **26,** 238–239. doi:https://doi.org/10.1016/0375-9601(68)90623-3 (1968).

110. Boev, M. V. Photon drag of superconducting fluctuations in two-dimensional systems. en. *Phys. Rev. B* **101,** 104512. doi:10.1103/PhysRevB.101.104512 (2020).

111. Plastovets, V. & Buzdin, A. Fluctuation-mediated inverse Faraday effect in superconducting rings. *Physics Letters A,* 129001. doi:10.1016/j.physleta.2023.129001 (2023).

112. Varlamov, A. A., Galda, A. & Glatz, A. Fluctuation spectroscopy: From Rayleigh-Jeans waves to Abrikosov vortex clusters. *Rev. Mod. Phys.* **90,** 015009. doi:10.1103/RevModPhys.90.015009 (2018).

113. Gilabert, Alain. Interaction between light and superconductors. *Ann. Phys. Fr.* **15,** 255–283. doi:10.1051/anphys:01990001503025500 (1990).

114. Kampfrath, T., Tanaka, K. & Nelson, K. A. Resonant and nonresonant control over matter and light by intense terahertz transients. *Nature Photonics* **7,** 680–690. doi:10.1038/nphoton.2013.184 (2013).

115. Schmid, A. A time dependent Ginzburg-Landau equation and its application to the problem of resistivity in the mixed state. *Physik der kondensierten Materie* **5,** 302–317 (1966).

116. Abrahams, E. & Tsuneto, T. Time Variation of the Ginzburg-Landau Order Parameter. *Phys. Rev.* **152,** 416–432. doi:10.1103/PhysRev.152.416 (1966).

117. Kramer, L. & Watts-Tobin, R. J. Theory of Dissipative Current-Carrying States in Superconducting Filaments. *Phys. Rev. Lett.* **40,** 1041–1044. doi:10.1103/PhysRevLett.40.1041 (1978).

118. Aronov, A. G. & Gurevich, V. L. Response of a pure superconductor to a slowly varying perturbation. *Sov. Phys. - Solid State (Engl. Transl.); (United States)* **16:9** (1974).

119. Larkin, A. & Ovchinnikov, Y. Non-linear effects during the motion of vortices in superconductors. *Zh. Eksp. Teor. Fiz.* **73,** 7 (1977).

120. Altland, A. & Simons, B. D. *Condensed matter field theory* (Cambridge university press, 2010).

121. Beekman, A. J., Rademaker, L. & van Wezel, J. An introduction to spontaneous symmetry breaking. *SciPost Phys. Lect. Notes,* 11. doi:10.21468/SciPostPhysLectNotes.11 (2019).

122. Gulian, A. M. & Zharkov, G. F. *Nonequilibrium electrons and phonons in superconductors* (Springer Science & Business Media, 1999).

123. Anderson, P. W. Coherent excited states in the theory of superconductivity: Gauge invariance and the Meissner effect. *Physical review* **110,** 827. doi:10.1103/PhysRev.110.827 (1958).

124. Higgs, P. W. Broken Symmetries and the Masses of Gauge Bosons. *Phys. Rev. Lett.* **13,** 508–509. doi:10.1103/PhysRevLett.13.508 (1964).

125. Pekker, D. & Varma, C. Amplitude/Higgs Modes in Condensed Matter Physics. *Annual Review of Condensed Matter Physics* **6,** 269–297. doi:10.1146/annurev-conmatphys-031214-014350 (2015).

126. Schmid, A. The approach to equilibrium in a pure superconductor the relaxation of the Cooper pair density. *Physik der kondensierten Materie* **8,** 129–140 (1968).

127. Matsunaga, R. & Shimano, R. Nonequilibrium BCS state dynamics induced by intense terahertz pulses in a superconducting NbN film. *Phys. Rev. Lett.* **109,** 187002. doi:10.1103/PhysRevLett.109.187002 (2012).

128. Matsunaga, R. *et al.* Higgs amplitude mode in the BCS superconductors $\mathrm{Nb}_{1-x}\mathrm{Ti}_x\mathrm{N}$ induced by terahertz pulse excitation. *Phys. Rev. Lett.* **111,** 057002. doi:10.1103/PhysRevLett.111.057002 (2013).

129. Matsunaga, R. & Shimano, R. Nonlinear terahertz spectroscopy of Higgs mode in s-wave superconductors. *Physica Scripta* **92,** 024003. doi:10.1088/1402-4896/aa5327 (2017).

130. Shimano, R. & Tsuji, N. Higgs Mode in Superconductors. *Annual Review of Condensed Matter Physics* **11,** 103–124. doi:10.1146/annurev-conmatphys-031119-050813 (2020).

131. Langenberg, D., Larkin, A. & Larkin, A. *Nonequilibrium Superconductivity (Modern problems in condensed matter sciences)* (North-Holland, 1986).

132. Volkov, A. F. & Kogan, S. M. Collisionless relaxation of the energy gap in superconductors. *Soviet Journal of Experimental and Theoretical Physics* **38,** 1018 (1974).

133. Kulik, I. O., Entin-Wohlman, O. & Orbach, R. Pair susceptibility and mode propagation in superconductors: A microscopic approach. *Journal of Low Temperature Physics* **43,** 591–620. doi:10.1007/BF00115617 (1981).

134. Moor, A., Volkov, A. F. & Efetov, K. B. Amplitude Higgs Mode and Admittance in Superconductors with a Moving Condensate. *Phys. Rev. Lett.* **118,** 047001. doi:10.1103/PhysRevLett.118.047001 (2017).

135. Nakamura, S. *et al.* Infrared Activation of the Higgs Mode by Supercurrent Injection in Superconducting NbN. *Phys. Rev. Lett.* **122,** 257001. doi:10.1103/PhysRevLett.122.257001 (2019).

136. Bellitti, M., Laumann, C. R. & Spivak, B. Z. Incoherent excitation of coherent Higgs oscillations in superconductors. *Phys. Rev. B* **105,** 104513. doi:10.1103/PhysRevB.105.104513 (2022).

137. Papenkort, T., Axt, V. M. & Kuhn, T. Coherent dynamics and pump-probe spectra of BCS superconductors. *Phys. Rev. B* **76,** 224522. doi:10.1103/PhysRevB.76.224522 (2007).

138. Matsunaga, R. *et al.* Light-induced collective pseudospin precession resonating with Higgs mode in a superconductor. *Science* **345,** 1145–1149. doi:10.1126/science.1254697 (2014).

139. Matsunaga, R. *et al.* Higgs Amplitude Mode in the BCS Superconductors $Nb_{1-x}Ti_xN$ Induced by Terahertz Pulse Excitation. *Phys. Rev. Lett.* **111,** 057002. doi:10.1103/PhysRevLett.111.057002 (2013).

140. Kemper, A. F., Sentef, M. A., Moritz, B., Freericks, J. K. & Devereaux, T. P. Direct observation of Higgs mode oscillations in the pump-probe photoemission spectra of electron-phonon mediated superconductors. *Phys. Rev. B* **92,** 224517. doi:10.1103/PhysRevB.92.224517 (2015).

141. Buzdin, A. I. Proximity effects in superconductor-ferromagnet heterostructures. *Reviews of Modern Physics* **77,** 935–976. doi:10.1103/RevModPhys.77.935 (2005).

142. Eschrig, M. Spin-polarized supercurrents for spintronics: a review of current progress. *Reports on Progress in Physics* **78,** 104501. doi:10.1088/0034-4885/78/10/104501 (2015).

143. Heikkilä, T. T., Silaev, M., Virtanen, P. & Bergeret, F. S. Thermal, electric and spin transport in superconductor/ferromagnetic-insulator structures. *Progress in Surface Science* **94,** 100540. doi:10.1016/j.progsurf.2019.100540 (2019).

144. Houzet, M. Ferromagnetic Josephson Junction with Precessing Magnetization. *Phys. Rev. Lett.* **101,** 057009. doi:10.1103/PhysRevLett.101.057009 (2008).

145. Barnes, S. E., Aprili, M., Petković, I. & Maekawa, S. Ferromagnetic resonance with a magnetic Josephson junction. *Superconductor Science and Technology* **24,** 024020. doi:10.1088/0953-2048/24/2/024020 (2011).

146. Richard, C., Houzet, M. & Meyer, J. S. Andreev Current Induced by Ferromagnetic Resonance. *Phys. Rev. Lett.* **109,** 057002. doi:10.1103/PhysRevLett.109.057002 (2012).

147. Petkovi ć, I., Aprili, M., Barnes, S. E., Beuneu, F. & Maekawa, S. Direct dynamical coupling of spin modes and singlet Josephson supercurrent in ferromagnetic Josephson junctions. *Phys. Rev. B* **80,** 220502. doi:10.1103/PhysRevB.80.220502 (2009).

148. Takahashi, S., Hikino, S., Mori, M., Martinek, J. & Maekawa, S. Supercurrent Pumping in Josephson Junctions with a Half-Metallic Ferromagnet. *Phys. Rev. Lett.* **99,** 057003. doi:10.1103/PhysRevLett.99.057003 (2007).

149. Li, L.-L., Zhao, Y.-L., Zhang, X.-X. & Sun, Y. Possible Evidence for Spin-Transfer Torque Induced by Spin-Triplet Supercurrents*. *Chinese Physics Letters* **35,** 077401. doi:10.1088/0256-307X/35/7/077401 (2018).

150. Golovchanskiy, I. *et al.* Magnetization Dynamics in Proximity-Coupled Superconductor-Ferromagnet-Superconductor Multilayers. II. Thickness Dependence of the Superconducting Torque. *Phys. Rev. Appl.* **19,** 034025. doi:10.1103/PhysRevApplied.19.034025 (2023).

151. Silaev, M. Anderson-Higgs Mass of Magnons in Superconductor-Ferromagnet-Superconductor Systems. *Phys. Rev. Appl.* **18,** L061004. doi:10.1103/PhysRevApplied.18.L061004 (2022).

152. Vadimov, V. L., Khaymovich, I. M. & Mel'nikov, A. S. Higgs modes in proximized superconducting systems. *Phys. Rev. B* **100,** 104515. doi:10.1103/PhysRevB.100.104515 (2019).

153. Tang, G., Belzig, W., Zülicke, U. & Bruder, C. Signatures of the Higgs mode in transport through a normal-metal–superconductor junction. *Phys. Rev. Res.* **2,** 022068. doi:10.1103/PhysRevResearch.2.022068 (2020).

154. Mironov, S. V. & Buzdin, A. I. Collective magnetic and plasma excitations in Josephson ψ junctions. *Phys. Rev. B* **104,** 134502. doi:10.1103/PhysRevB.104.134502 (2021).

155. Lu, Y., Ilić, S., Ojajärvi, R., Heikkilä, T. T. & Bergeret, F. S. Reducing the frequency of the Higgs mode in a helical superconductor coupled to an LC-circuit. *arXiv:2212.11615* (2022).

156. Silaev, M. A., Ojajärvi, R. & Heikkilä, T. T. Spin and charge currents driven by the Higgs mode in high-field superconductors. *Physical Review Research* **2,** 033416. doi:10.1103/PhysRevResearch.2.033416 (2020).

157. Lu, Y., Ojajärvi, R., Virtanen, P., Silaev, M. A. & Heikkilä, T. T. Coupling the Higgs mode and ferromagnetic resonance in spin-split superconductors with Rashba spin-orbit coupling. *Phys. Rev. B* **106,** 024514. doi:10.1103/PhysRevB.106.024514 (2022).

158. Sarma, G. On the influence of a uniform exchange field acting on the spins of the conduction electrons in a superconductor. *Journal of Physics and Chemistry of Solids* **24,** 1029–1032. doi:https://doi.org/10.1016/0022-3697(63)90007-6 (1963).

159. Abrikosov, A. *Fundamentals of the Theory of Metals* ISBN: 9780486819013 (Dover Publications, 2017).

160. Tewari, S., Stanescu, T. D., Sau, J. D. & Sarma, S. D. Topologically non-trivial superconductivity in spin–orbit-coupled systems: bulk phases and quantum phase transitions. *New Journal of Physics* **13,** 065004. doi:10.1088/1367-2630/13/6/065004 (2011).

161. Ketterson, J., Ketterson, J., Song, S. & B, K. *Superconductivity* ISBN: 9780521565622 (Cambridge University Press, 1999).

162. Barankov, R. A., Levitov, L. S. & Spivak, B. Z. Collective Rabi Oscillations and Solitons in a Time-Dependent BCS Pairing Problem. *Phys. Rev. Lett.* **93,** 160401. doi:10.1103/PhysRevLett.93.160401 (2004).

163. Yuzbashyan, E. A., Tsyplyatyev, O. & Altshuler, B. L. Relaxation and Persistent Oscillations of the Order Parameter in Fermionic Condensates. *Phys. Rev. Lett.* **96,** 097005. doi:10.1103/PhysRevLett.96.097005 (2006).

164. Yuzbashyan, E. A. & Dzero, M. Dynamical Vanishing of the Order Parameter in a Fermionic Condensate. *Phys. Rev. Lett.* **96,** 230404. doi:10.1103/PhysRevLett.96.230404 (2006).

165. Abrikosov, A. A. Sov. Phys. JETP. **5,** 1174 (1957).

166. Barone, A. & Paterno, G. *Physics and Applications of the Josephson Effect* (Wiley, New York, 1982).

167. Gurevich, A. Nonlocal Josephson electrodynamics and pinning in superconductors. *Phys. Rev. B* **46,** R3187. doi:10.1103/PhysRevB.46.3187 (1992).

168. Horide, T. *et al.* Magnetic-field-induced crossover from flux-flow to Josephson-junction behavior in a highly transparent weak link. *Phys. Rev. B* **75,** 020504(R). doi:10.1103/PhysRevB.75.020504 (2007).

169. Horide, T. *et al.* Tilt angle dependences of vortex structure and critical current density at low-angle grain boundaries in $YBa_2Cu_3O_{7-x}$ films. *Phys. Rev. B* **77,** 132502. doi:10.1103/PhysRevB.77.132502 (2008).

170. Khlyustikov, I. N. & Buzdin, A. I. Twinning-plane superconductivity. *Adv. Phys.* **36,** 271. doi:10.1080/00018738700101012 (1987).

171. Gurevich, A. *et al.* Flux Flow of Abrikosov-Josephson Vortices along Grain Boundaries in High-Temperature Superconductors. *Phys. Rev. Lett.* **88,** 097001. doi:10.1103/PhysRevLett.88.097001 (2002).

172. Hilgenkamp, H. & Mannhart, J. Grain boundaries in high-T_c superconductors. *Rev. Mod. Phys.* **74,** 485. doi:10.1103/RevModPhys.74.485 (2002).

173. Jooss, C., Warthmann, R. & Kronmuller, H. Pinning mechanism of vortices at antiphase boundaries in $YBa_2Cu_3O_{7-\delta}$. *Phys. Rev. B* **61,** 12433. doi:10.1103/PhysRevB.61.12433 (2000).

174. Djupmyr, M., Cristiani, G., Habermeier, H. U. & Albrecht, J. Anisotropic temperature-dependent current densities in vicinal $YBa_2Cu_3O_{7-\delta}$. *Phys. Rev. B* **72,** 220507(R). doi:10.1103/PhysRevB.72.220507 (2005).

175. Tafuri1, F. & Kirtley, J. R. Weak links in high critical temperature superconductors. *Rep. Prog. Phys.* **68,** 2573. doi:10.1088/0034-4885/68/11/R03 (2005).

176. Golubov, A. A., Kupriyanov, M. Y. & Il'ichev, E. The current-phase relation in Josephson junctions. *Rev. Mod. Phys.* **76,** 411. doi:10.1103/RevModPhys.76.411 (2004).

177. Hess, H. F., Robinson, R. B., Dynes, R. C., J. M. Valles, J. & Waszczak, J. V. Scanning-Tunneling-Microscope Observation of the Abrikosov Flux Lattice and the Density of States near and inside a Fluxoid. *Phys. Rev. Lett.* **62,** 214. doi:10.1103/PhysRevLett.62.214 (1989).

178. Hoogenboom, B. W. *et al.* Shape and motion of vortex cores in $Bi_2Sr_2CaCu_2O_{8+\delta}$. *Phys. Rev. B* **62,** 9179. doi:10.1103/PhysRevB.62.9179 (2000).

179. Guillamon, I. *et al.* Superconducting Density of States and Vortex Cores of $2H-NbS_2$. *Phys. Rev. Lett.* **101,** 166407. doi:10.1103/PhysRevLett.101.166407 (2008).

180. Karapetrov, G., Fedor, J., Iavarone, M., Rosenmann, D. & Kwok, W. K. Direct Observation of Geometrical Phase Transitions in Mesoscopic Superconductors by Scanning Tunneling Microscopy. *Phys. Rev. Lett.* **95,** 167002. doi:10.1103/PhysRevLett.95.167002 (2005).

181. Roditchev, D., Brun, C., Serrier-Garcia, L. & et al. Direct observation of Josephson vortex cores. *Nature Physics* **11,** 332. doi:10.1038/nphys3240 (2015).

182. Guinea, F. & Pogorelov, Y. Vortex Viscosity in Superconductors with Short Coherence Length. *Phys. Rev. Lett.* **74,** 462. doi:10.1103/PhysRevLett.74.462 (1995).

183. Feigel'man, M. & Skvortsov, M. Anomalous Flux-Flow Dynamics in Layered Type-II Superconductors at Low Temperatures. *Phys. Rev. Lett.* **78,** 2640. doi:10.1103/PhysRevLett.78.2640 (1997).

184. Skvortsov, M., Ivanov, D. & Blatter, G. Vortex viscosity in the moderately clean limit of layered superconductors. *Phys. Rev. B* **67,** 014521. doi:10.1103/PhysRevB.67.014521 (2003).

185. Mel'nikov, A. S. & Samokhvalov, A. V. Abrikosov vortex escape from a columnar defect as a topological electronic transition in a vortex core. *JETP Lett.* **94,** 759. doi:10.1134/S0021364011220085 (2011).

186. Andreev, A. F. *Zh. Eksp. Teor. Fiz.* **46,** 1823 (1964).

187. Volovik, G. E. *The Universe in a Helium Droplet* (Clarendon Press, 2003).

188. Tanaka, Y., Kashiwaya, S. & Takayanagi, H. Theory of Superconducting Quantum Dot under Magnetic Field. *Jpn. J. Appl. Phys.* **34,** 4566. doi:10.1143/JJAP.34.4566 (1995).

189. Eschrig, M., Rainer, D. & Sauls, J. A. *Vortices in unconventional superconductors and superfluids* (eds Huebener, R., Schopohl, N. & Volovik, G.) (2001).

190. Mel'nikov, A., A.V.Samokhvalov & Vadimov, V. *JETP Lett.* **102,** 886. doi:10.1134/S0021364015230101 (2015).

191. Vadimov, V. & Mel'nikov, A. Electronic Structure of Vortices Pinned by Columnar Defects in $p_x + ip_y$ Superconductors. *J. Low Temp. Phys.* **183,** 342. doi:10.1007/s10909-016-1519-7 (2016).

192. Landau, L. & Pitaevskii, L. *Statistical Physics, Part 2* (Clarendon Press, 1980).

193. Kopnin, N. B. *et al.* Giant Oscillations of Energy Levels in Mesoscopic Superconductors. *Phys. Rev. Lett.* **95,** 197002. doi:10.1103/PhysRevLett.95.197002 (2005).

194. Kopnin, N. B. *et al.* Enhanced vortex heat conductance in mesoscopic superconductors. *Phys. Rev. B* **75,** 024514. doi:10.1103/PhysRevB.75.024514 (2007).

195. Mel'nikov, A. S., Ryzhov, D. A. & Silaev, M. A. Local density of states around single vortices and vortex pairs: Effect of boundaries and hybridization of vortex core states. *Phys. Rev. B* **79,** 134521. doi:10.1103/PhysRevB.79.134521 (2009).

196. Lifshits, I. M. *Zh. Eksp. Teor. Fiz.* **38,** 1569. doi:http://www.jetp.ac.ru/cgi-bin/dn/e_011_05_1130 (1960).

197. Blanter, Y. M., Kaganov, M. I., Pantsulaya, A. V. & Varlamov, A. A. The theory of electronic topological transitions. *Phys. Reports* **245,** 159. doi:10.1016/0370-1573(94)90103-1 (1994).

198. Volovik, G. E. *Pis'ma Zh. Eksp. Teor. Fiz.* **49,** 343 (1989).

199. Mel'nikov, S. & Silaev, M. A. Intervortex quasiparticle tunneling and the electronic structure of multivortex configurations in type-II superconductors. *Pis'ma Zh. Eksp. Teor. Fiz.* **83,** 675. doi:10.1134/S0021364006120113 (2006).

200. Beenakker, C. W. J. & van Houten, H. Josephson current through a superconducting quantum point contact shorter than the coherence length. *Phys. Rev. Lett.* **66,** 3056. doi:10.1103/PhysRevLett.66.3056 (1991).

201. Kopnin, N. B. & Volovik, G. E. Singularity of the vortex density of states in d-wave superconductors. *Pis'ma Zh. Eksp. Teor. Fiz.* **64,** 641. doi:10.1134/1.567283 (1996).

202. Kopnin, N. B. & Volovik, G. E. Flux Flow in d-Wave Superconductors: Low Temperature Universality and Scaling. *Phys. Rev. Lett.* **79,** 1377. doi:10.1103/PhysRevLett.79.1377 (1997).

203. Basov, D. N., Fogler, M. M., Lanzara, A., Wang, F. & Zhang, Y. Colloquium: Graphene spectroscopy. *Rev. Mod. Phys.* **86,** 959. doi:10.1103/RevModPhys.86.959 (2014).

204. Neto, A. H. C., Guinea, F., Peres, N. M. R., Novoselov, K. S. & Geim, A. K. The electronic properties of graphene. *Rev. Mod. Phys.* **81,** 109. doi:10.1103/RevModPhys.81.109 (2009).

205. Janko, B. Theory of Scanning Tunneling Spectroscopy of Magnetic-Field-Induced Discrete Nodal States in a d-Wave Superconductor. *Phys. Rev. Lett.* **82,** 4703. doi:10.1103/PhysRevLett.82.4703 (1999).

206. Blatter, G., Feigel'man, M. V., Geshkenbein, V. B., Larkin, A. I. & Vinokur, V. M. Vortices in high-temperature superconductors. *Rev. Mod. Phys.* **66,** 1125. doi:10.1103/RevModPhys.66.1125 (1994).

207. Blonder, G. E., Tinkham, M. & Klapwijk, T. M. Transition from metallic to tunneling regimes in superconducting microconstrictions: Excess current, charge imbalance, and supercurrent conversion. *Phys. Rev. B* **25,** 4515. doi:10.1103/PhysRevB.25.4515 (1982).

208. Kopnin, N. B., Mel'nikov, A. S. & Vinokur, V. M. Single-electron transport through the vortex core levels in clean superconductors. *Phys. Rev. B* **68,** 054528. doi:10.1103/PhysRevB.68.054528 (2003).

209. Horide, T. *et al.* Magnetic-field-induced crossover from flux-flow to Josephson-junction behavior in a highly transparent weak link. *Phys. Rev. B* **75,** 020504. doi:10.1103/PhysRevB.75.020504 (2007).

210. Horide, T. *et al.* Tilt angle dependences of vortex structure and critical current density at low-angle grain boundaries in $YBa_2Cu_3O_{7-x}$ films. *Phys. Rev. B* **77,** 132502. doi:10.1103/PhysRevB.77.132502 (2008).

211. Beenakker, C. W. J. & van Houten, H. Josephson current through a superconducting quantum point contact shorter than the coherence length. *Phys. Rev. Lett.* **66,** 3056–3059. doi:10.1103/PhysRevLett.66.3056 (1991).

212. Beenakker, C. W. J. Universal limit of critical-current fluctuations in mesoscopic Josephson junctions. *Phys. Rev. Lett.* **67,** 3836–3839. doi:10.1103/PhysRevLett.67.3836 (1991).

213. Haberman, R. *Applied partial differential equations with Fourier Series and Boundary Value Problems (5th edition)* (Pearson, 2012).

214. Landau, L. D. & Lifshitz, E. M. *Quantum Mechanics. Nonrelativistic theory* (Pergamon Press, 1991).

215. Tinkham, M. *Introduction to Superconductivity (2nd edition)* (Dover Publication, 2004).

216. Iguchi, Y. *et al.* Superconducting vortices carrying a temperature-dependent fraction of the flux quantum. *Science* **380,** 1244–1247. doi:10.1126/science.abp9979 (2023).

217. Rotter, M., Tegel, M. & Johrendt, D. Superconductivity at 38 K in the Iron Arsenide $(Ba_{1-x}K_x)Fe_2As_2$. *Phys. Rev. Lett.* **101,** 107006. doi:10.1103/PhysRevLett.101.107006 (2008).

218. Babaev, E. Vortices with fractional flux in two-gap superconductors and in extended Faddeev model. *Phys. Rev. Lett.* **89,** 067001. doi:10.1103/PhysRevLett.89.067001 (2002).

219. Fistul, M. V. & Giuliani, G. F. Critical current of a long Josephson junction in the presence of a perturbing Abrikosov vortex. *Phys. Rev. B* **58,** 9343. doi:10.1103/PhysRevB.58.9343 (1998).

220. Mironov, S. *et al.* Anomalous Josephson effect controlled by an Abrikosov vortex. *Phys. Rev. B* **96,** 214515. doi:10.1103/PhysRevB.96.214515 (2017).

221. Ge, J. Y., Gutierrez, J., Gladilin, V. N., Devreese, J. T. & Moshchalkov, V. V. Bound vortex dipoles generated at pinning centres by Meissner current. *Nat. Commun.* **6,** 6573. doi:10.1038/ncomms7573 (2015).

222. Mironov, S., Devizorova, Z., Clergerie, A. & Buzdin, A. Magnetic mapping of defects in type-II superconductors. *Appl. Phys. Lett.* **108,** 212602. doi:10.1063/1.4952617 (2016).

223. Golubov, A. A., Kupriyanov, M. Y. & Il'Ichev, E. The current-phase relation in Josephson junctions. *Rev. Mod. Phys.* **76,** 411. doi:10.1103/RevModPhys.76.411 (2004).

224. De Gennes, P. G. *Superconductivity of Metals and Alloys* (Westview Press, 1999).

225. Buzdin, A. I. & Brison, J. P. Vortex structures in small superconducting disks. *Physics Letters A* **196,** 267–271. doi:10.1016/0375-9601(94)91238-6 (1994).

226. Buzdin, A. & Feinberg, D. Electromagnetic pinning of vortices by non-superconducting defects and their influence on screening. *Physica C* **256,** 303. doi:10.1016/0921-4534(95)00664-8 (1996).

227. Bespalov, A. A. & Melnikov, A. S. Abrikosov vortex pinning on a cylindrical cavity inside the vortex core: formation of a bound state and depinning. *Superconductor Science and Technology* **26,** 085014. doi:10.1088/0953-2048/26/8/085014 (2013).

228. Gaber, T. *et al.* Nonideal artificial phase discontinuity in long $0-\kappa$ Josephson junctions. *Phys. Rev. B* **72,** 054522. doi:10.1103/PhysRevB.72.054522 (2005).

229. Barone, A. & Paternò, G. *Physics and Applications of the Josephson Effect* (John Wiley & Sons, Inc, 1982).

230. Golod, T., Pagliero, A. & Krasnov, V. M. Two mechanisms of Josephson phase shift generation by an Abrikosov vortex. *Phys. Rev. B* **100,** 174511. doi:10.1103/PhysRevB.100.174511 (2019).

231. Golod, T. *et al.* Reconfigurable Josephson phase shifter. *Nano Letters* **21,** 5240–5246. doi:10.1103/PhysRevB.63.174511 (2021).

232. Kogan, V. G. & Kirtley, J. R. Meissner response of superconductors with inhomogeneous penetration depths. *Phys. Rev. B* **83,** 214521. doi:10.1103/PhysRevB.83.214521 (2011).

233. Abrikosov, A. A., Buzdin, A. I., Kulic, M. L. & Kuptsov, D. A. Phenomenological theory for twinning-plane superconductivity in $YBa_2Cu_3O_{7-x}$. *Superconductor Science and Technology* **1,** 260. doi:10.1088/0953-2048/1/5/008 (1989).

234. Gutfreund, A. *et al.* Direct observation of a superconducting vortex diode. *Nature Communications* **14,** 1630. doi:10.1038/s41467-023-37294-2 (2023).

235. Mironov, S. V. & Buzdin, A. I. Giant demagnetization effects induced by superconducting films. *Applied Physics Letters* **119.** doi:10.1063/5.0059149 (2021).

236. Rusanov, A. Y., Hesselberth, M. B. S. & Aarts, J. Depairing currents in superconducting films of Nb and amorphous MoGe. *Phys. Rev. B* **70,** 024510. doi:10.1103/PhysRevB.70.024510 (2004).

237. Vodolazov, D. Y. *et al.* Considerable enhancement of the critical current in a superconducting film by a magnetized magnetic strip. *Phys. Rev. B* **72,** 064509. doi:10.1103/PhysRevB.72.064509 (6 Aug. 2005).

238. Touitou, N. *et al.* Nonsymmetric current-voltage characteristics in ferromagnet/superconductor thin film structures. *Applied Physics Letters* **85,** 1742–1744. doi:10.1063/1.1789231 (Sept. 2004).

239. Kogan, V. G. Interaction of vortices in thin superconducting films and the Berezinskii-Kosterlitz-Thouless transition. *Phys. Rev. B - Condensed Matter and Materials Physics* **75.** doi:10.1103/PhysRevB.75.064514 (2007).

240. Koshelev, A. E., Buzdin, A. I., Kakeya, I., Yamamoto, T. & Kadowaki, K. Fluctuating pancake vortices revealed by dissipation of the Josephson vortex lattice. *Phys. Rev. B - Condensed Matter and Materials Physics* **83.** doi:10.1103/PhysRevB.83.224515 (2011).

241. Bean, C. P. Magnetization of Hard Superconductors. *Phys. Rev. Lett.* **8,** 250–253. doi:10.1103/PhysRevLett.8.250 (1962).

242. Zeldov, E., Clem, J. R., McElfresh, M. & Darwin, M. Magnetization and transport currents in thin superconducting films. *Phys. Rev. B* **49,** 9802–9822. doi:10.1103/PhysRevB.49.9802 (1994).

243. Gor'kov, L. P. & M., E. G. Generalization of the Ginzburg-Landau equations for non-stationary problems in the case of alloys with paramagnetic impurities. *Soviet Phys.-JETP* **27,** 328–334 (1968).

244. Watts-Tobin, R. J., Krähenbühl, Y. & Kramer, L. Nonequilibrium theory of dirty, current-carrying superconductors: Phase-slip oscillators in narrow filaments near T_c. *Journal of Low Temperature Physics* **42,** 459–501 (1981).

245. Golub, A. A. Dinamicheskie uravneniya Ginzburga-Landau i kalibrovochnaya invariantnost zaryada. *ZHETF* **71,** 341 (1976).

246. Schön, G. & Ambegaokar, V. Collective modes and nonequilibrium effects in current-carrying superconductors. *Phys. Rev. B* **19,** 3515. doi:10.1103/PhysRevB.19.3515 (1979).

247. Ivlev, B. I. & Kopnin, N. B. Theory of current states in narrow superconducting channels. *Phys. Usp.* **27,** 206–227. doi:10.1070/PU1984v027n03ABEH004037 (1984).

248. Gorkov, L. & Eliashberg, G. Superconducting alloys in a strong alternating field. *SOV PHYS JETP* **29,** 698–703 (1969).

249. Kopnin, N. Time dependent theory of gapless d-wave superconductors: Application to the flux flow. *Journal of low temperature physics* **110,** 885–898 (1998).

250. Abrahams, E. & Tsuneto, T. Time variation of the Ginzburg-Landau order parameter. *Physical Review* **152,** 416. doi:10.1103/PhysRev.152.416 (1966).

251. Maki, K. Hall Effect in Dirty Type-II Superconductors. *Phys. Rev. Lett.* **23,** 1223. doi:10.1103/PhysRevLett.23.1223 (1969).

252. Gor'kov, L. P. On the energy spectrum of superconductors. *Sov. Phys. JETP* **7,** 158 (1958).

253. Aronov, A. & Rapoport, A. Hall effect in superconductors above T_c. *Modern Physics Letters B* **6,** 1083–1088. doi:10.1142/S0217984992001939 (1992).

254. Abrikosov, A. A., Gorkov, L. P. & Dzyaloshinski, I. E. *Methods of quantum field theory in statistical physics* (Courier Corporation, 2012).

255. Van Otterlo, A., Golubev, D. S., Zaikin, A. D. & Blatter, G. Dynamics and effective actions of BCS superconductors. *The European Physical Journal B-Condensed Matter and Complex Systems* **10,** 131–143. doi:10.1007/s100510050836 (1999).

256. Angilella, G. G. N., Pucci, R., Varlamov, A. A. & Onufrieva, F. Effects of proximity to an electronic topological transition on normal-state transport properties of the high$-T_c$ superconductors. *Phys. Rev. B* **67,** 134525. doi:10.1103/PhysRevB.67.134525 (2003).

257. Pitaevskii, L. & Stringari, S. *Bose-Einstein condensation and superfluidity* (Oxford University Press, 2016).

258. Pitaevskii, L. Phenomenological theory of superfluidity near the l point. *Sov. Phys.—JETP* **8,** 282 (1959).

259. Kopnin, N. B. Introduction to Ginzburg-Landau and Gross-Pitaevskii theories for superconductors and superfluids. *Journal of low temperature physics* **129,** 219–262. doi:10.1023/A:1021456311824 (2002).

260. Carlson, R. V. & Goldman, A. M. Propagating Order-Parameter Collective Modes in Superconducting Films. *Phys. Rev. Lett.* **34,** 11–15. doi:10.1103/PhysRevLett.34.11 (1975).

261. Schmid, A. & Schön, G. Collective Oscillations in a Dirty Superconductor. *Phys. Rev. Lett.* **34,** 941–943. doi:10.1103/PhysRevLett.34.941 (1975).

262. Artemenko, S. N. & Volkov, A. Electric fields and collective oscillations in superconductors. *Soviet Physics Uspekhi* **22,** 295 (1979).

263. Sun, Z., Fogler, M. M., Basov, D. N. & Millis, A. J. Collective modes and terahertz near-field response of superconductors. *Phys. Rev. Res.* **2,** 023413. doi:10.1103/PhysRevResearch.2.023413 (2020).

264. Van der Ziel, J. P., Pershan, P. S. & Malmstrom, L. D. Optically-Induced Magnetization Resulting from the Inverse Faraday Effect. *Phys. Rev. Lett.* **15,** 190–193. doi:10.1103/PhysRevLett.15.190 (1965).

265. Tokman, I. The inverse Faraday effect in a harmonic "atom" and the generalized Kohn's theorem. *Physics Letters A* **252,** 83–86. doi:https://doi.org/10.1016/S0375-9601(98)00932-3 (1999).

266. Tokman, I. D. *et al.* Inverse Faraday effect in graphene and Weyl semimetals. *Phys. Rev. B* **101,** 174429. doi:10.1103/PhysRevB.101.174429 (2020).

267. Ghinovker, M., Shapiro, I. & Shapiro, B. Y. Explosive nucleation of superconductivity in a magnetic field. *Phys. Rev. B* **59,** 9514–9521. doi:10.1103/PhysRevB.59.9514 (1999).

268. Hernández, A. D., Baelus, B. J., Domínguez, D. & Peeters, F. M. Effects of thermal fluctuations on the magnetic behavior of mesoscopic superconductors. *Phys. Rev. B* **71,** 214524. doi:10.1103/PhysRevB.71.214524 (2005).

269. Ivlev, B., Kopnin, N. & Larkin, I. Low-frequency oscillations in the resistive state of narrow superconductors. *Sov. Phys. - JETP (Engl. Transl.); (United States)* **61:2** (1985).

270. Yokoyama, T. Creation of Superconducting Vortices by Angular Momentum of Light. *Journal of the Physical Society of Japan* **89,** 103703. doi:10.7566/JPSJ.89.103703 (2020).

271. Berman, R., Foster, E. & Ziman, J. M. Thermal conduction in artificial sapphire crystals at low temperatures I. Nearly perfect crystals. *Proceedings of the Royal Society of London. Series A. Mathematical and Physical Sciences* **231,** 130–144 (1955).

272. Kirtley, J. R. *et al.* Scanning SQUID susceptometers with sub-micron spatial resolution. *Review of Scientific Instruments* **87,** 093702. doi:10.1063/1.4961982 (2016).

273. Martinez-Perez, M. J. & Koelle, D. NanoSQUIDs: Basics and recent advances. *Physical Sciences Reviews* **2,** 20175001. doi:doi:10.1515/psr-2017-5001 (2017).

274. Vasyukov, D. *et al.* A scanning superconducting quantum interference device with single electron spin sensitivity. *Nature Nanotechnology* **8,** 639–644. ISSN: 1748-3395. doi:10.1038/nnano.2013.169 (2013).

275. Thiel, L. *et al.* Quantitative nanoscale vortex imaging using a cryogenic quantum magnetometer. *Nature Nanotechnology* **11,** 677–681. ISSN: 1748-3395. doi:10.1038/nnano.2016.63 (2016).

276. Lenz, T., Wickenbrock, A., Jelezko, F., Balasubramanian, G. & Budker, D. Magnetic sensing at zero field with a single nitrogen-vacancy center. *Quantum Science and Technology* **6,** 034006. doi:10.1088/2058-9565/abffbd (2021).

277. Goa, P. E. *et al.* Real-time magneto-optical imaging of vortices in superconducting NbSe2. *Superconductor Science and Technology* **14,** 729–731. doi:10.1088/0953-2048/14/9/320 (2001).

278. Correa, A. *et al.* Attractive interaction between superconducting vortices in tilted magnetic fields. *Communications Physics* **2,** 31. doi:10.1038/s42005-019-0132-x (2019).

279. Llorens, J. B. *et al.* Observation of a gel of quantum vortices in a superconductor at very low magnetic fields. *Phys. Rev. Research* **2,** 013329. doi:10.1103/PhysRevResearch.2.013329 (2020).

280. Bleszynski-Jayich, A. C. *et al.* Persistent Currents in Normal Metal Rings. *Science* **326,** 272–275. doi:10.1126/science.1178139 (2009).

281. Kirtley, J. R. Fundamental studies of superconductors using scanning magnetic imaging. *Reports on Progress in Physics* **73,** 126501. doi:10.1088/0034-4885/73/12/126501 (2010).

282. Aslamazov, L. & Larkin, A. Effect of fluctuations on the properties of a superconductor at temperatures above the critical temperature(Electron fluctuation coupling effect on superconductor kinetic properties at temperature above critical temperature). *Fizika tverdogo tela* **10,** 1104–1111 (1968).

283. Maki, K. Critical fluctuation of the order parameter in a superconductor. I. *Progress of Theoretical Physics* **40,** 193–200. doi:10.1143/PTP.40.193 (1968).

284. Thompson, R. S. Microwave, flux flow, and fluctuation resistance of dirty type-II superconductors. *Phys. Rev. B* **1,** 327. doi:10.1103/PhysRevB.1.327 (1970).

285. Sergeev, A., Reizer, M. Y. & Mitin, V. Particle-hole asymmetry in fluctuating thermoelectric and Hall effects. *Phys. Rev. B* **66,** 104504. doi:10.1103/PhysRevB.66.104504 (2002).

286. Schmidt, V. V. *in Proceedings of the 10th International Conference on Low Temperature Physics (VINITI, Moscow), C2, 205* 1967.

287. Buhrman, R. A. & Halperin, W. P. Fluctuation Diamagnetism in a "Zero-Dimensional" Superconductor. *Phys. Rev. Lett.* **30,** 692–695. doi:10.1103/PhysRevLett.30.692 (1973).

288. Glazman, L. I., Hekking, F. W. J. & Zyuzin, A. Nonlocal resistance oscillations near the superconducting transition. *Phys. Rev. B* **46,** 9074–9081. doi:10.1103/PhysRevB.46.9074 (1992).

289. Buzdin, A. I. & Varlamov, A. A. Critical Fluctuations in a Mesoscopic Superconducting Ring. en. *Phys. Rev. Lett.* **89,** 076601. doi:10.1103/PhysRevLett.89.076601 (2002).

290. Schwiete, G. & Oreg, Y. Fluctuation persistent current in small superconducting rings. en. *Phys. Rev. B* **82,** 214514. doi:10.1103/PhysRevB.82.214514 (2010).

291. Little, W. A. & Parks, R. D. Observation of Quantum Periodicity in the Transition Temperature of a Superconducting Cylinder. *Phys. Rev. Lett.* **9,** 9–12. doi:10.1103/PhysRevLett.9.9 (1962).

292. Daumens, M., Meyers, C. & Buzdin, A. Little-Parks effect for arbitrary geometry: fluctuations of the magnetic moment of mesoscopic loops. *Physics Letters A* **248,** 445–452. doi:https://doi.org/10.1016/S0375-9601(98)00741-5 (1998).

293. Mironov, S. V. & Buzdin, A. Fluctuations in a Mesoscopic Superconducting Ring: Resonant Behavior of Conductivity and Specific Heat in the Two-Mode Critical Regime. *Phys. Rev. B* **84,** 064527. doi:10.1103/PhysRevB.84.064527 (2011).

294. Behrle, A. *et al.* Higgs mode in a strongly interacting fermionic superfluid. *Nature Physics* **14,** 781–785. doi:10.1038/s41567-018-0128-6 (2018).

295. Wang, P., Yi, W. & Xianlong, G. Topological phase transition in the quench dynamics of a one-dimensional Fermi gas with spin-orbit coupling. *New Journal of Physics* **17,** 013029. doi:10.1088/1367-2630/17/1/013029 (2015).

296. Dong, Y., Dong, L., Gong, M. & Pu, H. Dynamical phases in quenched spin–orbit-coupled degenerate Fermi gas. *Nature communications* **6,** 6103. doi:10.1038/ncomms7103 (2015).

297. Genwang Fan Xiao-Long Chen, P. Z. Probing two Higgs oscillations in a one-dimensional Fermi superfluid with Raman-type spin-orbit coupling. *Frontiers of Physics* **17,** 52502. doi:10.1007/s11467-022-1155-4 (2022).

298. Samokhin, K. V. Goldstone modes in Larkin-Ovchinnikov-Fulde-Ferrell superconductors. *Phys. Rev. B* **81,** 224507. doi:10.1103/PhysRevB.81.224507 (2010).

299. Huang, Z., Ting, C. S., Zhu, J.-X. & Lin, S.-Z. Gapless Higgs mode in the Fulde-Ferrell-Larkin-Ovchinnikov state of a superconductor. *Phys. Rev. B* **105,** 014502. doi:10.1103/PhysRevB.105.014502 (2022).

300. Ivakhnenko, O. V., Shevchenko, S. N. & Nori, F. Nonadiabatic Landau-Zener-Stückelberg-Majorana transitions, dynamics, and interference. *Physics Reports* **995,** 1–89. doi:10.1016/j.physrep.2022.10.002 (2023).

301. Gor'kov, L. P. & Rashba, E. I. Superconducting 2D System with Lifted Spin Degeneracy: Mixed Singlet-Triplet State. *Phys. Rev. Lett.* **87,** 037004. doi:10.1103/PhysRevLett.87.037004 (2001).

302. Note that here we focus on the problem with a single pairing channel. The collective modes in systems with several pairing channels may be of interest in the context of theoretical and experimental studies of multicomponent superconductors and superfluids. In particular, in a helium system the breaking of complex symmetry (including gauge transformation as well as spin and orbital rotations) by the matrix order parameter leads to the appearance of multiple Higgs modes [319, 320].

303. Frigeri, P. A., Agterberg, D. F. & Sigrist, M. Spin susceptibility in superconductors without inversion symmetry. *New Journal of Physics* **6,** 115. doi:10.1088/1367-2630/6/1/115 (2004).

304. Szombati, D. B. *et al.* Josephson ϕ-junction in nanowire quantum dots. *Nature Physics* **12,** 568–572. doi:10.1038/nphys3742 (2016).

305. Kirilyuk, A., Kimel, A. V. & Rasing, T. Ultrafast optical manipulation of magnetic order. *Reviews of Modern Physics* **82,** 2731–2784. doi:10.1103/RevModPhys.82.2731 (2010).

306. Kirilyuk, A., Kimel, A. V. & Rasing, T. Laser-induced magnetization dynamics and reversal in ferrimagnetic alloys. *Reports on Progress in Physics* **76,** 026501. doi:10.1088/0034-4885/76/2/026501 (2013).

307. El-Ghazaly, A., Gorchon, J., Wilson, R. B., Pattabi, A. & Bokor, J. Progress towards ultrafast spintronics applications. *Journal of Magnetism and Magnetic Materials* **502,** 166478. doi:https://doi.org/10.1016/j.jmmm.2020.166478 (2020).

308. Hurand, S. *et al.* Field-effect control of superconductivity and Rashba spin-orbit coupling in top-gated LaAlO3/SrTiO3 devices. *Scientific reports* **5,** 12751 (2015).

309. Hurand, S. *et al.* Top-gated field-effect LaAlO3/SrTiO3 devices made by ion-irradiation. *Applied Physics Letters* **108,** 052602. doi:10.1063/1.4941672 (2016).

310. Gershenzon, E. *et al.* Electron-phonon interaction in ultrathin Nb films. *Sov. Phys. JETP* **70,** 505–511 (1990).

311. Kardakova, A. *et al.* The electron-phonon relaxation time in thin superconducting titanium nitride films. *Applied Physics Letters* **103,** 252602. doi:10.1063/1.4851235 (2013).

312. Tsuchiya, S., Yamamoto, D., Yoshii, R. & Nitta, M. Hidden charge-conjugation, parity, and time-reversal symmetries and massive Goldstone (Higgs) modes in superconductors. *Phys. Rev. B* **98,** 094503. doi:10.1103/PhysRevB.98.094503 (2018).

313. Liu, C.-X., Liu, D. E., Zhang, F.-C. & Chiu, C.-K. Protocol for Reading Out Majorana Vortex Qubits and Testing Non-Abelian Statistics. *Phys. Rev. Appl.* **12,** 054035. doi:10.1103/PhysRevApplied.12.054035 (5 Nov. 2019).

314. Posske, T., Chiu, C.-K. & Thorwart, M. Vortex Majorana braiding in a finite time. *Phys. Rev. Res.* **2,** 023205. doi:10.1103/PhysRevResearch.2.023205 (2 May 2020).

315. Hua, C., Halász, G. B., Dumitrescu, E., Brahlek, M. & Lawrie, B. Optical vortex manipulation for topological quantum computation. *Phys. Rev. B* **104,** 104501. doi:10.1103/PhysRevB.104.104501 (10 Sept. 2021).

316. Linder, J. & Robinson, J. W. Superconducting spintronics. *Nature Physics* **11,** 307–315. doi:10.1038/nphys3242 (2015).

317. Yang, G., Ciccarelli, C. & Robinson, J. W. Boosting spintronics with superconductivity. *APL Materials* **9.** doi:10.1063/5.0048904 (2021).

318. Bergeret, F. S., Silaev, M., Virtanen, P. & Heikkilä, T. T. Colloquium: Nonequilibrium effects in superconductors with a spin-splitting field. *Rev. Mod. Phys.* **90,** 041001. doi:10.1103/RevModPhys.90.041001 (4 Oct. 2018).

319. Volovik, G. & Zubkov, M. Higgs bosons in particle physics and in condensed matter. *Journal of Low Temperature Physics* **175,** 486–497. doi:10.1007/s10909-013-0905-7 (2014).

320. Zavjalov, V., Autti, S., Eltsov, V., Heikkinen, P. & Volovik, G. Light Higgs channel of the resonant decay of magnon condensate in superfluid 3He-B. *Nature communications* **7,** 10294. doi:10.1038/ncomms10294 (2016).